AD-A160 403 CHEMICAL BONDING INTERDIFFUSION AND ELECTRONIC STRUCTURE AT INP GAAS ANN SI--ETAL INTERFACES(U) XEROX WEBSTER RESEARCH CENTER NY L J BRILLSON 01 OCT 85 1/3

UNCLASSIFIED N00014-80-C-0778 F/G 20/12 NL

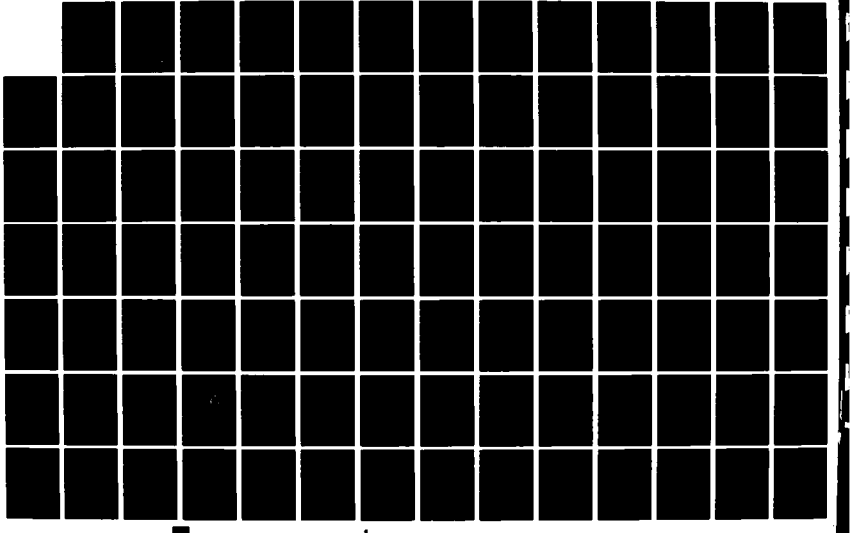

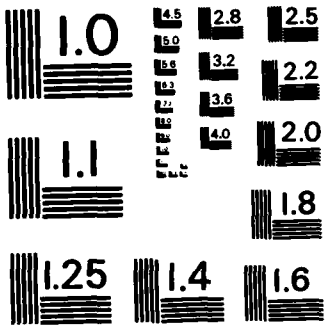

MICROCOPY RESOLUTION TEST CHART
NATIONAL BUREAU OF STANDARDS - 1963 - A

(1)

AD-A160 403

XEROX WEBSTER RESEARCH CENTER

CHEMICAL BONDING, INTERDIFFUSION AND ELECTRONIC STRUCTURE AT InP, GaAs, AND Si-METAL INTERFACES: ANNUAL SUMMARY REPORT

L.J. Brillson, Principal Investigator
Xerox Webster Research Center
Webster, NY 14580
Telephone (716) 422-6468

October 1, 1985

Office of Naval Research
800 North Quincy Street
Arlington, VA 22117

Sponsored by

Office of Naval Research
NR #372-098
Proposal No. 80-10-199
Contract No. N00014-80-C-0778

SECURITY CLASSIFICATION OF THIS PAGE (When Data Entered)

REPORT DOCUMENTATION PAGE		READ INSTRUCTIONS BEFORE COMPLETING FORM
1. REPORT NUMBER	2. GOVT ACCESSION NO. AD-A160403	3. RECIPIENT'S CATALOG NUMBER
4. TITLE (and Subtitle) Chemical Bonding, Interdiffusion and Electronic Structure at InP, GaAs and Si-Metal Interfaces: Annual Summary Report		5. TYPE OF REPORT & PERIOD COVERED Summary Report - Oct. 1, 1984 - Sept. 30, 85 6. PERFORMING ORG. REPORT NUMBER
7. AUTHOR(s) Leonard J. Brillson		8. CONTRACT OR GRANT NUMBER(s) N00014-80-C-0778
9. PERFORMING ORGANIZATION NAME AND ADDRESS Xerox Webster Research Center 800 Phillips Road 114-41D Webster, NY 14580		10. PROGRAM ELEMENT, PROJECT, TASK AREA & WORK UNIT NUMBERS
11. CONTROLLING OFFICE NAME AND ADDRESS Office of Naval Research Electronics Div. Code 414 800 N. Quincy St., Arlington, VA 22217-5000		12. REPORT DATE October 1, 1985 13. NUMBER OF PAGES 266
14. MONITORING AGENCY NAME & ADDRESS(if different from Controlling Office) Office of Naval Research		15. SECURITY CLASS. (of this report) UNCLASSIFIED 15a. DECLASSIFICATION/DOWNGRADING SCHEDULE

16. DISTRIBUTION STATEMENT (of this Report)

Approved for public release; Distribution unlimited.

17. DISTRIBUTION STATEMENT (of the abstract entered in Block 20, if different from Report)

18. SUPPLEMENTARY NOTES

19. KEY WORDS (Continue on reverse side if necessary and identify by block number)

20. ABSTRACT (Continue on reverse side if necessary and identify by block number)

An annual report of research performed under Office of Naval Research Grant No. N00014-80-C-0778.

DD FORM 1 JAN 73 1473 EDITION OF 1 NOV 65 IS OBSOLETE

S/N 0102-LF-014-6601

Unclassified

SECURITY CLASSIFICATION OF THIS PAGE (When Data Entered)

1. Overview

Over the past year, we have carried out an experimental program to investigate the interface electronic states and band structure at GaAs, InP, and Si-metal interfaces formed by chemical reaction and interdiffusion at room temperature, elevated temperatures, as well as following pulsed-laser annealing. We have used soft x-ray photoemission spectroscopy (SXPS) and Auger electron spectroscopy (AES)/depth profiling to characterize atomic redistribution and new chemical bonding near the surfaces and interfaces on an atomic scale. We have refined the technique of cathodoluminescence spectroscopy (CLS) for investigations of new compound and defect formation at "buried" metal-semiconductor interfaces. We have employed temperature-dependent current-voltage and capacitance-voltage measurements to characterize the electronic properties and spatial distribution of interface states of metal-InP interfaces prepared and processed under carefully controlled conditions. This annual report for the period October 1, 1984, through September 30, 1985, defines (Sec. II) and summarizes (Sec. III) the bulk of this research and includes the papers published or in press as a result of this effort. A list of the papers published under Navy Contract #N00014-80-C-0778 (NR #372-098) as well as the papers themselves are included in (Sec. IV) of this report. Also attached are: the cumulative list of publications (Sec. V), serially numbered, a list of postdoctoral fellows involved in the contract (Sec. VI), a list of Publications/Patents/Presentations/Honors (Sec. VII), money spent on equipment (Sec. VIII), transitions of research to industry (Sec. IX) and a list of collaborations with workers from academic institutions (Sec. X).

II. Background

It is now clear that substantial chemical interactions can occur between semiconductors and metals or other adsorbates, even near room temperature. Furthermore, such interactions can strongly modify the surface or interface electronic properties.[1-3] These chemical interactions can affect Schottky barrier formation by producing defects[4-6] of various types, interfacial regions with new dielectric properties[7], metallic alloy layers with new effective work functions[8,9] as well as new interface states at the intimate semiconductor-metal interface.[10,11] Each of these mechanisms may play a role in modifying electronic behavior at different interfaces, yet each is difficult to characterize unambiguously - particularly if these interfaces are characterized at only one stage of the metal-semiconductor interaction.

We are now investigating the detailed relationships between chemical interactions and electronic structure at metal-GaAs, InP, and Si interfaces by promoting these interactions at elevated temperatures and under nonequilibrium thermal conditions. By studying the evolution of electronic properties with chemical changes under carefully controlled conditions, we can begin to identify which factor or factors dominate the Fermi level movement, the type and distribution of interface states, and the Schottky barrier as measured by conventional electrical techniques. To promote these chemical interactions on a microscopic scale near the interface, we have used pulsed-laser annealing and rapid thermal annealing under ultrahigh vacuum conditions. To measure electronic properties at the interface after "burying" it with bulk metal films, we have employed a variation of cathodoluminescence spectroscopy (CLS) with sub-surface sensitivity. Thus, with our complement of ultrahigh vacuum techniques, we have developed the capability

to measure surface (SXPS) and subsurface (CLS) electronic properties and surface (AES, SXPS) and subsurface (AES/depth profiling) chemical properties. This combination of techniques reveals new electronic/chemical relationships and suggests new approaches to controlling these properties by atomic scale techniques.

III. Results

The work ~~under this contract~~ can be grouped into four ~~related~~ areas: 1) chemical and electronic structure of "buried" III-V and II-VI compound semiconductor-metal interfaces, 2) localized chemical reactions at Al interfaces with III-V compound semiconductors promoted by pulsed-laser annealing as well as laser-induced oxidation of Si, 3) electrical characterization of the UHV-prepared Al-InP (110) interface, and 4) control of competitive Ti-Si and Ti-SiO_2 interfacial reactions by rapid thermal annealing.

In the first area, we have used AES combined with Ar^+ sputtering to obtain depth profiles of atomic composition vs. distance from the intimate interface for a variety of common metals deposited on UHV-cleaved InP (110) surfaces.[14] Interface composition can change with increasing overlayer thickness as more semiconductor outdiffusion can be accommodated. Analysis of the free surface alone can not provide this information. Special care is taken to minimize ion-induced mixing of the overlayer-substrate system. In this way, we are able to demonstrate that anion and cation outdiffusion is a general phenomenon at thick (70Å) metal-InP interfaces, even near room temperature. The relative stoichiometry of In and P atoms changes substantially between the substrate, the interfacial region, the overlayer, and the free surface. Nevertheless the same patterns of diffusion are observed for "unreactive" (Au and Cu) and "reactive"[12] (Al, Ni, and Ti) metal overlayers. These patterns are

highly sensitive to the strength of metal-anion and metal-cation bonding and can be altered dramatically by thin (40Å) interlayers. Our depth-profiling studies allow us to demonstrate that "chemical trapping"[13] at the interface can change the interfacial region from In-rich ("unreactive" to P-rich ("reactive"). Comparison with vacancy and antisite defect calculations of energy levels reveals that our identification of interfacial atomic composition is inconsistent with Fermi level pinning by such simple native defects. Hence, our results for this prototypical III-V compound semiconductor point to either more complex defect combinations or other electronic mechanisms - chemical or otherwise[1] - as the dominant factor in Fermi level pinning.

The evolution of metal-semiconductor interfaces with temperature is of considerable interest in identifying the dominant factors in Schottky barrier formation and interface degradation. Yet surface-sensitive techniques are not optimum for studies of such evolution occurring at "buried" interfaces - i.e., many monolayers below the free surface of the metal overlayer. We have adapted the technique of cathodoluminescence spectroscopy (CLS) to monitor changes in buried metal-semiconductor interfaces with room temperature deposition and with pulsed-laser annealing.[15] By choosing incident electron energies in the range of 0.5 to 2 keV, one can vary the excitation depth in the range of several tens to several hundreds of Å respectively. These incident electrons can excite optical transitions characteristic of the semiconductor band-to-band emission, new interface compound emission, as well as new deep levels within the band gap(s). Thus, by spectrally resolving this emission, it is possible to identify chemical and electronic features from optical transitions below the surface and, by varying the electron energy, discriminate between electronic states distributed at different depths below the free surface with

microscopic resolution of less than hundreds of Å. We have demonstrated this capability for metals on CdS, for which identification of luminescent features is relatively straightforward. CLS provides evidence for Cu_2S formation after laser-annealing Cu on UHV-cleaved CdS. On the other hand, Al deposition on CdS followed by laser annealing leads to formation of at least two deep levels distributed at different depths from the interface. The relative intensities and spatial distribution of these features changes with subsequent processing, highlighting the utility of the energy-dependent CLS technique for *in-situ* electronic characterization under real device conditions.

In the second area, we have used pulsed ultraviolet (UV) laser anneling to prepare highly localized chemical reactions at metal-semiconductor interfaces.[18-20] These interfaces were annealed in UHV and characterized by surface-sensitive techniques in order to monitor the chemical processes on a scale of monolayers. Because of the extremely short laser pulse (5 nsec) and resultant heating (~ 100 nsec), interdiffusion of the metal and semiconductor atoms could be limited to tens of Å even though temperatures near the melting point are reached. Longer heat treatments, even at low temperatures, would produce extended diffusion and a broadening of the interfacial structure below the detection level of our surface-sensitive techniques. In addition, the step-wise nature of the pulsed annealing allows us to characterize the nature of the spatially-localized interface chemical reactions in discrete stages, using successive pulses. We used SXPS and AES to characterize the atomic movement and chemical structure which occur at pulsed-laser-annealed Al-InP (110) interfaces. In addition, for Al on each of the semiconductors GaP, GaAs, GaSb, InP, InAs, and InSb, we have found a finite range of energy density above a characteristic threshold such that a chemical reaction occurs without disruption of the surface morphology.

The systematic change in threshold across the III-V semiconductors indicates a thermally-activated reaction occurring in a molten phase of the Al overlayer and a thin (~ 100-200Å) substrate later. Excellent agreement between the observed thresholds and calculations which model the heat flow demonstrate that the thermal properties of the semiconductor have a dominant influence on the interfacial temperature profile and the threshold energy density for reaction. Hence we have demonstrated how to enhance the observed microreactions at room temperature on a scale of nanometers and in a controllable, predictable fashion. These reactions can modify junction electronic properties[1] and may prove useful in modifying charge transport, surface recombination and open-circuit voltage, among other applications.

We have also used the pulsed laser technique to induce ultrafast oxidation of Si.[21,22] This process represents an efficient low temperature technique for depositing thin dielectric films in semiconductor device fabrication. Low temperature techniques can reduce or eliminate substrate warpage, dopant redistribution, defect generation and propagation associated with conventional high temperature process steps. While researchers have used continuous-wave (CW) lasers extensively to grow SiO_2 layers on Si, growth rates are comparable to or only slightly larger than the rate of conventional thermal oxidation. With the pulsed UV laser under an oxygen ambient of 1 atmosphere, we are able to produce oxide growth rates of 100 Å/sec between thicknesses of 300 to 1800 Å. This growth rate is comparable to that found for deposition of SiO_2 by laser-assisted chemical vapor deposition (CVD) techniques. Taking into account that the Si wafer surface is at elevated temperatures for only 1 μsec after each pulse, one obtains growth rates orders of magnitude greater than thermal oxidation processes. The electrical quality of the interface is acceptable - 3 to 8×10^{11} cm^{-2}, and can be reduced substantially by

postannealing. An important advantage of this technique is the use of a focussed laser beam with which to grow a patterned oxide. Hence, two steps in the fabrication of integrated circuits are eliminated - masking and subsequent etching to remove patterned oxide areas for metallization. Since the oxidation process is very strongly temperature-dependent, the oxide profile is usually much steeper than the laser beam profile, yielding abrupt oxide sidewalls. By varying the energy density, it is also possible to modulate the oxide thickness in a controlled manner during the growth process.

In a third area of activity, we have carried out electrical measurements on interfaces of Al deposited on UHV-cleaved InP (100).[23] Improved understanding of this interface is desirable for both theoretical and technological reasons. First, simple metals such as Al on a prototypical III-V compound such as InP represent a useful test bed for the variety of current Schottky barrier models. Factors which impact such models include: the Fermi level pinning position in the band gap, the density of interface states or traps, the shape of the Schottky barrier and whether tunneling takes place through the barrier. If, as is frequently the case, the Schottky barrier exhibits non-ideal behavior, what is the correct procedure to extract the effective barrier height? Considerable work on Fermi level pinning at monolayer metal coverages is now available for metal-semiconductor interfaces.[1] Yet the relation between such results to electrically-measured barrier heights has only begun.[24-26] Of particular importance is whether Fermi level pinning in the band gap changes due to screening as the monolayer films increase to bulk metallic contacts.[27,28] Technologically, the Al/InP interface is particularly stable under heating and can shield the junction from ambient contamination. Contact stability is particularly desirable for high power InP devices such as microwave oscillators and injection

lasers. Our results show that a low but non-zero (0.21-0.26 eV) barrier is present at all temperatures at the UHV-cleaved InP/Al interface. Careful analysis taking into account both forward and reverse bias data over a wide range of temperatures reveals barrier characteristics which can not be analyzed as an ideal Schottky diode. The barrier is described accurately only by allowing for the presence of a thin interfacial layer of trapped charge. This charge resides in acceptor-like electron traps separated by only 0.1 eV from the conduction band edge. The traps are not restricted to the surface, but penetrate hundreds of Å into the depletion region. The traps are distinct from the donors invoked to explain certain InP barrier heights[6] according to the unified defect model.[5] While the measured electrical barrier agrees with Fermi level movements extracted from SXPS data[29,30] the actual mechanism by which the barrier is formed differs substantially from the interface models currently assumed. These results emphasize the importance of a full range of temperature-dependent forward and reverse bias measurements of Schottky barrier height and highlight the complexity of even these representative metal-semiconductor junctions.

In the last area of activity, we have developed a new technique for controlling the competitive reactions which take place at metal-semiconductor interfaces.[31] For metals on Si and SiO_2, the reactions which dominate will determine the success of specific semiconductor wafer processing steps for device fabrication. In addition, for semiconductor-metal interfaces in general, the dominant interdiffusion and reaction process will determine the resultant Schottky barrier formed. We focussed primarily on Ti reactions with Si and SiO_2, since the formation of titanium silicide is of considerable importance for low-resistivity applications such as MOS gate electrodes and VLSI circuit interconnects. We have discovered that 1) thin film reactions occur

at Ti/Si and Ti/SiO_2 interfaces on a short timescale (seconds at conventional processing temperatures) and not over the course of tens of minutes or hours, 2) these thin film (< 100 nm) reactions parallel closely thick film (multimicron) reactions, 3) SiO_2 dissociation and Ti silicide formation occur at the Ti/SiO_2 interface which will destroy the self-aligned gate device structure, and most importantly, 4) low temperature (400-500^{o}C), rapid thermal annealing (tens of seconds) provides a process window in time and temperature in which a desirable reaction ($TiSi_2$ formation at the Ti/Si interface) can be promoted while suppressing an undesirable reaction (SiO_2 dissociation and Ti-silicide formation at the Ti/SiO_2 interface). Thus, our work expands the control we now have in Si wafer scale processing technology for a key interfacial structure. From a broader, more fundamental viewpoint, such low temperature rapid thermal annealing may permit new control over competitive processes such as cation and anion outdiffusion and metal indiffusion at compound semiconductor/metal interfaces, the balance of which will determine the Schottky barrier formation.

Overall, we have applied combinations of interface techniques and have developed new analytical methods to characterize electronic and chemical structure at technologically relevant metal-semiconductor interfaces. By elucidating the relationships between chemical interactions on a microscopic scale and the macroscopic electronic properties, we aim to achieve a broader understanding of the fundamental physical processes which control Schottky barrier formation at ideal and non-ideal metal-semiconductor intefaces.

References

1. See for example, L.J. Brillson, Surf. Sci. Repts. 2, 123 (1982) and references therein.

2. L.J. Brillson, J. Phys. Chem. Solids 44, 703 (1983).

3. L.J. Brillson, in Handbook of Synchrotron Radiation, Ed. G.V. Marr (North-Holland, Amsterdam, 1985), Volume 2, in press.

4. H.H. Wieder, J. Vac. Sci. Technol. 15, 1498 (1978).

5. W.E. Spicer, I. Lindau, P. Skeath, C.Y. Su, and P. Chye, Phys. Rev. Lett. 44, 420 (1980).

6. R.H. Williams, J. Vac. Sci. Technol. 16, 1418 (1979).

7. L.J. Brillson, J. Vac. Sci. Technol. 15, 1378 (1978); 16, 1137 (1979).

8. J.L. Freeouf, Solid State Commun. 33, 1059 (1980).

9. J.M. Woodall and J.L. Freeouf, J. Vac. Sci. Technol. 19, 784 (1981).

10. R. Ludeke, T.-C. Chiang, and T. Miller, J. Vac. Sci. Technol. B1, 581 (1983).

11. J. Tersoff, Phys. Rev. Lett. 57, 465 (1984).

12. L.J. Brillson, Phys. Rev. Lett. 40, 260 (1978).

13. L.J. Brillson, G. Margaritondo, and N.G. Stoffel, Phys. Rev. Lett. 44, 667 (1980).

14. Y. Shapira, L.J. Brillson, A.D. Katnani, and G. Margaritondo, Phys. Rev. B30, 4586 (1984).

15. L.J. Brillson, H.W. Richter, M.L. Slade, B.A. Weinstein, and Y. Shapira, J. Vac. Sci. Technol. A3, 1011 (1985).

16. L.J. Brillson, Applications Surf. Sci. 22/23, 948 (1985).

17. L.J. Brillson, Surf. Sci., in press.

18. H. Richter, L.J. Brillson, R. Daniels, M. Kelly, and G. Margaritondo, J. Vac. Sci. Technol. B2, 591 (1984).

19. H. Richter and L.J. Brillson, Proceedings of the 17th International Conf. on Physics of Semiconductors, (Springer-Verlag, New York, 1985), p. 137.

20. H.W. Richter and L.J. Brillson, submitted to Physical Review.

21. T.E. Orlowski and H. Richter, Appl. Phys. Lett. 45, 241 (1984).

22. H. Richter, T.E. Orlowski, M. Kelly, and G. Margaritondo, J. Appl. Phys. 56, 2351 (1984).

23. J.H. Slowik, H.W. Richter, and L.J. Brillson, J. Appl. Phys., in press.

24. N. Newman, T. Kendelewicz, D. Thomson, S.H. Pan, S.J. Eglash, and W.E. Spicer, Solid State Electron. 28 307 (1985).

25. N. Newman, K.K. Chin, W.G. Petro, T. Kendelewicz, M.D. Williams, C.E. McCants, and W.E. Spicer, J. Vac. Sci. Technol. A3, 996 (1985).

26. N. Newman, T. Kendelewicz, L. Bowman, and W.E. Spicer, Appl. Phys. Lett. 46, 1176 (1985).

27. A. Zur, T.C. McGill, and D.L. Smith, J. Vac. Sci. Technol. A1, 608 (1985).

28. W.E. Spicer, S. Pan, D. Mo, N. Newman, P. Mahowald, T. Kendelewicz, and S. Eglash, J. Vac. Sci. Technol. B2, 476 (1984).

29. L.J. Brillson, C.F. Brucker, A.D. Katnani, N.G. Stoffel, R. Daniels, and G. Margaritondo, J. Vac. Sci. Technol. 21, 564 (1982).

30. T. Kendelewicz, N. Newman, R.S. List, I. Lindau, and W.E. Spicer, J. Vac. Sci. Technol. B3, 1206 (1985).

31. L.J. Brillson, M.L. Slade, H.W. Richter, H. Vander Plas, and R.T. Fulks, Appl. Phys. Lett., in press.

IV. Papers Published and Submitted Under Navy Contract #N00014-80-C-0778 During Period October 1, 1984, to September 30, 1985.

80-C-0778 - 21. Ultrafast Laser-Induced Oxidation of Silicon: A New Approach Towards High Quality, Low Temperature, Patterned SiO_2 Formation, T.E. Orlowski and H. Richter, Applied Physics Letters 45, 241 (1984).

80-C-0778 - 22. Ultrafast UV-Laser-Induced Oxidation of Silicon: Control and Characterization of the Si-SiO_2 Interface, H. Richter, T.E. Orlowski, M. Kelly, and G. Margaritondo, Journal of Applied Physics 56, 2351 (1984).

80-C-0778 - 23. Interdiffusion and Chemical Trapping at InP (110) Interfaces with Au, Al, Ni, Cu and Ti, Y. Shapira, L.J. Brillson, A.D. Katnani and G. Margaritondo, Physical Review B30, 4586 (1984).

80-C-0778 - 24. Control and Characterization of Metal-InP and GaAs Interfaces Formed by Laser-Enhanced Reactions, H. Richter, L.J. Brillson, R. Daniels, M. Kelly, and G. Margaritondo, Journal of Vacuum Science and Technology B2, 591 (1984).

80-C-0778 - 25. Laser-Induced Chemical Reactions at the Al/III-V Semiconductor Interface, H. Richter and L.J. Brillson, Proceedings of the 17th International Conference on the Physics of Semiconductors (Springer-Verlag, New York, 1985), p. 137.

80-C-0778 - 26. Advances in Characterizing and Controlling Metal-Semiconductor Interfaces, Applications of Surface Science 22/23, 948 (1985).

80-C-0778 - 27. Cathodoluminescence Spectroscopy Studies of Laser-Annealed Metal-Semiconductor Interfaces, Journal of Vacuum Science and Technology A3, 1011 (1985).

80-C-0778 - 28. Laser-Induced Chemical Reaction at the Al/III-V Compound Semiconductor Interface, H.W. Richter and L.J. Brillson, submitted to Physical Review B.

80-C-0778 - 29. UPS, XPS and AES Studies of CaF_2-CdSe, C.F. Brucker, Y. Shapira and L.J. Brillson, submitted to Thin Solid Films.

80-C-0778 - 30. Acceptor-Like Electron Traps and Thermally-Reversible Barrier Heights for Al on UHV-Cleaved (110) InP, John H. Slowik, H.W. Richter, and L.J. Brillson, Journal of Applied Physics, in press.

80-C-0778 - 31. Promoting and Characterizing New Chemical Structure at Metal-Semiconductor Interfaces, L.J. Brillson, Surface Science, in press.

80-C-0778 - 32. Control of Titanium-Silicon and Silicon Dioxide Reactions by Low Temperature Rapid Thermal Annealing, L.J. Brillson, M.L. Slade, H.W. Richter, H. Vander Plas, and R.T. Fulks, Applied Physics Letters, in press.

INTERDIFFUSION AND CHEMICAL TRAPPING AT InP (110) INTERFACES WITH Au, Al, Ni, Cu, AND Ti

Yoram Shapira* and L.J. Brillson

Xerox Webster Research Center

Webster, NY 14580

and

A.D. Katnani and G. Margaritondo

Physics Dept., University of Wisconsin-Madison

Madison, WI 53706

We have studied UHV-cleaved (110) surfaces of InP covered with a large variety of metal layers and interlayers, using Auger electron spectroscopy (AES) in conjuction with Ar^+ ion sputtering. All measurements were made under identical experimental conditions, other than the thickness or type of the metal films, in order to minimize ion-beam-induced distortion of the data. We find that In and especially P are segregated at unreactive metal surfaces such as Au or Cu. Very thin interlayers of "reactive" metals between Au and InP completely reverse the outdiffusion process of the phosphorus, which is accumulated at the interface due to chemical trapping by the reactive metal interlayers. Indium outdiffusion is found to be unaffected by these interlayers while Au indiffusion depends sensitively on the type of metal interlayer. The results are correlated with soft X-ray photoemission spectroscopy measurements to reveal the diffusant spatial distribution on a microscopic scale while illustrating the relative limitations of the SXPS technique. The contrasting effects of the unreactive versus reactive metal interfaces are correlated with Schottky barrier heights and with energy level calculations of associated surface defects.

1. INTRODUCTION

Recent years have seen a considerable interest in InP both as a prototypical III-V compound suitable for basic studies and a potential candidate for a variety of electronic and opto-electronic devices. The feasibility of various useful devices, such as MISFET's[1-4] for high speed applications, Schottky diodes[5], solar cells[6] and photoelectrochemical cells[7], based on InP has been extensively demonstrated. Understanding and knowledge about the electronic and chemical properties of InP surfaces and metal interfaces are of major technological importance for improving the performance of such devices. Experimental works in this direction have used a wide variety of techniques for electrical[8,9] electronic[10,11] compositional[12,13] and structural[14] analyses of InP surfaces[15,16] and interfaces[17]. The experimental techniques comprised I-V[18] and C-V[19] measurements, ultra-violet, soft X-ray and X-ray photoelectron spectroscopies[12-14], (UPS, SXPS and XPS), low energy electron diffraction[20] (LEED), Auger electron spectroscopy (AES) and sputter profiling[21-23] and surface photovoltage spectroscopy[24].

The data reveal that the metal-InP interface is not abrupt[9,25,26]. Rather, a number of phenomena occur upon metal deposition including interdiffusion[13], reactions which create new interfacial compounds[26], defects formation[9,25] and removal or addition of gap surface states[11]. These phenomena depends very sensitively on the reactivity of the deposited metal and can be dramatically altered by extremely thin interlayers of different metals[10]. In turn, these interfacial processes and properties seem to be crucial in determining the Schottky barrier height observed at such inter-

faces. An extremely important task remains that is to find a correlation between the interfacial properties of InP and its electrical characteristics, and possibly to extend it to compound semiconductors in general.

In this paper we present results of an extensive study of InP (110) surfaces covered with thin films and interlayers of various metals with different thicknesses. We have endeavoured to find a general pattern of anion and cation outdiffusion and metal atom indiffusion as a function of metal type and thickness. We have kept all other experimental parameters unchanged in order to cancel out any inherent artifacts and causes for misinterpretation due to the sputtering process. Thus, we were able to probe the InP-metal interfaces post factum and compare the results with UPS and SXPS data[12-14,25,26], which are taken at very low metal coverages during the buildup of the junction. The experimental techniques we have used are described in Sec. 2. Sec. 3 presents the experimental results, which describe well-characterized patterns of redistribution of the semiconductor and metal constituents at the interfaces as well as the metal surface due to interdiffusion and reaction, depending on the reactivity of the metal layer or interlayer. These results are discussed in Sec. 4 and compared with other results and theoretical predictions.

2. EXPERIMENTAL

The InP crystals studied were supplied in the form of 5x5x15 mm^3 bars with $p = 4.3 \times 10^{15}$ cm^{-3} (Zn) by MCP Electronic materials (Alperton, Middlesex, England). These were cleaved in a UHV system with a base pressure

$\leq 5\times10^{-11}$ Torr to expose visually smooth (110) surfaces. These surfaces were covered with metal layers by deposition from shielded W filament sources at pressures in the low 10^{-9} Torr range. The deposition thickness were monitored by a quartz crystal oscillator. The surfaces were then analyzed by AES using a double pass CMA and a grazing incidence electron gun. All spectra were acquired with a 2 keV electron beam energy and 2 eV CMA modulation voltage. Electron current was restricted to ≤ 2 μA focused on a spot 0.1 mm in diameter in order to minimize electron beam effects. For sputter profiling, we used a grazing incidence Ar^+ gun operated at 2×10^{-4} Torr Ar pressure (system Ar background pressure $\leq 3\times10^{-8}$ Torr), 25 mA emission current, and 1 keV beam energy which was typically rastered over a 4x4 mm^2 area on the sample. The electron beam was directed to the center of the rastered area. Each spectrum was obtained by signal averaging for 100 sec during which the sputtering rate (for Au) was estimated to be about 3 monolayers (ML). Mild annealing (200°C) was carried out using a focussed Quartz halogen lamp external to the chamber. We also performed angle-integrated SXPS experiments using synchrotron radiation at the University of Wisconsin Synchrotron Radiation Center and a double pass CMA in a similar UHV chamber.

3. RESULTS

Fig. 1 shows an Auger electron spectrum of a typical UHV-cleaved (110) surface of InP. There are no traces of contaminants on the surface. However, the P:In peak-to-peak (p-p) height ratio is much higher than the one shown in Fig. 2 which was obtained from the same crystal after prolonged Ar^+ bombardment. Fig. 3 is a depth profile of the In and P atomic concentrations as a function of sputtering time. There is a sharp change

at the surface, followed by a slower decrease (increase) of the P(In) peak to peak height. The latter is evidence of the phosphorus preferential sputtering[22] but the topmost layer behaviour is a strong indication of a P-rich surface produced by the cleavage. This is further supported by surface photovoltage measurements[11] and by comparison with InP (100) surfaces[24]. After Ar^+ sputtering of the cleaved surface, a constant In/P peak-to-peak height ratio is achieved. In Fig. 3 only, the relative In/P Auger sensitivity was taken to match In and P intensities after prolonged sputtering. Taking the subsurface as representative of the clean, stoichiometric InP, we have adjusted the relative In/P Auger sensitivity accordingly and used the new sensitivity ratio to normalize all subsequent depth profiles.

Fig. 4 shows a typical Auger electron spectrum obtained from a 30 A thick Au film deposited on a UHV-cleaved (110) surface. Besides the Au peak, In and P are also present. No other peaks can be detected. These AES Au, P and. In p-p heights were recorded as a function of sputtering time, during 1 keV Ar^+ ion-bombardment of a 4x4 mm^2 area. The normalized depth profiles obtained from five different thicknesses of Au films are shown in Fig. 5. Sputtering and AES parameters are identical for all the interfaces shown. Several points should be noted: 1. As the Au film thickness is increased, a redistribution pattern emerges, which indicates a strong P and In segregation at the free metal surface, small In and no P concentration within the film (in accordance with their solid solubilities[27]) and a non-abrupt interface. 2. The phosphorus surface segregation is up to a factor two higher than the In. 3. The bulk In peak precedes the bulk P peak when the interface is approached. This is due to the fact that the In MNN electrons have a larger escape depth than the P LMM electrons. However, this effect is superimposed on the In excess (or P deficiency) induced at the interface by the Au deposition. Results pre-

sented later point to this interface redistribution of P as the origin of the segregated P at the metal surface. 4. The segregated layer is not apparent at Au thicknesses below 30 Å which may indicate that 10 or 20 Å are below a typical threshold thickness for segregation or more probably that at such thin layers, the transition from the segregated layer to the substrate semiconductor is masked by the inherent escape depth of the Auger electrons and the width of the disordered layer caused by the sputtering. We estimate that 10-20 Å represent a characteristic depth resolution of the results. 5. The Au signal is detectable after the In and P signal seem to have reached their bulk values. This indicates gold in-diffusion simultaneously with In and P outdiffusion, a process which is confirmed by results presented later. 6. The segregated layer shows an almost constant P concentration, while the In concentration seems to decrease, with increasing Au thickness. We estimate the segregated P layer to be about 10 Å thick. These results suggest a "floating" process of the excess surface P on top of the Au film being deposited.

In order to gain insight into the microscopic details of the latter process, SXPS measurements were carried out under similar experimental conditions. Fig. 6 shows a photoemission spectrum for the In 4d levels for increasing Au coverage of a UHV-cleaved InP (110) surface. We have used a photon energy of 70 eV in order to obtain maximum surface sensitivity, analyzing photoelectrons with 50 eV kinetic energy which have a minimal escape depth. Indeed the spectra show that starting at Au coverages above a monolayer the In 4d core level exhibits an initial 0.9 eV shift to lower binding energies while retaining its spin-orbit splitting. This shift is

in good agreement with other Au/InP results.[28] Further Au deposition causes an additional shift until stabilization of the level at 1.05 eV below the cleaved binding energy state. Such shifts are due to both band bending and chemical bonding change. Specifically, the results indicate that Au deposition causes dissociation of the In-P bonds, while covering the surface with a continuous layer of Au intermixed with metallic In and P atoms. This is confirmed by the absence of an unshifted In 4d peak. Thus it seems that some of the dissociated In and P, including the initial excess P, segregate to the top of the deposited layer. The rest remains at the interface, creating the concentration gradient from the InP substrate to the level soluble in the Au film.

These processes may be supported by Fig. 7 which shows the surface concentrations of In and P (in percent of their cleaved InP surface concentration) as a function of increasing Au coverage. The concentrations are obtained by integration of the In 4d and P 2p peak areas, taken by 70 eV and 175 eV photons, respectively. The initial drop in concentration corresponds to a uniform Au-InP interface without substantial interdiffusion, as compared with the AES findings. However, the SXPS and AES results can be reconciled by the low sputtering rate of InP, which causes a diffusional broadening of ~10 A. At Au film thicknesses above 20 Å the In and P maintain a relatively constant concentrations, the P more so and at a higher level, than the In. The Fig. 7 and 5 data are in good agreement if the "floating" P is taken into account. The excess P in the SXPS spectra (Fig. 7) should not be interpreted as a uniform distribution extending into the Au overlayer.

Additional information regarding the microscopic distribution in the segregated layer can be obtained by SXPS measurements at different photon energies, corresponding to different photoelectron escape depths. Table 1 summarizes these results, which are taken on the cleaved surface, on 20 A thick, and on 50 Å thick Au films as small as on the latter film after mild annealing. The ratios represent the peak areas taken at 130 eV and 100 eV for the Au 4f peak, at 175 eV, 150 eV and 140 eV for the P 2p peak at 70 eV and 40 eV photon energies for the In 4d peaks. Those energies represent estimated probing depths of 2-4 Å and 6-8 Å respectively and 10-15 Å for the 140 eV photons used to probe the P 2p level.[29] All areas are normalized to the most surface sensitive peak area, which is taken as unity. These areas can be compared with the data shown in Fig. 5. Thus, the Au peak area ratio is 1:1/2 at 20 Å coverage while at 50 Å coverage the Au signal below the surface exhibits a relative increase and has the same area as the "surface" peak. This is in accordance with the segregation data for Au given by Figs. 5b and 5d, i.e., the segregated In and P decrease the surface Au concentration. The In ratio shows that at depths of 6-8 Å from the free Au surface there is a higher In concentration than at the surface itself, referred to the cleaved surface ratio. The same trend is seen by the P data, but probing deeper (10-15 Å) by the 130 eV photons shows a decrease relative to the cleaved surface ratio. This hints at the possibility that the 10 Å thick segregated layer of In and P on the Au film actually has a spatial distribution which peaks at around 5 A deep, decreases towards the free Au surface and falls off towards the film "bulk". The microsopic details at the surface cannot be yielded by AES data due to the fixed escape depth of the Auger electrons. This particular surface behavior is not en-

tirely clear at the present time.

Subsequent mild annealing of the 50 Å thick Au film causes an increase in the Au 4f peak area (not shown), an increase of the In 4d peak and a decrease of the P-2p peak areas. The variable photon energy results in Table 1 suggest that the annealing causes a broadening of the segregated P layer with a preferential loss of surface P while the surface Au concentration increases. Simultaneously, somewhat more In diffuses out to the free surface during the annealing process.

A similar segregation and interdiffusion pattern, as encountered in the gold films, is repeated with other unreactive metals[30]. Fig. 8 is an example of a sputter depth profile taken from a 60 Å thick Cu film deposited on a UHV cleaved (110) surface. Cu is relatively unreactive with InP[8]. Some differences are noted compared with Au: The In segregation is less evident, the P concentration in the Cu film is higher, and the Cu indiffusion is deeper. Regarding the first difference, it is not clear whether the particular pattern of surface distribution reflects the conclusion obtained from the SXPS segregation data. Also, it is not clear whether the anion accumulation at the interface is not an artifact of the sputter profile data acquisition. This effect is not repeated in thinner Cu films and therefore could reflect an enhanced knock-in effect of the phosphorus in the copper film. As in the Au films, the In and P segregation pattern does not become evident for Cu thicknesses below 20-30 Å.

Dramatic changes in the In and P outdiffusion and segregation patterns

at the Au-InP interface are caused by very thin interlayers of reactive metals[10]. Fig. 9 is a sputter depth profile taken from a 70 Å thick Au film deposited on a 2 Å thick Al interlayer on a UHV-cleaved InP (110) surface. The $\geq$ 1 ML Al interlayer is the only difference in experimental condition between Fig. 9 and Fig. 5d. Yet the P segregation is totally eliminated. Similar experiments with Al thicknesses of 5 Å, 10 Å and 20 Å yield the same result. The In outdiffusion does not seem to be affected by the interlayer. Unfortunately, the Au and the Al Auger peaks fall at approximately the same energy and could not be resolved, so the exact interlayer distribution cannot be seen. However, judging from results of other reactive interlayers shown later, it seems that the Au indiffusion is also unaffected by the interlayer presence.

A similar experiment was carried out using SXPS in order to probe the initial steps of the interface formation. Fig. 10 shows the In 4d photoemission spectra taken by 70 eV photons from a UHV cleaved surface, 2 Å Al coverage and subsequent Au coverage with increasing thickness. Deposition of 2 A of Al causes a 0.3 eV shift of the bulk In 4d level superimposed on a 0.7 eV shifted In-4d level of the dissociated In. Subsequent Au deposition leaves the dissociated peak only. The surface P was monitored by observing the P 2p photomission spectrum. Such SXPS measurements are given in fig. 11 which was taken, using 175 eV photons, from a UHV-cleaved surface before and after 2Å Al deposition. The latter case shows considerable broadening of the peak indicative of surface reaction with Al. Subsequent Au deposition causes the P 2p photoemission to fall below the detectable level.

In order to focus on the reactive metal interfacial reaction, SXPS measurements were performed on InP (110) surfaces covered with increasing Al film thicknesses. Fig. 12 shows the In 4d photoemission spectra taken by 70 eV electrons from a UHV-cleaved (110) surface covered with an increasing Al film thickness. Even at the very early stages of Al deposition one can observe the initial 0.3 eV shift, apparently due to band bending, superimposed on the shifted In 4d peak indicating dissociated In. These results suggest that the metallic, dissociated In "floats" on top of the reacted Al-P layer, segregating to its surface, in agreement with our AES results. Furthermore, the observation of the In core level associated with InP even after 8 A Al deposition strongly suggest that the reacted layer may be discontinuous.

Further information about the reacted interfacial layer may be obtained from fig. 13, which shows the Al 2p photemission spectra taken by 130 eV photons from a UHV-cleaved InP (110) surface covered with increasing thicknesses of Al. At low coverages the Al core level is shifted towards higher binding energies, strongly pointing to Al-P reaction which forms the thermodynamically favorable AlP compound. At coverages below a monolayer, cluster formation may also shift the Al 2p peak to higher binding energies.[31] Subsequent depositions show the evolution of spectra in which the metallic Al core level emerges. It should be noted that a mild heat treatment increases the reacted Al "shoulder" (topmost spectrum) indicating a thicker Al-P layer induced by annealing. This is consistent with recent LEED and AES work of Kahn et al.[32]

The joint AES and SXPS results suggest a reaction of the Al interlayer with the surface excess P which forms an Al-P compound. This "chemical trapping" of P creates a layer which may even be discontinuous but proves to be an excellent barrier for additional P outdiffusion.

Indium is able to diffuse through the reacted layer to segregate at the free Au surface. The effect on Au indiffusion is difficult to perceive at such low Al coverages.

A more conclusive support for this process can be given by reactive metals, other than Al, whose AES peaks can be distinguished from Au. Fig. 14 is a sputter depth profile of a 70 Å Au film on a 10 Å Ti interlayer deposited on a UHV-cleaved InP surface. Again a total elimination of P outdiffusion and segregation is noted. The In seems to be unaffected by the interlayer. As the interface is approached, the Ti LMM peak rises while the P peak, which has a smaller electron escape depth, lags somewhat behind. The latter seems to stabilize at a certain level, indicative of a compound formation, in the Ti film. The Au peak also shows a saturated level in the Ti film indicating a certain solubility in the reacted layer. Further into the interface, the In and P rise to their bulk levels, while Au shows definite signs of indiffusion as in the Al interlayer case. A similar result was obtained with a 5 Å thick Ti interlayer, the difference being a small signal of segregated P at the free Au surface in this case.

Fig. 15 shows an Auger sputter profile of another 70 Å thick Au layer on a UHV-cleaved InP surface with a 20 Å thick Ni interlayer. Again the reactive interlayer proves to be an effective barrier for P outdiffusion, chemically trapping it at the interface, while the In is unperturbed from following the same outdiffusion trend. However, the Ni interlayer seems to be also a very strong diffusion barrier for Au, unlike the Ti case. The deeper Ni concentration "tail" may indicate stronger knock-in effects in

this case.

In view of the results yielded by reactive metal interlayers, it is interesting to note that a 20 A thick Cu interlayer between the Au film and the InP (110) surface gives the Auger sputter profile shown in Fig. 16. The interdiffusion and segregation patterns seem to be identical to the pure Au case. A comparison of Figs. 12 and 13 leads to a realization of the importance of interlayer reactivity in determining the interface and free surface chemical composition.

The type of metal interlayer is not the only important factor in determining interdiffusion. In this study we have focused on UHV-cleaved surfaces. If these surfaces are ion-bombarded prior to metal deposition, the results are markedly different. Fig. 17 is a sputter depth profile of a 70 Å thick Au film on a 10 Å thick Al interlayer deposited on an Ar^+-bombarded (110) surface. The In and P are distributed throughout the Au film probably due to a mixture of outdiffusion and film discontinuity. No segregation pattern is evident and the interface seems to be very extended. This enhanced interdiffusion due to ion sputtering of the InP substrate in in agreement with results obtained for Al-Si interfaces[33].

4. DISCUSSION

The results obtained by Auger depth profiling highlight the power of this technique in obtaining important information about atomic spatial distribution at metal-semiconductor interfaces after the junction is prepared.

The inherent interpretational difficulties of AES are avoided by performing a series of many experiments under identical conditions. Complementary to SXPS measurements, Auger sputter profiling reveals in-depth information about the microscopic spatial distribution of the atomic components starting at the metal surface and through the film to the metal-semiconductor interface and the InP bulk.

The results indicate that UHV-cleaved InP (110) surfaces are P-rich. Such effects have also been observed on cleaved GaAs surfaces[34]. The P-rich surfaces are affected in a dramatically different way by unreactive and reactive metals. The results show that Au as a representative of the former group seems to sink into the topmost layers, dissociating the lattice without reacting with it. The dissociated In and P tend to segregate to the top of the Au film and maintain that position apparently by microdiffusion simultaneously with the deposition process. Increasing thickness of the Au films shows no detectable P content, but various low concentrations of In diffused throughout the Au film itself. This is in accordance with the published solid solubilities of P and In in Au.[27] The variance in In concentration could be due to small differences in substrate temperature during deposition. However, the pattern of the In and P surface segregation appears to gradually decrease as a function of the metal film thickness, especially for thicknesses above 30 Å. Below this value the segregation pattern may be screened by the inherent Auger electrons escape depth or it may be insignificant due to the segregated layer width itself. For segregated layers thinner than the overlayer, the effect may cause misinterpretation of SXPS data, especially those taken at higher coverages and at a single wavelength.

A survey of the results for the various thicknesses of Au films leads us to the conclusion that the Au-InP interface is 10-20 A thick[26] and that for Au films above that thickness there is a formation a segregated layer of dissociated In and P about 10 Å thick at the free surface. This segregated layer has a peculiar spatial distribution-namely that the dissociated elements may reach their peak concentration slightly (~ 5 Å) below the surface proper.

A very different pattern of outdiffusion is observed in the case of reactive metal deposition. These metals, exemplified by our results with Al, Ni and Ti, tend to remain on the cleaved surface, and to react strongly with the phosphorus. This reacted layer creates a strong diffusion barrier for P which is chemically trapped at the interface. However, the outdiffusion of atomic In is not perturbed by the reacted layer. The reacted layer itself can be made very thin (several Å only) and may not even be continuous but is apparently a very effective chemical trap even if used as an extremely thin interlayer. If the reactive metal interlayer is discontinuous it is probably on a microscopic scale. This is emphasized by the results on Ar^+-bombarded surface, where the effects of the interlayer as a barrier is eliminated (see Fig. 17).

Thus the results on reactive and unreactive metal-InP interfaces demonstrate the importance of the chemical and physical interactions in determining the spatial distribution of the constituents over the formed junction. The unreactive metals appear to "sweep" the excess P to the free metal surface and thus leave a P-depleted interface. This type of inter-

face has been shown to have higher Schottky barrier heights[9] and surface state concentrations at the reported Fermi level pinning positions for such barriers[11,35]. The reactive metal interfaces, on the other hand, trap the anion by chemical reaction while allowing the In to diffuse out. Thus an In-depleted interface is created, which can be associated with the lower Schottky barrier heights reported for such junctions[10,13].

Our results cannot identify a particular set of defects or other electrically-active sites as directly responsible for the reported Fermi level positions. Calculations of energy levels for various surface defects have to be reported by several research groups in recent years[36,37]. The calculations indicate a P vacancy (V_P) level in[36] or just below[37] the conduction band, an In vacancy (V_{In}) around midgap and antisite defects (In_P and P_{In}) deep in the InP band gap[36]. Our results on unreactive metals could indicate V_P formation at the interface, but such a level cannot account for the reported higher Schottky barrier heights at unreactive metal interfaces. Similarly the reactive metal interface results which can be associated with In depletion (V_{In}) are not consistent with the lower Schottky barriers reported on such interfaces. The only level which appears to be consistent with AES, SXPS and electrical results could be the In_P level, where In occupies P sites which are vacated by anion segregation to the free metal surface. One should however bear in mind that these calculations are based on an assumed free, relaxed surface which may be very far from the disrupted, interdiffused interface, even in the nonreactive metals case. For want of more adequate theoretical treatment, we therefore limit our conclusions to the role of the metal reactivity in determining

the electrical parameters of the junction. This role seems to be dominant even at extremely low coverages on the UHV-cleaved surfaces. Obviously, one cannot rule out the possibility of Schottky barrier height determination by interfacial defects which can include antisite vacancy and interstitial defects or combinations thereof.

Acknowledgements

We wish to thank Dr. C.F. Brucker for designing the computer program used for acquiring depth profiles and for many productive discussions. Thanks also to Dr. H. Richter for valuable refinements to the data analysis routines. We gratefully acknowledge J. Iseler (Lincoln Labs) for supplying the InP crystals and Jim Zesch (Xerox Palo Alto Research Center) for orienting and cutting them. This work is supported in part by Office of Naval Research Contract N00014-80-C-0778 (G.B. Wright). One of us (Y.S.) is grateful to the Belfer Center for Energy Research and the Israel Ministry of Energy for their support.

* On sabbatical leave from the Faculty of Engineering, Tel-Aviv University, Ramat Aviv 69978, Israel.

REFERENCES

1. L. Messick, D.L. Lile and A.R. Clawson, Appl. Phys. Lett., 32, (1975), 494.

2. K. Kamimura and Y. Sakai, Thin Solid Films, 56, 215 (1979).

3. L.G. Meiners, D.L. Lile and D.A. Collins, J. Vac. Sci. Technol, 16, (1979), 1458.

4. D.L. Lile and M.J. Taylor, J. Appl. Phys. 54, 260 (1983).

5. K. Hattori and Y. Izumi, J. Appl. Phys. 52, 5699 (1981).

6. P. Sheldon, R.K. Ahrenkiel, R.E. Hayes and P.E. Russel, Appl. Phys. Lett. 41, 727 (1982).

7. A. Heller and R.G. Vadimsky, Phys. Rev. Lett., 46, 1153 (1981).

8. R.H. Williams, V. Montgomery and R.R. Varma, J. Phys. C: Solid St. Phys. 11, L735 (1978).

9. R.H. Williams, R.R. Varma and V. Montgomery, J. Vac. Sci., Technol. 16, 1418 (1979).

10. L.J. Brillson, C.F. Brucker, A.D. Katnani, N.G. Stoffel and G. Margaritondo, J. Vac. Sci. Technol. 19, 661 (1981).

11. Y. Shapira, L.J. Brillson and A. Heller, J. Vac. Sci. Technol., A1, 766 (1983).

12. P.W. Chye, I. Lindau, P. Pianetta, C.M. Garner, C.Y. Su and W.E. Spicer, Phys. Rev. B18, 5545 (1978).

13. L.J. Brillson, C.F. Brucker, A.D. Katnani, N.G. Stoffel and G. Margaritondo, Appl. Phys. Lett. 38, 784 (1981).

14. A. McKinley, A.W. Parke and R.H. Williams, J. Phys. C: Solid St. Phys. 13, 6723 (1980).

15. D.L. Kirk and C. Jones, J. Phys. D: Appl. Phys. 12, 651 (1979).

16. S. Singh, R.S. Williams, L.G. Van Uitert, A. Schlierr, J. Camlibel and W.A. Bonner, J. Electrochem. Soc. 447 (1982).

17. L.J. Brillson, Surf. Sci. Repts. 2, 123 (1982).

18. E. Hokelek and G.Y. Robinson, Solid St. Electronics 24, 99 (1981).

19. B.L. Smith, J. Phys. D: Appl. Phys. 6, 1358 (1973).

20. R.H. Williams and J.T. McGovern, Surf. Sci. 51, 41 (1975).

21. R.S. Williams, R.J. Nelson and A.R. Schlierr, Appl. Phys. Lett. 36, 827 (1980).

22. D.K. Skinner, J.G. Swanson and C.V. Haynes, Surf. and Interf. Analysis, 5, 38 (1983).

23. Y. Shapira and L.J. Brillson, to appear in J. Vac. Sci. Technol. B1 618 (1983).

24. L.J. Brillson, Y. Shapira and A. Heller, Appl. Phys. Lett. 43, 174 (1983).

25. W.E. Spicer, P.W. Chye, P.R. Skeath, C.Y. Su and I. Lindau, J. Vac. Sci. Technol. 16, 1422 (1979).

26. L.J. Brillson, C.F. Brucker, N.G. Stoffel, A.D. Katnani and G. Margaritondo, Phys. Rev. Lett. 46, 838 (1981).

27. M. Hansen and K. Anderko, Constitution of Binary Alloys (McGraw Hill, New York 1958).

28. I.A. Babalola, W.G. Petro, T. Kendelewicz, I. Lindau and W.E. Spicer, J. Vac. Sci. Technol. A1, 762 (1983).

29. M.P. Seah and W.A. Dench, Surf. Interf. Anal. 1, 2 (1979).

30. L.J. Brillson, Phys. Rev. Lett. 40, 260 (1978).

31. T-X. Zhao, R.R. Daniels, A.D. Katnani, G. Margaritondo, and A. Zunger, J. Vac. Sci. Technol. B1, 610 (1983).

32. A. Kahn, C.R. Bonapace, C.B. Duke, and A. Paton, J. Vac. Sci. Technol. B1, 613 (1983).

33. L.J. Brillson, M.L. Slade, A. Katnani, M. Kelly and G. Margaritondo 44, 110 (1984).

34. W. Mönch and H. Gant, Surf. Sci. (in press).

35. H. Tempkin, B.V. Duff, W.A. Bonner and V.G. Keramidas, J. Appl. Phys. 53, 7529 (1982).

36. J.D. Dow and R.E. Allen, J. Vac. Sci. Technol, 20, 659 (1982).

37. M.S. Daw and D.L. Smith, Appl. Phys. Lett. 36, 690 (1979) and Phys. Rev. B20, 5150 (1979).

FIGURE CAPTIONS

Fig. 1 AES features of a UHV-cleaved InP (110) surface taken with a 2 keV, 2 μA electron beam focused to a 0.1 mm diameter spot and 2 eV CMA modulation.

Fig. 2 AES features taken under same experimental conditions and from same sample as in Fig. 1 after 40 min. of Ar^+ ion bombardment after a constant In:P p-p ratio had been achieved).

Fig. 3 Normalized AES intensities of P (solid curve) and In (dashed curve) as a function of sputtering time taken from an initially UHV-cleaved InP (110) surface.

Fig. 4 AES features taken from 30 Å thick Au film deposited on a UHV-cleaved InP (110) surface. AES parameters same as in Fig. 1.

Fig. 5 AES Au, In and P depth profiles for different Au overlayer thicknesses on a UHV-cleaved InP (110) surface. Sputtering conditions were identical throughout the profiles for all five interfaces. Ion beam raster dimensions were 4 by 4 mm^2.

Fig. 6 Soft X-ray photoemission spectra of the In 4d core level as a function of increasing Au deposition on a UHV-cleaved InP (110) surface using $h\nu$ = 70 eV.

Fig. 7 Surface concentration of In (open circles) and P (solid circles) (in percent of cleaved surface In 4d and P 2p peak areas) as a function of increasing Au coverage using $h\nu$ = 70 eV and 175 eV, respectively.

Fig. 8 AES depth profiles of Cu (triangles), In(solid circles) and P(open circles) from 60 Å Cu film on a UHV-cleaved InP (110) surface.

Fig. 9 AES depth profiles of Au, In and P from a 70 Å Au film on 2Å Al interlayer on UHV-cleaved InP (110) surface.

Fig. 10 Soft X-ray photoemission spectra of the In 4d core level as a function of increasing Au deposition on a 2 Å Al interlayer on a UHV-cleaved InP (110) surface using $h\nu$ = 70 eV.

Fig. 11 Soft X-ray photoemission spectra of the P 2p core level on a UHV-cleaved InP (110) surface before and after 2 Å deposition using $h\nu$ =175eV.

Fig. 12 Soft X-ray photoemission spectra of the In 4d core level as a function of increasing Al deposition on a UHV-cleaved InP (110) surface using $h\nu$ =70eV.

Fig. 13 Soft X-ray photoemission spectra of the Al 2p core level as a function of increasing Al deposition on a UHV-cleaved InP (110) surface using $h\nu$ =175eV.

Fig. 14 AES depth profiles of Au, Ti In and P from a 70 Å Au film on a 10 A Ti interlayer on a UHV-cleaved InP (110) surface.

Fig. 15 AES depth profiles of Au, Ni, In and P from a 70 Å Au film on a 20 A Ni interlayer on a UHV-cleaved (110) surface.

Fig. 16 AES depth profiles of Au (triangles), Cu(squares) In(solid circles) and P(open circles) from a 70 Å Au film on a 20 Å Cu interlayer on a UHV-cleaved InP (110) surface.

Fig. 17 AES depth profiles of Au, In and P from a 70 Å Au film on a 10 Å Al interlayer on an ion-bombarded InP (110) surface.

Table 1 SXPS peak intensity ratios for Au 4f, In 4d, P 2p core levels (columns 2-4) for different surface coverage (column 1) taken at their respective photon energies (in parentheses in eV). Corresponding photoelectron escape depths appear in row 5.

Table 1

Surface coverage	$I^{4f}_{Au}(130)/I^{4f}_{Au}(100)$	$I^{2p}_{P}(175)/I^{2p}_{P}(150)/I^{2p}_{P}(140)$	$I^{4p}_{In}(70)/I^{4p}_{In}(40)$
cleaved InP(110)	-	1:12:12	1:1
cleaved + 20Å Au	1:1/2	1:13:8	1:2
cleaved + 50Å Au	1:1	1:15:10	1:2.2
cleaved + 50Å Au + annealing	1:2	1:18:30	1:2
escape depth (Å)	2-4/6-8	2-4/6-8/10-15	2-4/6-8

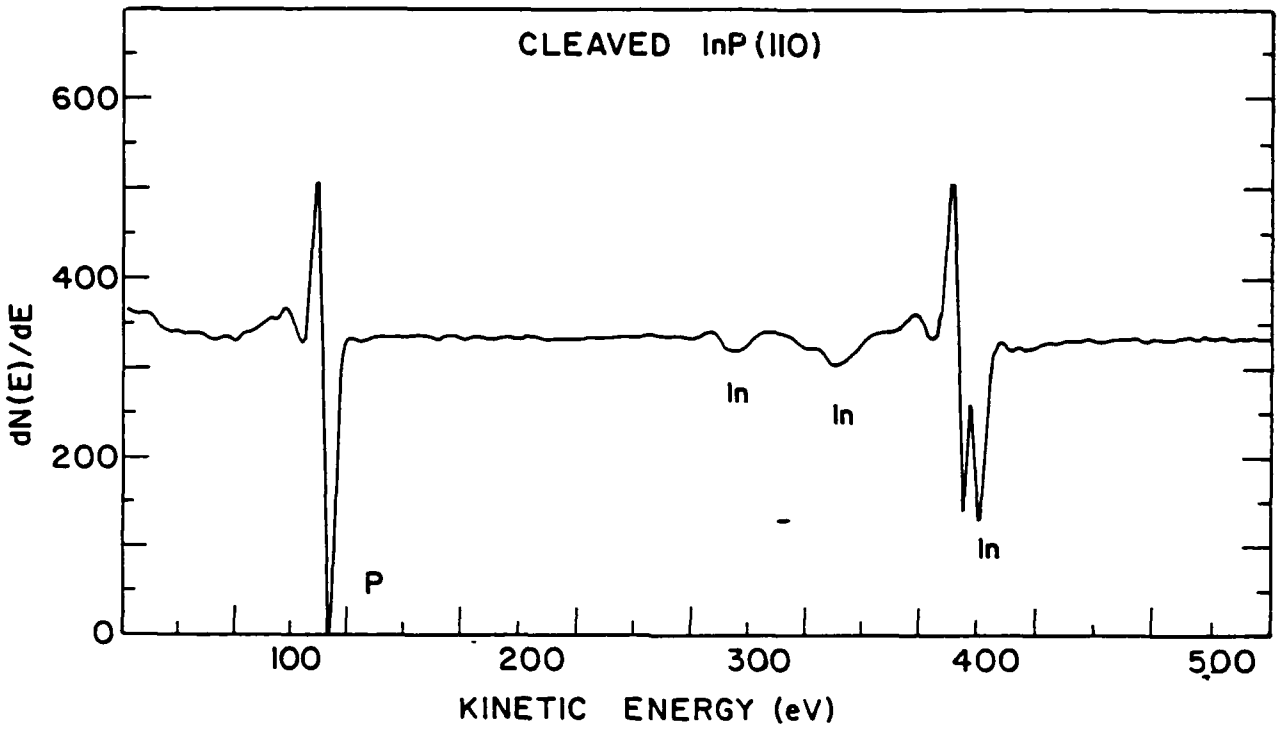
CLEAVED InP(110)
600
400
200
0
dN(E)/dE
In
In
In
P
100
200
300
400
500
KINETIC ENERGY (eV)

Fig. 1

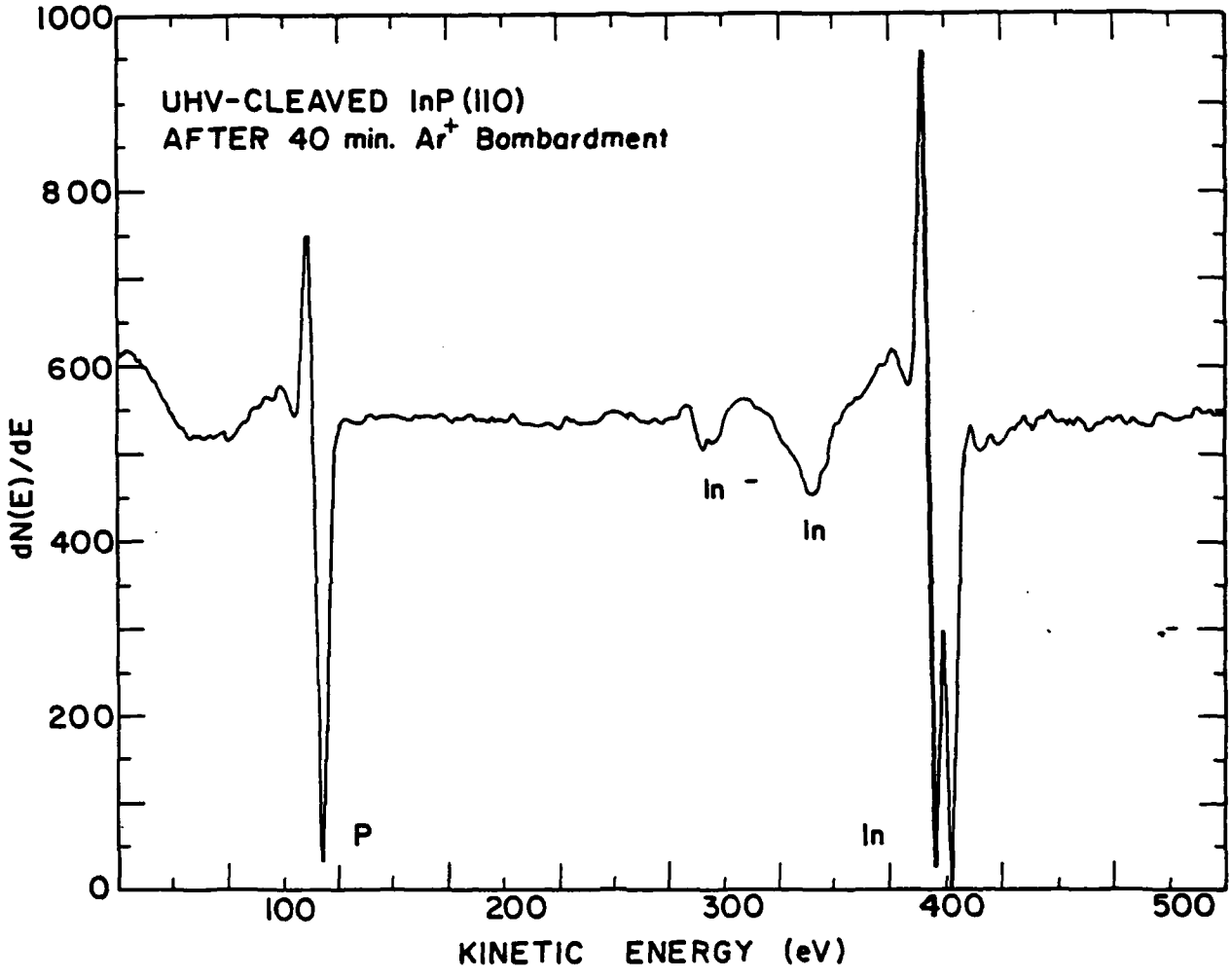
UHV-CLEAVED InP(110)
AFTER 40 min. Ar+ Bombardment
1000
800
600
400
200
0
dN(E)/dE
100
200
300
400
500
KINETIC ENERGY (eV)
P
In
In
In

Fig. 2

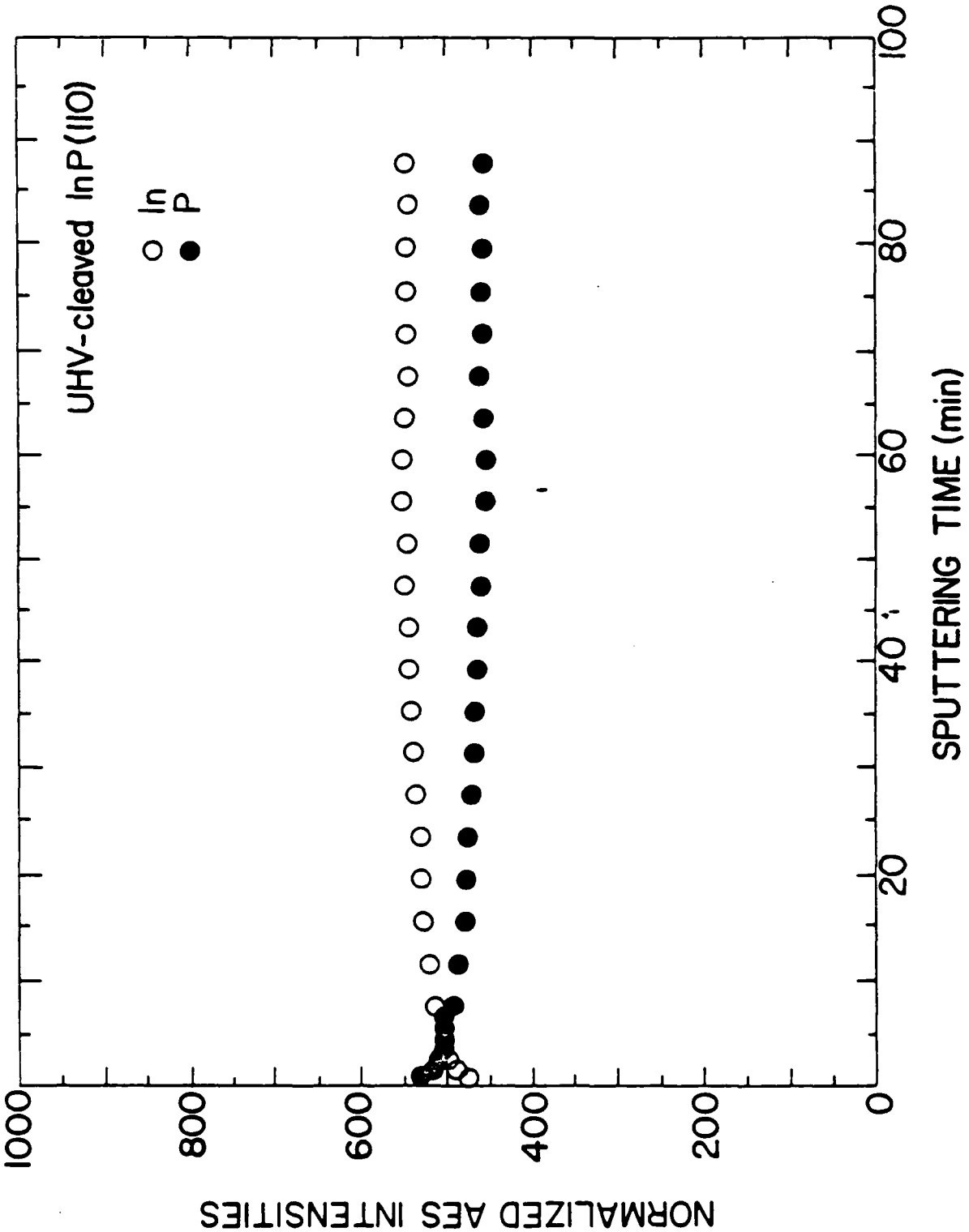
UHV-cleaved InP(110)
In
P
NORMALIZED AES INTENSITIES
SPUTTERING TIME (min)
1000
800
600
400
200
0
100
80
60
40
20

Fig. 3

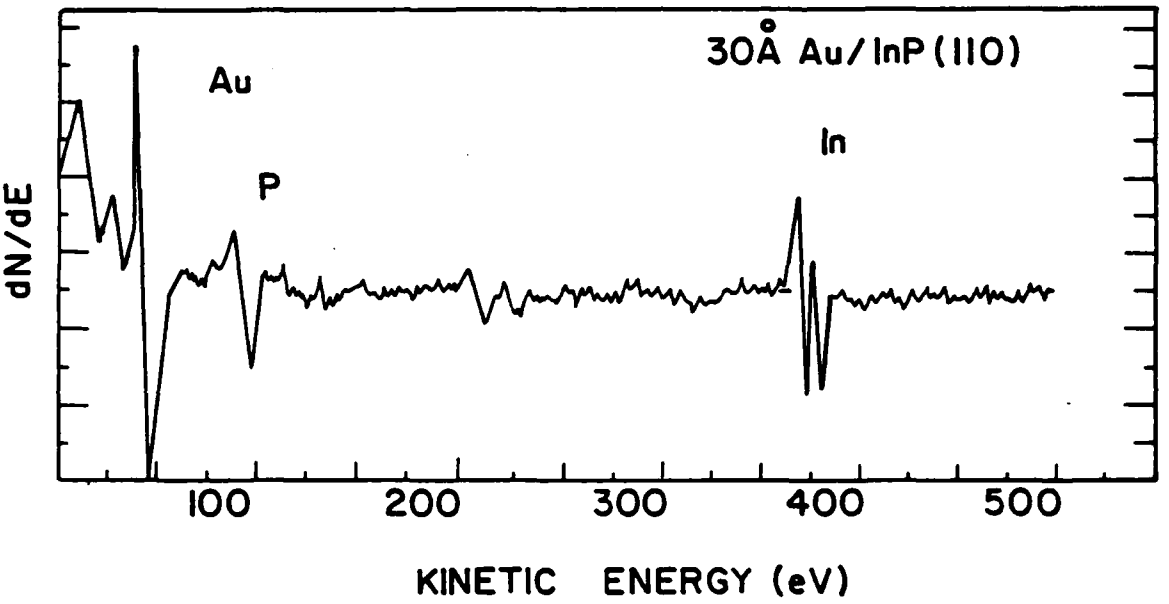
30Å Au/InP(110)
Au
P
In
dN/dE
100
200
300
400
500
KINETIC ENERGY (eV)

Fig. 4

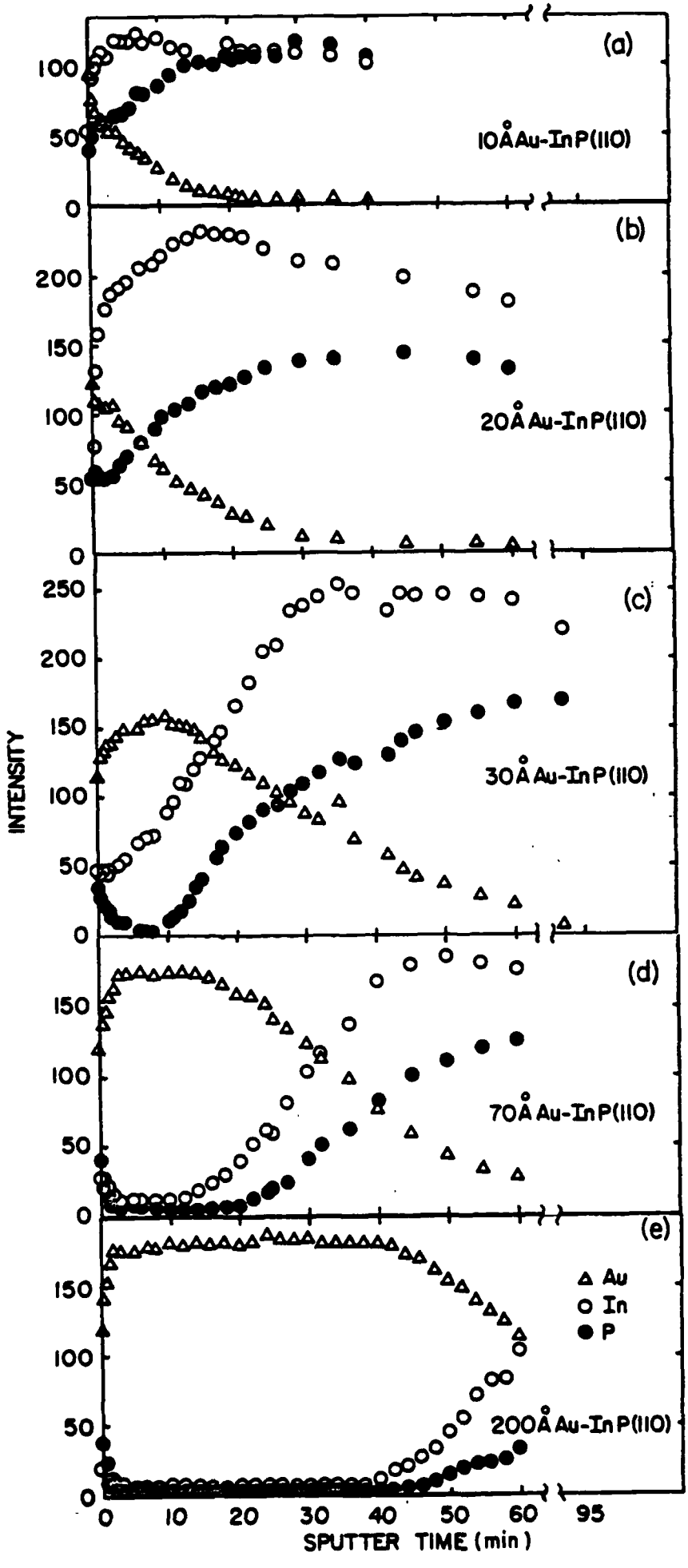
(a)
10Å Au-InP(110)
(b)
20Å Au-InP(110)
(c)
30Å Au-InP(110)
(d)
70Å Au-InP(110)
(e)
200Å Au-InP(110)
Au
In
P
INTENSITY
SPUTTER TIME (min)
0
10
20
30
40
50
60
95

Fig. 5

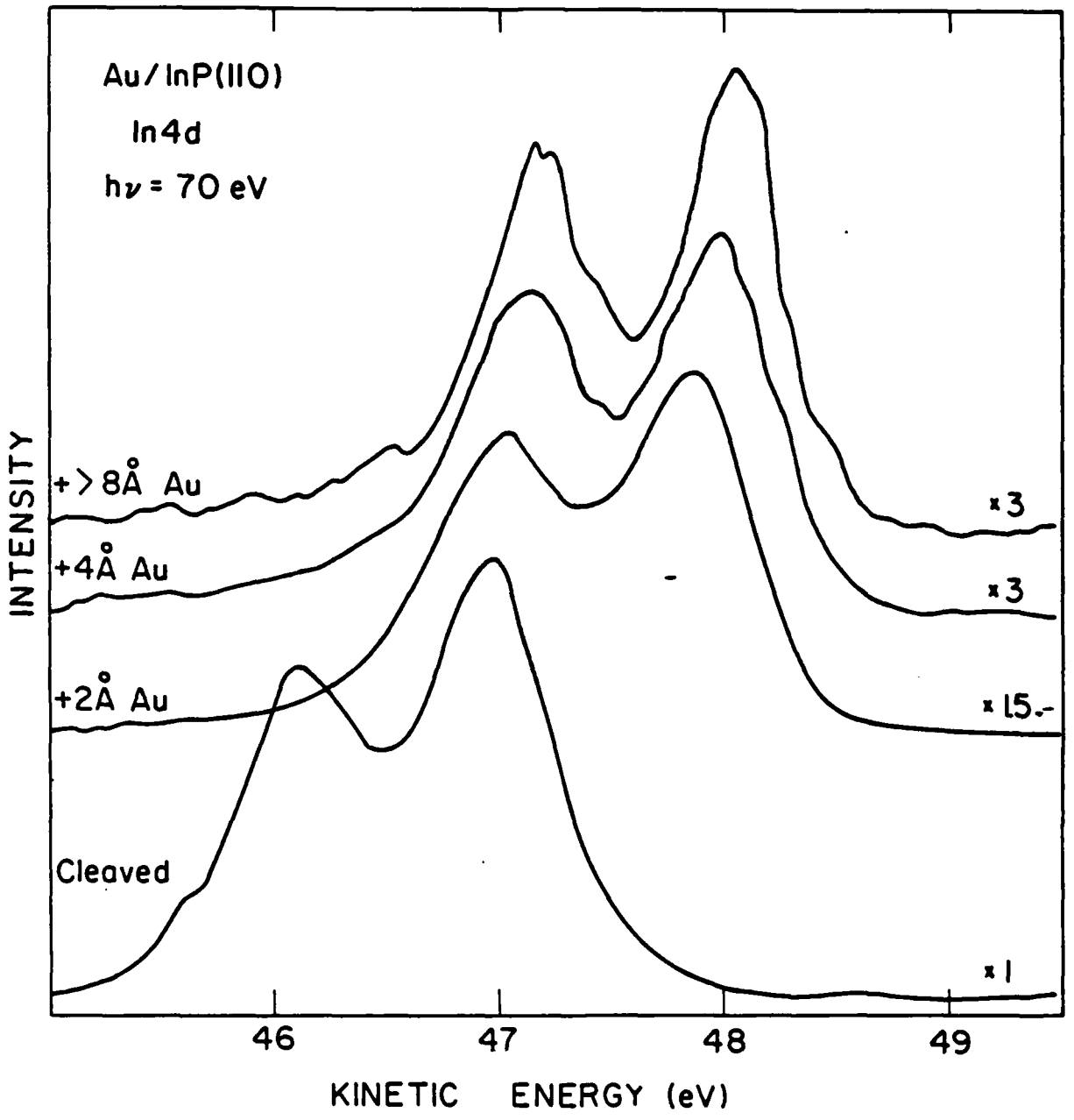
Au/InP(110)
In4d
hν = 70 eV
+>8Å Au
+4Å Au
+2Å Au
Cleaved
x3
x3
x15
x1
INTENSITY
46
47
48
49
KINETIC ENERGY (eV)

Fig. 6

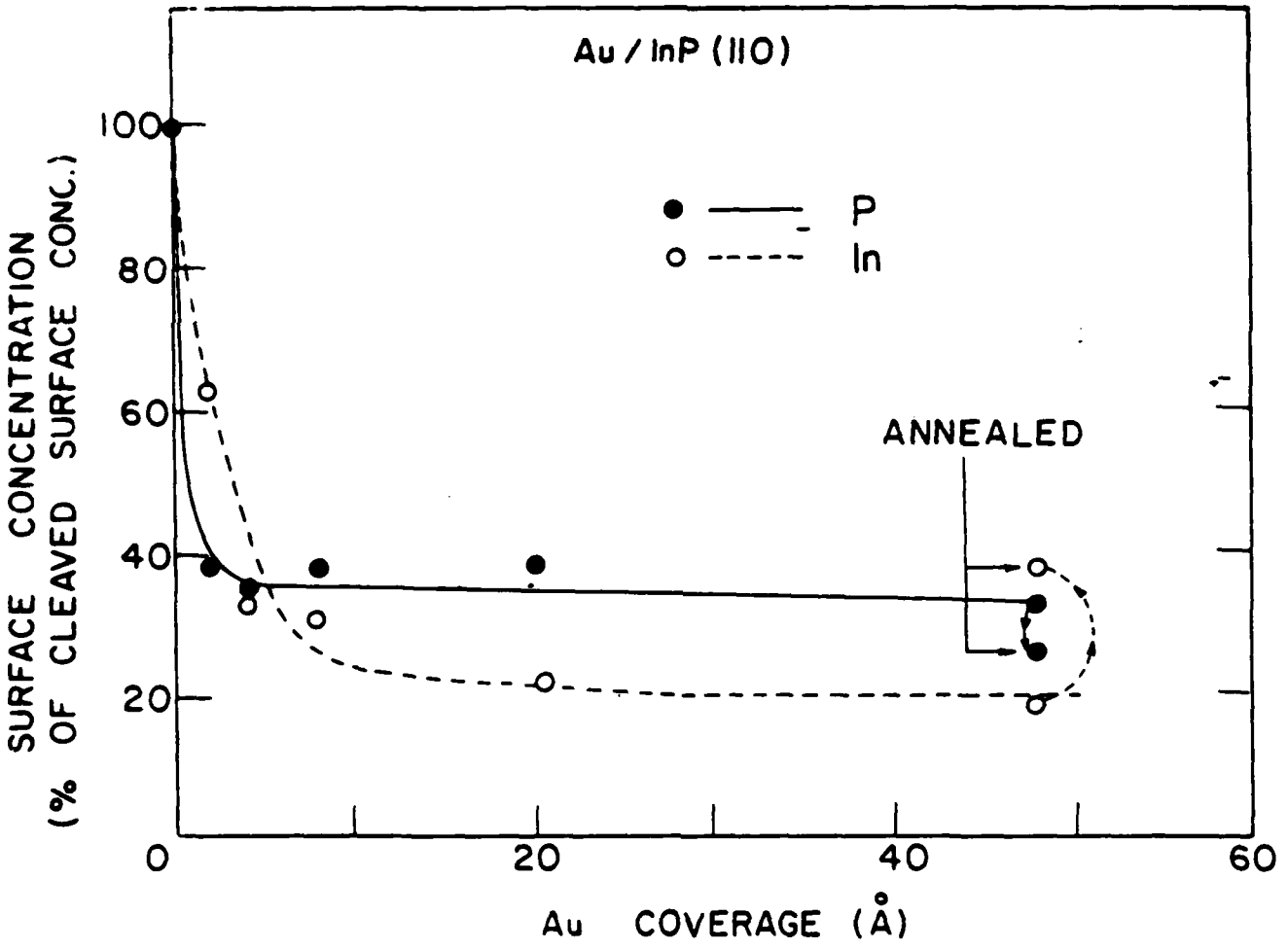
Au / InP (110)
SURFACE CONCENTRATION
(% OF CLEAVED SURFACE CONC.)
100
80
60
40
20
0
20
40
60
P
In
ANNEALED
Au COVERAGE (Å)

Fig. 7

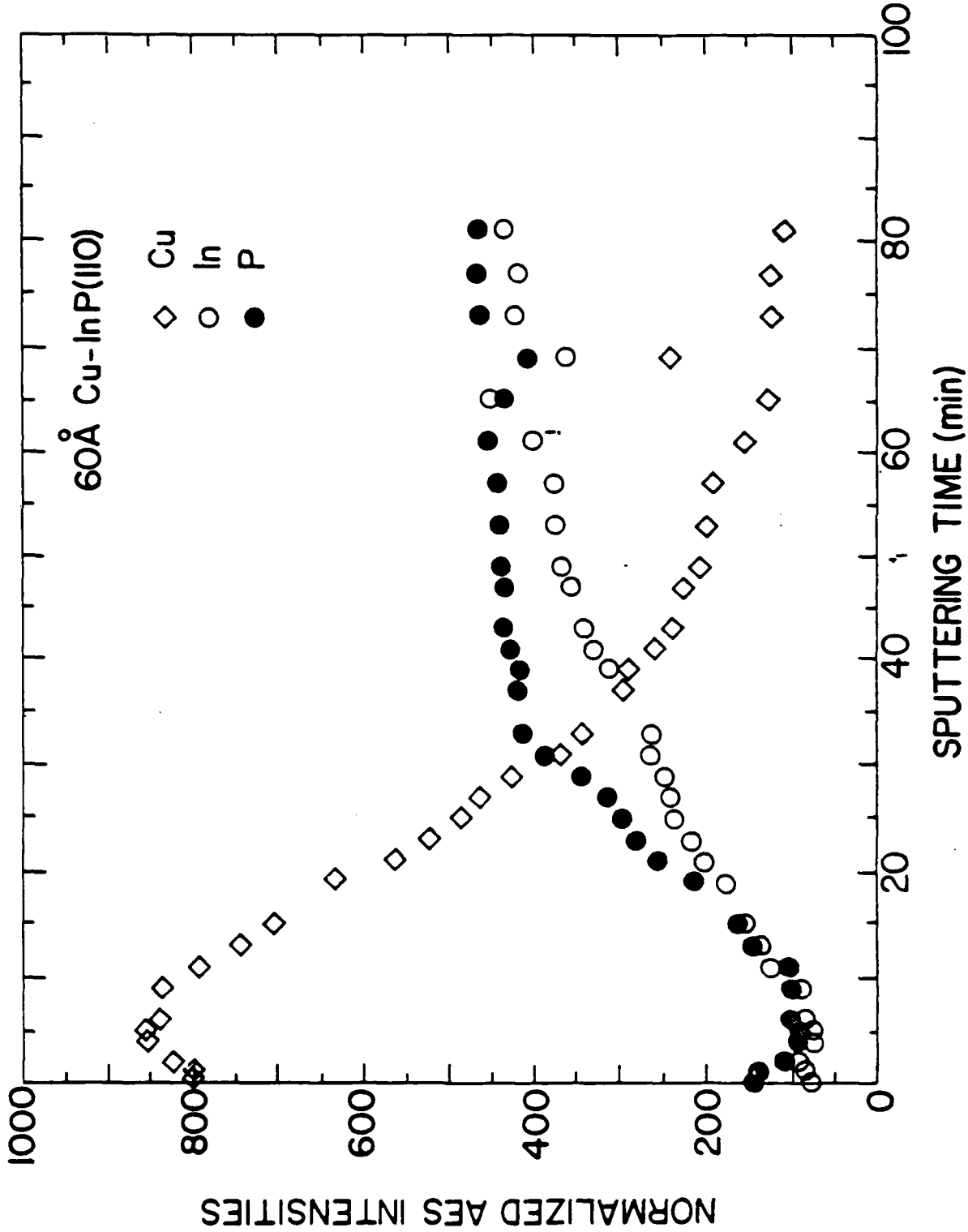
60Å Cu-InP(110)
Cu
In
P
NORMALIZED AES INTENSITIES
SPUTTERING TIME (min)
1000
800
600
400
200
0
100
80
60
40
20

Fig. 8

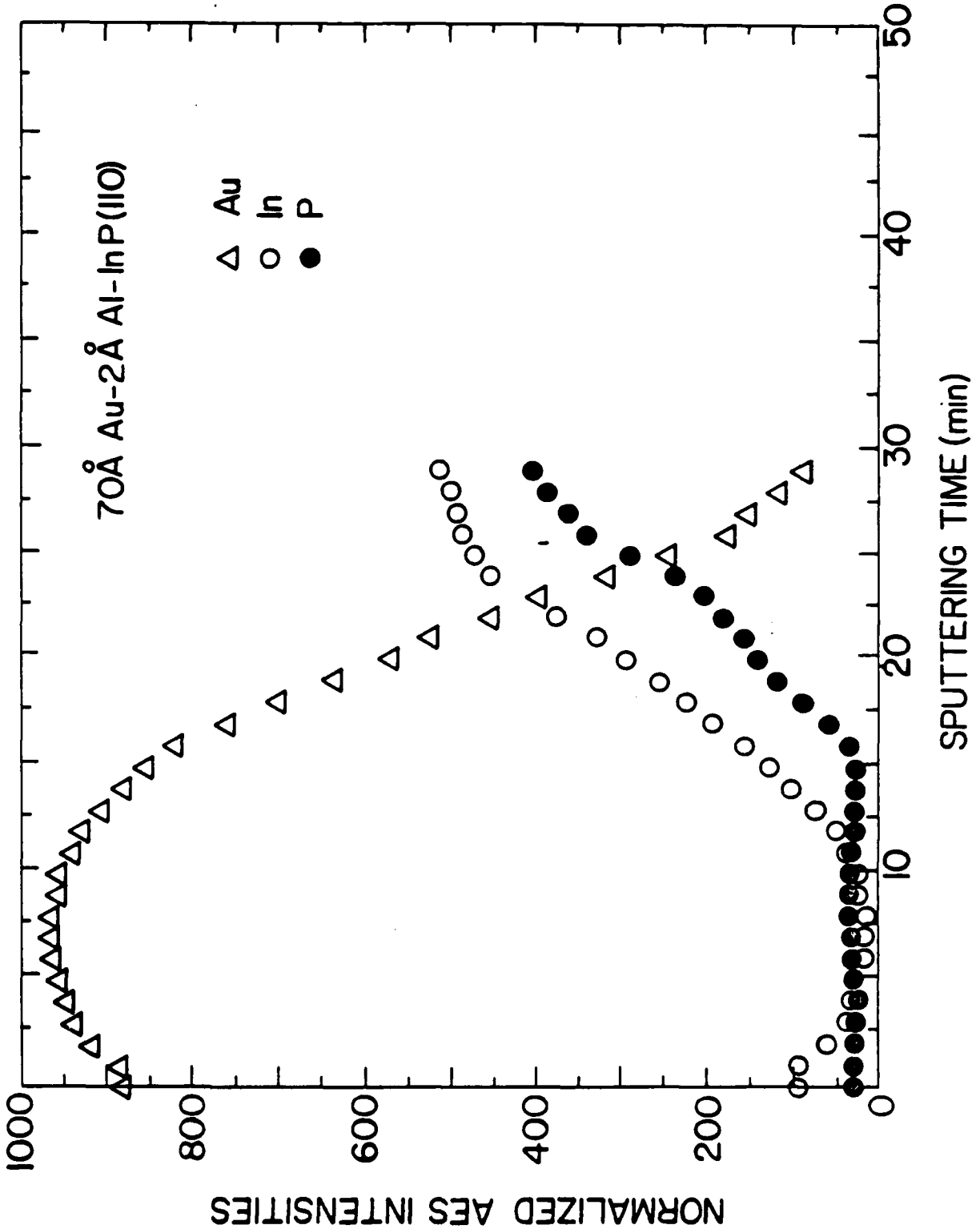
70Å Au-2Å Al-InP(110)
Au
In
P
NORMALIZED AES INTENSITIES
1000
800
600
400
200
0
SPUTTERING TIME (min)
50
40
30
20
10

Fig. 9

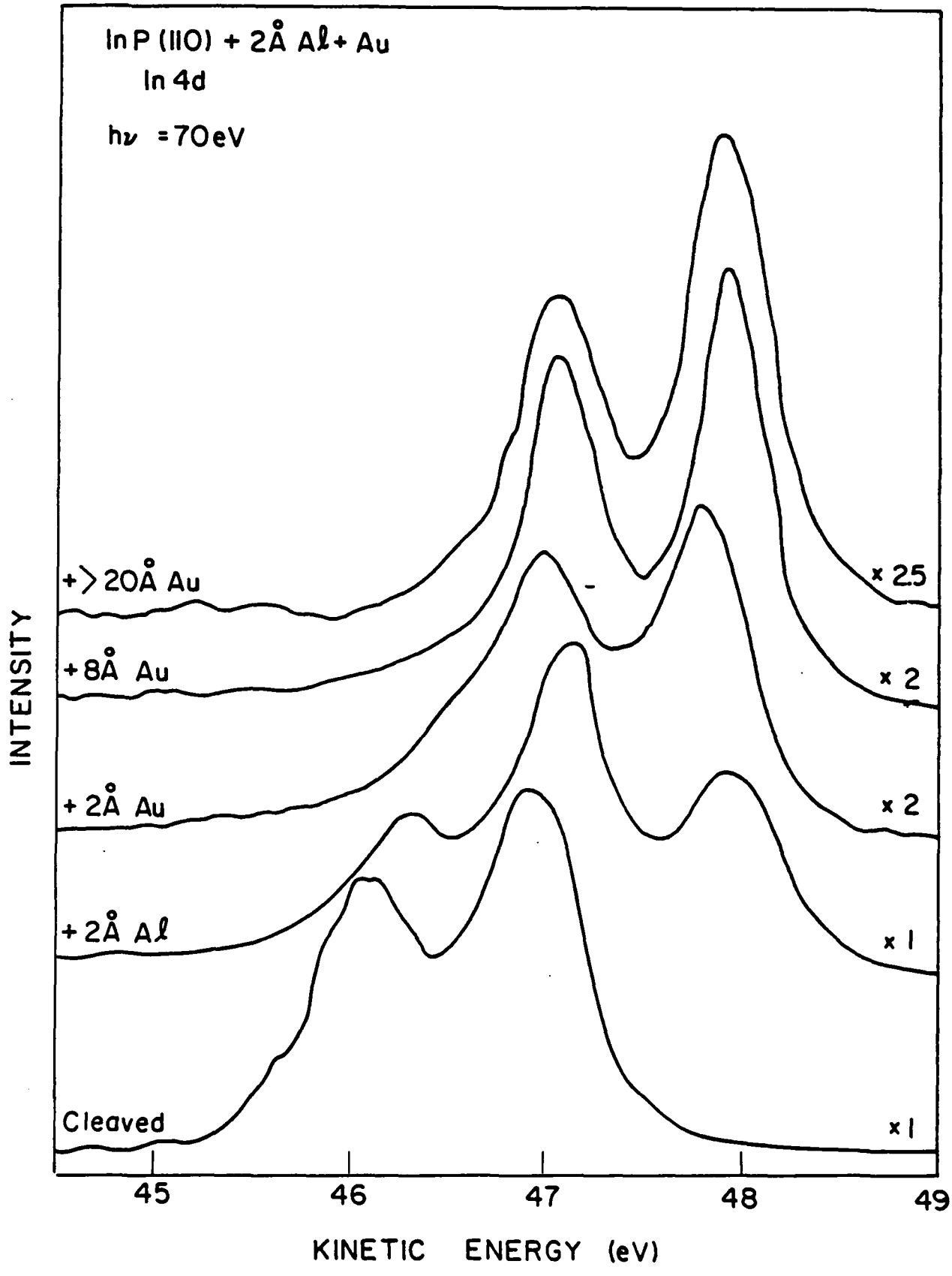
InP (110) + 2Å Al + Au
In 4d
hν = 70eV
+ > 20Å Au
+ 8Å Au
+ 2Å Au
+ 2Å Al
Cleaved
x 25
x 2
x 2
x 1
x 1
INTENSITY
45
46
47
48
49
KINETIC ENERGY (eV)

Fig. 10

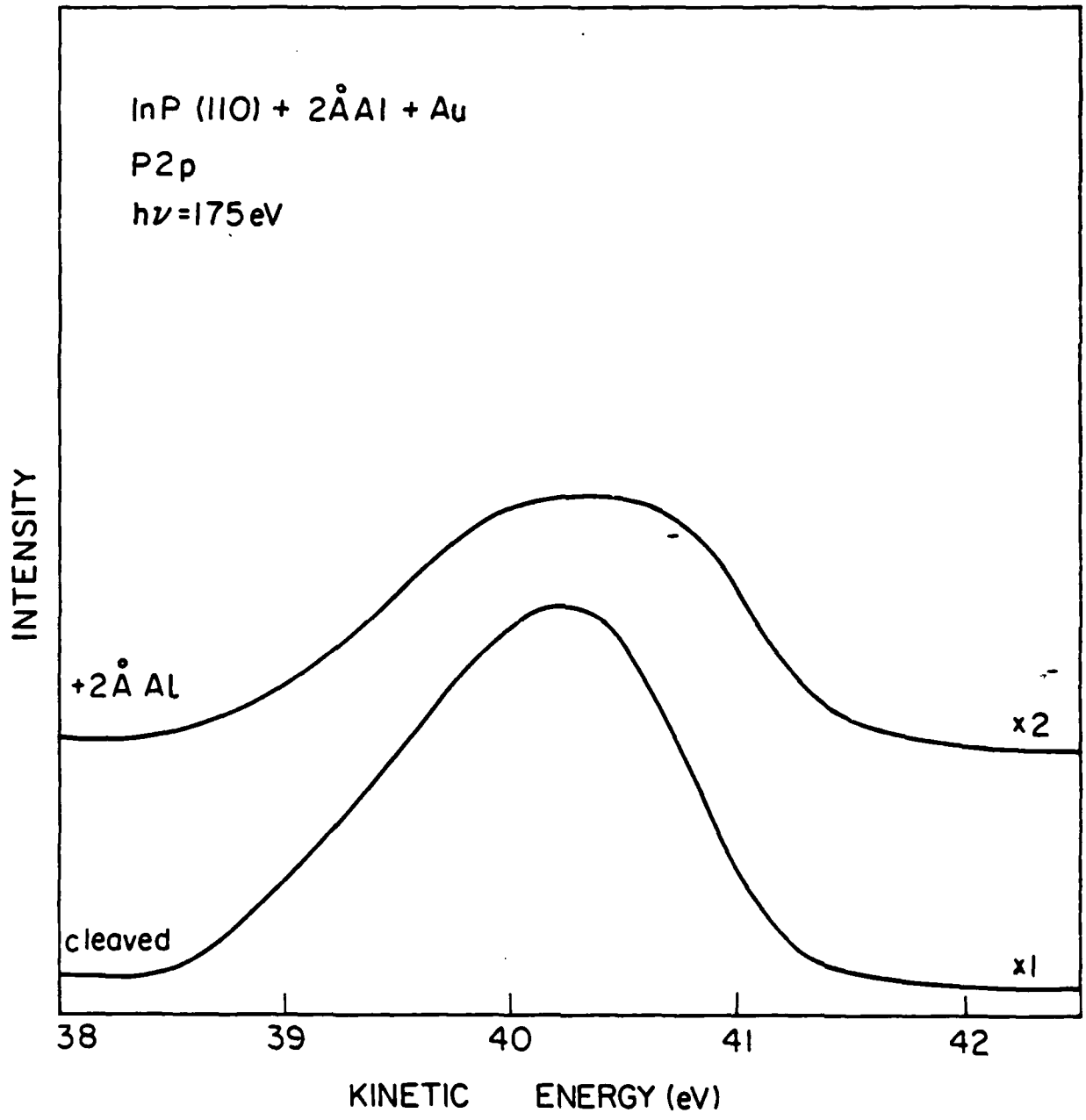
InP (110) + 2ÅAl + Au
P2p
hν=175eV
INTENSITY
+2Å Al
x2
cleaved
x1
38
39
40
41
42
KINETIC ENERGY (eV)

Fig. 11

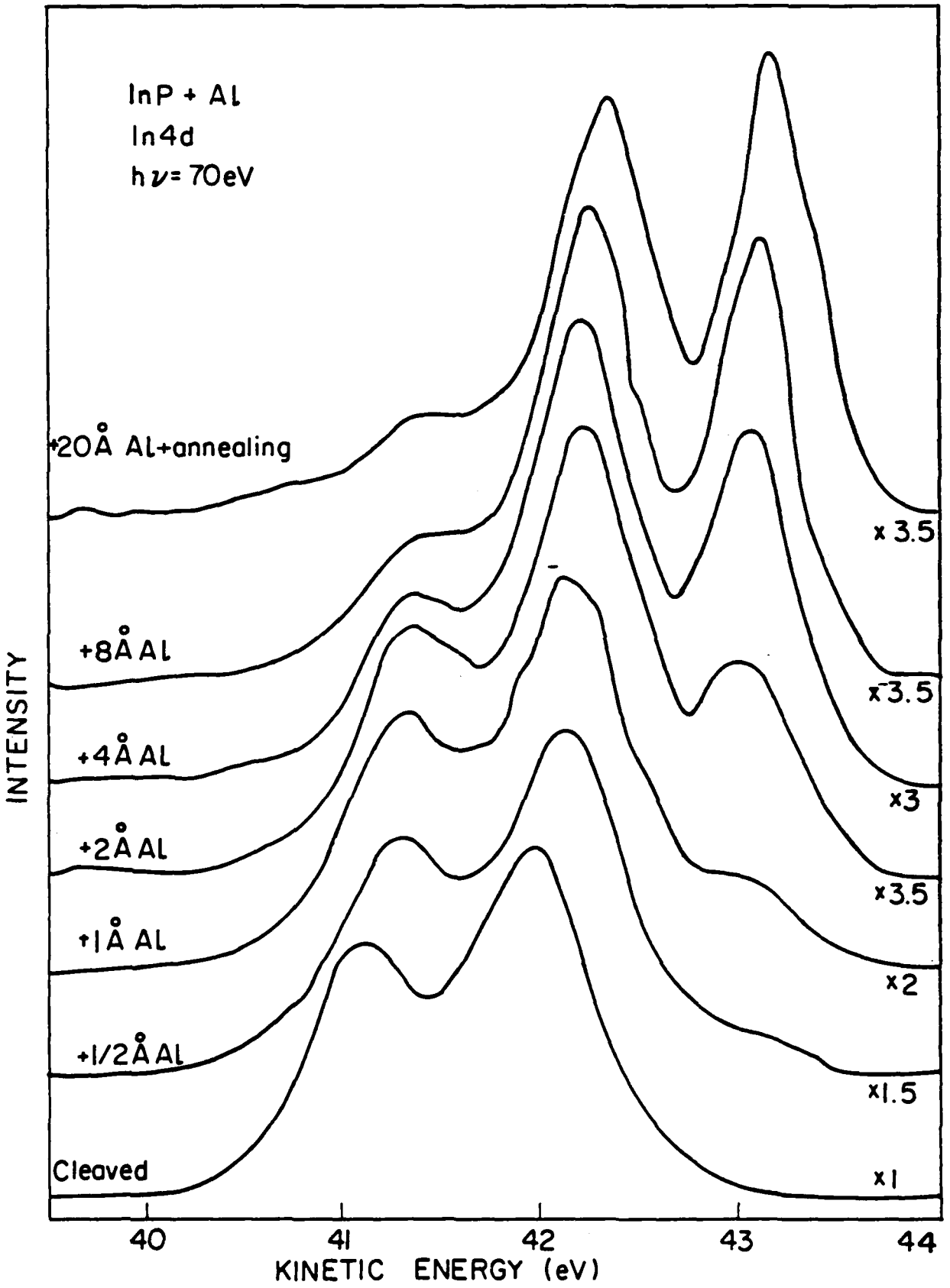
InP + Al
In4d
hν = 70eV
+20Å Al+annealing
+8Å Al
+4Å Al
+2Å Al
+1Å Al
+1/2Å Al
Cleaved
x 3.5
x3.5
x3
x3.5
x2
x1.5
x1
INTENSITY
40
41
42
43
44
KINETIC ENERGY (eV)

Fig. 12

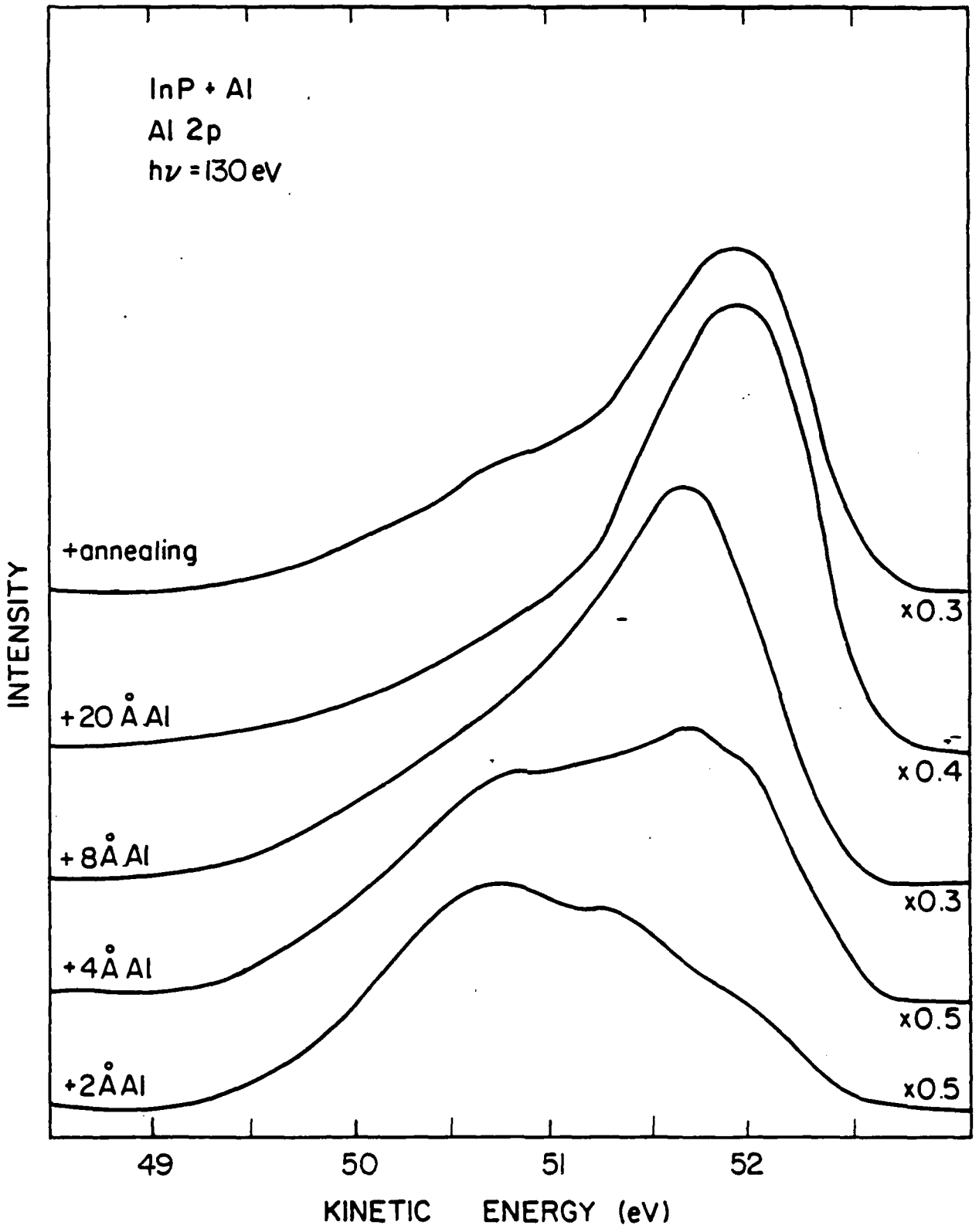
InP + Al
Al 2p
hν = 130 eV
+annealing
+20 Å Al
+8Å Al
+4Å Al
+2Å Al
x0.3
x0.4
x0.3
x0.5
x0.5
INTENSITY
49
50
51
52
KINETIC ENERGY (eV)

Fig. 13

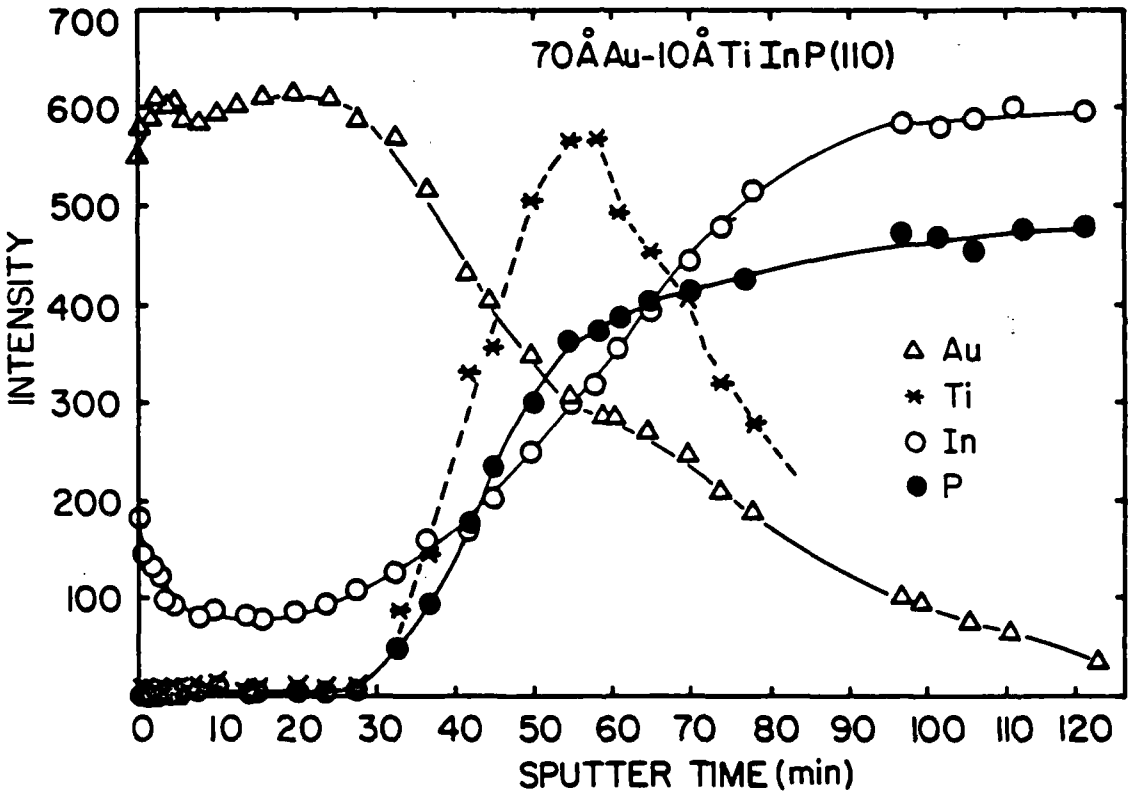
70Å Au-10Å Ti InP(110)
INTENSITY
SPUTTER TIME (min)
Au
Ti
In
P
700
600
500
400
300
200
100
0
10
20
30
40
50
60
70
80
90
100
110
120

Fig. 14

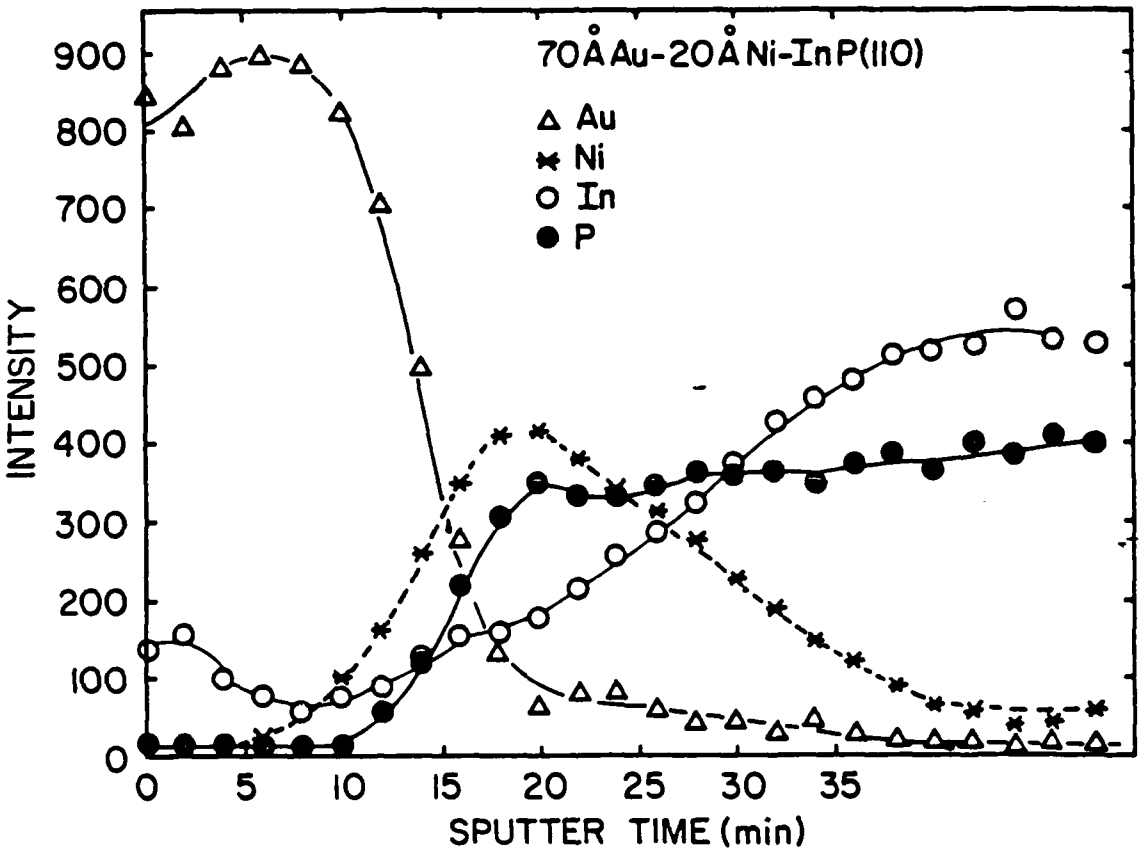
70Å Au-20Å Ni-InP(110)
Au
Ni
In
P
INTENSITY
SPUTTER TIME (min)
0
100
200
300
400
500
600
700
800
900
0
5
10
15
20
25
30
35

Fig. 15

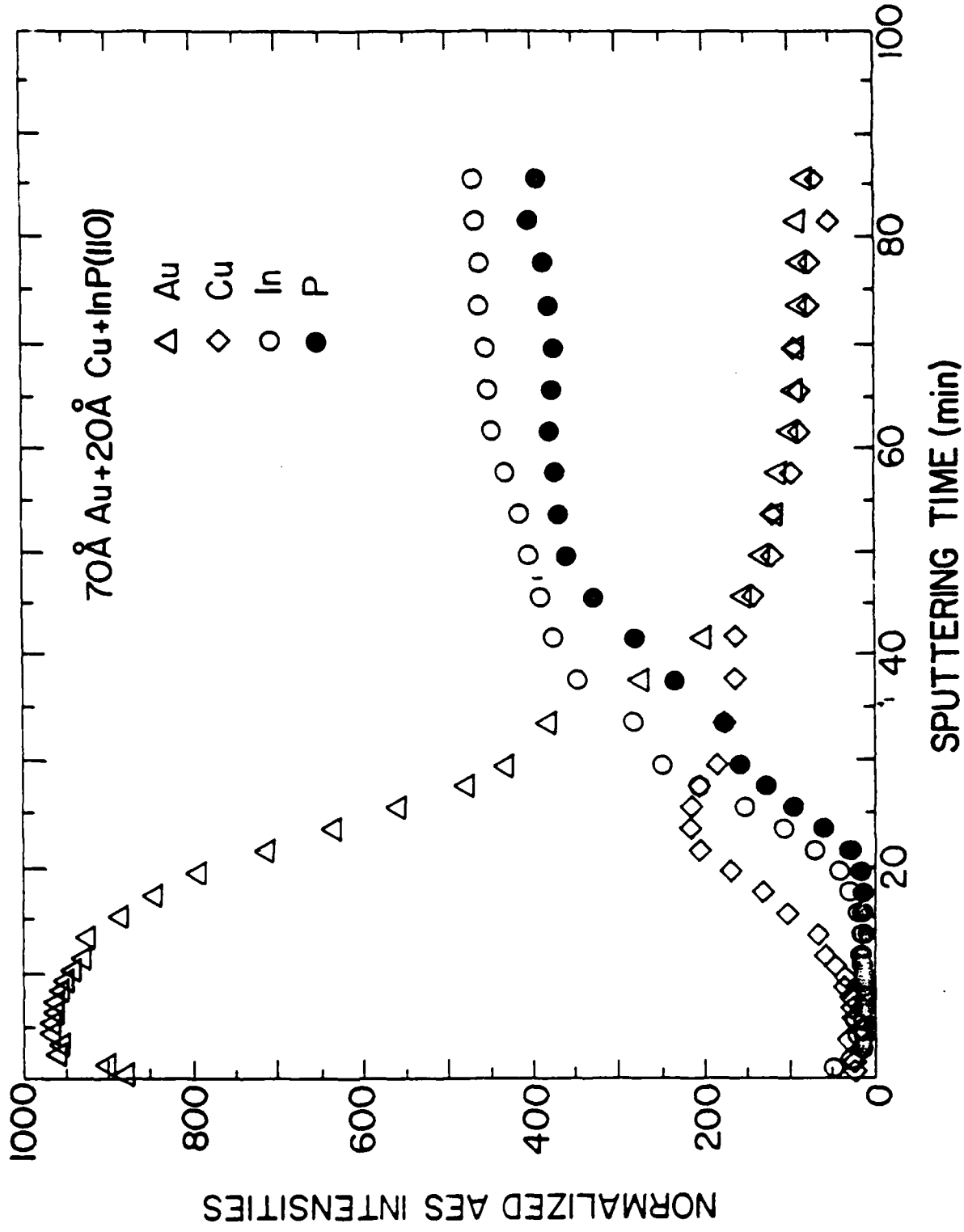
70Å Au+20Å Cu+InP(110)
Au
Cu
In
P
NORMALIZED AES INTENSITIES
SPUTTERING TIME (min)
0
200
400
600
800
1000
20
40
60
80
100

Fig. 16

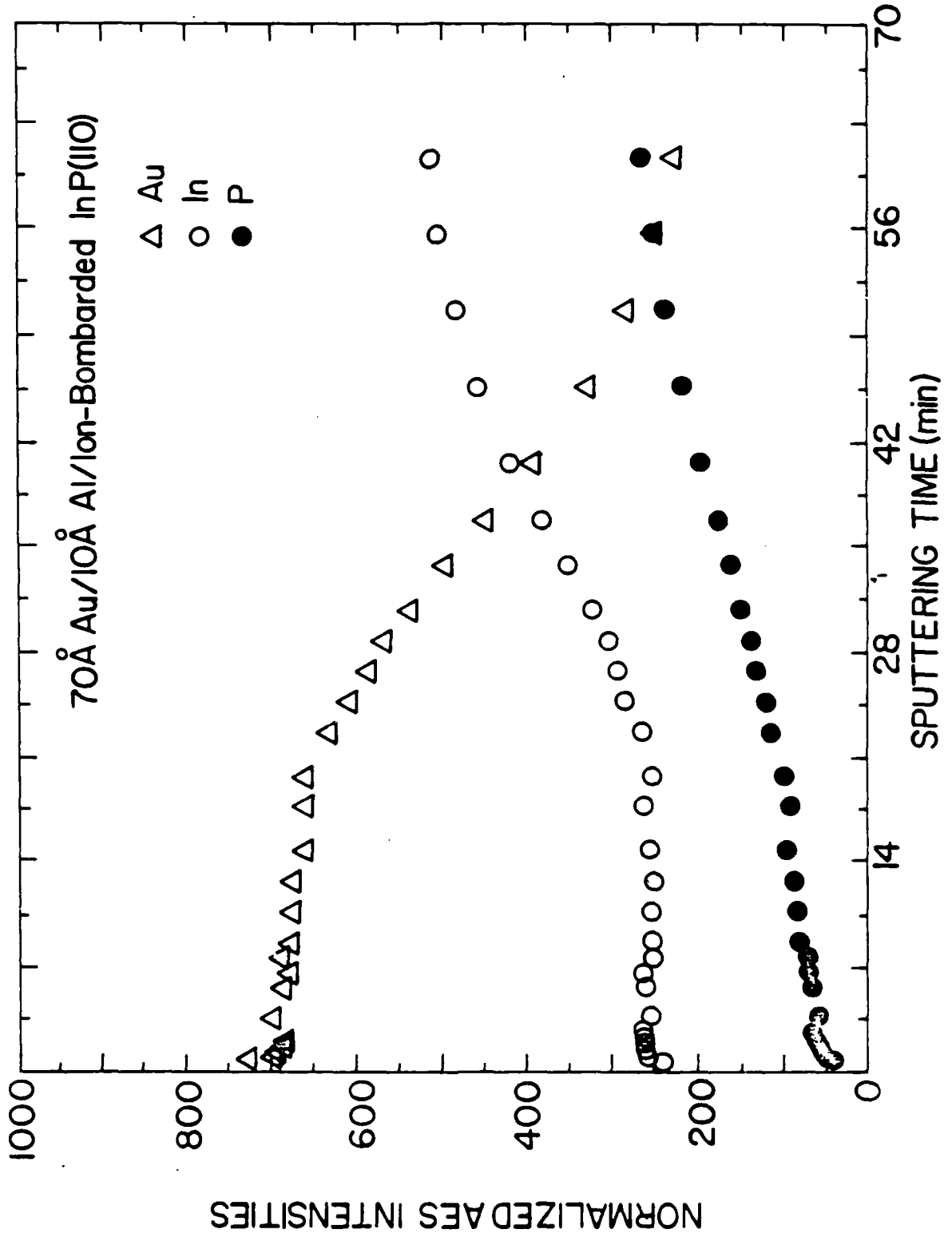
70Å Au/10Å Al/Ion-Bombarded InP(110)
Au
In
P
NORMALIZED AES INTENSITIES
SPUTTERING TIME (min)
0
200
400
600
800
1000
14
28
42
56
70

Fig. 17

Cathodoluminescence Spectroscopy Studies of Laser-Annealed Metal-Semiconductor Interfaces

L.J. Brillson, H.W. Richter†, M.L. Slade, B.A. Weinstein and Y. Shapira††

Xerox Webster Research Center
800 Phillips Road W114
Webster, NY 14580

Abstract

We have extended cathodoluminescence spectroscopy (CLS) to the study of new compound and defect formation at metal-semiconductor interfaces. CLS provides evidence for Cu_2S and/or impurity band formation after laser annealing Cu on UHV-cleaved CdS. Al deposition on UHV-cleaved CdS followed by laser annealing leads to formation of at least two deep levels distributed at different depths from the initial interface. The energies, densities and spatial distribution of these levels depend sensitively on the laser intensity and the presence or absence of particular metal overlayers. These results demonstrate the utility of CLS in revealing electronic features of the buried metal-semiconductor interface while still maintaining depth resolution on the order of hundreds of Å or less.

1. INTRODUCTION

Interface studies by surface science techniques suggest that strong changes in chemical and electronic structure can take place at the metal-semiconductor contact.[1-3] In particular, chemical reactions and diffusion at the microscopic interface and their associated defects, dipoles, and alloy layers can have a profound influence on the macroscopic Schottky barrier. While many of these effects can occur near room temperature, they are expected to become more pronounced upon annealing, and their evolution with temperature is of considerable interest in understanding Schottky barrier formation and degradation. Unfortunately, surface-sensitive techniques are not optimum for studies of such evolution, especially for changes occurring at "buried" interfaces - i.e., below the free surface of the overlayer. In this paper, we present results illustrating the use of cathodoluminescence spectroscopy (CLS) to monitor changes in buried metal-semiconductor interfaces after pulsed laser annealing. While CLS is a relatively old

technique[4] whose surface sensitivity has already been demonstrated,[5] we apply it here for the first time to interface-specific phenomena. Furthermore, by irradiating metal-semiconductor interfaces with strongly absorbed light from a pulsed excimer laser, we can induce chemical changes over depths on the order of 1000A.[6] This is in contrast to the macroscopic changes produced by conventional annealing. As a result, our interface-specific effects remain spatially microscopic during thermal processing. We show that with incident electron energies of 0.5 keV to 2 keV, it is possible to identify chemical and electronic features below the free surface induced by laser annealing and, by varying the energy, discriminate between electronic states distributed at different depths from the free surface with a resolution of only hundreds of A or less. Thus, CLS provides information unobtainable by standard surface science techniques while maintaining a microscopic depth resolution.

II. EXPERIMENTAL

CLS experiments were carried out in an ultrahigh vacuum (UHV) chamber (base pressure $p = 5X10^{-11}$ Torr) incorporating a variety of characterization techniques. Figure 1 illustrates schematically the CLS apparatus in vertical cross section. Specimens mounted on a manipulator are positioned at the common focal point of both a glancing incidence electron gun and transmitted, focused light from a Leiss double-prism monochromator. In the CLS experiments, electrons impinging upon the specimen produce luminescence which is focused by a quartz lens in UHV through a quartz window into the monochromator. A S-1 photomultiplier, cooled to liquid nitrogen temperature, detected the transmitted signal with a sensitivity which dropped sharply below 1 eV (1.3 μm). In order to filter out light emitted from the electron gun filament, we chopped the electron beam current and detected the photomultiplier current in phase with a lock-in amplifier. Both the monochromator scan energies and the signal acquisition were controlled by a Nova 2/10 minicomputer. Incident electron beam energies were varied between 0.5 and 2 keV to vary the depth of electron excitation. Incident beam currents were kept below 0.1uA to minimize any degradation of the target material.

Photoluminescence spectroscopy was performed using the 4579 A line of Ar^+ laser, a Spex 1401 grating monochromator scanned in second order, and another S-1 photomultiplier. Both the incident laser beam and the photoluminscence were transmitted by the same glass window in the UHV chamber. For these experiments,

Cu/CdS interfaces were annealed in UHV by a focused 300 W projection lamp (Sylvania ELH tungsten halogen), resulting in a temperature rise of 200-300°C.

The CdS specimens used were of "ultrahigh purity" single crystals, supplied by Eagle Picher Industries with resistivities up to 10^9 Ω-cm (carrier concentrations below 10^{16} cm^{-3}) and single crystals supplied by Cleveland Crystals with nominal resistivity of 1 Ω-cm. (1-2 x 10^{16} cm^{-3} donor concentration). The CdS from Cleveland Crystals appeared orange in color, while "ultrahigh purity" Eagle Picher CdS exhibited a yellow hue, the latter due to postannealing of the as-grown material in a S overpressure.[7] This S treatment compensates for the high concentration of S vacancies in the as-grown material and lowers the associated free electron concentration. The CdS crystals were cleaved in UHV to obtain smooth, clean mirror-like surfaces oriented in the $(10\bar{1}0)$ plane.

Metals were evaporated from heated tungsten filaments with deposited thickness monitored by a quartz crystal oscillator. During evaporation, the pressure rose into the high 10^{-9} torr or low 10^{-8} torr range.

We performed laser annealing in UHV by focusing an excimer laser (λ = 308 nm, 5 ns pulse width) through a sapphire viewport, onto the UHV-cleaved, metallized surfaces. The 300 by 600 mm diameter (1/e intensity) spot was rastered across the outer surface in a serpentine pattern with 100 μm row spacing and at rates such that each spot received 4 pulses. The rastered beam was also controlled by our minicomputer using Oriel micropositioners to move the quartz focusing lens (350 mm focal length).

III. RESULTS

Cu on CdS

Figure 2 illustrates CL spectra from UHV-cleaved, yellow CdS supplied by Eagle-Picher Ind. The UHV-cleaved surface before evaporation and laser annealing exhibits only a single peak at 2.42 eV corresponding to band-edge luminescence at room temperature. It should be noted that light emitted from the electron gun, reflected off the target surface and sampled by the collection optics produces a peak feature at ~1.2 eV which is completely removed by phase-sensitive detection. Also absent are peak features at 1.2 and 1.6 eV which appeared in CL spectra from UHV-

cleaved CdS provided by Cleveland Crystals (not shown). These orange-colored crystals are expected to contain significant concentrations of bulk defects, as mentioned above. All of the CL results presented in this paper are from "yellow" CdS supplied by Eagle-Picher Ind. only.

Deposition of 50 Å Cu on the UHV-cleaved surface produces no dramatic changes in luminescence features but an increased background extending to lower energies below the band edge peak and a weak peak at ~1.27 eV. These new features increase in intensity relative to the band edge luminescence following laser annealing with an energy density of 0.1 J/cm^2, resulting in a large peak at 1.28 eV. We will discuss the origin of this peak later.

Figure 3 illustrates the dependence of the laser-annealed Cu-CdS CL spectrum on incident electron energy. As shown, there is a dramatic decrease in the band gap *vs* 1.28 eV peak luminescence intensity as electron beam energy is reduced. Since electron scattering lengths decrease with kinetic energies, between 2 and 0.5 keV,[8] the lower energy spectra represent excitation preferentially near the laser annealed free surface. Of course, luminescence transitions occur at depths beyond the electron scattering length since electron-hole pairs generated by the incident beam can diffuse before recombining. The difference in 2keV spectra between Figs. 2 and 3 is due to either beam damage or a time-dependent change in the Cu-CdS interface resulting from diffusion over the course of one hour.[9]

We have observed a feature similar to this 1.28 eV peak in photoluminescence experiments carried out with the 4579 Å line of an Ar^+ laser. Instead of pulsed laser annealing, we used the focused light of a tungsten halogen lamp to promote Cu/CdS interdiffusion. Figure 4 illustrates photoluminescence spectra obtained for UHV-cleaved CdS from Cleveland Crystals, before and after Cu deposition and annealing. For these measurements, the CdS specimens rested on a copper cold finger of a Lakeshore Cryotronics cryopump. The surface temperature of the laser-irradiated CdS surface was ~50°C, as extracted from the 2.54 eV band gap emission. Other peaks evident in Figure 4 are at 2.03 eV and 1.70 eV and are due to bulk defects. With the deposition of 100 Å Cu and 135 min annealing at 200-300°C (the error is due to uncertainty in the emissivity of the Cu/CdS surface), a new peak emerges at 1.26 eV with a 0.1 eV FWHM. The energy of this peak corresponds almost exactly to the peak induced by pulsed laser annealing in Figs. 2 and 3 but has

a narrower width due to the lower specimen temperature. The signal to noise ratio of this Cu-annealed peak in photoluminescence is much worse than that evident for the corresponding CLS peak in Figs 2 and 3. This is due in large measure to the larger absorption depth (~600 Å at 4579 Å) for photoluminescence *vs* CLS. With an additional 185 min. annealing, the 1.26 eV peak diminishes relative to the 1.67 eV peak and a large new feature at 2.36 eV. Besides its lower sensitivity to new surface features, photoluminescence spectroscopy provides no straightforward method to vary the depth of excitation significantly.

Al on CdS

Different luminescence features appear for Al on CdS after laser annealing. Figure 5 shows that, as with the Cu-CdS case, room temperature deposition of Al produces no new features below the band gap energy. The UHV-cleaved surface exhibits weak peak structures at 1.3 eV and 1.65 eV which may be due to residual damage produced during cleavage. These weak structures increase dramatically upon laser annealing at an energy density of 0.1 J/cm^2. A subsequent laser anneal at 0.2 J/cm^2 decreases these features relative to the gap luminescence peak. The correspondence of the 1.65 eV with one of the bulk photoluminescence features in Figure 4 coupled with the reduction of both 1.3 and 1.65 eV peaks by further pulsed laser annealing suggest that both of these peaks are due to lattice damage.

The energy dependence of the CL spectra provide further information about these damage-related peaks. At 0.1 J/cm^2, comparison of 05. and 2keV spectra in Fig. 6a reveals that the 1.3 eV and 1.65 eV transitions both occur preferentially near the specimen surface. Band gap luminescence appears in the 2 keV but not the 0.5 keV spectrum, indicating a large change in defect density between the volumes sampled with these two excitation energies. Furthermore, we observe a large increase in the 1.3 eV peak relative to the 1.65 eV peak at 0.5 keV. This suggests that the 1.3 eV transitions occur closer to the surface than do the 1.65 eV transitions.

The spatial distribution of these transitions changes with additional laser annealing. Furthermore, the 1.3 eV peak shifts to 1.35 eV. Fig. 6b shows that a preferential enhancement of the 1.3 eV peak does not occur for the 0.5 keV spectrum. In addition, the enhancement of both peaks relative to the band edge luminescence is not as large as observed in Figure 6a. These differences indicate that the 0.2 J/cm^2

results in a decrease in the defect density near the surface and that the density of defects associated with the 1.35 eV luminescence decreases relative to the 1.65 eV luminescence as well. Thus, the CL technique permits us to distinguish between lattice defect features with different depth distributions and to monitor changes in these distributions with thermal processing.

Discussion

Several possibilities can account for the spectral features produced by Cu deposition and annealing. These include the formation of: a) a Cu-S compound, b) a Cu impurity level deep within the CdS band gap, c) bulk defect levels, and d) Cu impurity - lattice defect complexes. Strong evidence for compound formation arises from cathodoluminescence studies of bulk Cu_2S[10] which exhibit a peak at 1.26 eV with a FWHM of 0.12 eV at 300°K. At 77°K, this peak shifts to 1.28 eV with a FWHM of 0.09 eV. With the slight exception of the 0.2 eV FWHM for the room temperature CLS peak, the Ref. 10 results are in agreement with our CLS and photoluminescence measurements. Our CLS peak could be broadened by lattice disorder which smears the band edges.

Cu impurity levels can not be ruled out in explaining the Figure 2 through 4 results. Cu diffuses rapidly through CdS[11] and may establish an equilibrium between interstitial and substitutional Cu during the diffusion.[12] Depending upon the impurity (acceptor) relative to the bulk donor concentration, Cu may exhibit luminescence transitions at 1.2 eV (low concentration) and 1.5 eV (high concentration).[13,14] Fluorescence emission of Cu-doped CdS exhibits 80°K peaks at 1.57 eV, 1.18 eV, and 0.75 eV[15] - the latter outside our spectral range. The 1.18 eV peak has a FWHM of 0.24 eV but differs significantly from our 1.28 eV peak. Figs. 2 and 3 show no evidence for the 1.57 eV Cu transition. Interstitial Cu donors have been associated with a level 0.27 eV below the conduction band.[16] We see no evidence for transitions from this level at 2.42 - 0.27 = 2.15 eV. Thus supporting evidence for identifying the 1.28 eV CLS peak with a Cu impurity alone is rather limited.

Native defects created by annealing must be considered as well. For example, the 1.7 eV peak in Figure 4 has been identified with a S vacancy while the 2.35 eV feature is associated with a S interstitial.[17,18] These transitions are also observed

after Ar^+ bombardment of UHV-cleaved CdS.[19] A more recent luminescence studies attributes the 1.7 eV transition to a complexed S interstitial.[20] Other transitions relevant to our results include 2.05 eV and 1.20 eV fluorescence bands attributed to Cd interstitials and vacancies respectively.[21] A 1.20 eV peak has also been associated with Cu in a particular ionization state[22] as well as with Cu interstitials associated with Cd vacancies.[23] Given the single peak observed for laser-annealed Cu on CdS, and the excellent agreement with the cathodoluminescence peak energy of Cu_2S, we believe that Cu_2S formation is the most likely explanation of the many possibilities discussed.

The two peaks produced by pulsed laser annealing of Al on CdS are evidence that a different interaction has occurred from that of Cu or CdS. Unlike the Cu/CdS case, one can not argue for compound formation since the $Al_2 S_3$ absorption edge lies at 3.7-4.1 eV[24] and no CLS structure is observed in that region (not shown). The absence of such structure could be due to quenching by lower energy transitions. More likely, however, the annealing of Al on CdS results in the formation of CdS native defects. Halsted *et al*[15] list luminescence transitions for native defects at 1.4 and 1.7 eV at 80°k, consistent with our CLS peaks at room temperature. These peaks are also similar to the structure evident after cleavage, which can be attributed to mechanical damage. Furthermore, the reduction of these peak intensities with additional heating suggests lattice disorder which is being reduced by thermal annealing. The 1.65 eV peak can also be related to Al doping of CdS. Susa *et al*[25] propose Al complexed with a Cd vacancy to account for a 1.65 eV photoluminescence peak at 77°K. Such a defect complex could contribute along with a native defect to the CLS peak at 1.65 eV, particularly for the 0.1 J/cm^2 case in which this peak is dominant. It is likely that defects form which are related to a S deficiency near the semiconductor surface since we observe evaporation of S from the Al/CdS interface during pulsed laser annealing. We detect such evaporation from the appearance of S vapor (amu 32) as measured by a residual gas analyzer. The different density and spatial distribution of two laser-induced defects is not surprising given the atomic diffusion out of the crystal and chemical interactions at the microscopic metal-semiconductor interface. The variation in CLS features between Figs. 2, 3, 5, and 6 emphasize that the distribution and density of defect complexes and chemical products depends sensitivitely on both the chemical nature of metal overlayer as well as on the annealing conditions.

The spectral data presented here suggest that CLS can be effectively applied to the analysis of metal-semiconductor interactions - especially "buried" interfaces at elevated temperatures for which chemical interactions can produce new interfacial phases and electrically-active sites extending over nanometers or more. Furthermore, CLS can be spatially localized to analyze particular surface features.

The CLS technique has relatively high depth resolution (e.g., nanometers) despite the fact that injected electrons can produce lower energy secondaries which diffuse before recombining radiatively. The depth resolution of luminescence can be estimated from the depth resolution of backscattered secondary electrons as measured by scanning electron microscopy. Fractional backscattering measurements of Cosslett and Thomas[26] for normal incidence yield an extrapolated variation from 100 A for 2 keV to less than 20 A for 0.5 keV. In fact these measurements represent upper limits. Monte Carlo calculations of Murata[27] show lower values for the glancing incidence irradiation employed in our experiment.

Cathodoluminescence has a number of problems which can complicate any quantitative analysis. These include a dependence of relative peak amplitudes on injection level, a dependence of cross section for luminescence on incident energy, thermal effects and other electron beam damage, as well as on an exact determination of electron range at particular incident angles. On balance, however, the CLS may prove useful in characterizing metal-semiconductor interfaces since it can provide information on basic mechanisms of Schottky barrier formation and changes under various process conditions - fundamental issues which are far from understood.

ACKNOWLEDGMENTS

The authors wish to thank William Greene for assistance in constructing the Leiss monochromator drive and Harvey Scher for his constant support. This work was supported in part by the Office of Naval Research (Grant No. 00014-80-C-0778).

†Permanent address: Max Planck Institute for Festkörperforschung, Stuttgart, West Germany

††Permanent address: Dept. of Electron devices, Faculty of Engineering, Tel Aviv University, Ramat Aviv, 69978, Israel

References

1. L.J. Brillson, Surf. Sci. Rpts. 2, 123, (1982): Int. J. Phys. Chem. Solids 44, 703 (1983) and references therein.

2. G. Margaritondo, Solid State Electron. 26, 499 (1983)

3. R.H. Williams, Contempt. Phys. 23, 329 (1982).

4. See, for example, F.G.J. Garlick, Adv. Electron. 2, 151 (1950) and references therein.

5. C.B. Norris, C.E. Barnes, and W. Beezhold, J. Appl. Phys. 44, 3209 (1973).

6. H. Richter and L.J. Brillson, Proc. 17th Int. Conf. on Physics of Semiconductors, in press.

7. J. Powderly, Eagle Picher Ind., private communication.

8. M.P. Seah and W.A. Dench, Surf. Interf. Anal. 1, 2 (1979)

9. M. Cardona and G. Harbeke, Phys. Rev. 137, A1467 (1965).

10. F. Guastavino, S. Duchemin, B. Rezig, B. Grault,, and M. Savelli, Conf. Rec. IEEE Photovoltaic Spec. Conf., Series 13, 303 (1978).

11. H. Woodbury, J. Appl. Phys. 36, 228 (1965).

12. W. Szeto and G.A. Somarjai, J. Chem. Phys. 44, 3490 (1966).

13. R.H. Bube, Photoconductivity of Solids (Wiley, New York, 1960).

14. W. VanGool, Philips Research Rept. 13, 157 (1958).

15. R.E. Halsted, M. Aven, and H.D. Coghill, J. Electrochem. Soc. 112, 177 (1965).

16. M.A. Rizakhanou, Yu.N. Emirov, and N.A. Abilova, Sov. Phys. Semicond. 14, 991 (1980).

17. B.A. Kulp and R.H. Kelley, J. Appl. Phys. 31, 1057 (1960).

18. J.W. Corbett, in: Electron Radiation Damage in Semiconductors and Metals, Suppl 7: Solid State Physics Eds. F. Seitz and D. Turnbull (Academic, New York, 1966) p. 192.

19. L.J. Brillson, Surf. Sci. 51, 45 (1975).

20. C.N. Elsby and J. M. Meese IEEE Trans. Nucl. Sci. NS-21, 14 (1974).

21. B.A. Kulp, Phys. Rev. 125, 1865 (1962).

22. B.A. Kulp, J. Appl. Phys. 32, 1966 (1961).

23. I.B. Ermolovich, G.I. Matvievskaya, G.S. Pekar, and M.K. Sheinkman, Utr. Fiz. Zh. 18, 732 (1973).

24. Von E. Kauer and A. Rabenau, Z. Natur. Forschg. 13a, 531 (1958).

25. N. Susa, H. Watanake, and M. Wada, Jap. J. appl. Phys. 14, 1733 (1975).

26. V. E. Cosslett and R. N. Thomas, Brit. J. Appl. Phys. 16, 779 (1965).

27. K. Murata, Phys. Stat. Sol. (a) 36, 527 (1976).

Figure Captions

Figure 1 Schematic experimental arrangement for cathodoluminescence (CL) spectroscopy under ultrahigh vacuum conditions.

Figure 2 CL spectra obtained with 2 keV electrons incident on UHV-cleaved CdS($11\bar{2}0$), after *in-situ* deposition of 50 Å Al, and after *in-situ* laser annealing with increasing energy density 0.1 J/cm^2.

Figure 3 CL spectra as a function of incident electron energy for UHV-cleaved CdS($11\bar{2}0$) with a 50 Å Cu overlayer, laser-annealed with energy density 0.1 J/cm^2.

Figure 4 Photoluminescence spectra for UHV-cleaved CdS($11\bar{2}0$) before and after deposition of Cu overlayers and annealing. The 100 Å Cu/CdS interface was annealed by a focussed 300 W projector lamp, first for 135 min, then for an additional 180 min. Excitation source was a 100 mW, 4579 Å line of an Ar^+ laser.

Figure 5 CL spectra obtained with 2 keV electrons incident on UHV-cleaved CdS($11\bar{2}0$), after *in-situ* depositon of 50 Å Al;, and after *in-situ* laser annealing with increasing energy density.

Figure 6 CL spectra as a function of incident electron energy for UHV-cleaved CdS($11\bar{2}0$) with a 50 Å Al overlayer, laser-annealed with energy density a) 0.1 J/cm^2 and b) 0.2 J/cm^2.

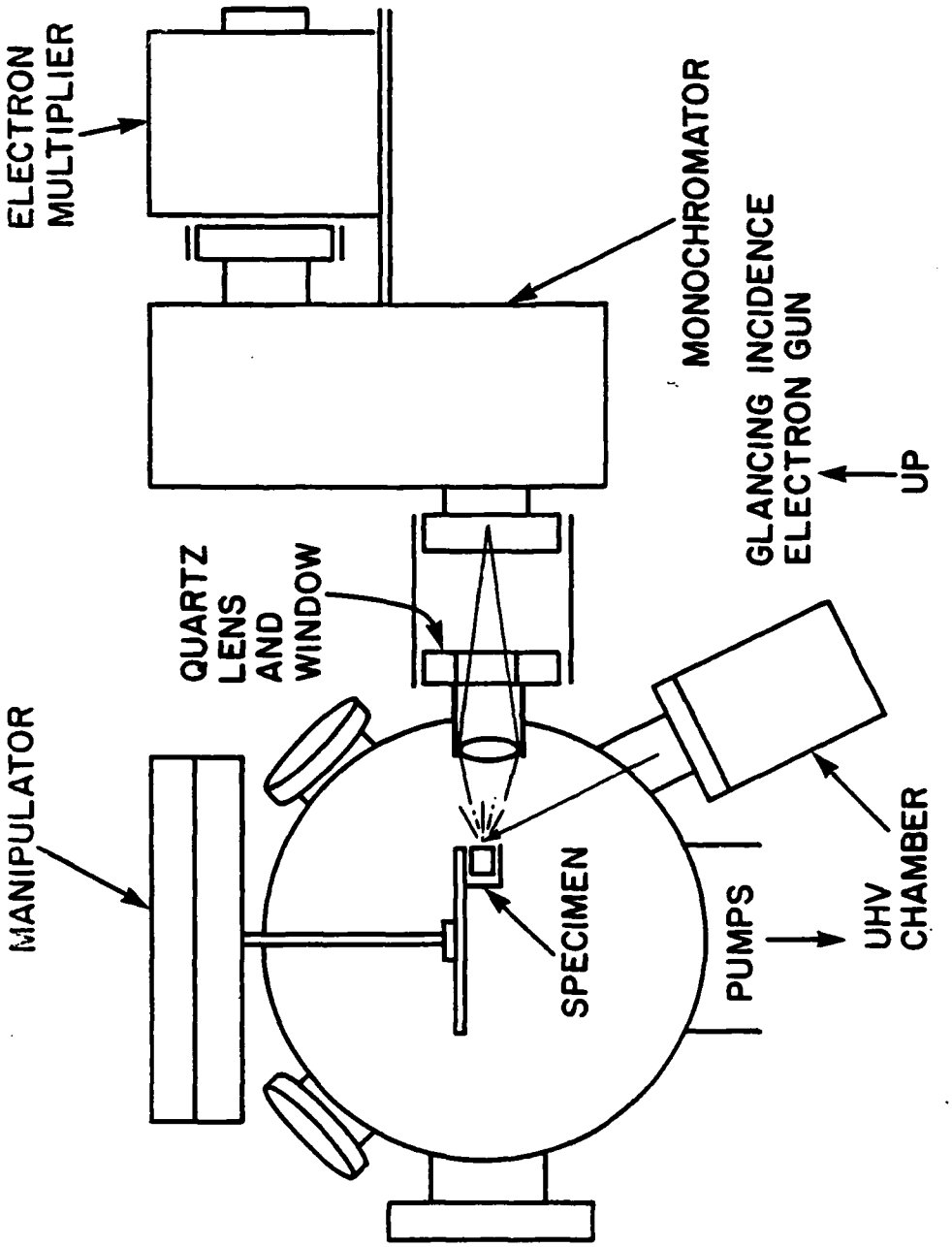
ELECTRON MULTIPLIER
MONOCHROMATOR
GLANCING INCIDENCE ELECTRON GUN
UP
QUARTZ LENS AND WINDOW
MANIPULATOR
SPECIMEN
PUMPS
UHV CHAMBER

Fig. 1

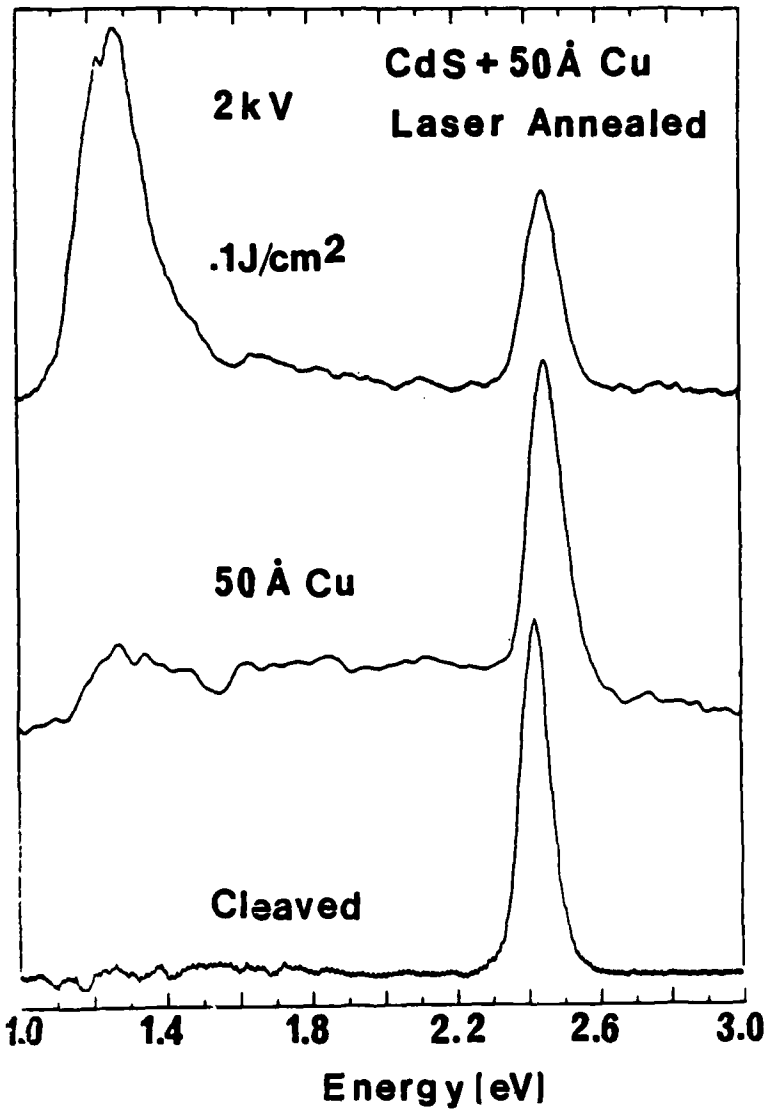
CdS + 50Å Cu
Laser Annealed
2 kV
.1J/cm2
50 Å Cu
Cleaved
1.0
1.4
1.8
2.2
2.6
3.0
Energy [eV]

Fig. 2

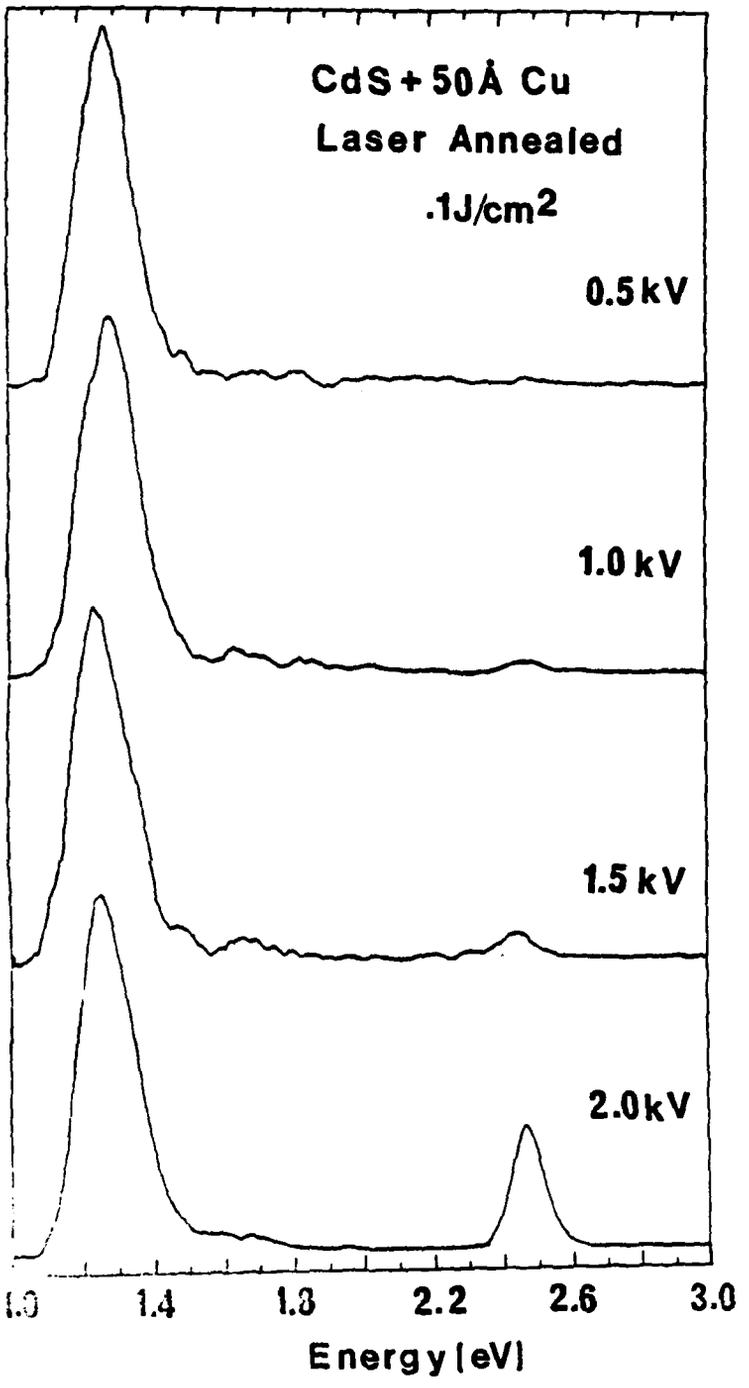
CdS + 50Å Cu
Laser Annealed
.1J/cm2
0.5kV
1.0kV
1.5kV
2.0kV
1.0
1.4
1.8
2.2
2.6
3.0
Energy (eV)

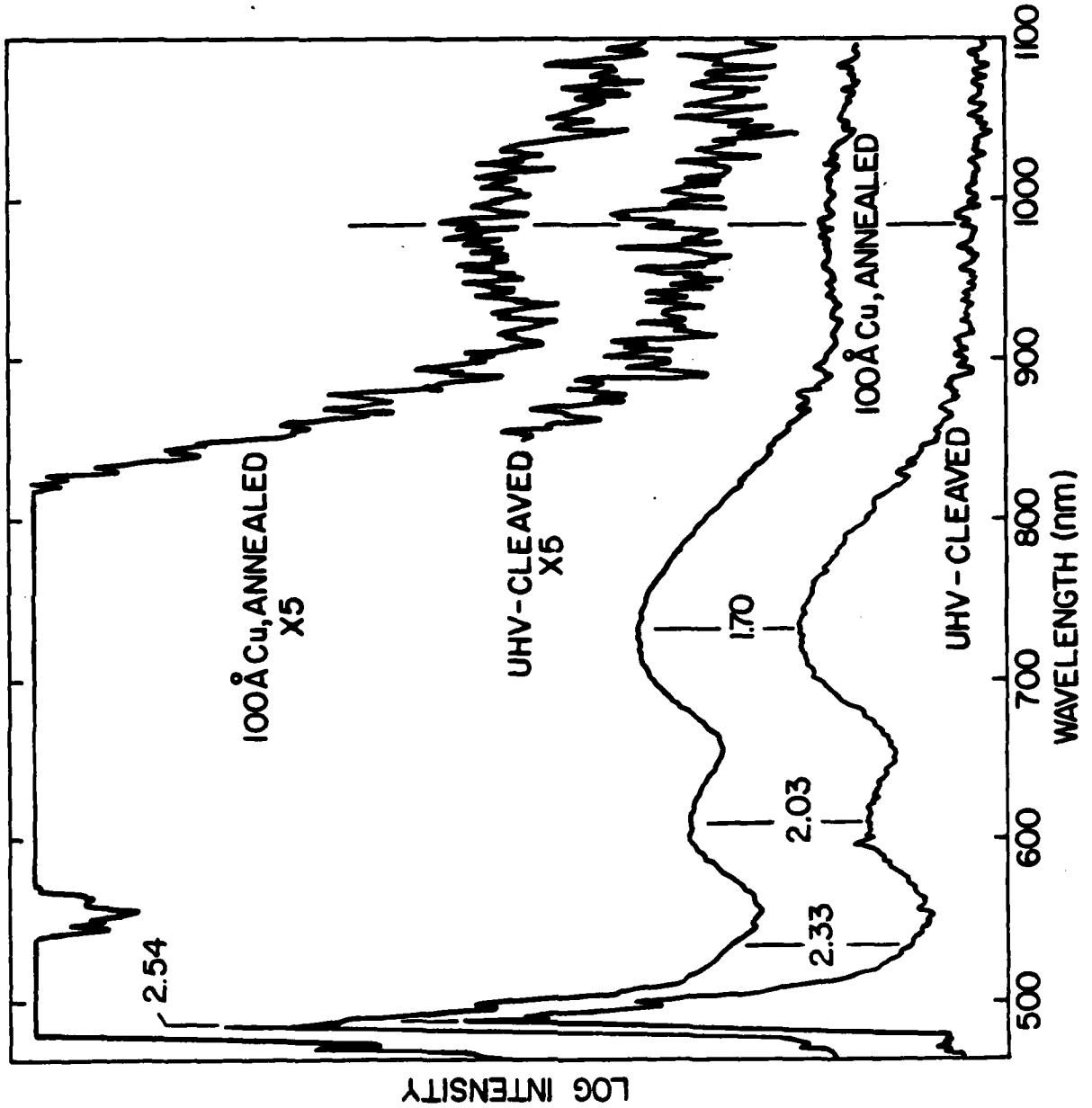
100Å Cu, ANNEALED
X5
UHV-CLEAVED
X5
100Å Cu, ANNEALED
UHV-CLEAVED
2.54
2.33
2.03
1.70
500
600
700
800
900
1000
1100
WAVELENGTH (nm)
LOG INTENSITY

Fig. 4

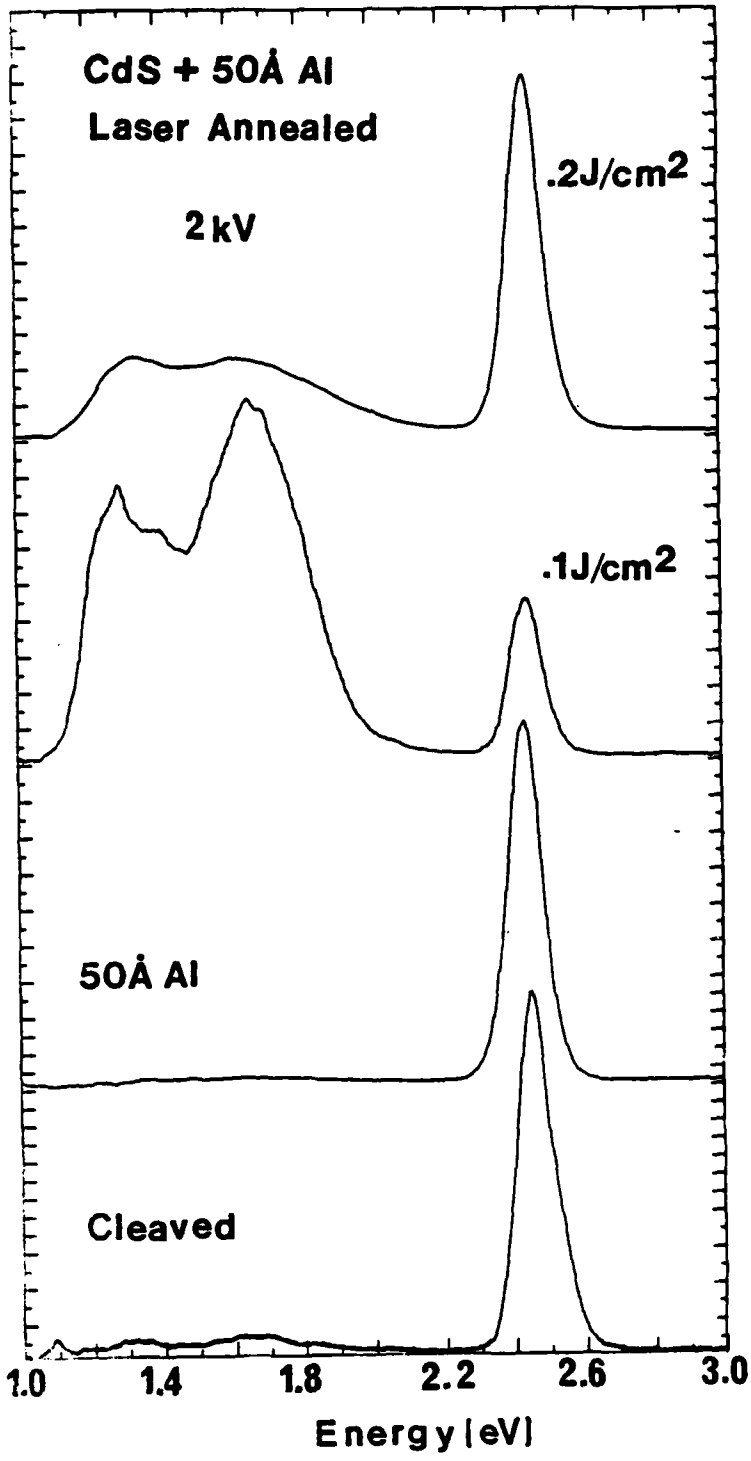
CdS + 50Å Al
Laser Annealed
2kV
.2J/cm2
.1J/cm2
50Å Al
Cleaved
1.0
1.4
1.8
2.2
2.6
3.0
Energy [eV]

Fig. 5

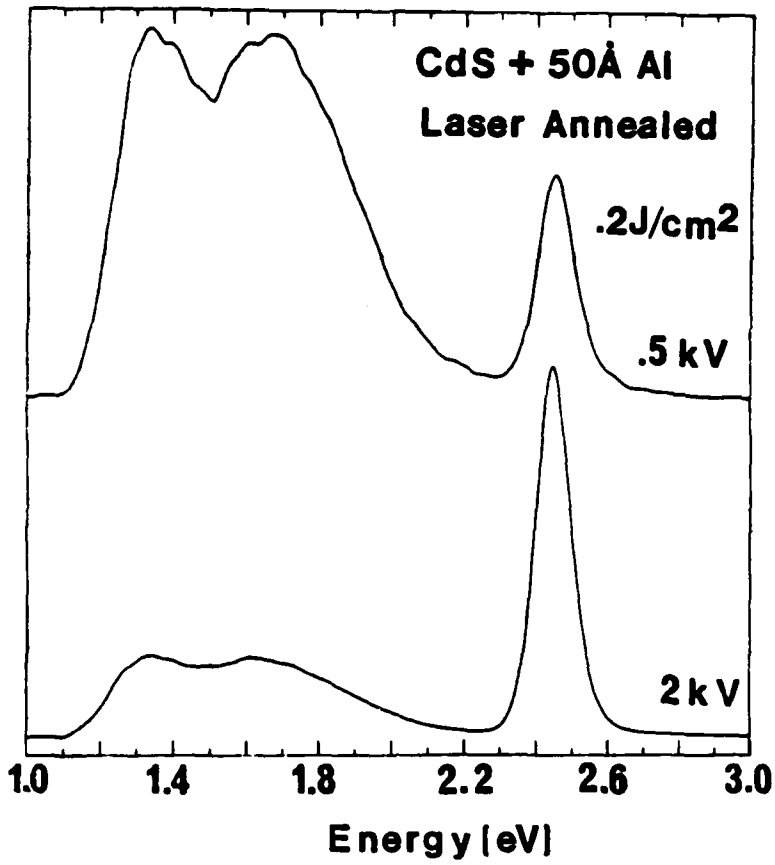
CdS + 50Å Al
Laser Annealed
.2J/cm2
.5 kV
2 kV
1.0
1.4
1.8
2.2
2.6
3.0
Energy [eV]

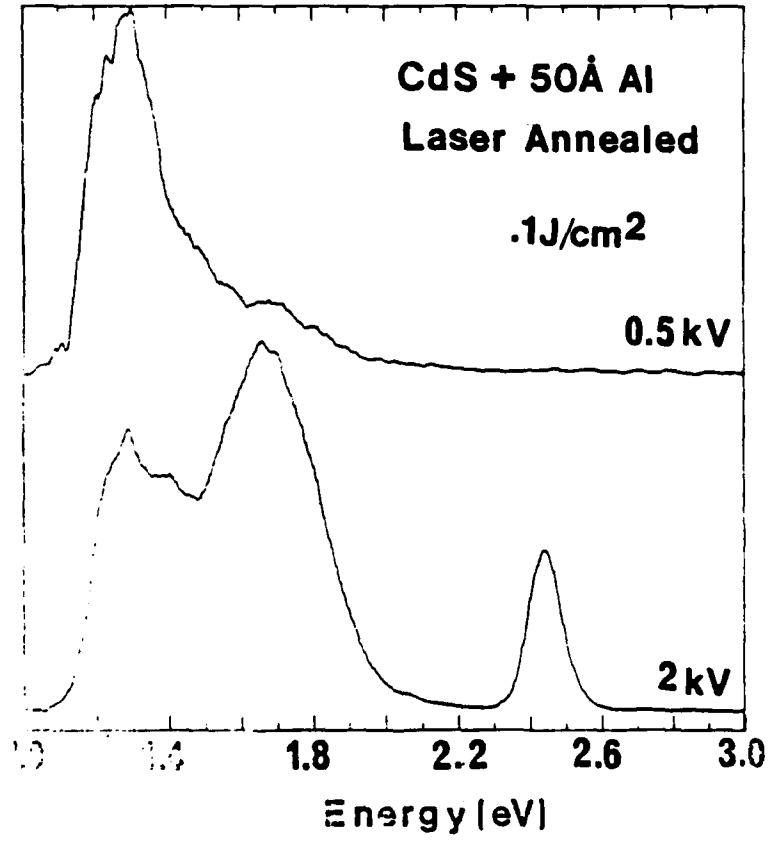
CdS + 50Å Al
Laser Annealed
.1J/cm2
0.5 kV
2 kV
1.8
2.2
2.6
3.0
Energy [eV]

Advances in Characterizing and Controlling Metal-Semiconductor Interfaces*

L. J. Brillson

Xerox Webster Research Center

800 Phillips Rd. W-114

Webster, NY 14580

Abstract

We have used a variety of novel approaches in characterizing metal-semiconductor interfaces - soft X-ray photoemission spectroscopy with interlayers or markers, surface photovoltage spectroscopy cathodoluminescence spectroscopy, coupled with pulsed laser annealing - to reveal new systematics between interface chemical and electronic structure. The chemical basis for these interfacial properties suggest new avenues for controlling electronic structure on a microscopic scale.

I. INTRODUCTION

With the application of surface science techniques to the study of metal-semiconductor interfaces, considerable progress has been achieved in understanding the interactions which take place at the microscopic junction and their influence on macroscopic electronic properties. [1-6] In particular, it is now generally accepted that the extrinsic electronic states of a metal-semiconductor interface - e.g. those due to some interaction between metal and semiconductor - rather than any intrinsic states present at the semiconductor surface-dominate the Schottky barrier formation. Considerable evidence for these conclusions has been derived from contact

*This work reported here was carried out in collaboration with C. F. Brucker, A. Katnani, M. Kelly, G. Margaritondo, H. Richter, Y. Shapira, M. Slade, and N. G. Stoffel.

potential,[7,8] surface photovoltage, low energy electron loss,[9,10] UV,[12,13] and soft X-ray photoemission spectroscopies.[14-21] With these techniques, research groups around the world have found strong charge transfer and atomic redistribution occuring with the deposition of only a few monolyers or less of deposited metal on clean, ordered semiconductor surfaces. Thus related phenomena such as chemical reactions, diffusion, formation of defects, dipoles, and alloy layers at the metal-semiconductor interface are observed which can account for Schottky barrier formation on an atomic scale. Within the last few years, this body of work has been extended to reveal further evidence that the strength and nature of chemical bonding plays a key role in forming interface electronic properties.

Our group has used soft x-ray photoemission spectroscopy (SXPS) to show that substantial differences exist between chemistry at metal interfaces with II-VI versus III-V compounds. Auger electron spectroscopy (AES) with depth profiling reveals pronounced segregation of anion and cation to the free metal surface and "chemical trapping" which depend strongly on metal-semiconductor reactivity. This chemical trapping leads to anion accumulation at the interface which can be associated with lower Schottky barrier heights. Surface photovoltage spectroscopy (SPS) provides direct observation of gap states at UHV-cleaved, metal-deposited, and wet-chemically-treated InP surfaces which correlate with the Fermi level pinning. For metals on Si, depth-dependent and marker studies of SXPS core levels demonstrate that atomic redistribution depends strongly on local chemical bonding and solubility. In some cases (e.g., Al-Si), more abrupt and lower resistance contacts than conventionally available may be prepared by UHV techniques.

The chemical basis for these interface properties suggests new avenues for controlling electronic structure on microscopic scale. These new directions involve modifying the diffusion and reaction processes which normally occur at the interfaces, either by introducing new chemical species (i.e., reactive interlayers[22] or gas ambients[23]), processing the metal-semiconductor interface at elevated temperatures and times sufficient to produce novel atomic rearrangment, or a combination of both. Another alternative not to be considered here involves epitaxial growth of interfacial structures having desired band gap, internal electric field, barrier, and doping density characteristics.[24,25] In order to prepare localized reacted layers with new dielectric properties without resorting to molecular beam

epitaxy or metallorganic chemical vapor deposition[26] techniques, we have employed pulsed lasers to anneal metal films on III-V and II-VI compound semiconductors. The new reacted species and electrically active impurity and defect levels induced can be analyzed *in situ through relatively thick (20-50Å) metal overlayers* using cathodoluminescence spectroscopy. Coupled with the other surface science techniques, these methods provide a means to characterize buried interfaces before and after high temperature annealing. Further the systematics uncovered provide new data with which to understanding and perhaps predict the corresponding changes in electronic properties.

2. SYSTEMATICS OF III-V VS. II-VI COMPOUND SEMICONDUCTOR/METAL INTERFACE CHEMISTRY

A variety of ultrahigh vacuum (UHV) techniques have shown that diffusion of anions and cations can occur at room termperature from a compound semiconductor into a metal overlayer.[27-29] For III-V compound semiconductors, the stoichiometry of this outdiffusion is sensitive to the chemical reactivity with the metal. Fig. 4 shows that the stoichiometry varies from anion-rich to cation-rich with increasing metal-anion heat of reaction ΔH_R.[30] ΔH_R values were calculated per metal atom for the reaction

$$M + (1/x)CA \rightarrow (1/x)[M_x A + C] \qquad (1)$$

so that

$$\Delta H_R = (1/x)[H_F(CA) - H_F(M_xA)] \qquad (2)$$

where ΔH_R is the difference in heat of formation[31-33] H_F for a compound semiconductor CA and the most stable metal-anion product M_xA, normalized per metal atom. In Fig. 4, the stoichiometry was measured as the ratio of integrated P 2p to In 4d core level intensities, as determined from SXPS. The difference is stoichiometry becomes more apparent with increasing thickness of deposited metal. The Fig. 4 inset[34] illustrates the ΔH_R associated with many of these metals, as well as their correlation with Schottky barrier heights ϕ_{SB}.[35] Fig. 4 demonstrates that anion (cation) rich diffusion corresponds to unreactive (reactive) outdiffusion and high (low) n-type ϕ_{SB}.

Using Auger electron spectroscopy (AES) with sputter depth-profiling, we have found an accumulation or deficiency of anion atoms at the formed metal-semiconductor interface depending on whether the interface couple are reactive or unreactive.[36] For 70Å Au on InP (110), Fig. 2a shows a P excess on the surface but an apparent excess of In within the Au interface and at the interior interface. Fig. 2b illustrates the effect of "reactive" metal interlayers on the In and P outdiffusion. Here the presence of a Ti interlayer results in a complete attenuation of P within Au film and at the free Au surface. Significantly however, the P intensity exceeds that of the In at the position of the Ti film (e.g., the metal-semiconductor interface). Analogous behavior occurs for other Ni and Ti interlayer thicknesses as well as for Al interlayers. Thick overlayers of reactive metals also produce preferential decreases of P relative to In in comparison to unreactive metals such as Au, Cu, or Ag.[37]

Our studies of chemical interdiffusion and reaction at metal/III-V compound semiconductor interfaces suggest a chemical basis for their Schottky barrier formation. For this class of semiconductors, the $\varnothing_{SB}$ values tend to fall into two energy categories. For the case of InP, the I-V data compiled by Williams et. al.[34] indicates a high and low energy range which are well-separated. For other III-V compounds such as GaP,[35] GaAs,[38] and narrower gap semiconductors,[39] the energy separation is smaller but nevertheless recognizable. The presence of two "plateau" values of $\varnothing_{SB}$ with few if any intermediate values for different metals suggests that the semiconductor Fermi level E_F is "pinned" at either of two levels within the band gap. A number of semiconductor defect models have been proposed to account for the formation of similar $\varnothing_{SB}$ with different adsorbates on III-V compounds,[40-45] although emphasizing a single pinning position for all adsorbates on the same n-type or the same p-type surface.[44,43] Several theoretical approaches have been employed to calculate the energies of simple native defects and defect complexes and are reviewed at this Conference by J. D. Dow and coworkers.[46] Nevertheless, very little information exists regarding the detailed nature of such defects. The data in Figs. 1 and 2 provide at least an indication of which defects are not likely (i.e., P vacancies at the P-rich Ti-InP interface) to form and contribute to Fermi level pinning. Furthermore, the separation of $\varnothing_{SB}$ levels into reactive and unreactive regimes[35] provides the basis for predicting and indeed controlling Schottky barriers on the basis of chemistry - as will be discussed later.

3. CONTROL OF II-VI AND III-V COMPOUND SEMICONDUCTOR BARRIERS

The II-VI compounds exhibit a qualitative difference in interface chemical behavior with respect to III-V compound semiconductors.[47,48] In addition, SXPS data for a large set of II-VI compounds shows that II-VI chemical behavior varies with compound ionicity, resembling III-V behavior with decreasing ionicity.[49,50] A major difference between these two classes of compounds is that the stoichiometry of outdiffusion does not appear to reverse with reactive vs. unreactive metals on the II-VI's as it does on the III-V's. Both semiconductor classes exhibit anion-rich outdiffusion into unreactive metals, but reactive metals appear to enhance anion outdiffusion and retard cation outdiffusion for many II-VI compounds instead of chemically trapping the anion as for III-V compounds.[48] Fig. 3 demonstrates that chemical behavior at II-VI/metal interfaces can vary, depending upon the semiconductor. Here SXPS anion and cation core level intensities have been normalized to their cleaved surface values. For Al interlayers between UHV-cleaved CdS ($10\bar{1}0$) surfaces and Au overlayers (Fig. 3a and b), the level of cation (Cd) outdiffusion decreases with increasing interlayer thickness at a given overlayer thickness while the anion levels increase. Cu interlayers produce a similar enhancement for CdS and CdSe.[29] For the same overlayer (Au) - interlayer (Al) depositions on ZnSe, a less ionic II-VI compound, the level of cation (Zn) again decreases in Fig. 3c. However, Fig. 3d shows that the anion (Se) intensity decreases as well, similar to behavior of III-V compounds. The behavior of all other II-VI compounds resembles that of either CdS or ZnSe Furthermore, the effect of the reactive metal interlayer varies monotonically with the semiconductor ionicity,[49,50] producing the most "chemical trapping" for the least ionic compound ZnTe and increasing the effect of reactive outdiffusion in the sequence ZnTe, CdTe, ZnSe, CdSe, ZnS, and CdS.[48]

The absence of II-VI stoichiometry reversal in our photoemission studies and wider $\varnothing_{SB}$ range of II-VI vs. III-V compound semiconductor/metal interfaces suggest that factors other than defect pinning can play a role in II-VI Schottky barrier formaton.

One such factor is a doping of the interface by localized cations.[29,51,52] The anion diffusion promoted by reactive metals leaves a preferentially cation-rich region near the metal-semiconductors interface. Dissociated cation features have been detected in photoemission spectra for Al on CdS,[53] CdSe[29], CdTe[47] and the Zn chalcogenides,[47] and Cu on CdS.[29,54] Since a cation excess within the semiconductor surface results in an increase in doping density, reactive metal overlayers and interlayers on II-VI compound semiconductors can give rise to a high doping and sharp band bending near the semiconductor surface. If this band bending reduces the width of the surface space charge region to the point at which tunneling occurs, then it can reduce the effective Schottky barrier height.

This rapid band bending is indeed observed for reactive interlayers of Al between Au and CdSe or CdS.[12] For example, a comparison of the Se 3d core linewidth for low surface sensitivity ($h\upsilon = 70$eV, escape depth = 90-100Å) vs high surface sensitivity ($h\upsilon$ = 130 eV, escape depth = 6-10Å) reveals an anomalous broadening when the subsurface Se contributes to the photoemission. Furthermore, such broadening is absent for Au-CdSe or Al-CdSe interfaces without an interlayer. Capacitance-voltage (C-V) measurements of the interfaces with Al interlayers reveal a narrowing of the surface space charge region and an increase in doping density.[12,56]

The extent of the doping can be controlled by the thickness of the reactive interlayer, leading to dramatic effects on the measured Schottky barrier height. Fig. 4 shows that very thin interlayers of Al between Au and UHV-cleaved CdS (10$\bar{1}$0) can change the Schottky barrier from 0.8eV to "ohmic". The softening of the otherwise rectifying characteristic requires only 2Å Al and appear to be controllable by even smaller (randomly distributed) Al deposits. Presumably, thicker Al deposits on CdS narrow the Schottky barrier width to zero. Williams et. al. has reported similar barrier lowering by Al interlayers for Au-CdTe interfaces as well.[57]

Control of Schottky barrier heights at metal/III-V interfaces is possible using reactive metal interlayers as well as gas ambients. For example, introducing a 10Å Al interlayer between Au dots or UHV-cleaned InP (110) produces a 0.1eV ϕ_{SB} decrease relative to Au-InP diodes without interlayers on the same semiconductor surface.[30] Montgomery *et al.* have described substantial decreases of InP-Au and Ag

barriers with exposure of InP to H_2S, Cl or H_20.[58,59] Massies *et al.* have reported a 0.4eV modulation of the Al-GaAs (100) $\varnothing_{SB}$ by H_2S exposure.[60,61] Grant *et al.* have used different surface treatments to produce at least four different pinning levels for Gats (110) and (100) which can range over 0.7eV - half the band gap.[62]

SXPS core level and electrical measurements appear to rule out localized doping at metal/reactive metal interlayer/III-V interfaces. Thus, localized cation doping provide an additional mechanism which extends the range of II-VI but not III-V $\varnothing_{SB}$ values, as observed experimentally.[39] Nevertheless, metal interlayers do affect the Schottky barrier values significantly and it appears that alternative processing by ambient gases can produce even larger shifts in the Fermi level pinning.

Associated with different surface treatments of compound semiconductors are surface states with different energies within the band gap. For example, surface photovoltage spectroscopy (SPS) and AES studies of UHV-cleaved (110) and chemically-treated (100) InP reveal direct optical transitions to and from a variety of states which correlate with Fermi level pinning behavior. These transitions can be identiied from the slope changes of the SPS features.[63] Figure 5 illustrates SPS features for InP (100) surfaces after etching in Br_2-methanol, Br_2-methanol, Br_2-methanol plus KAg $(CN)_2^-$ aqua-regia, aqua-regia plus Ag or Au, aqua-regia plus 10^{12} Langmuir oxygen exposure, as well as Ar^+ bombardment.[64] With the exception of Br_2-methanol and aqua-regia which produce similar spectra, each treatment results in a unique distribution of surface states. Thus Br_2 methanol etching produces states at 1.05eV above the valence band Ev, while subsequent immersion of the etched surface in KAg $(CN)_2$ - shifts this state and yields an additional state at 1.25ev below the conduction band E_c. Deposition of Au or Ag produce states at energies in good agreement with observed Fermi level E_f position of the macroscopic Schottky barrier.[34]

AES results indicate significant changes in stoichiometry and chemical bonding between the various surfaces in Fig. 5. The state produced by KAg $(CN)_2^-$ can be associated with formation of a volatile P compound and an In oxide surface layer. This layer provides an explanation for the reduced recombination velocity produced by KAg $(CN)_2^-$ treatment.[65] Ar^+ bombardment removes these features completely, thereby, demonstrating their surface nature. Coupled with the SPS effects are

changes in surface work function, consistent with E_f shifts. The three chemically-etched surfaces are all P-deficient, yet each exhibit a unique set of multiply-bonded P features. UHV-cleaved surfaces exhibit cleavage-dependent features and stoichiometry changes which can even affect the sign of band bending within the surface space charge region. SPS characterization provides a link between surface electronic states and chemical structure. Furthermore, the variation of electronic features with surface chemical preparation can account for the substantial effect of interfacial chemical processing on the Schottky barriers discussed above.

4. CHARACTERIZATION AND CONTROL OF METAL-Si INTERFACES

Another example of characterization and control of metal-semiconductor interfaces arises from SXPS studies of Al on Si. This interface is of widespread technological interest because of the widespread use of Al as interconnects in integrated circuit structures.[65] Despite the massive diffusion reported for the Al-Si interface at *relatively low temperatures* (400-450°C), SXPS core level spectra reveal that the Al-Si interface is abrupt to within only a few atomic layers at temperatures of 200°C or more. Fig. 6 illustrates Si 2p core level spectra taken as a function of (a) deposited Al thickness at constant photon energy $h\nu$ (130eV) and (b) $h\nu$ at constant thickness (20Å).[66] At $h\nu = 130$eV, photoelectrons excited from Si 2p core levels have a scattering length λ_e of only 4-6Å[67] and therefore yield highly surface-sensitive core level spectra. For $\lambda_e = 120$; 110; and 107eV, λ_e = 6-10Å, 10-20Å, and 20-50Å respectively, so that Fig. 6b represents 20Å Al on Si (111) with variable depth resolution. The initial deposition of 1Å Al on Si in Fig. 6a produces a core level shift to lower binding energy, consistent with an increase in n-type band bending. Further deposition attenuates the Si intensity and produces a shoulder at lower binding energy due to Si segregated at the free Al surface. The escape depth-dependent spectra in Fig. 6b confirm this relatively small segregation for the case of 20Å Al or Si (111). As $h\nu$ decreases, the escape depth increases. The surface contribution becomes a small portion of the sampled volume, and the shoulder disappears almost completely. This behavior is in contrast to metals such as Au, for which Si diffuses throughout the metal overlayer, and for which special features due

to the diffused Si do not change appreciably with probe depth.[68] Except for some increased Si segregation to the free Al surface, the SXPS Al-Si spectra do not change appreciably with elevated temperatures up to 600°C, near the Si-Al eutectic temperature of 577°C. Only above this point did we observe extensive Si-Al interdiffusion. At lower temperatures, SXPS data indicated negligible Si mixing within the Al overlayer, consistent with the low solubility of Si in Al.[69]

We performed marker experiments to identify the diffusing species for the limited Al-Si interdiffusion.[68] The marker layer between the metal and semiconductor was a 1Å layer of Ni, chosen for its strong bonding to Si.[70] Only a monolayer was used in order to minimize any effects on the interdiffusion process itself. These experiments are analogous to marker studies carried out via Rutherford backscattering and AES except that movement on a monolayer rather than a mirror scale is being probed. The movement of Si into the metal overlayer vs the movement of metal into the Si was monitored by the SXPS intensity ratio I_{Si}^{2p}/I_{Ni}^{3d} as a function of metal overlayer thickness. An increase in these ratios corresponds to diffusion of metal atoms past the Ni layer into the Si lattice. As shown in Fig. 7, the deposition of Al and Au lead to opposite changes in the I_{Si}^{2P}/I_{Ni}^{3d} ratio[68]. In the case of Al, the overall increase indicates Si outdiffusion only. For Au on Si, the decrease followed by an increase suggests that Au first diffuses into Si with the first few monolayers followed by predominantly Si diffusion into the Au overlayer at higher coverages. The qualitatively diifferent results for Au and Al suggest that the thin Ni marker does not significantly alter the interdiffusion processes.

The marker results for Al-Si interdiffusion are particularly significant since they coincide with predictions of the Si-Al binary phase diagram[69] - namely, that Al has no solubility in Si and that Si has but a limited solubility in Al below 577°C. Given the latter property, the SXPS results shown in Fig. 6 become significant since they confirm the limited interaction between Al and Si at temperatures below their eutectic point.

AES sputter depth profiles of thicker Al films on Si confirm the relatively abrupt nature of the Al-Si interface and suggest an explanation for more conventional results. Fig. 8a exhibits the depth profile for 200Å Al deposited in UHV on Si (100) after a 1250°C preanneal and a 400°C, 30-min post-anneal for 30 min[66]. The preanneal is known to yield clean, highly-ordered Si surfaces. Even after the post-

anneal, the Al-Si interface width (here taken between 10% - 90% Al and Si limits) is 200-400Å, e.g. orders of magnitude more abrupt than measured for conventionally-prepared interfaces.

By way of contrast, Fig. 8b demonstrates the effect of intentionally disordering the Si surface prior to Al deposition with a 5kV Ar^+ bombardment. As shown, Si diffuses through the Al overlayer with no evident attenuation. The resultant Si concentration in Al is 100 times its solid solubility at 400°C. Thus lattice disorder, strain and/or Ar^+ intersitials produced by Ar^+ bombardment promote a massive outdiffusion into Al. These results suggest that contact interpenetration of the semiconductor, one of the limiting factors in preparing submicron devices, may be overcome without the need for complex metallic diffusion barriers. Indeed, we have been able to form ohmic contacts between Al-Si which are abrupt on a scale of nonometers simply by depositing Al on preannealed Si in UHV.

5. LASER ANNEALED METAL-SEMICONDUCTOR INTERFACES

Another approach to controlling chemical and electronic properties at metal-semiconductor interfaces is to prepare localized reacted layers with new dielectric properties. Using pulsed laser annealing, metal films on compound semiconductors can be heated to their melting point and reacted without substantial diffusion taking place. For example, using pulsed UV excimer lasers, such results are acheivable because of the short pulse widths (5n sec), fast thermal relaxation (~100n sec), and associated shallow absorption depths (~1000Å). We have studied the systematics of such laser-induced interface reactions and have been able to produce new interfacial phases over only a few hundred Å or less. Figure 9 shows the Al 2p SXPS core level spectra for 20Å Al on UHV-cleaved InP as a function of input energy density[71]. Besides the major contribution from the metallic Al, we observe a wing of significant intensity at lower kinetic energy. This spectrum agrees with earlier observations which indicate that Al reacts with the InP substrate and Al-P bands are formed at the Al-InP interface. With increasing energy density, we observe little or no change in the Al 2p (or the In 4d and P 2p) spectra at 0.1 J/cm^2, a shift to higher binding

energy of the major Al 2p intensity distribution between 0.17 J/cm^2 and 0.3 J/cm^2, and a reappearance of the In4d and P2p substrate features (not shown) for higher energy densities. Thus we find an energy window in which it is possible to react the entire Al overlayer without disrupting the surface morphology. Contrary to laser-annealing experiments of free III-V semiconductor surfaces, we find no significant loss of anion.

AES sputter profiling of the laser-annealed metal-semiconductor interface demonstrates the highly localized structure of the reacted layer. Fig. 10 illustrates the sputter-depth profile of a 50Å Al overlayer in InP annealed with an energy density of 0.14 J/cm^2 [72]. We observe a slight In segregation at the surface, a region of constant composition (8-32 min) sputter time, a very gradual decrease in Al concentration (40-80 min) and a rather sharp drop-off of the Al concentration above 80 min. This rapid drop is remarkably abrupt, considering the expected smearing of the Al boundary by the anion beam mixing and because the surface was annealed by multiple laser shots. The Al concentration above 100 min sputter time is an upper limit and is considered negligible. Given the average Al concentration of 25% of the initial 50Å Al deposit, we may conclude that the reaction and diffusion of the Al overlayer is well defined with a steep edge and is localized to a depth of 200Å. The formation of thin reacted layers at metal-semiconductor interfaces may provide a new method for controlling Schottky barriers if one can obtain desirable dielectric properties. For Al/InP interfaces annealed by a pulsed excimer laser, J-V characteristics with Al cover electrodes indicate substantial changes in apparent barrier height, interface state density, and ideality factor which require further analysis[73]. Such characteristics may depend sensitively on the detailed conditions of pulsed laser annealing.

6. "BURIED" METAL-SEMICONDUCTOR INTERFACES

While considerable progress has been made in characterizing metal monolayers on semiconductors by surface sensitive techniques, new approaches must be developed to probe the "buried" interface under thick metal overlayers. Such analysis is

particularly important in characterizing chemical and electronic structure of interfaces at elevated temperature, for which chemical interactions can easily extend over hundreds of Å or more. The associated changes at the initial contact can be detected only by techniques which probe below the free surface, and to detect features at particular depths require even further control. Raman spectroscopy has recently been extended to studying new interfacial phases at annealed compound semiconductor[74] and Si/metal[75] interfaces. Electric field-induced Raman scattering may also provide a measure of the band bending within the semiconductor's surface space charge region. Inverse photoemission spectroscopy provides another method for observing band structure via electron-beam induced luminescence. We have used a lower energy luminescence technique cathodoluminescence spectroscopy (CLS) - to demonstrate the value of subsurface interface analysis. Fig. 11 exhibits CLS spectra for UHV-cleaved CdS ($10\bar{1}0$) before and after 50Å Au deposition and pulsed laser annealing.[76] The peak feature at 2.42eV is due to the band gap luminescence of CdS. Au deposition produces only a mild increase in signal at subgap energies, especially at ~1.3eV. Pulsed laser annealing (5ns, 308n sec, XeCl excimer laser) produces an intense feature at 1.27eV which can be identified with Cu_2S formation,[77] along with a weak shoulder at ~1.6eV. In contrast, laser annealing of 50Å Al on UHV-cleaved CdS ($10\bar{1}0$) produces a pair of peaks at 1.3-1.35 and 1.7eV which can be attributed to bulk defects. Furthermore, by varying the incident electron beam energy, CLS can emphasize the regions toward or away from the free surface. Thus, Fig. 12a illustrates a relative increase in the 1.3eV peak at more surface sensitive (0.5kV) *vs* more bulk-sensitive (2kV) excitation energies. Note that for 0.5kV excitation, both laser induced features are enhanced relative to the bulk gap luminescence. The reannealing of this surface at $0.2J/cm^2$ changes the relative intensities of these peaks. Both lower energy peaks are reduced relative to the gap luminescence and the preferential enhancement of the 1.3eV feature at 0.5kV is also removed. This indicates a preferential reduction in density of 1.3eV transitions near the twice-annealed surface. Comparison of Figs. 11 and 12 demonstrate the influence of different metal overlayers and annealing processes on the resultant interface electronic structure.

The results of the past several years suggest that new techniques must be applied to characterize the electronic and chemical structure of metal-semiconductor interfaces in greater detail. Besides "buried" interface methods, high resolution microscopy

techniques can be employed to define interface structure on an atomic scale and to identify structural influences on Schottky barrier formation. Scanning Auger microscopy can provide valuable determination of overlayers films in the lateral dimension especially at elevated temperatures where grain boundaries, precipitates, and other phases can play an active role in reaction and diffusion. Extended X-Ray Fine Structure (EXAFS) experiments of near-interface atoms may also provide evidence for new bonded phases and possibly the structure of interfacial defects.

The chemical basis for the interface properties presented in this paper suggest new avenues for controlling electronic structure on a microscopic scale. In addition to these techniques, other new methods include rapid thermal annealing to drive chemical reactions selectively, ion implantation to alter surface doping and conductivity of electronic materials, and the use of epitaxially-grown semiconductor interfaces (via molecular beam epitaxy or metallorganic chemical vapor deposition) to design interface band structure and doping to order. Thus a wide variety of opportunities exist for characterizing and controlling metal-semiconductor interfaces which, over the next few years, should add to our knowledge of these complex materials systems.

7. ACKNOWLEDGMENTS

This work was supported in part by the Office of Naval Research (Grant No. 000 14-80-C-0778) and is gratefully acknowledged.

Figure Captions

Fig. 1 SXPS ratio of surface anion/cation core level intensities I_P^{2p}/I_{In}^{4d} versus Ag, Pd, Cu, Au, Al, Ti, or Ni coverages in InP (110) relative to its UHV-cleaned surface ratio. $\varnothing_{SB}$ versus ΔH^R is plotted in the inset (after Williams *et. al.*[34]). This plot illustrates the correspondence between $\varnothing_{SB}$ and the stoichiometry of outdiffusion (After Brillson *et al.*[30]).

Fig. 2 AES Au, In, P, and Ti interlayer metal depth profiles for a) 70Å Au - InP (110) and b) 70Å Au - 10Å Ti-InP (110) interfaces (after Shapira and Brillson).[36] Arrows indicate the relative anion/cation excess near the interior interfaces.

Fig. 3 Integrated SXPS peak areas for a) Cd 4d, b) S 2p, c) Zn 3d, and d) Se 3d core levels as a function of coverage for different Al interlayer thicknesses. Each curve correspond to a different interlayer thickness. Intensities are normalized to the cleaned surfaces. Insets show corresponding diffusion of anions and cations through the metal. Al interlayers increase (decrease) anion outdiffusion for CdS (ZnSe) (after Brillson *et al.* [47,48]).

Fig. 4 J-V characteristics of the Au-CdS (10$\bar{1}$0) Schottky diodes as a function of Al interlayer thickness. $\varnothing_{SB}$ measured by capacitance-voltage techniques are given for each curve. Inset shows cross sectional schematic of interlayer structure (after Brucker and Brillson[56]).

Fig. 5 SPS features of p-InP (100) surfaces under various conditions. The monolayers (ML) of metal are vapor-deposited. The features labelled E_C-E (E_V+E) correspond to transitions to the conduction band (from the valence band) which depopulate (populate) the surface state.

Fig. 6 SXPS Si 2p core level spectra for Al deposited on UHV-cleaned Si (111) surfaces as a function of (a) deposited Al thickness at constant photon energy $h\upsilon$ (130eV) and (b) $h\upsilon$ at constant thickness (20Å)

Fig. 7 SXPS intensity ratios of I_{Si}^{2p} (130eV)/I_{Ni}^{3d} (130eV) for Au and I_{Si}^{2p} (130eV)/I_{Ni}^{3d} (110eV) for Al overlayers on Si (100). Intensity ratios are arbitrarily normalized to unity at zero overlayer coverage.

Fig. 8 AES depth profiles for 200Å Al deposited on Si (100) in UHV after (a) high-temperature preanneal and a 400°C, 30-min post-anneal and (b) a 5-kV Ar^+ bombardment prior to Al deposition and a 400°C, 30-min post-anneal.

Fig. 9 Al 2p SXPS core level spectra taken at 120eV photon energy: 20Å Al in InP (110) surface as evaporated and after laser annealing with increasing energy density.

Fig. 10 Sputter depth profile of 50Å Al in InP annealed to an energy density of 0.14J/cm^2 per pulse. The excess In above 120 min is due to preferential sputtering of P.

Fig. 11 Cathodoluminescence spectra of UHV-cleaved CdS (10$\bar{1}$0) before and after 50Å Cu deposition and pulsed laser annealing at an energy density 0.1J/cm^2. Incident electron beam energy is 2kV.

Fig. 12 Cathodoluminescence spectra of UHV-cleaved CdS (10$\bar{1}$0) as a function of excitation depth for a 50Å Al overlayer annealed to 0.1J/cm^2 and 0.2J/cm^2 energy density. The 0.5kV vs 2kV beam energy corresponds to surface *vs* surface plus bulk excitation.

References

1. L.J. Brillson, Surf. Sci. Repts. 2 (1982) 123; L.J. Brillson, Int. J. Phys. Chem. Solids 44 (1983) 703.

2. G. Margaritondo, Solid St. Electron. 26 (1983) 499.

3. R.H. Williams, Contemp. Phys. 23 (1982) 329.

4. M. Schlüter, Thin Solid Films 93 (1983) 3.

5. A. Zunger, Thin Solid Films, 104 (1983) 301.

6. R.Z. Bachrach, in: Metal-Semiconductor Schottky Barrier Junctions. Ed. B. L. Sarma (Plenum, New York, 1984) in press.

7. J. Van Laar and J.J. Scheer, Surface Sci. 8 (1967) 342; A. Huijser and J. Van Laar, Surface Sci, 52 (1975) 202.

8. W. Mönch and H. Gant, Phys. Rev. Letters 48 (1982) 512.

9. L.J. Brillson, Surface Sci. 51 (1975) 45; L.J. Brillson, Proc. 13th Intern. Conf. on the Physics of Semiconductors, Ed. F.G. Fumi (Typografica Marves, Rome, (1975) p. 665.

10. J.E. Rowe, S.B. Christman, and G. Margaritondo, Phys. Rev. Letters 35 (1975) 1471.

11. L.J. Brillson, Phys. Rev. Letters 38 (1977) 245; L.J. Brillson, Phys. Rev. 18 (1978) 2431.

12. C.F. Brucker and L.J. Brillson, Thin Solid Films 89 (1982) 67.

13. P.S. Keath, I. Lindau, P.W. Chye, C.Y. Su, and W.E. Spicer, J. Vacuum Sci. Technol. 16 (1979) 1143.

14. For example, W.E. Spicer, I. Lindau, P. Skeath, and C.Y. Su, J. Vacuum Sci Technol. 17 (1980) 1019 and references therein.

15. L.J. Brillson, J. Vacuum Sci. Technol. 20, 652 (1982), L.J. Brillson, Proc. Brookhaven Conf. on Advances in Soft X-Ray Science and Technol., Eds F.J. Himpsel and R.W. Klaffky (SPIE, Bellingham, WA, 1984) p. 89.

16. G. Margaritondo and J.E. Rowe, J. Vacuum Sci. Technol. 17, (1980) 561.

17. R.S. Bauer and H.W. Sang, Jr., Surface Sci. 132 (1983) 479 and references therein; R.Z. Bachrach and R.S. Bauer, J. Vacuum Sci. Technol. 16 (1979) 1149 and references therein.

18 R.Z. Bachrach, Prog. Crystal Growth Charact. 2 (1979) 115 and references therein.

19. R. Ludeke, Surface Sci. 132 (1983) 143 and references therein.

20. G.W. Rubloff, Surface Sci. 132 (1983) 268 and references therein.

21 R.H. Williams, Surface Sci. 132 (1983) 122 and references therein.

22. L.J. Brillson, G. Margaritondo, and N.G. Stoffel, Phys. Rev. Letters 44 (1980) 667; L.J. Brillson, G. Margaritondo, N.G. Stoffel, R.S. Bauer, R.Z. Bachrach, and G. Hansson, J. Vacuum Sci. Technol. 17 (1980) 880.

23. V. Montgomery and R.H. Williams, J. Phys. C: Solid State Phys. 15 (1983) 5887.

24. L.F. Eastman, J. Physique C7 (1981) 263; A.Y. Cho, J. Vacuum Sci. Technol. 16 (1979) 275.

25. F. Capasso, J. Vacuum Sci. Technol. B1 (1983) 457; F. Capasso, Surface Sci. 132 (1983) 527.

26. R.D. Burnham, W. Streifer, and T.L. Paoli, J. Crystal Growth (1984 - in press).

27. A. Hiraki, K. Shuts, F. Kim. W. Kammura, and W. Iwami, Appl. Phys. Letters 31 (1978) 611 and references therein.

28. P.W. Chye, I. Lindau, P. Pianetta, C.M. Garner, and W.E. Spicer, Phys. Rev. B17 (1978) 2682.

29. C.F. Brucker and L.J. Brillson, J. Vac. Sci. Technol. 18 (1981) 617.

30. L.J. Brillson, C.F. Brucker, A.D. Katnani, N.G. Stoffel, and G. Margaritondo, Appl. Phys. Letters 38 (1981) 784.

31. D.D. Wagman, W.H. Evans, V.B. Parker, I. Halow, S.M. Bailey, and R.H. Schumm, NBS Technical Notes 270-3-270-7 (US GPO Washington, DC, 1968-1971).

32. K.C. Mills, Thermodynamic Data for Inorganic Sulphides, Selenides, and Tellurides (Butterworths, London, 1974).

33. O. Kubachewski, E.Ll. Evans, and C.B. Alcock, Mettalurgical Thermochemistry (Pergamon, New York, 1967).

34. R.H. Williams, V. Montgomery, and R.R. Varma, J. Phys. C11 (1978) L735.

35. L.J. Brillson, Phys. Rev. Letters 40 (1978) 260.

36. Y. Shapira and L.J. Brillson, J. Vac. Sci, Technol. B1 (1983) 618.

37. Y. Shapira, L.J. Brillson, A. Katroni, and G. Margoritondo (unpublished).

38. J.R. Waldrop, Appl. Phys. Letters 41 (1982) 350.

39. C.A. Mead, Solid State Electron 9 (1966) 1023, and references therein.

40. I. Lindau, P.W. Chye, C.M. Garner, P. Pianetta, and W.E. spicer, J. Vac. Sci. Technol. 15 (1978) 1332.

41. P.W. Chye, I. Lindau, P. Pianetta, C.M. Garner, and W.E. Spicer, Phys. Rev. B17 (1978) 2682.

42. H.H. Weider, J. Vac. Sci. Technol. 15 (1978) 1498.

43. R.H. Williams, J. Vac. Sci. Technol. 16 (1979) 1418.

44. W.E. Spicer, I. Lindau, P.W. Chye, P. Skeath, and C.Y. Su, J. Vac. Sci. Technol. 16 (1979) 1422.

45. W.E. Spicer, I. Lindau, P.R. Skeath, C.Y. Su, and P.W. Chye, Phys. Rev. Letters 44 (1980) 420.

46. J.D. Dow *et. al.*, this proceeding.

47. L.J. Brillson, C.F. Brucker, N.G. Stoffel, A.D. Katnani, R. Daniels, and G. Margaritondo, Physica 117/118B (1983) 848.

48. L.J. Brillson, C.F. Brucker, A.D. Katnani, N.G. Stoffel, R. Daniels, and G. Margaritondo, Surface Sci. 132 (1983) 212.

49. L. Pauling, The Nature of the Chemical Bond (Cornell Univ. Press, Ithaca, NY, 1939).

50. J.C. Phillips and J.A. Van Vechten, Phys. Rev. Letters 23 (1969) 1115; J.C. Phillips and J.A. Van Vechten, Phys. Rev. B2 (1970) 2147.

51. C.F. Brucker and L.J. Brillson, Appl. Phys. Letters 39 (1981) 96.

52. E.C. Freeman and J. Slowik, Appl. Phys. Letters 39 (1981) 96.

53. L.J. Brillson, R.S. Bauer, R.Z. Bachrach, and J.C. McMenamin, J. Vac. Sci. Technol. 17 (1980) 476.

54. N.G. Stoffel, R.R. Daniels, G. Margaritondo. C.F. Brucker, and L.J. Brillson, J. Vac. Sci. Technol. 20 (1982) 701.

55. C.F. Brucker, L.J. Brillson, A.D. Katnani, N.G. Stoffel, and G. Margaritondo 21 (1982) 590.

56. C.F. Brucker and L.J. Brillson, Appl. Phys. Letters 39 (1981) 67.

57. M.H. Patterson and R.H. Williams, J. Crystal Growth 59 (1982) 281.

58. V. Montgomery, R.H. Williams, and G.P. Srivastava, J. Phys. C: Solid St. Phys. 14 (1981) L191.

59. V. Montgomery and R.H. Williams, J. Phys. C; Solid State Phys. 15 (1982) 5887.

60. J. Massies, J. Chaplart, M. Laviron, and N.T. Linh, Appl. Phys. Letter 38 (1981) 693.

61. J. Massies, F. Dezaly, and N.T. Linh, J. Vac. Sci, Technol. 17 (1980) 1134.

62. R.W. Grant, J.R. Waldrop, S.P. Kowalczyke and E.A. Karut, J. Vac. Sci. Technol. 19 (1981) 477.

63. H.C. Gatos and J. Lagowski, J. Vacuum Sci. Technol. 10 (1973) 130; L.J. Brillson, Surface Sci, 69 (1977) 62.

64. L.J. Brillson, Y. Shapira, and A. Heller, Appl. Phys. Lett 43 (1983) 174.

65. See, for example, D. Pramanik and A.N. Saxena, Solid State Technol. 26 (1983) 127.

66. L.J. Brillson, M.L. Slade, A. D. Katnani, M. Kelly, and G. Margaritondo, Appl. Phys. Lett. 44 (1984) 110.

67. M.P. Seah and W.A. Dench 1 (1979) 1.

68. L.J. Brillson, A.D. Katnani, M. Kelly, and G. Margaritondo, J. Vacuum Sci. Technol. A2 (1984) 551.

69. M. Hansen, Constitution of Binary Alloys (McGraw-Hill, New York, 1958).

70. K.N. Tu and J.W. Mayer, in: Thin Films - Interdiffusion and Reactions, Ed. J.M. Poate, K.N. Tu, and J.W. Mayer (Wiley-Interscience, New York, 1978) p. 359.

71. H.W. Richter, L.J. Brillson, M.K. Kelley, R.R. Daniels, and G. Margaritondo, J. Vacuum Sci. Technol. B1 (1984) in press.

72. H.W. Richter and L.J. Brillson, Proc. 17th Int. Conf. on the Physics of Semiconductors (Springer-Verlog, New York, 1984) in press.

73. J. Slowik, H.W. Richter and L.J. Brillson, unpublished.

74. J.C. Tsang, J. Vacuum Sci. Technol, in press.

75. R.J. Nemanich, M.J. Thompson, W.B. Jackson, C.C.Tsai, and B.L. Stafford, J. Vacuum Sci. Technol B1 (1983) 519; R.J. Nemanich, this proceeding.

76. L.J. Brillson, H.W. Richter, M.L. Slade, B.A. Weinstein, and Y. Shapira, submitted to J. Vacuum Sci. Technol.

77. Von E. Kauer and A. Rabenau, Z. Naturforschg. 139 (1958) 531.

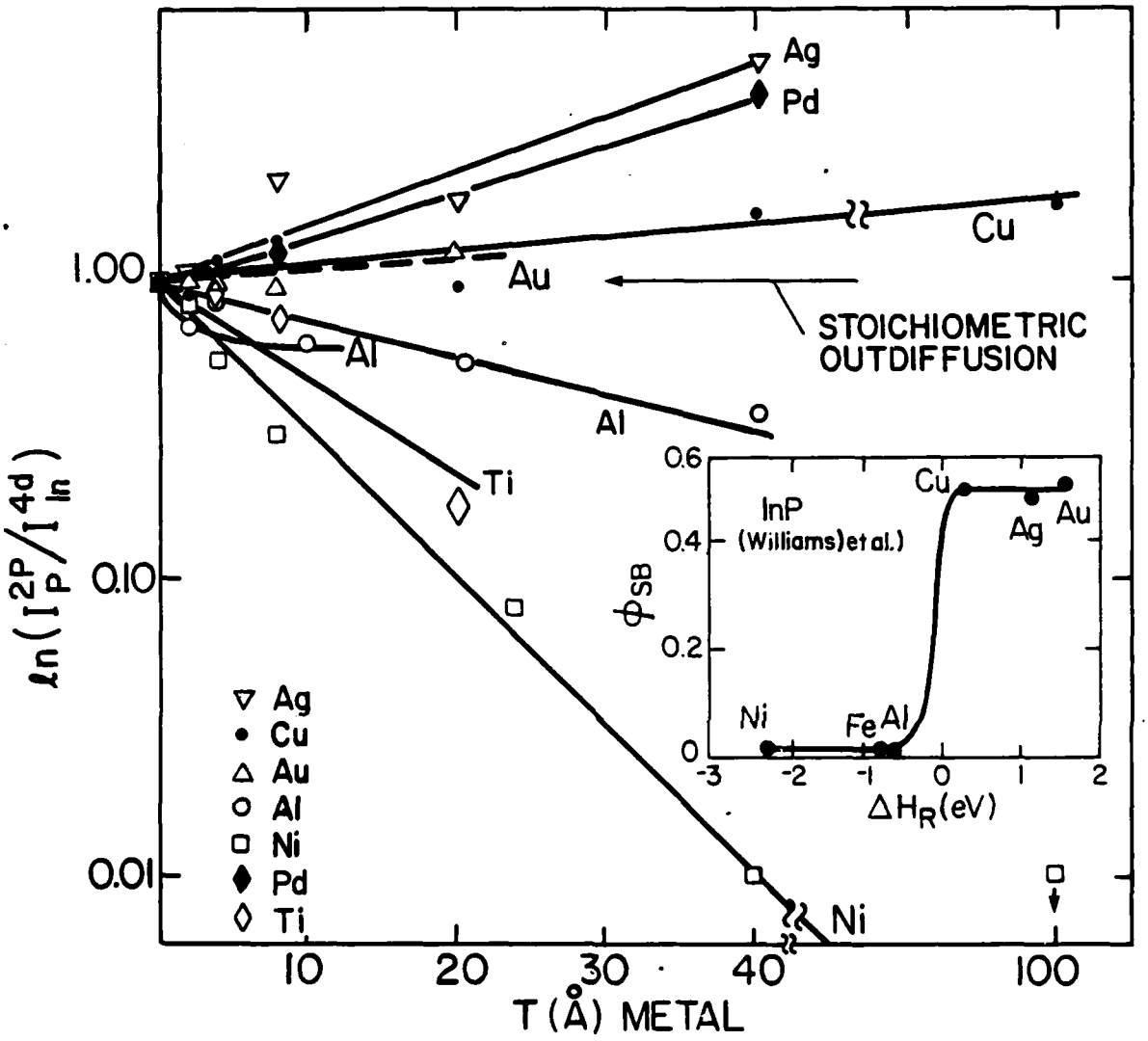
Ag
Pd
Cu
Au
STOICHIOMETRIC
OUTDIFFUSION
Al
Al
Ti
Ni
1.00
0.10
0.01
$\ln(I_P^{2P}/I_{In}^{4d})$
Ag
Cu
Au
Al
Ni
Pd
Ti
10
20
30
40
100
T (Å) METAL
InP
(Williams) et al.
ϕ_{SB}
0.6
0.4
0.2
0
Cu
Ag
Au
Ni
Fe
Al
-3
-2
-1
0
1
2
ΔH_R(eV)

Fig. 1

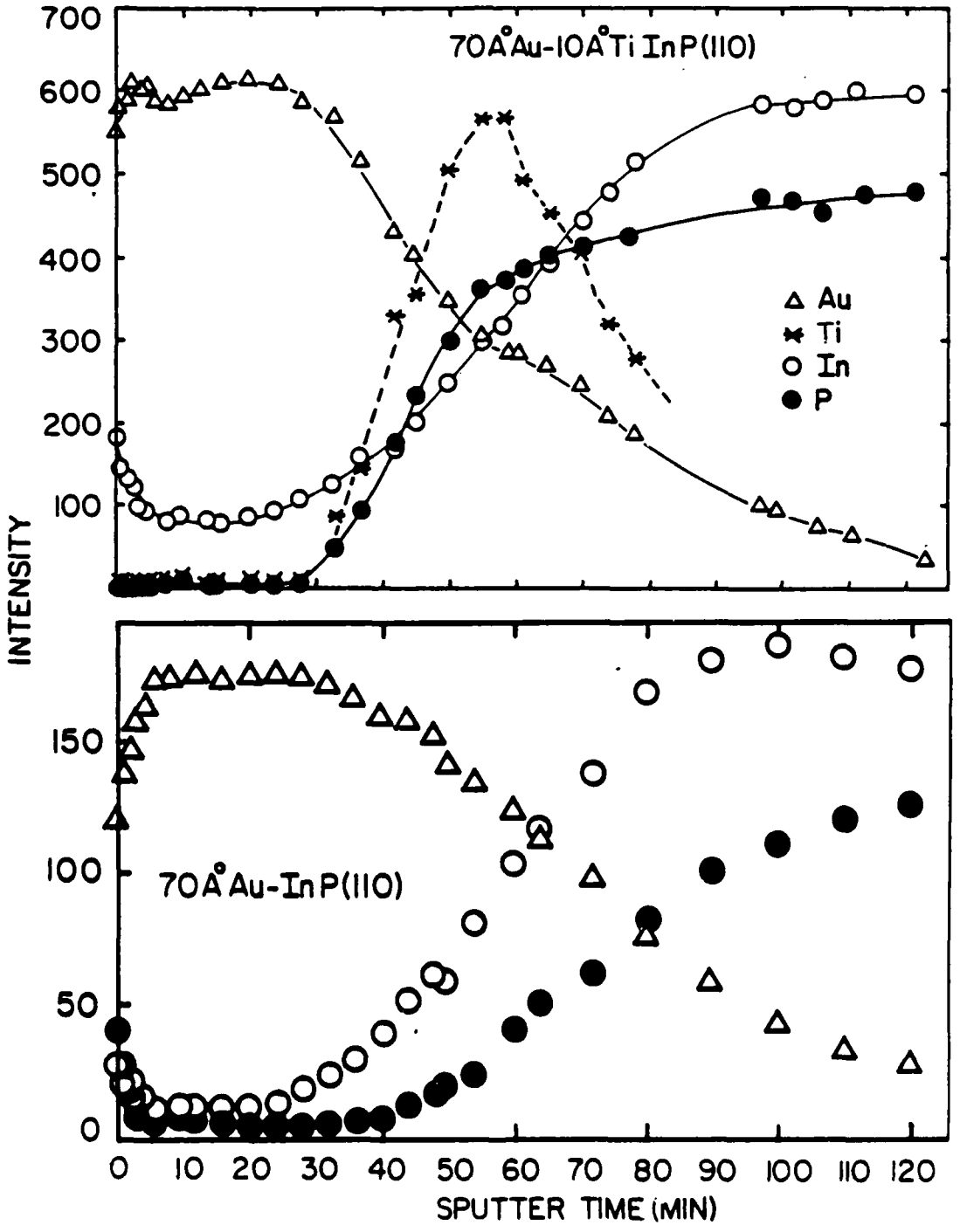
70Å Au-10Å Ti InP(110)
Au
Ti
In
P
INTENSITY
700
600
500
400
300
200
100
70Å Au-InP(110)
150
100
50
0
0 10 20 30 40 50 60 70 80 90 100 110 120
SPUTTER TIME (MIN)

Fig. 2

AD-A160 403 CHEMICAL BONDING INTERDIFFUSION AND ELECTRONIC STRUCTURE AT INP GAAS ANN SI--ETAL INTERFACES(U) XEROX WEBSTER RESEARCH CENTER NY L J BRILLSON 01 OCT 85 2/3

UNCLASSIFIED N00014-80-C-0778 F/G 20/12 NL

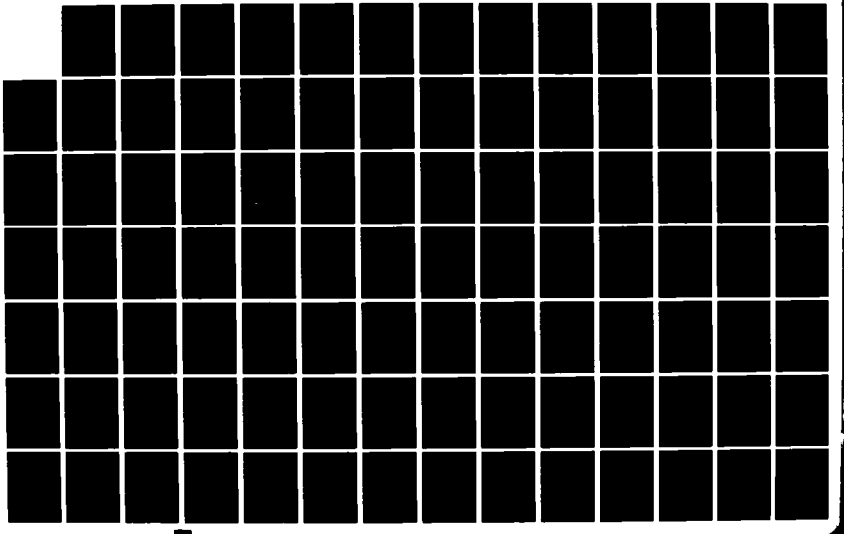

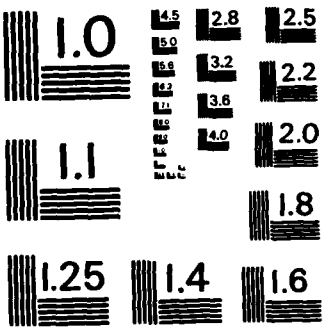

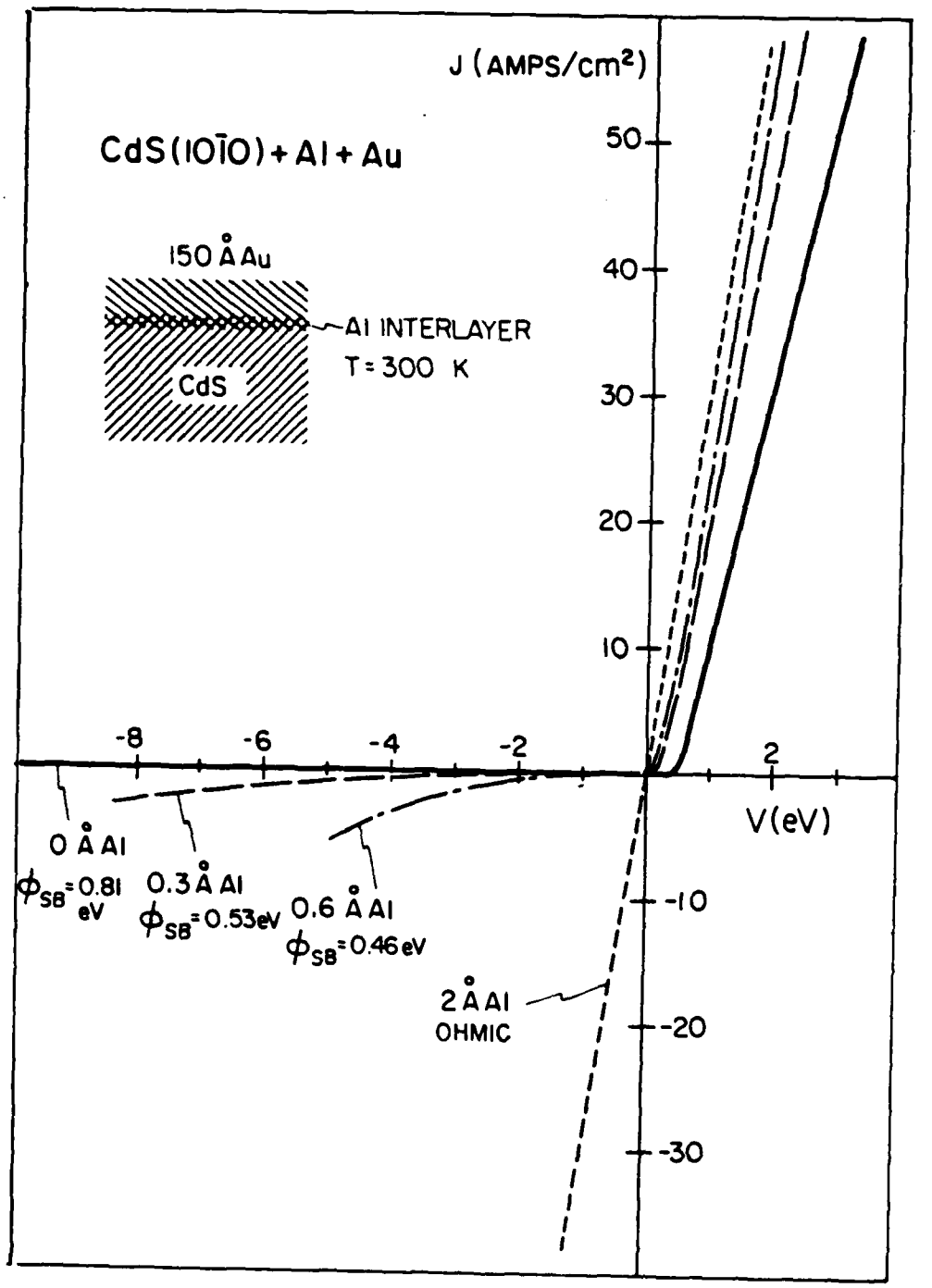
J (AMPS/cm²)
CdS(10$\bar{1}$0) + Al + Au
150 Å Au
Al INTERLAYER
T = 300 K
CdS
50
40
30
20
10
-8
-6
-4
-2
2
V(eV)
0 Å Al
ϕ_{SB} = 0.81 eV
0.3 Å Al
ϕ_{SB} = 0.53eV
0.6 Å Al
ϕ_{SB} = 0.46 eV
2 Å Al
OHMIC
-10
-20
-30

Fig. 4

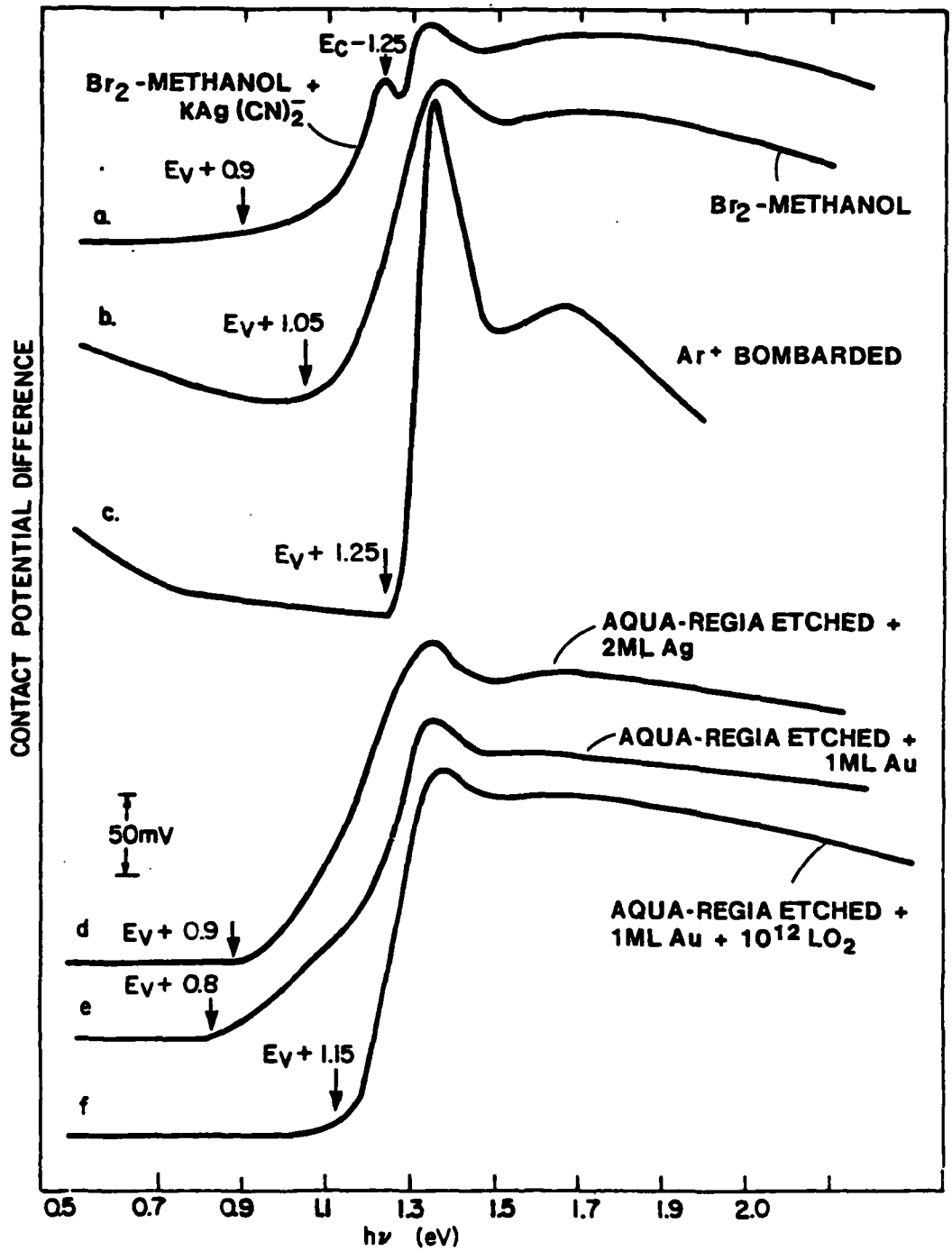
Ec-1.25
Br2-METHANOL + KAg(CN)2
Ev+0.9
a.
Br2-METHANOL
b.
Ev+1.05
Ar+ BOMBARDED
c.
Ev+1.25
AQUA-REGIA ETCHED + 2ML Ag
AQUA-REGIA ETCHED + 1ML Au
50mV
d Ev+0.9
Ev+0.8
e
Ev+1.15
f
AQUA-REGIA ETCHED + 1ML Au + 10^12 LO2
CONTACT POTENTIAL DIFFERENCE
0.5
0.7
0.9
1.1
1.3
1.5
1.7
1.9
2.0
hν (eV)

Fig. 5

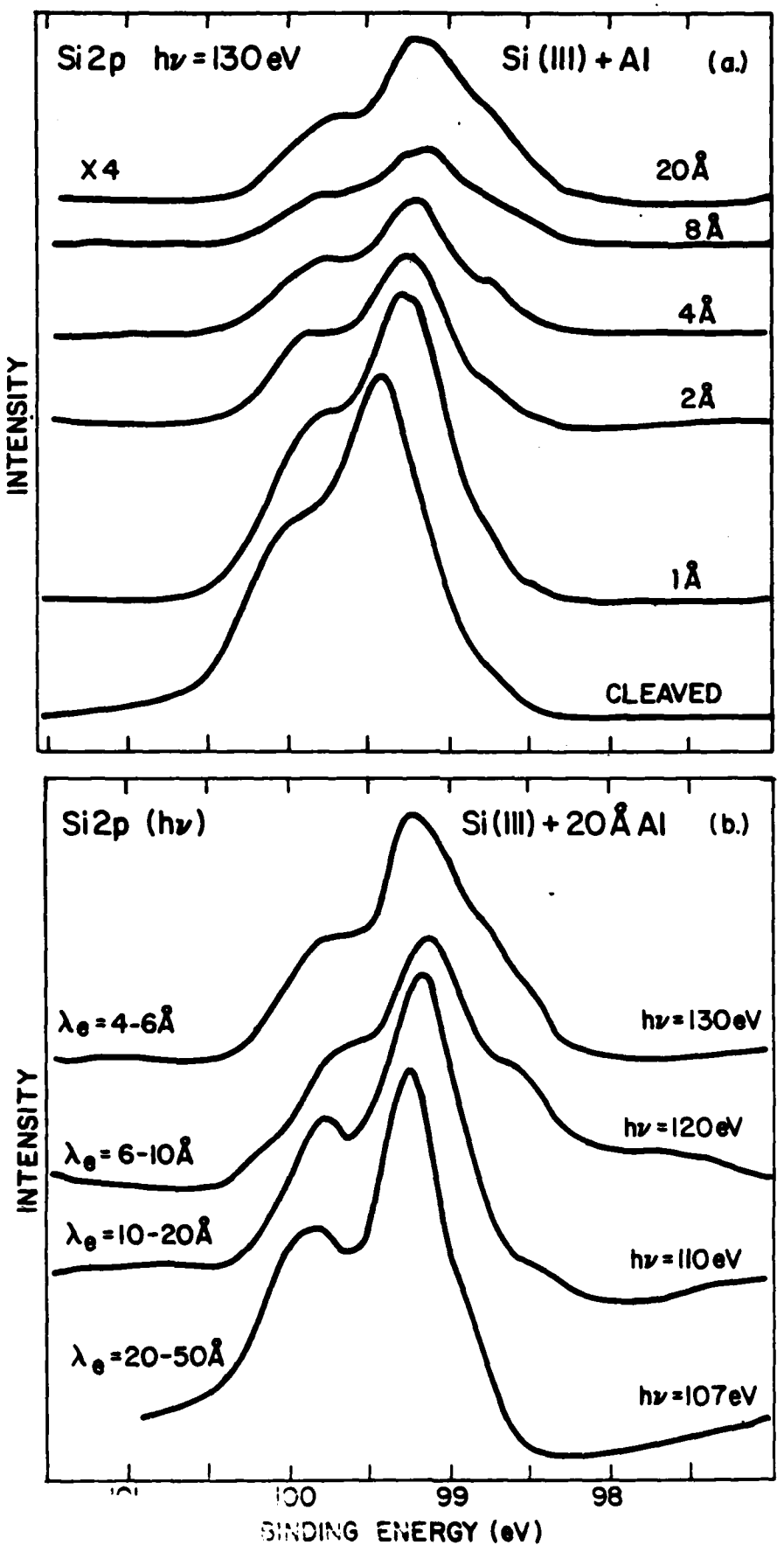
Si2p hν = 130 eV
Si (III) + Al
(a.)
X4
20Å
8Å
4Å
2Å
1Å
CLEAVED
INTENSITY
Si2p (hν)
Si(III) + 20Å Al
(b.)
λe = 4-6Å
hν = 130eV
λe = 6-10Å
hν = 120eV
λe = 10-20Å
hν = 110eV
λe = 20-50Å
hν = 107eV
INTENSITY
100
99
98
BINDING ENERGY (eV)

Fig. 6

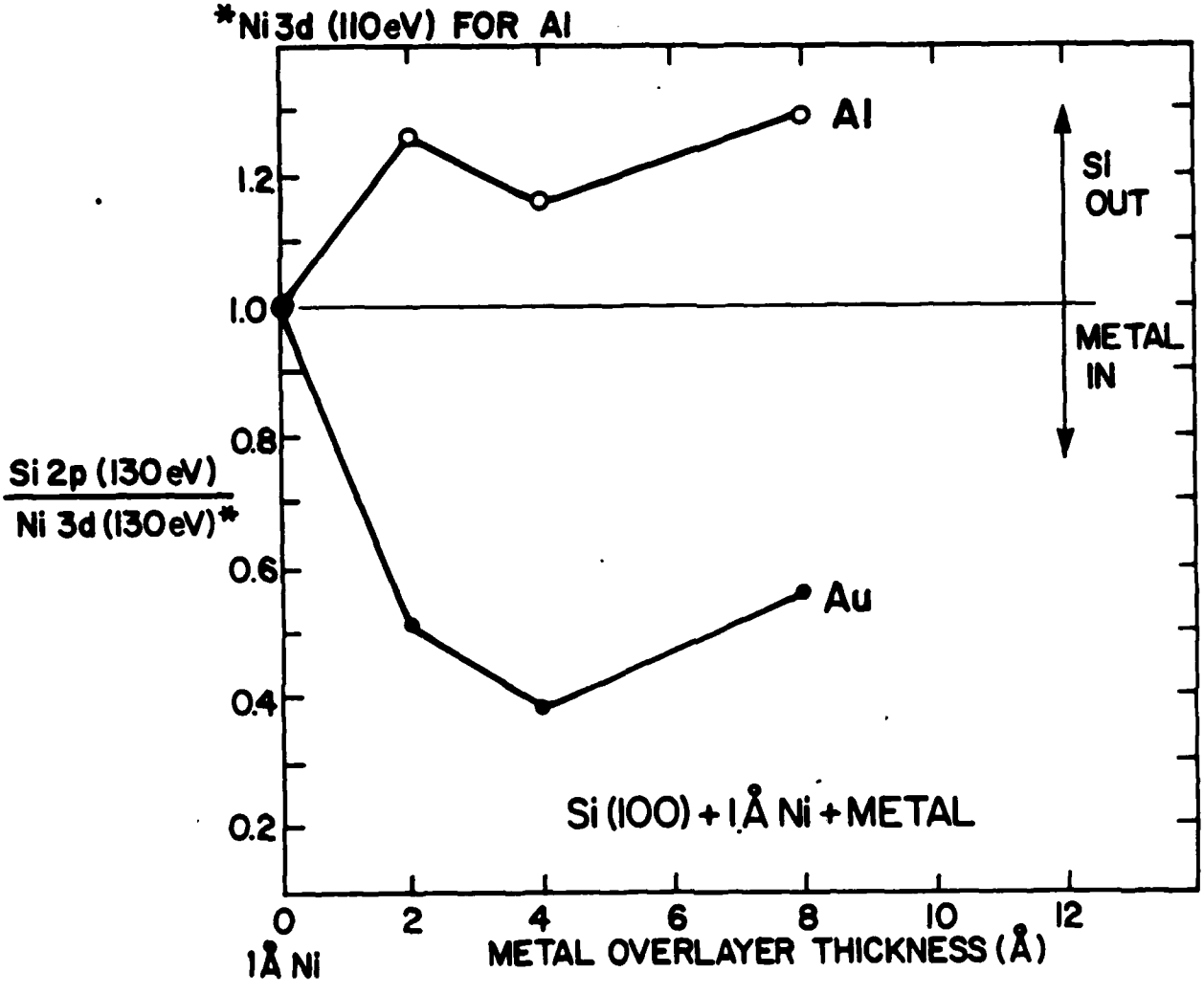
*Ni 3d (110eV) FOR Al
Al
Au
SI OUT
METAL IN
Si 2p (130 eV) / Ni 3d (130eV)*
1.2
1.0
0.8
0.6
0.4
0.2
Si (100) + 1Å Ni + METAL
0
2
4
6
8
10
12
1Å Ni
METAL OVERLAYER THICKNESS (Å)

Fig. 7

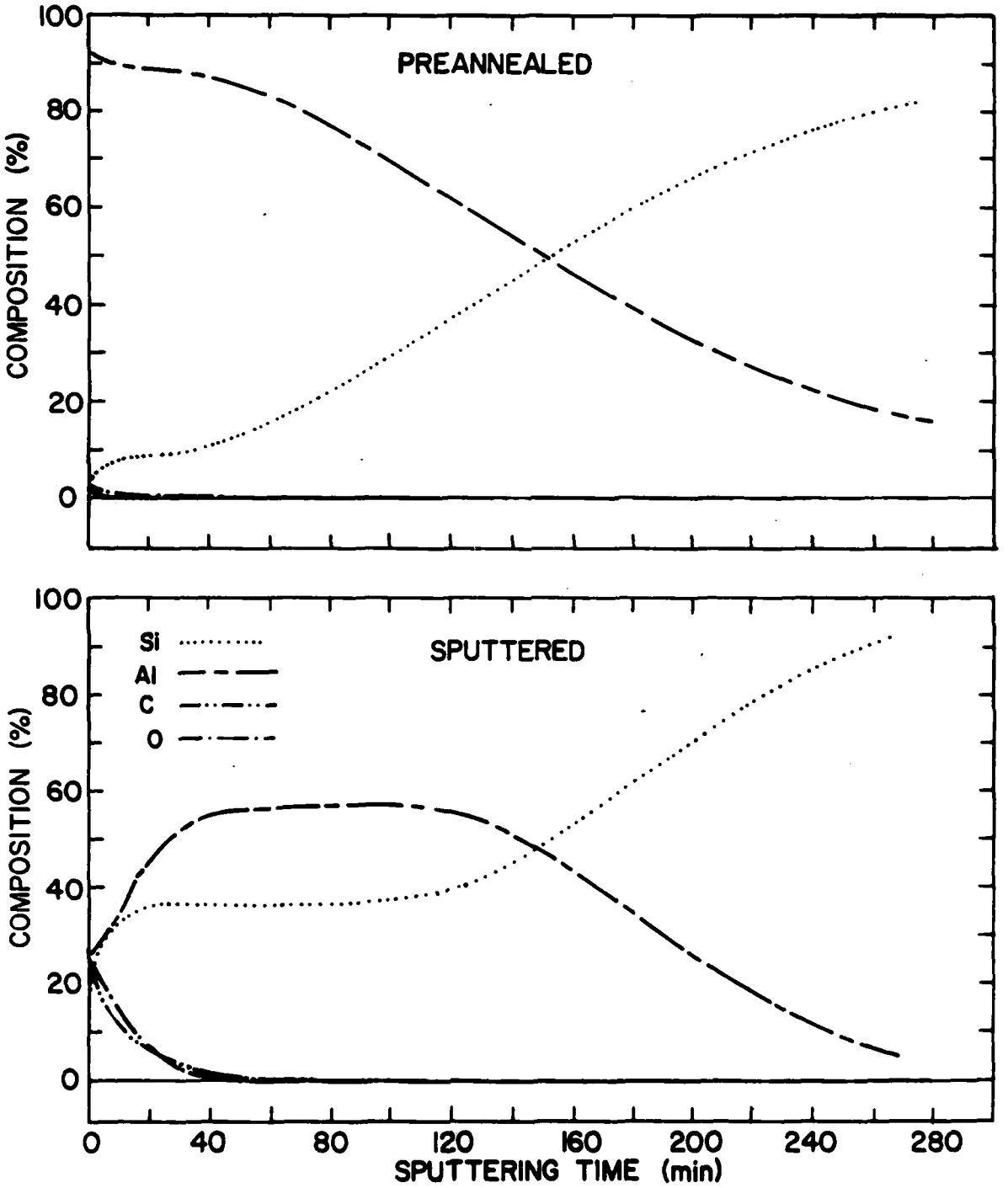
PREANNEALED
SPUTTERED
COMPOSITION (%)
100
80
60
40
20
0
Si
Al
C
O
0
40
80
120
160
200
240
280
SPUTTERING TIME (min)

Fig. 8

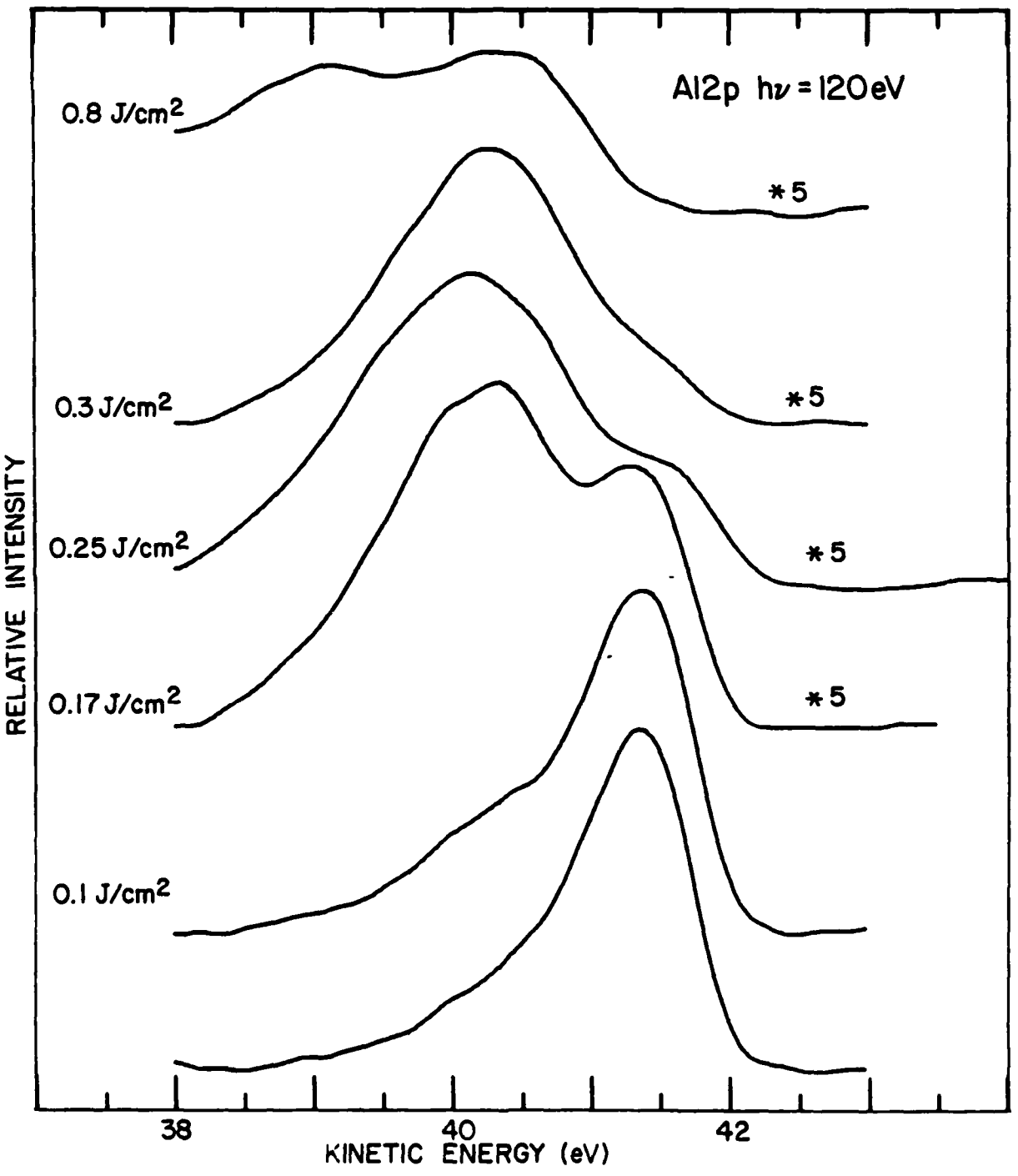
Al2p hν = 120eV
0.8 J/cm2
*5
0.3 J/cm2
*5
0.25 J/cm2
*5
0.17 J/cm2
*5
0.1 J/cm2
RELATIVE INTENSITY
38
40
42
KINETIC ENERGY (eV)

Fig. 9

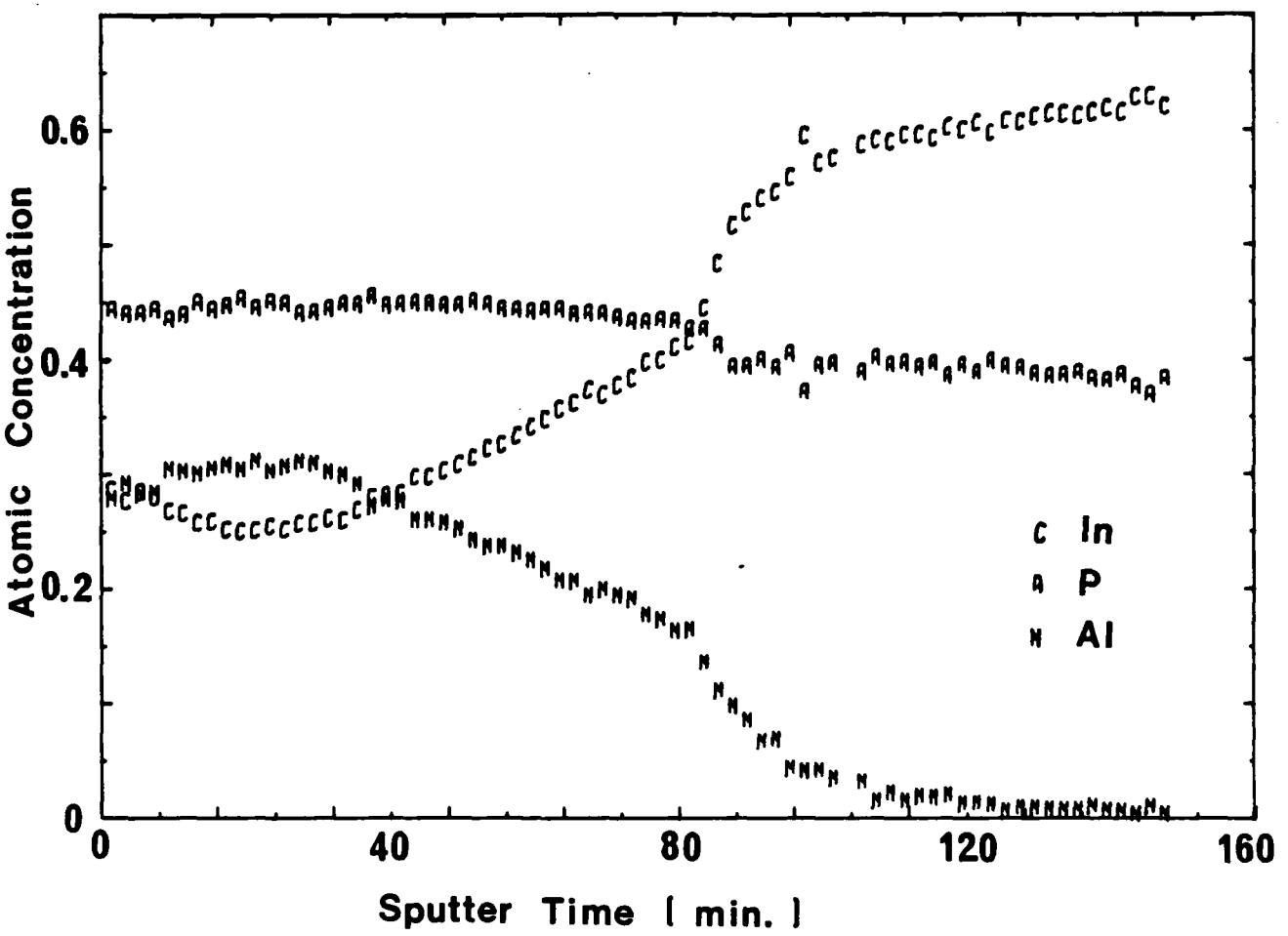
Atomic Concentration
0.6
0.4
0.2
0
0
40
80
120
160
Sputter Time (min.)
C In
A P
N Al

Fig. 10

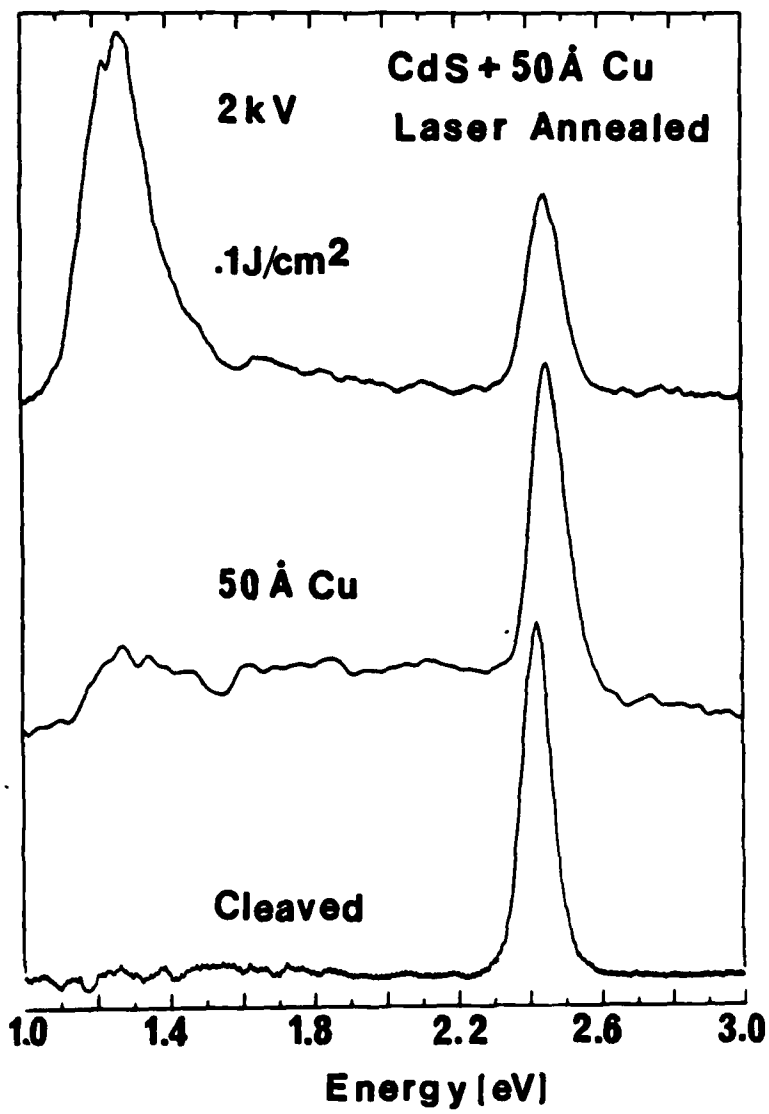
CdS + 50Å Cu
Laser Annealed
2kV
.1J/cm2
50 Å Cu
Cleaved
1.0
1.4
1.8
2.2
2.6
3.0
Energy [eV]

Fig. 11

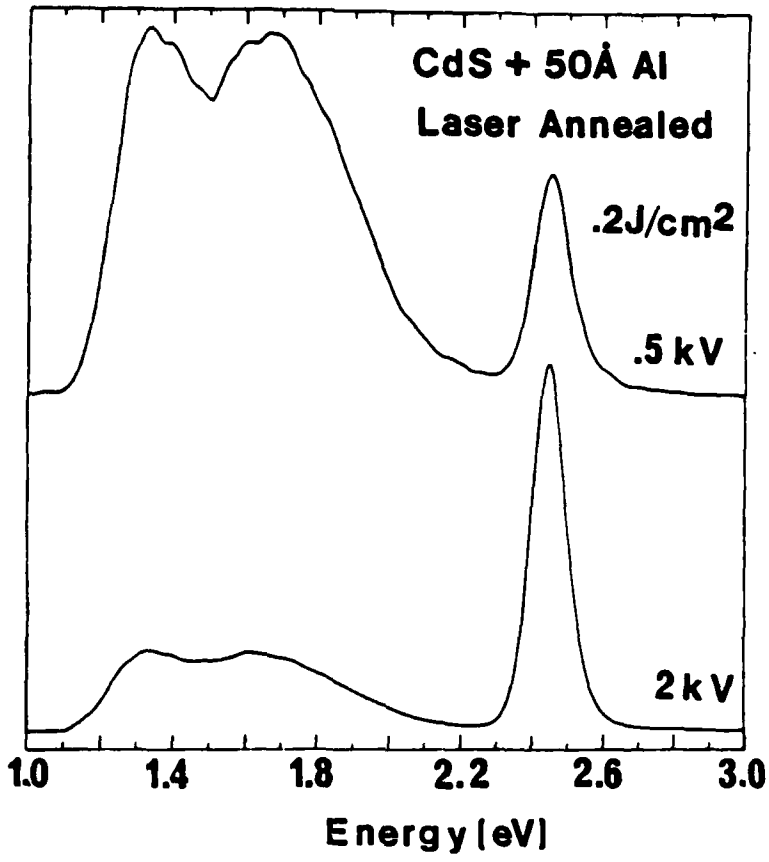
CdS + 50Å Al
Laser Annealed
.2J/cm2
.5 kV
2 kV
1.0
1.4
1.8
2.2
2.6
3.0
Energy [eV]

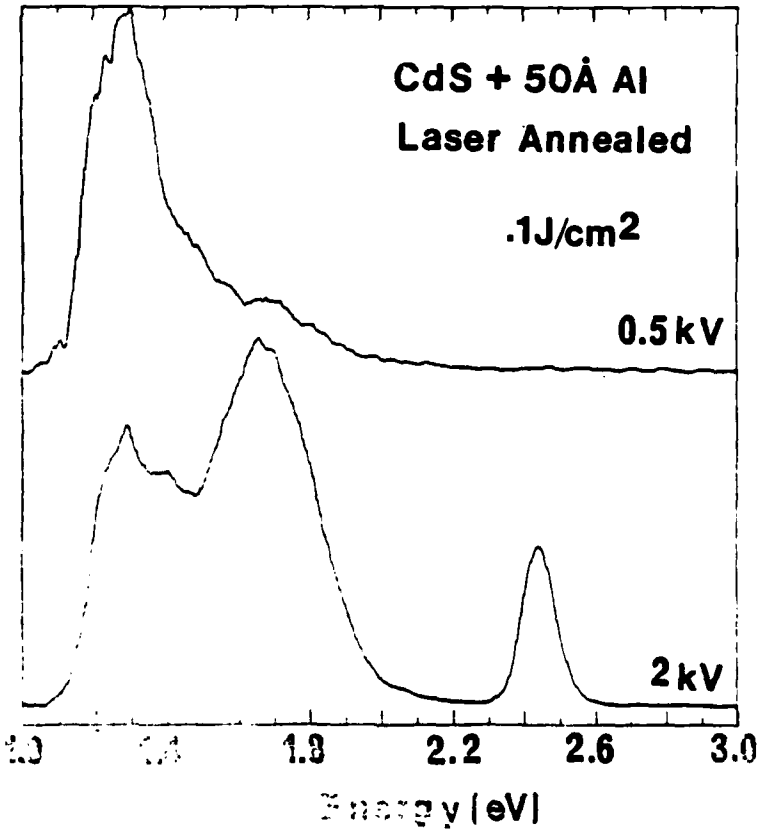
CdS + 50Å Al
Laser Annealed
.1J/cm2
0.5 kV
2 kV
1.8
2.2
2.6
3.0
Energy [eV]

PROMOTING AND CHARACTERIZING NEW CHEMICAL STRUCTURE AT METAL-SEMICONDUCTOR INTERFACES†

L.J. Brillson
Xerox Webster Research Center, 800 Phillips Road 114-41D, Webster, NY 14580

Abstract

A variety of surface and "buried interface" techniques reveal that thermal processing can influence strongly the interface interdiffusion, the dominant chemical reactions, and the nature and spatial distribution of deep level defects which contribute to the electronic barrier. We present here examples of thermally-processed interfaces ranging from Si to III-V to II-VI compound semiconductor-metal interfaces and using isothermal, rapid thermal, and pulsed laser annealing techniques.

†This paper based in part on work carried out in collaboration with A. Katnani, R. Daniels, M. Kelly, P. Kirschner, G. Margaritondo, D. Niles, H. Richter, Y. Shapira, M. Slade, N. Stoffel, N. Tache, B. Weinstein, and J. Woodall.

I. INTRODUCTION

Surface science techniques have been used extensively over the past decade to study the electronic and chemical properties of metal-semiconductor interfaces [1-5]. These studies have revealed that chemical reactions and interdiffusion are quite common at metal-semiconductor interfaces, even near room temperature. Such chemical interactions may result in a variety of electronically-active material phases: interfacial dielectric layers, dipoles, metallic alloy overlayers, as well as native defects, impurities and their complexes. Hence the ultimate electronic structure can depend sensitively on the strength and nature of chemical bonding at the microscopic metal-semiconductor junction.

In general, interface chemical and electronic structure may evolve with metal coverage on the semiconductor beyond monolayer coverage, especially at elevated temperature. Such evolution can present both a challenge and an opportunity for interface studies: a challenge to characterize chemical and electronic features of "buried" interfaces with surface science techniques and an opportunity to identify key Schottky barrier parameters which vary systematically with thermal treatment.

Here we present examples of thermally-processed interfaces ranging from Si to III-V to II-VI compound semiconductor-metal interfaces which are modified by isothermal, rapid thermal, and pulsed laser annealing techniques. In addition to standard soft x-ray photoemission spectroscopy (SXPS) and Auger electron spectroscopy (AES)/depth profiling analysis, we employ cathodoluminescence spectroscopy (CLS) to characterize compound phase and deep level defect formation at the "buried", thick metal-semiconductor interface. Our results indicate that at well-defined temperatures and process intervals, thermal processing can influence strongly the interface interdiffusion, the dominant chemical reactions, and the nature and spatial distribution of deep level defects which contribute to the Schottky

barrier.

Our results involve thermal processing in three ways: surface preparation, interface processing, and chemical/electronic characterization. We present AES/depth profiling studies of Al-Si interfaces which involve isothermal annealing to prepare surfaces and process interfaces and which demonstrate the importance of lattice disorder in controlling junction interdiffusion. AES/depth profiling studies of Ti-SiO_2/Si interfaces provide another example of preparation and processing which shows that rapid low-temperature thermal annealing can help control competitive chemical reactions at electrically-active interface arrays. SXPS investigation of Al/III-V compound semiconductor interfaces illustrate how pulsed laser annealing contributes to both interface processing and characterization. Similarly, CLS analysis of Al and Cu/CdS interfaces represents both processing and characterization of "buried" interfaces. Finally, we include SXPS studies of metals on the ternary alloys $In_xGa_{1-x}As$. Isothermal processing of As-capped $In_xGa_{1-x}As$ surfaces provides clean semiconductor surfaces which exhibit unexpectedly large variations in Schottky barrier heights.

2. Isothermally-Annealed Al-Si Interfaces

AES depth profiling studies of annealed Al-Si interfaces demonstrate the importance of lattice disorder in metal-semiconductor interdiffusion. The Al-Si junction finds widespread use as interconnects in integrated circuit structures [6]. At temperatures of 400-500°C, Si from a single-crystal substrate diffuses into an Al metallization layer and Al penetrates through the dissociated interfaces to form Al "spikes" and recrystallized Si layers doped with Al which can extend up to tens of microns [7]. It is desirable to minimize such diffusion in the fabrication of ultrasmall devices, where the semiconductor thickness may be only a fraction of a micron. SXPS studies of Al-Si interfaces performed at room temperature and above indicate that, below the Si-Al

eutectic temperature of 577°C, there is relatively little interaction between 20Å Al overlayers and clean, ordered Si [8]. Except for a relatively small amount of Si segregation to the free Al overlayer surface, Si-Al interfaces are abrupt to within tens of Å. Consistent with the low Si solubility in Al [9], SXPS data indicated negligible Si mixing within the Al overlayer, even at temperatures of 200-400°C [8].

AES depth profiling measurements confirm these conclusions for thicker Al films. As with the SXPS experiments, we prepared Si surfaces from Si (100) wafer sections which were annealed first at 1250°C for 1 min. then at 950°C for 10 min. AES and low-energy electron diffraction (LEED) revealed atomically clean, ordered (1x1) surfaces. We monitored surface temperature using an optical radiometer focussed through a sapphire viewport into the UHV chamber and using emissivity values for Si previously calibrated at different temperatures [8]. During Al evaporation, pressure rose from 10^{-10} torr to the high 10^{-9} torr range only.

Figure 1(a) demonstrates that 200Å Al overlayers on clean, ordered Si exhibit relatively abrupt junctions even after postannealing at 400°C for 30 min. [8]. Here the Al-Si interface width is 200-400Å, based on the time required to sputter through the crossover point, using 1 kV Ar^+ ions to minimize surface damage. Sputter-induced mixing effects limit the depth resolution of this AES technique to only 10-20 Å (minimized by the low incident ion energies). Without the 400°C postanneal, the same interface is ten times more abrupt (not shown). Even with postannealing, the Al-Si interdiffusion is two to three orders of magnitude more abrupt than conventionally reported.

Figure 1(b) illustrates the effect of intentionally disordering the Si surface prior to Al deposition, using a 5 kV Ar^+ sputtering for 30 min. to clean the Si surface. As shown, Si diffuses through the Al overlayer with no evident attenuation. The Si

concentration within the Al is 100x its bulk solubility at 400°C, so that the Al film thickness is not a factor in limiting Si outdiffusion on this scale. Significantly there appears to be no enhancement of Al extending into the Si over the preannealed, unsputtered surface. This is consistent with Si movement into Al as the primary diffusion process, as determined from SXPS marker experiments [10]. Hence, Fig. 1(b) reveals that lattice disorder, strain, and/or Ar^+ interstitials promote a massive Si outdiffusion into Al. Lattice disorder may account for the high interdiffusion of Al with amorphous Si [11].

These results demonstrate the importance of eliminating near-surface disorder to reduce metal-semiconductor diffusion. For Al-Si junctions, high temperature annealing reduces lattice defects and stress, leading to highly uniform interface plane. It is not yet known to what extent crystal cleavage introduces subsurface stress and disorder which could contribute to enhanced interdiffusion.

Besides ion bombardment, the presence of strongly interacting species at the intimate metal-semiconductor interface may lead to enhanced interdiffusion. SXPS studies of Au-Si interfaces [10,12] reveal that a pronounced interdiffusion occurs at the interface, resulting in formation of an extended Au-Si eutectic phase. Au deposits on Si do not yet exhibit bulk metallic features until coverages above 10Å - 20Å [10]. In Fig. 1(c), a clean, ordered Si (100) surface and a 200Å Al overlayer (analogous to Fig. 1(a)) with a 10Å Au interlayer exhibits a pronounced Al-Si interdiffusion after a 400°C, 30 min. postanneal of the Al/Au/Si (100) junction. Analogous to Fig. 1(b), the AES depth profile shows Si diffusion throughout the Al overlayer. In contrast to Fig. 1(b) however, Al now appears to penetrate past the interface into the Si substrate. Hence Au interlayers at the intimate Si interface appear to catalyze the interdiffusion at the otherwise relatively, abrupt Al-Si interface. Presumably, other metals can promote similar atomic redistribution which can result in electronic band

bending changes.

3. Rapid Thermal Annealing of Ti-SiO2/Si Interfaces

Rapid thermal annealing (RTA) provides a new technique to promote chemical reactions at interfaces without extended furnace annealing. The RTA technique can, for example, activate dopants by annealing ion-implantation damage in a semiconductor wafer without extensive dopant redistribution [13]. AES/depth profiling studies show that RTA at relatively low temperatures can enhance preferentially one of two competitive reactions within the same interface array [14].

Ti films deposited on Si are used commonly to produce low resistivity interconnects by formation of $TiSi_2$. AES and photoemission studies indicate that such silicide formation can occur over the course of several minutes at moderate (600-1000°C) temperatures rather than over a conventional half to one-hour anneal [15-16]. For heating intervals of only a few minutes, the stoichiometry of such silicides changes consistently with annealing temperatures consistent with the silicide phases reported by Murarka [17].

Reactions can also occur at the interface between Ti and SiO_2. Figure 2 illustrates an AES depth profile of 400Å Ti on 1400Å SiO_2 on a Si substrate which was annealed for 2 min. at 700°C. Here the resultant interface structure consists of a layer of Ti oxide at the outer (free) surface, a layer of Ti silicide, the SiO_2 film and the Si substrate. In only 2 min., the entire Ti film is consumed by Si and O from dissociated SiO_2. The O segregates to the outer surface, consistent with predictions for surface segregation of the phase with the lowest heat of vaporization [18]. Assuming thermal equilibrium is reached, consideration of the ternary phase diagram [19] leads to an identification of Ti_5Si_3 as the only stable silicide phase in contact with both a Ti oxide and SiO_2. On this basis, the Ti oxide stoichiometry is that of

TiO.

The presence of O on the free Ti surface in Fig. 2 is an indicator of SiO_2 dissociation. Such dissociation is usually undesirable in an active device structure since it results in conducting silicide pathways across the insulating SiO_2 layer. Likewise, the presence of Si on the free Ti over Si surface is an indicator of Ti silicide formation. One can use these signs to uncover a process window in time during which Ti silicide can form on Si before significant SiO_2 dissociation occurs. Figure 3 demonstrates this for 425∘C annealing at 400Å Ti on Si and SiO_2 on the same heat-cleaned wafer. Note the immediate appearance of Si on Ti/Si in Fig. 3(a), whereas the appearance of O on Ti/SiO_2 in Fig. 3(b) requires between 8 and 12 minutes. Hence, a conformal Ti film deposited over both Si and SiO_2 on the same substrate can be processed to promote silicide formation at the Si but not the SiO_2 interface.

The ability of low-temperature RTA to enhance one of several simultaneous reactions illustrates another avenue to modify interfacial chemical and electronic structure. This presents new opportunities for metal-semiconductor interfaces involving several chemical changes, i.e., Au diffusion into GaAs *versus* Ga and As diffusion out of the GaAs lattice. A relative alteration of these chemical changes is significant because the diffusion of each atomic species can influence the Schottky barrier in a different way.

4. Pulsed Laser Annealing of Al/III-V Compound Semiconductor Interfaces

We have used pulsed laser annealing to prepare highly localized chemical reactions at metal-semiconductor interfaces. Furthermore, we have utilized the step-wise nature of the pulsed annealing to characterize the nature of the spatially localized interfacial chemical reactions. These reactions can modify junction electronic

properties [1,20,21] and may prove useful in modifying charge transport, surface recombination and open-circuit photovoltage among other applications.

Figure 4 illustrates an AES depth profile of 50Å Al on UHV-cleaved InP(110), annealed at an energy density of 0.145/cm^2 [22]. A 308 nm excimer laser with 5ns pulse width generates a transient temperature rise lasting ~100ns. The duration of this transient is long enough to heat and perhaps even melt the solid without significant atomic diffusion beyond the annealed volume. The focussed laser beam is rastered in a serpentine pattern across the surface of a cleaved InP crystalline UHV. From the integrated Al signal, one may infer a sputter rate of 2.25Å/min. Thus the reacted interface region in Fig. 4 is only 200Å deep. The composition profile suggests that Al has mixed with the In and P to form an AlInP ternary alloy layer. Note the almost flat P concentration extending away from the InP substrate. The apparent increase in In concentration beyond 200Å is due to preferential sputtering of P from the InP substrate. Note the rather abrupt decrease in Al concentration at the reacted layer/InP interface, indicative of minimal atomic diffusion beyond the reacted region. This is particularly remarkable since every point on the Al-InP(110) surface was annealed on average by at least 5 pulses. Hence, the reaction and diffusion of the Al overlayer is well-defined and localized to a microscopic surface layer.

SXPS studies of 20Å Al deposits on UHV-cleaved InP after pulsed laser annealing demonstrate that the Al reacts with the lattice, giving rise to a ternary layer and some dissociated In which segregates to the free surface. The core level intensities provide a guide to the evolution of the Al-InP reaction with increasing laser energy density [23]. In Fig. 5(a) the ratio of covalently bonded to total Al 2p photoemitted core electrons increases with increasing energy density. The total P2p *versus* In4d core level intensity ratio in Fig.5(b) decreases abruptly upon Al deposition, as reported

earlier [24], remains constant for intermediate energy densities, then increases as part of the free surface layer is removed at high energy densities. Deconvolution of the dissociated In4d doublet from the bound components lead to a metallic *versus* total In4d intensity ratio in Fig. 5(c) which increases at low energy density as dissociated In segregates to the free surface. Above $0.3J/cm^2$, this ratio decreases strongly, suggesting that higher energy densities cause evaporation of atoms from the surface.

We have used AES peak intensities and Al LVV Auger line shifts to identify the onset of chemical reaction with increasing laser energy density [22,25]. For Al on each six III-V compounds - GaAs, GaP, GaSb, InAs, InP, InSb - we have found a finite range of energy density above a characteristic energy density such that a chemical reaction is promoted without disrupting the surface morphology. These threshold energy densities exhibit an excellent linear correlation with the semiconductor heat of fusion, indicating that melting of a thin layer of III-V compound with the metal overlayer initiates the chemical reaction. Furthermore, calculations of the energy needed to melt the Al overlayer and a 250Å layer of the particular underlying semiconductor agree with the observed threshold for the reaction [22,25].

SXPS analysis of CdTe, CdSe, and CdS/Al interfaces after pulsed laser annealing reveal significant differences [26], consistent with chemical interactions observed at room temperature [27]. Furthermore, the change in near surface stoichiometry and distribution of dissociated species depend sensitively on laser energy density and annealing prior to metal deposition [27].

Several features of pulsed laser annealing emerge from these interface studies - the manifestation of microreactions on a larger, controlled scale, the step-wise analysis and the consistency between observations of reaction thresholds and calculated heat transfer based on thermodynamic data.

5. Cathodoluminescence of "Buried" Metal-Semiconductor Interfaces

The evolution of metal-semiconductor interfaces with temperature is of considerable interest in understanding Schottky barrier formation. Yet surface-sensitive technique are not optimum for studies of such evolution occuring at "buried" interfaces – i.e., below the free surface of the overlayer. We have adapted the technique of cathodoluminescence spectroscopy (CLS) to monitor changes in buried metal-semiconductor interfaces with pulsed laser annealing [28]. By choosing incident electron energies in the range of 0.5 to 2 keV, one can vary the excitation depth in the range of several tens to several hundreds of Å respectively. Thus, it is possible to identify chemical and electronic features from optical transitions below the free surface and, by varying the electron energy, discriminate between electronic states distributed at different depths below the free surface with microscopic resolution of less than hundreds of Å.

Figure 6(a) illustrates CLS results for Cu-CdS interfaces with pulsed laser annealing. The UHV-cleaved CdS exhibits only a single peak at 2.42 eV corresponding to band-edge luminescence at room temperature. Deposition of 50Å Cu produces no dramatic changes but an increased background extending to lower energies below the band edge peak and a weak peak at ~1.27 eV. Following laser annealing, with 0.1 J/cm^2 energy density, these new features increase in intensity, resulting in the large peak at 1.28 eV. This feature provides strong evidence for the formation of Cu_2S, the main bulk CLS feature of which is a peak at 1.26 eV [29]. At 0.9 keV excitation energy, the 1.28 eV feature increases relative to the CdS edge luminescence, indicative of its near-surface origin.

CLS results for Al-CdS interfaces with pulsed laser annealing exhibit qualitatively different features from Fig. 6(a). In Fig. 6(b), the UHV-cleaved surface exhibits weak peak structures at 1.3 and 1.65 eV probably due to residual damage produced

during cleavage. These features increase dramatically upon laser annealing at an energy density of 0.1 J/cm^2. Subsequent annealing at 0.2 J/cm^2 decreases these features relative to the gap luminescence peaks [28] along with their reduction upon further laser annealing suggests that both are due to lattice damage.

The energy dependence of CLS provides additional information about these damage-related peaks. At 0.1 J/cm^2 energy density, both 1.3 and 1.65 eV transitions occur preferentially near the surface (not shown). At 0.5 keV incident electron energy, these features dominate the gap luminescence feature completely relative to the 2 keV spectrum – indicating a large change in defect density between the two volumes sampled by these two excitation energies. Furthermore, the 1.3 eV feature increases relative to the 1.65 eV peak, revealing that the transitions associated with the former occur closer to the surface.

With additional annealing, the spatial distribution of the transitions change. In particular, the enhancement of the 1.3 eV peak feature no longer occurs for 0.5 keV excitation (not shown). Furthermore, both sub-bandgap transition decrease relative to the edge luminescence at both excitation energies, indicating that the higher energy density reduces the density of these defects. Thus, the CLS technique provides a means to distinguish between lattice defect features and to monitor their near-surface spatial distribution with thermal processing. In addition, the metal/CdS results reveal the changes in interface electronic features and their spatial distribution which occur with different metal overlayers and thermal process steps on the same semiconductor surface. The extension of the CLS technique to other semiconductor systems promises to uncover considerable information concerning new electronic states and band structure resulting from metal-semiconductor interactions.

6. Metal Interfaces with Thermally Cleaned $In_xGa_{1-x}As$ Surfaces

A final and relatively straightforward example of thermal processing to study Schottky barrier formation is the preparation of clean $In_xGa_{1-x}As$ (100) ternary alloy faces. These surfaces are obtained by desorption of an As "cap" which protects the outer semiconductor layer from ambient contamination [30]. Desorption of this cap by isothermal annealing eliminates the need to study the alloys in a molecular beam epitaxy (MBE) chamber. This is particularly helpful in carrying out synchrotron radiation studies, which impose their own unique set of experimental constraints.

Figure 7 illustrates SXPS In4d and Ga3d core level features obtained from a clean, LEED-ordered $In_{0.25}Ga_{0.75}As$ (100) single-crystal (unstrained) surface with increasing deposits of Al [31]. With a photon energy $h\nu = 40$ eV, (resolution = 0.2 eV) the photoemitted core electrons leave the solid with minimal kinetic energy so that the escape depth extends below the outer semiconductor monolayers. As a result, the spectra deemphasize surface core level shifts due to chemical bonding changes which can otherwise interfere with shifts due to band bending changes.

The deposition of Al on $In_{0.25}Ga_{0.75}As$ leads to pronounced chemical changes in the near surface region. Even with an extended escape depth, the $h\nu = 40$ eV spectra exhibit formation of substantial dissociated In with the first 0.5Å Al deposition. This In4d component of dissociated In completely dominates the spectra with increasing Al coverage, demonstrating that an Al-In exchange reaction occurs at room temperature. Significantly, no comparable Ga dissociation is apparent, consistent with the higher Ga-As vs. In-As bond strength [32]. As 3d core level spectra obtained at $h\nu = 60$ eV with comparable depth sensitivity reveal strong anion versus total cation attenuation, consistent with the "chemical trapping" of anions at III-V compound semiconductor/metal interfaces reported earlier [33].

The energy shifts of bulk core level peaks in Fig. 7 indicate changes in band bending with Al deposition. Almost all such shifts for the In4d, Ga3d, and As3d

features occur within the first 2-4 A of metal coverage. For Al on $In_{0.25}Ga_{0.75}As$, the Fermi level, E_F moves toward the conduction band by 0.3-0.45 eV with metal coverage. Depending on the metal, this shift can be either toward or away from the conduction band with a range of 0.5-0.75 eV. Such a range of E_F movement represents a substantial portion of the alloy semiconductor band gap of 1.1 eV [34]. We observe similar phenomena for metals deposited on other InGaAs ternary alloy compositions [32]. This wide range of Schottky barriers on the same III-V compound semiconductor is similar to results obtained for GaAs (100) surfaces [35] but unlike those obtained for UHV-cleaved GaAs(110) surfaces [36].

Besides the preparation of clean surfaces, we have used isothermal annealing to promote *in-situ* changes in chemical structure of the InGaAs/metal interface. These chemical changes result in Schottky barrier changes which will be reported elsewhere [32].

7. Conclusions

In this paper we have described some methods by which isothermal, rapid thermal, and pulsed laser annealing can be employed in the study of metal-semiconductor interactions. Such thermal treatments can be used (a) to prepare clean or altered surfaces, (b) to process interfaces in time and temperature to enhance a particular reaction, or (c) to "step" through a metal-semiconductor interaction. The interface chemical reactions, interdiffusion, and formation of electrically-active sites depend strongly on the temperatures and process times employed. Thus, the promotion of interfacial chemistry in a controlled manner at elevated temperatures yields a promising new avenue by which to analyze the formation of electronically-active interfaces.

Acknowledgements

This work was supported in part by the Office of Naval Research (G.B. Wright) under Contract No. 000 14-80-C-0778.

References

1. L.J. Brillson, Surface Sci. Repts. 2 (1982) 123; L.J. Brillson, J. Phys. Chem. Solids 44 (1983) 703.

2. G. Margaritondo, Solid-State Electron. 44 (1983) 703, G. Margaritondo and A. Franciosi, Ann. Rev. Mater. Sci. 14 (1984) 67.

3. R.H. Williams, Contemp. Phys. 23 (1982) 329.

4. R.Z. Bachrach, in Metal-Semiconductor Schottky Barrier Junctions and their Applications (Plenum, New York, 1984).

5. W.E. Spicer and S.J. Eglash, in Surface and Interface Effects in VLSI, Ed. R.S. Bauer (Academic, New York, 1984).

6. See, for example, D. Pramanik and A.N. Saxena, Solid State Technol. 26 127, Jan. (1983).

7. R. Rosenberg, M.J. Sullivan, and J.R. Howard, in *Thin Films-Interdiffusion and Reaction*; Eds. J.M. Poate, R.N. Tu, and J.W. Mayer (Wiley-Interscience, New York, 1978) p. 13 and references therein.

8. L.J. Brillson, M.L. Slade, A.D. Katnani, M. Kelly and G. Margaritondo, Appl. Phys. Letters 44 (1984) 110.

9. M. Hansen, *Constitution of Binary Alloys* (McGraw-Hill, New York, 1958).

10. L.J. Brillson, A.D. Katnani, M. Kelly and G. Margaritondo, J. Vacuum Sci. Technol. A2 (1984) 551.

11. S. Ishihara, T. Hirao, K. Mori, M. Kitagawa, M. Ohno and S. Kohiki, J. Appl. Phys. 53 (1982) 3909.

12. L. Braicovitch, C.M. Garner, P.R. Skeath, C.P. Su, P.W. Chyc, I. Lindau, and W.E. Spicer, Phys. Rev. B20 (1979) 5131.

13. R.T. Fulks, C.J. Russo, P.R. Hanley and T.I. Kamins, Appl. Phys. Letters 39 (1981) 604.

14. L.J. Brillson, M.L. Slade, H. Vander Plas, and R.T. Fulks, unpublished.

15. R. Bulz, G.W. Rubloff, T.Y. Tan, and P.S. Ho, Phys. Rev. B30 (1984) 5421.

16. M.A. Taubenblatt and C.R. Helms, J. Appl. Phys. 53 (1982) 6308.

17. S.P. Murarka, *Silicides for VLSI Applications* (Academic, New York, 1983).

18. H.H. Brongersma, M.J. Sparnaay, and T.M. Buck, Surface Sic. 71 (1978) 657.

19. R. Byers, J. Appl. Phys. 56 (1984) 147.

20. K. Okamoto, C.E.C. Wood, and L.F. Eastman, Appl. Phys. Letters 38 (1981) 636.

21. J. Slowik, H.W. Richter and L.J. Brillson, unpublished.

22. H.W. Richter and L.J. Brillson, Proc. 17th Intern. Conf. on the Physics of Semiconductors, Eds. J.D. Chadi and W.A. Harrison (Springer-Verlag, New York, 1985).

23. H.W. Richter, L.J. Brillson, M.K. Kelly, R.R. Daniels, and G. Margaritondo, J. Vacuum Sci. Technol. B2 (1984) 591.

24. L.J. Brillson, C.F. Brucker, A.D. Katnani, N.G. Stoffel, R. Daniels and G. Margaritondo, J. Vacuum Sci. Technol. 21 (1982) 5641.

25. H.W. Richter and L.J. Brillson, unpublished.

26. L.J. Brillson, M.L. Slade, M.K. Kelly, D. Niles and G. Margaritondo, unpublished.

27. L.J. Brillson, C.F. Brucker, N.G. Stoffel, A.D. Katnani, R. Daniels and G. Margaritondo, Surface Sci. 132 (1983) 212.

28. L.J. Brillson, H.W. Richter, M.L. Slade, B.A. Weinstein, and Y. Shapira, T. Vacuum Sci. Technol., in press.

29. F. Guastavino, S. Duchemin, B. Rezig, B. Grault and M. Savelli, Conf. Rec. IEEE Photovoltaic Spec. Conf. Ser. 13 (1978) 303.

30. S.P. Kowalczyk, D.L. Miller, J.R. Waldrop, P.G. Newman and R.W. Grant, J. Vacuum Sci. Technol. 19 (1981) 255.

31. L.J. Brillson, M.L. Slade, P. Kirschner, J. Woodall, M.K. Kelly, L. Tache and G. Margaritondo, unpublished.

32. D.D. Wagman, W.H. Evans, V.B. Parker, I. Halow, S.M. Bailey and R.H. Schumm, Natl. Bur. Std. Technical Notes 270-3-270-7 (US Govt. Printing Office, Washington, DC, 1968-1971).

33. L.J. Brillson, G. Margaritondo, and N.G. Stoffel, Phys. Rev. Letters 44 (1980) 667.

34. E.W. Williams and V. Rehn, Phys. Rev. 172 (1969) 798.

35. R.W. Grant, J.R. Waldrop, S.P. Kowalczyk, and E.A. Kraut, J. Vacuum Sci. Technol. 19 (1981) 477.

36. W.E. Spicer, I. Lindau, P. Skeath, and C.Y. Su, J. Vacuum Sci. Technol. 17 (1980) 1019.

Figure Captions

1. AES depth profiles for 200Å Al deposited on Si(100) in UHV after (a) high temperature preanneal and a 400°C, 30 min. post-anneal, (b) a 5 kV Ar^+ bombardment prior to Al deposition and a 400°C, 30 min. post-anneal {after Brillson et al. [8]} and (c) a high temperature preanneal, predeposition of a 10Å Au interlayer, and a 400°C, 30 min. post-anneal {after L.J. Brillson, H.W. Richter and M.L. Slade, unpublished}.

2. Auger depth profile of 400Å Ti on heat cleaned SiO_2 on Si annealed at 700°C for 2 minutes. After Brillson et al. [14].

3. Evolution of Auger intensities as a function of 425°C anneal time for 400Å Ti on heat-cleaned Si (a) and SiO_2 (b). After Brillson et al. [14].

4. AES depth profile of 50Å Al on InP annealed at an energy density of 0.14 J/cm^2 per pulse. Excess In above 120 min. is due to preferential sputtering of P. Integration of the Al signal yields a sputter rate of 2.25Å/min. After Richter and Brillson [22].

5. Change in SXPS surface composition of 20Å Al overlayer on UHV-cleaned InP(110) surface as a function of annealing energy density - (a) covalently bonded vs. total Al:conversion of metallic into covalently bonded Al, (b) total P2p versus In4d:attenuation of P2p level at surface due to Al overlayer and recovery upon high energy density anneal, and (c) metallic versus total In4d:metallic In segregation then removal with increasing energy density. After Richter et al. [23].

6. Cathodoluminescence spectra as a function of incident electron energy for UHV-

cleaved CdS (1120), after *in-situ* deposition of (a) 50Å Cu or (b) 50Å Al, and pulsed laser annealing with energy density $0.1J/cm^2$. After Brillson et al. [28].

7. Ga3d/In4d core level spectra taken at 40eV photon energy: clean $In_{.25}Ga_{.75}As$ (100) surface obtained by isothermal desorption of an As "cap" and as a function of Al deposition. After Brillson et al. [31].

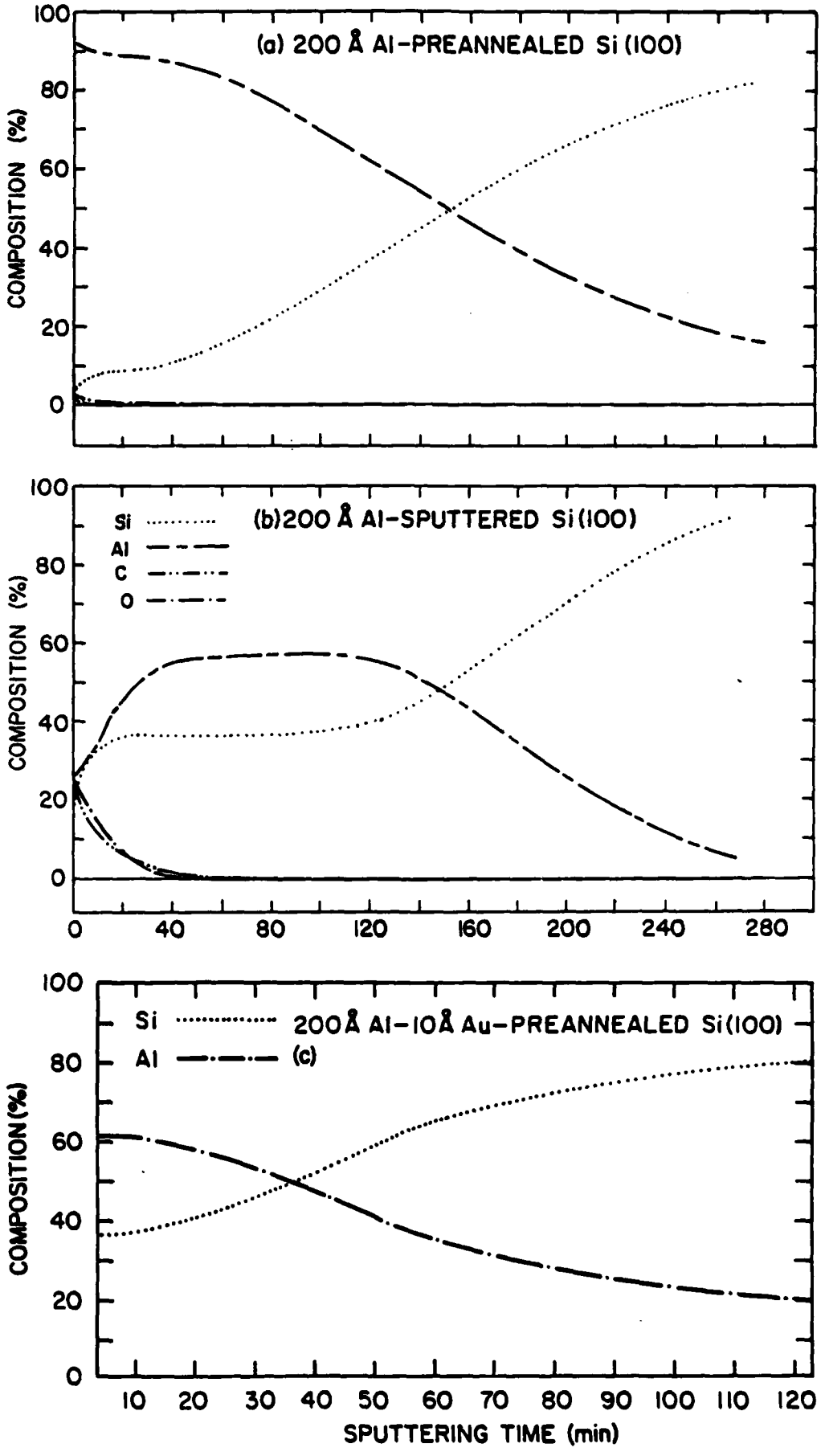
(a) 200 Å Al-PREANNEALED Si(100)
COMPOSITION (%)
100
80
60
40
20
0
(b)200 Å Al-SPUTTERED Si(100)
Si
Al
C
O
0
40
80
120
160
200
240
280
200Å Al-10Å Au-PREANNEALED Si(100)
(c)
10
20
30
40
50
60
70
80
90
100
110
120
SPUTTERING TIME (min)

Fig. 1

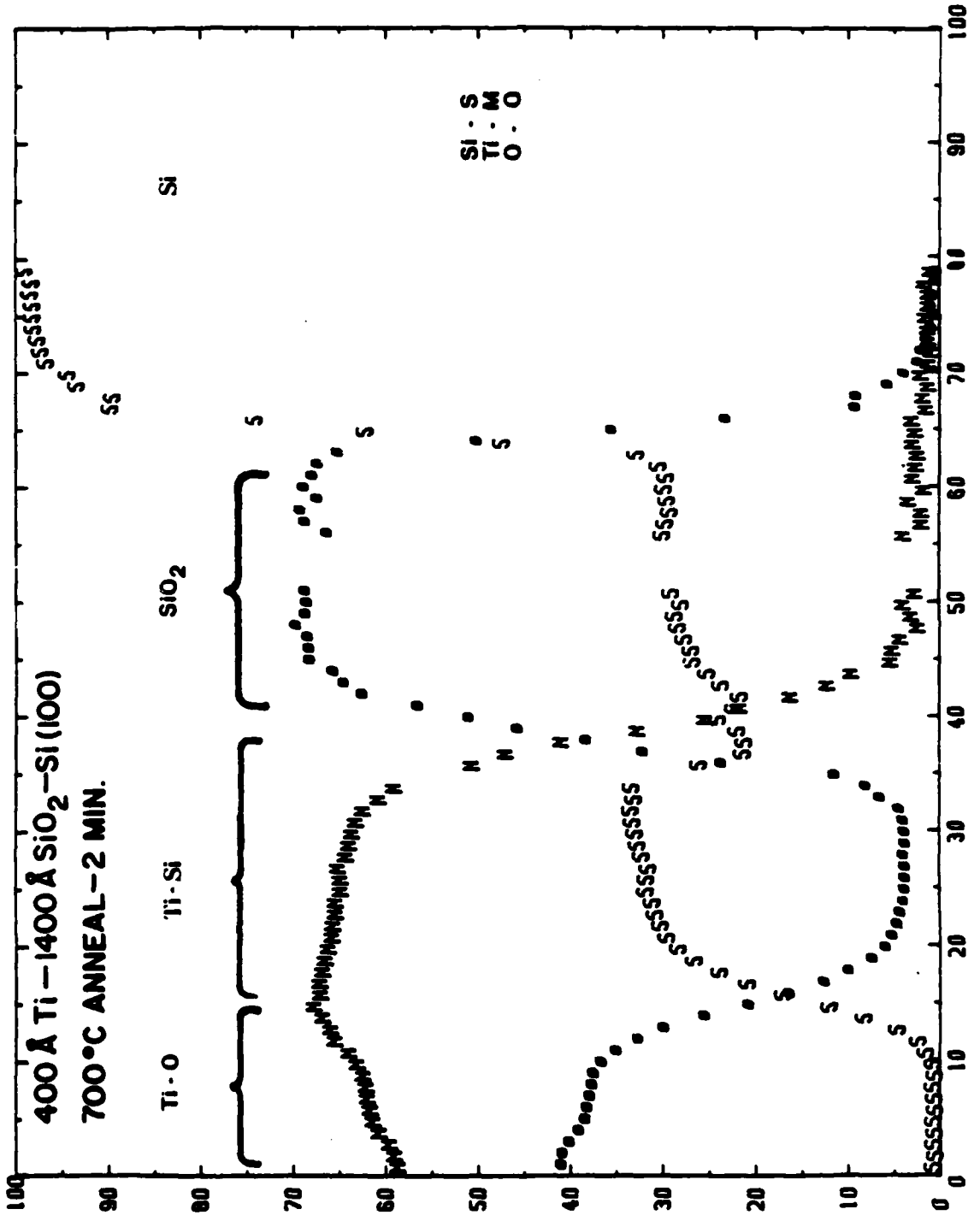
400 Å Ti – 1400 Å SiO_2 – Si (100)
700°C ANNEAL – 2 MIN.
Ti · O
Ti · Si
SiO_2
Si
Si · S
Ti · M
O · O
0
10
20
30
40
50
60
70
80
90
100

Fig. 2

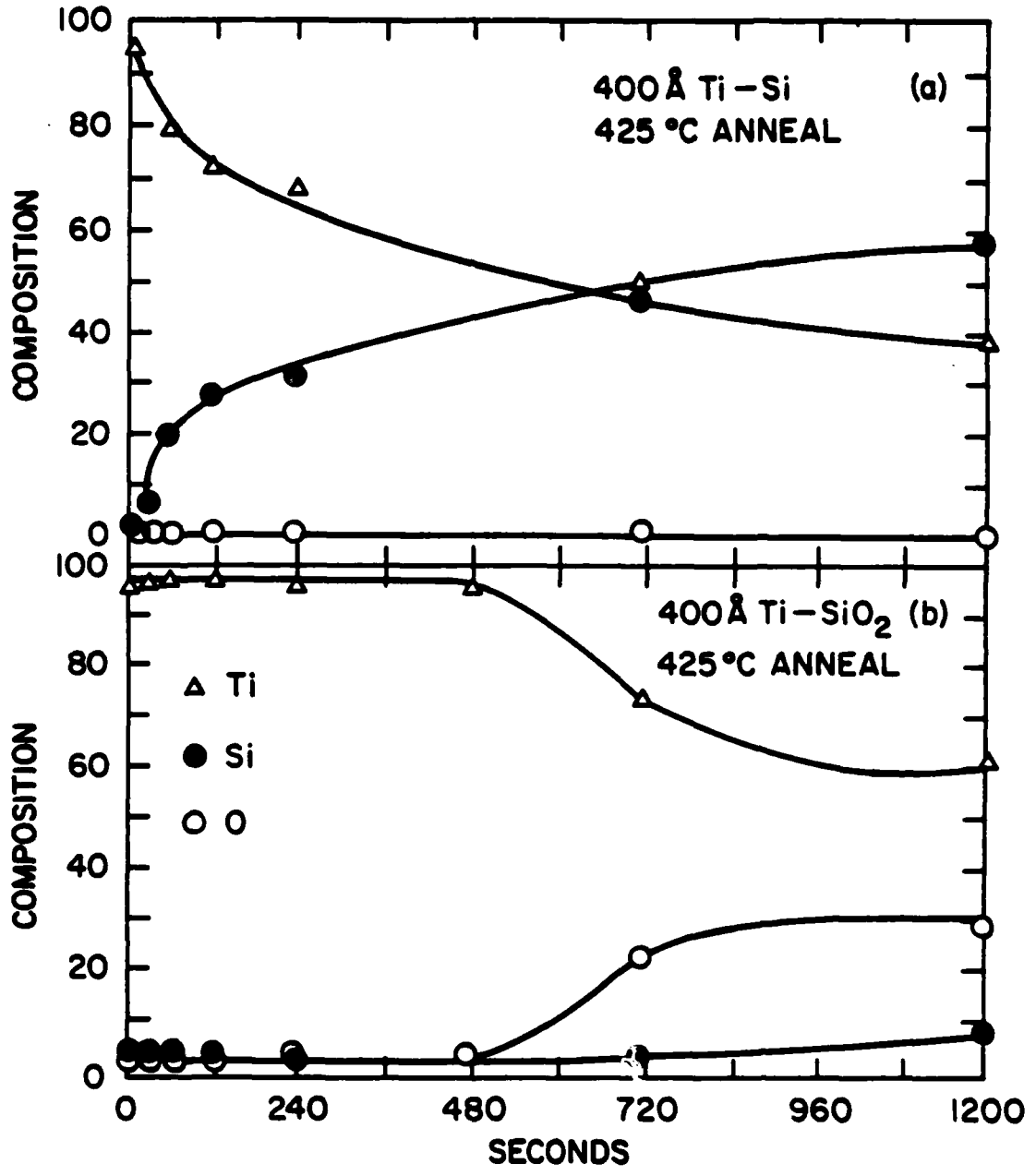
400Å Ti–Si
425 °C ANNEAL
(a)
400Å Ti–SiO2 (b)
425°C ANNEAL
Ti
Si
O
COMPOSITION
COMPOSITION
100
80
60
40
20
0
0
240
480
720
960
1200
SECONDS

Fig. 3

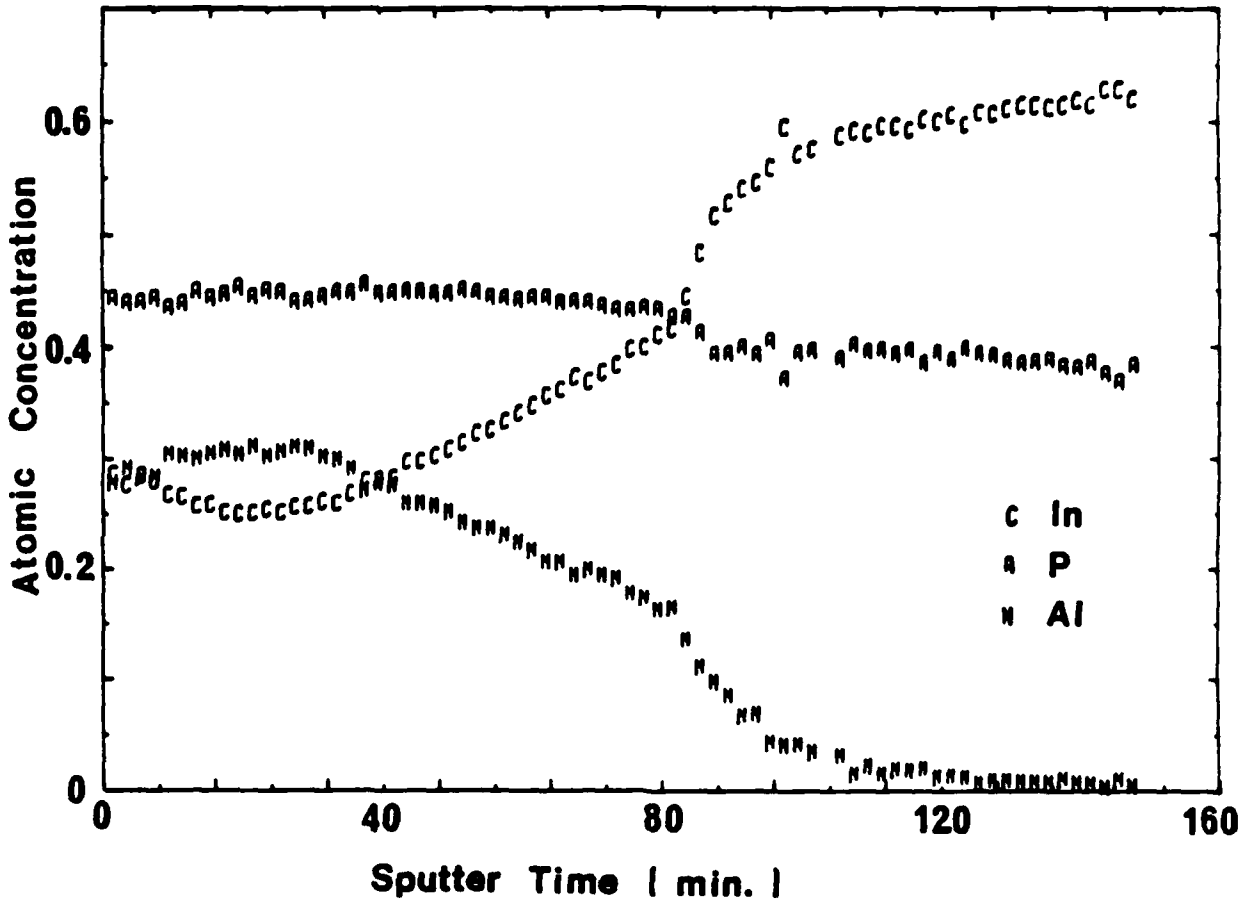
Atomic Concentration
0.6
0.4
0.2
0
0
40
80
120
160
Sputter Time (min.)
C In
P
N Al

Fig. 4

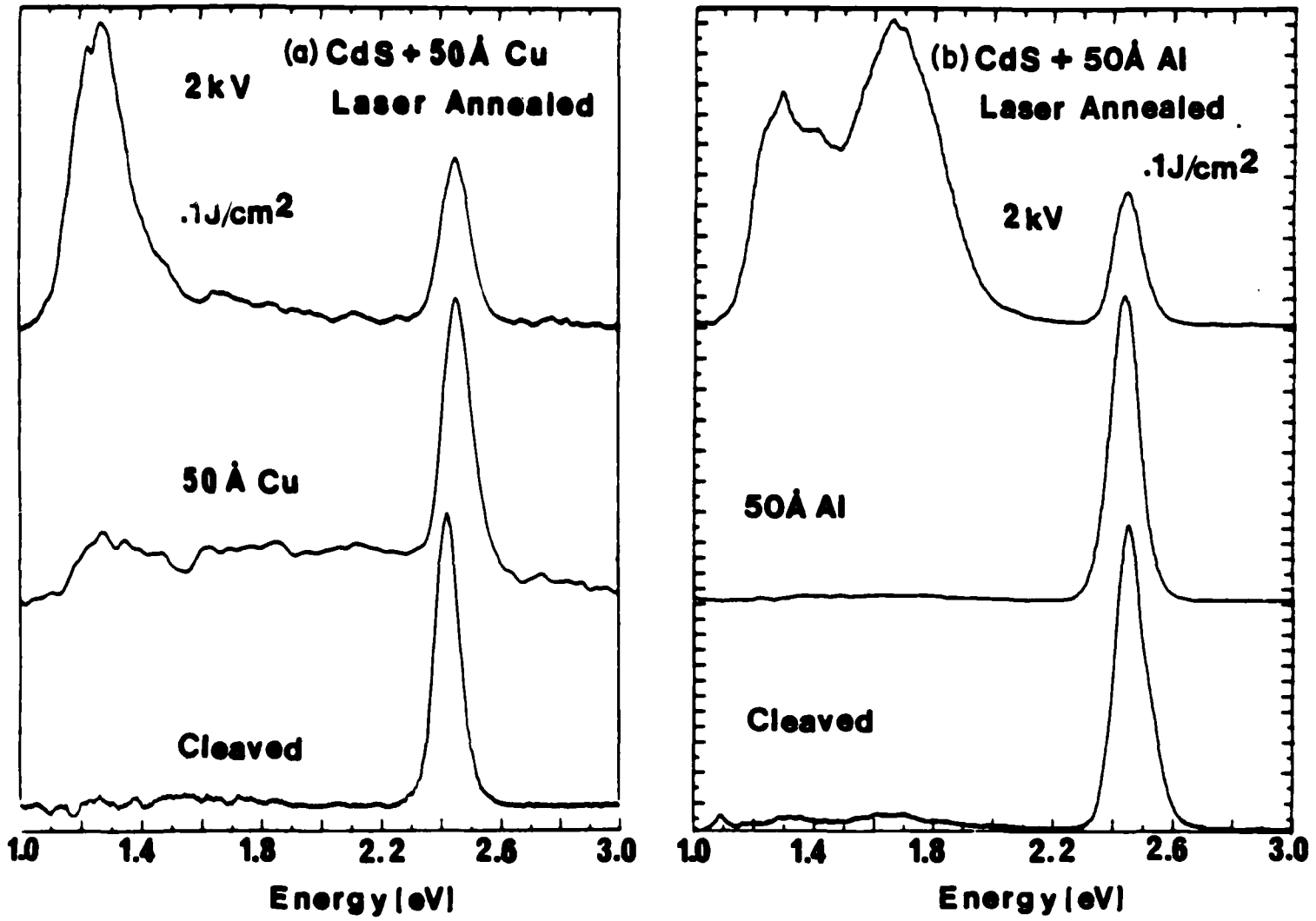
(a) CdS + 50Å Cu
Laser Annealed
2 kV
.1J/cm2
50 Å Cu
Cleaved
1.0
1.4
1.8
2.2
2.6
3.0
Energy (eV)
(b) CdS + 50Å Al
Laser Annealed
.1J/cm2
2 kV
50Å Al
Cleaved
1.0
1.4
1.8
2.2
2.6
3.0
Energy (eV)

Fig. 6

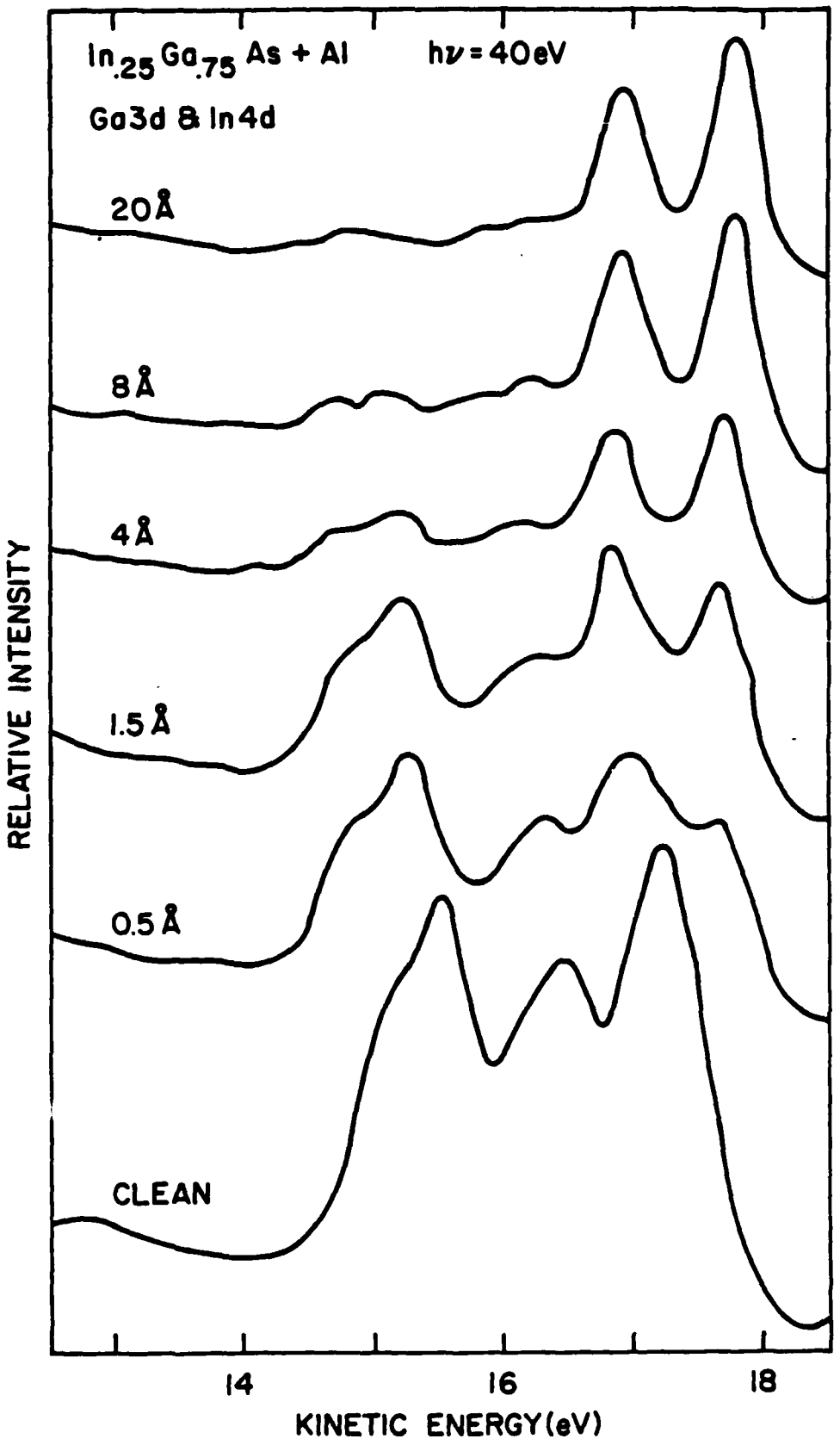
$In_{.25}Ga_{.75}As$ + Al
hν = 40eV
Ga3d & In4d
20Å
8Å
4Å
1.5Å
0.5Å
CLEAN
RELATIVE INTENSITY
14
16
18
KINETIC ENERGY(eV)

Fig.7

Control and Characterization of Metal-InP and GaAs Interface Structures Formed by Laser-Enhanced Reactions

H. Richter and L.J. Brillson
Xerox Webster Research Center, Webster, NY 14580

and

M. Kelly, R. Daniels and G. Margaritondo
Dept. of Physics, Univ. of Wisconsin, Madison, WI 52706

Abstract

We have used pulsed laser annealing to produce highly localized chemical reactions at the Al-InP and Al-GaAs interfaces. At successive stages of these laser induced reactions, we have monitored atomic movement and chemical structure on a microscopic scale using soft x-ray photoemission spectroscopy (SXPS) and Auger electron spectroscopy (AES). We have found a finite range of energy density such that a chemical reaction is promoted without disrupting the surface morphology. The reactions and atomic movements are explained by simultaneous melting of the Al overlayer and a thin layer of the semiconductor substrate.

1. Introduction

A number of studies using surface science techniques show that chemical reaction and diffusion are quite common at the metal semiconductor interface, even if all the process steps are carried out at or near room temperature.[1-3] Although such phenomena are usually localized to within tens of Å at room temperature, nevertheless the resultant changes in chemical structure can strongly effect the macroscopic electronic properties of the metal-semiconductor contact. Thus, it is of interest to study how these chemical processes evolve for higher temperatures at which greater atomic movement can occur. Such studies can provide new information on mechanisms of Schottky barrier formation, such as formation of interfacial dielectric layers or defects within the semiconductor. They can also reveal modes of interface degradation for semiconductor interfaces at lower temperatures over relatively long times.

We have used a pulsed ultra-violet (UV) laser to anneal metal-semiconductor interfaces and promote highly localized chemical reactions. These interfaces were annealed in ultrahigh vacuum (UHV) and characterized by surface-sensitive techniques in order to monitor the chemical processes on a scale of monolayers. Because of the extremely short laser pulse (5ns) and resultant heating (~ 100 ns), interdiffusion of the metal and semiconductor atoms could be limited to tens of Å. Longer heat treatments, even at lower temperatures, would produce extended diffusion, and a "washing out" of the interfacial structure, below the level of detectability of our spectroscopic techniques. In addition, the discrete laser pulses provide us with the means to monitor the laser-induced process in discrete steps, using successive pulses. The UHV environment excludes ambient contamination which could interfere with or otherwise mask the metal-semiconductor interaction.

Surface science techniques like soft x-ray photoelectron spectroscopy (SXPS) and Auger electron spectroscopy (AES) allow to follow atomic movements on a monolayer scale and to determine the chemical state of these atoms.

In this paper, we report on the laser-induced chemical reactions at the Al-InP (110) and Al-GaAs (110) interfaces, formed by depositing Al overlayers on InP and GaAs single crystals cleaved in UHV. Considerable spectroscopic evidence[4-10] suggests that a strong Al-P bonding takes place at this interface, even with the InP substrate held at room temperature. With our laser-induced annealing technique, we have discovered that it is possible to induce a strong chemical reaction at the Al-III-V semiconductor interface limited to depths on the order of a hundred Å in which all the Al-Al bonds are replaced by Al-anion bonds. This can be achieved without severely disrupting the surface morphology i.e., roughness as measured by optical microscopy and electron beam induced imaging with 3 μm resolution. We also find, that in contrast to most other studies on III-V semiconductors,[11-17] the stoichiometry of the semiconductor near the surface is not disturbed. Preliminary investigations show pronounced differences in the electronic behavior between the Al-InP contact and the Al contact with the laser reacted layer.

II. Experimental

SXPS measurements were performed using InP- and GaAs bars of dimension 5 x 5 x 15 mm, cleaved in an ultrahigh-vacuum chamber (pressure $\leq 5 \times 10^{11}$ torr) which was connected to the Stoughton electron storage ring Tantalus. Al-overlayers ranging from 20 to 50 Å thickness (monitored with a quartz-crystal oscillator) were evaporated onto visually-smooth (110) surfaces from a heated tungsten filament in the same chamber. These overlayers were exposed to 5 nsec pulsed laser light from

a 308 nm XeCl-excimer laser. The light was focussed onto the specimen with a 350 mm quartz lens to a spot size of 0.9 mm diameter. Special care was taken to align all specimens into exactly the same position realtive to the focussing lens in order to assure good reproducibility of energy density from anneal to anneal. We also eliminated laser reflections from the specimen to the UHV chamber, which could desorb gases and contaminate our clean interfaces by aligning the sample surface in a way, that the laser beam was reflected back onto the entrace window.

To anneal the 5x5 mm^2 cleaved surface completely, we used repetitive pulses while scanning the laser beam over the surface. Scan speed and pulse rate were chosen such that the individual laser spots overlapped with each surface point receiving 4 pulses. All energy densities quoted in the following are energy densities per pulse. While the absolute value of energy density is only accurate to about 25%, the relative accuracy and reproducibility between different anneals is estimated to be better than 10%. Up to the highest applied enrgy density of 0.8 J/cm^2, no visual damage was introduced on the InP surfaces. Photoelectrons were excited with light passing through a grasshopper monochromator; the angular-integrated photoelectron spactra were taken with a double-pass PHI-cylindrical mirror analyzer (CMA). The combined resolution of the monochromator plus CMA was kept at 0.25 eV for the In4d and Ga3d core level, 0.3 eV and 0.5 eV for the Al 2p and P2p core level respectively.

III. Results

Figures 1 and 2 illustrate the In4d and P2p core level spectra for the different stages of our experiment: cleaved surface, with deposition of 20 Å of Al, and after exposure to pulsed laser light with indicated energy density. The spectra were taken

with 60 eV and 140 eV photon energies respectively, corresponding to mean electron escape depths of 5 Å for the In 4d and 15 Å for the P2p core level.[18] In the case of the cleaved surface, both the In4d and the P2p core level show their characteristic spin-orbit splitting of 0.8 and 0.85 eV with intensity ratios of 2:1. The 20 Å Al overlayer strongly attenuates the P2p intensity, but as far as we can tell from the rather weak signal, there is no change in either peak position or peak shape. This indicates that the strength of chemical bonding between the P atoms and its neighbors is affected very little by the Al overlayer as it is expected because of the small difference between Al-P and In-P binding energies. In contrast, the In4d line changes drastically. We now find two major peaks separated by 0.8 eV of approximately equal intensity and a rather small shoulder at higher binding energy. It has been shown earlier[5,6,8] that this In4d structure is due to a combination of two components representing the two different chemical states In-atoms are in: a) In in a covalent bonded, semiconductor-like environment and b) In in a metallic bonded state. We have deconvoluted the two contributions by superimposing two "as-cleaved" spectra, treating the energy position of both components and the relative intenstiy as adjustable fit parameters. (The dotted line in Fig. 1 shows an example of such a fit.) For the unannealed Al overlayer, we find that 75% of the In-atoms within the detection depth are in the metallic state, thus comfirming that, even at room temperautre, In diffuses into the Al overlayer and to the surface.

Even though cluster formation can occur in some metal semiconductor systems especially at submonolayer coverage, we are confident that in our experiment, the 20 Å Al-layer forms a rather continuous overlayer, since the P intensity is attenuated by a factor of about 4, which is consistent with the expected attenuation due to an electron escape depth of 15 Å.

The Al2p spectrum of the 20 Å overlayer before laser annealing is shown in Fig. 3 (lowest curve). Beside the major contribution from the metallic Al, we observe a wing of significant intensity at lower kinetic (higher binding) energy. This spectrum agrees with earlier observations[5,6,8] which indicate that Al reacts with the InP substrate and Al-P bonds are formed at the Al InP interface.

Annealing the Al-overlayer with increasing energy densities, we observe the following: At the lowest applied energy density of 0.1 J/cm^2, we detect very little or no change in all three (In4d, P2p, Al2p) spectra, indicating that this energy density is too low to promote any kind of fast chemical reaction during the short annealing time. Between 0.17 J/cm^2 and 0.3 J/cm^2, the P2p spectra and the P2p/In4d intensity ratio change very little (Fig. 4b). This means, that the P is relatively unaffected by the annealing, and also that there is no significnat loss of the anion in contrast to other annealing experiments of InP or GaAs.[11-17]

The In4d spectra show a gradual change between 0.17 J/cm^2 and 0.3 J/cm^2: the low binding energy ("metallic") peak increases gradually with increasing power relative to the total In signal (Fig. 1), indicating that increasing amounts of In are driven out of the semiconductor and segregate as metallic In near the free surface. As shown in Fig. 4c, the metallic component increases from 75% after evaporation to 85% after 0.3 J/cm^2 annealing. The most obvious changes in this annealing regime occurred in the Al2p-spectra (Fig. 3). Between 0.1 J/cm^2, the major intensity contribution in the photoelectron spectrum is shifted from 41.3 eV kinetic energy to 40.3 eV kinetic energy, indicating that more and more Al change their chemical bonding from being bonded in a metal to a stronger covalent bond. This trend continues with higher annealing energy density until 0.3 J/cm^2, for which only a very small contribution from the 41.3 eV "metallic" peak is left. In order to quantify the two contributions

to the Al 2p spectra, we have modelled the 41.3 eV-component in the following way: two Lorentzian curves with spin-orbit splitting of 0.4 eV[19] and intensity ratio 2:1 are superimposed and convoluted with a Gaussian-function. The width of the Lorentzians and Guassian are adjusted to fit the high energy side of the measured spectrum of the unannealed sample. The "spectrum" generated in this way is then scaled and substracted from the measured spectra. For all spectra shown here, the model-spectrum fits the metallic component very well, indicating that this peak does not broaden, but the intensity is transfered into the peak at higher binding energy. The intensity contribution from the "covalent" peak is plotted in Fig. 4a, illustrating a sharp onset of the reaction between 0.1 and 0.17 J/cm^2.

Up to 0.3 J/cm^2, the total Al-intensity drops by only 40% compared to the initial 20 Å-Al, indicating that the reaction is limited to a small volume near the surface. Since the attenuation of the P and In-signal does not change in this energy regime, there is no evidence that lateral distribution of the Al is significantly changed i.e. by forming clusters. Above 0.3 J/cm^2 this behavior changes significantly - the Al-intensity drops by a factor of 5. Simultaneously, the P/In ratio recovers its initial value before evaporation of the Al and the contribution of the "metallic" In component is reduced significantly (Fig. 4c). Auger depth profiles taken at this stage of anneal reveal that the Al diffuses several hundred Å into the InP. However, the energy density of 0.8 J/cm^2 is probably also sufficiently higher to cause evaporation of atoms from the surface, thereby producing a more bulk-like composition. 50 Å-Al overlayers on InP show the same overall behavior, except that the energy density required to initiate the reaction is about 25% higher. Again the Al-bonds are completely converted to covalent bonds.

The results for Al on GaAs can be summarized as follows: the unannealed Al-overlayer shows a weaker interaction with the GaAs substrate: less Ga goes into the metallic phase (45% compared to 75% for the InP) and less Al-anion bonds are formed, as indicated by a less pronounced shoulder in the Al2p spectra. The reaction does not start until over 0.3 J/cm^2, but at 0.4 J/cm^2 the Al2p peak has mostly shifted by 1 eV to higher binding energy, leaving little traces of the metallic component.

IV. Discussion

Using SXPS, we have studied chemcial reactions at the Al-InP (110) and Al-GaAs (110) interface promoted by exposure to pulsed laser-light on a microsocic scale. We find, that both systems show very similar behavior: an energy density threshold characteristic for both materials exists for the onset of the reaction. We find an energy window where it is possible to react the entire Al-overlayer, by forming covalent bonds with the substrate, without disrupting the surface morphology, on a μm-scale, as explained earlier. Contrary to laser-annealing experiments of free III-V semiconductor surfaces,[11-17] we find no significant loss of anion within our probing depth. The Al diffuses into the semiconductor substrate over the order of hundred Å during the reaction time, which can be estimated to be on the order of 100 ns, based on heat-flow calculation in Si,[20] a material with comparable thermal conductivity. It has been shown[20] that 0.45 J/cm^2 (10 ns, 694 nm ruby-laser) is sufficient to melt a 1000 Å layer of GaAs. With decreasing pulse length and shorter wavelength causing shorter absorption depth, this threshold decreases.

Preliminary calculations based on Baeri's and Compisano's heat flow model[20] for InP yields an energy density threshold for melting of 0.15 J/cm^2. Experiments to

determine the threshold for the Al-III-V semiconductor reaction carried out with six different III-V compounds reveals a very strong linear correlation between the threshold and the heat of fusion of the semiconductor. The influence of the Al-overlayer on the threshold of melting for the semiconductor substrate can be estimated in the following way: bulk Al has a reflectivity of 92% at 308 nm at room temperature, but the reflectivity of a 20 Å or 50 Å Al layer on a GaAs substrate calculated by the formulas given in the AIP handbook[23], is only 51% or 59% compared to 40% for the bare GaAs substrate at room temperature. With increasing temperautre, the optical constants of Al change in a way, that the reflectivity is further reduced[22]. Therefore, the amount of energy deposited in the Al-semiconductor system is reduced by less than 20% compared to the bare semiconductor surface. In addition, the energy require to heat the 20Å Al layer from 300K to 1300K including the heat of fusion[23] is only 0.0007 J/cm^2, which is small compared to the melting threshold of the bare substrate (~ 0.15 J/cm^2). The melting threshold of the substrate should therefore be only slightly increased by the 20-50 Å Al overlayer.

From all these considerations we conclude that the observed reaction is promoted by simultaneous melting of the Al-overlayer and a thin layer of the semiconductor. In this molten layer atoms, a highly mobile and a fast intermixing occurs. The melting and subsequent resolidification also account for the rearrangement of bonds. Since the Al-P bond is stronger than the InP bond (heat of formation 40 kcal/mol compared to 21 kcal/mol[24]), the formation of Al-P bonds is favored and therefore In diffuses out of the substrate and segregates at the free surface. The large heat of formation for Al-P can also account for the effective trapping of P-atoms in the Al layer, whereas in similar annealing experiments of the free InP surface[25] up to 50% of the P-atoms escape.

Our work demonstrated that laser annealing of thin Al layers on III-V semiconductors can produce ultrathin layers of new materials, such as Al_xIn_yP or Al_xGa_yAs for the interfaces discussed here. One expects that such layers dramatically change the electronic properties of the metal-semiconductor contact. Preliminary measurements of the Al-InP system indicate that this is indeed the case. While Al forms a quasi-ohmic contact with InP, the Al_xIn_yP interlayer exhibits rectifying behavior, but more experiments must be performed to determine the exact electronic behavior of the interface layer.

Acknowledgements

Partial support by the Office of Naval Research (ONR N00014-80-C-0778 and NSF DMR 78-22205) is gratefully acknowledged. We thank J. Iseler (Lincoln Labs) for supply of our InP crystals, Jim Zesch (Xerox Palo Alto Research Center) for cutting and orienting them, the Synchrotron Radiation Center (funded by NSF Grant No. DMR-74-15089) for their cooperation, and Tom Orlowski (Xerox Webster Research Center) as well as Dave Zehner (Oak Ridge National Laboratory) for valuable discussions.

References

1. L.J. Brillson, Surf. Sci. Repts. 2, 123 (1982); Int. J. Phys. Chem. Solids 44, 703 (1983).

2. G. Margaritondo, Solid State Electron. 26, 499 (1983).

3. R.H. Williams, Contemp. Phys. 23, 329 (1982).

4. L.J. Brillson, C.F. Brucker, A.D. Katnani, N.G. Stoffel, G. Margaritondo, Phys. Rev. Lett. 46, 838 (1981); Appl. Phys. Lett. 38, 784 (1981); J. Vac. Sci. Techn. 19, 661 (1981).

5. L.J. Brillson, C.F. Brucker, A.D. Katnani, N.G. Stoffel, R. Daniels and G. Margaritondo, J. Vac. Sci. Techn. 21, 564 (1982).

6. T. Kendelewicz, W.G. Petro, I.A. Babalola, J.A. Silberman, I. Lindau, W.E. Spicer, J. Vac. Sci. Techn. B1, 623 (1983).

7. A. Kahn, C.R. Bonapace, C.B. Duke, A. Paton, J. Vac. Sci. Techn. B1, 613 (1983).

8. T.Z. Zhao, R.R. Daniels, A.D. Katnani, G. Margaritondo, A. Zunger, J. Vac. Sci. Techn. B1, 610 (1983).

9. A. McKinley, G.J. Hughes, R.H. Williams, J. Phys. C15, 7049 (1982).

10. R.H. Williams, R.R. Varma, A. McKinley, J. Phys. C10, 4545 (1977);R.H. Williams, A. McKinley, G.J. Hughes, V. Montgomery, I.T. McGovern, J. Vac. Sci. Techn. 21, 594 (1982).

11. D.M. Zener, C.W. White, in Laser Annealing of Semiconductors, ed. J.M. Poate, J.W. Mayer, Academic Press, New York, 1982, p. 281.

12. V. Gamo, Y. Yuba, A.H. Oraby, K. Murakami, S. Namba, Y. Kawasahi, in Laser and Electron Beam Processing of Materials, ed. by C.W. White and P.S. Percey, Academic Press, New York, 1980, p. 322.

13. H.B. Harrison, J.S. Williams, in Laser and Electron Beam Processing of Materials, ed. by C.W. White and P.S. Percey, Academic Press, New York, 1980, p. 481.

14. D. Eirug Davies, J.K. Kennedy, E.F. Kennedy, in Galium Arsenide and Related Compounds, ed. H.W. Thimm, Inst. of Phys., Conf. Series 56, London, 1980, p. 229.

15. J.S. Williams, in Laser Annealing of Semiconductors, ed. by J.M. Poate, J.W. Mayer, Academic Press, New York, 1982, p. 383.

16. M. Okigawa, T, Nakayama, K. Morita, N. Hoh, Appl. Phys. Lett. 43, 1054 (1983).

17. A.G. Cullis, H.C. Webber, D.S. Robertson, in Laser-Solid Interactions and Laser Processing 1978, ed. by S.D. Ferris, H.J. Leamy, J.M. Poate (Am. Inst. Phys., New York, 1979), p. 653.

18. M.P. Seah, W.A. Dench, Surf. Interf. Anal. 1, 2 (1979).

19. M. Cardona, Photoemission in Solids I, Springer, Berlin, 1978, p. 265.

20. P. Beari, S.U. Campisano, in Laser Annealing of Semiconductors, ed. by J.M. Poate, J.W. Mayer, Academic Press, New York, 1982, p. 75.

21. H. Richter, L.J. Brillson, to be published.

22. M.F. von Allmen, in Laser Annealing of Semiconductors, ed. by J.M. Poate, J.W. Mayer, Academic Press, New York, 1982, p. 43.

23. American Institute of Physics Handbook, ed. by D.E. Gray.

24. D.D. Wagman, W.H. Evans, V.B. Barker, I. Halow, S.M. Bailey, R.H. Schumm, Natl. Bur. Std. Technical Notes 270-3-270-7 (US Govt. Printing Office, Washington, DC, 1968-1971.

25. H. Richter, L.J. Brillson, M. Kelly, G. Margaritondo, to be published.

Figure Captions

Fig. 1 In4d SXPS core level spectra taken at 60 eV photon energy, yielding maximum surface sensitivity: UHV-cleaved (110) surface, with 20 Å Al overlayer, and after laser annealing with increasing energy density. The dots indicate the model spectrum as described in the text.

Fig. 2 P2p SXPS core level spectra taken at 140 eV photon energy, UHV-cleaved (110) surface, with 20 Å Al overlayer, and after laser annealing with increasing energy density.

Fig. 3 Al2p SXPS core level spectra taken at 120 eV photon energy: 20 Å Al on InP (110) surface as evaporated and after laser annealing with increasing energy density.

Fig. 4 Change in surface composition of 20 Å-Al overlayer on UHV-cleaved InP (110) surface as a function of annealing energy density.

a) covalent bonded Al versus total Al: conversion of metallic Al into covalent bonded Al.

b) P2p versus In4d: attenuation of P2p level at surface due to Al overlayer and recovery after high energy density ann al.

c) metallic In4d versus total In4d: metallic segregation due to Al overlayer increases with energy density up to 0.3 J/cm^2 and then drops at higher energy densities.

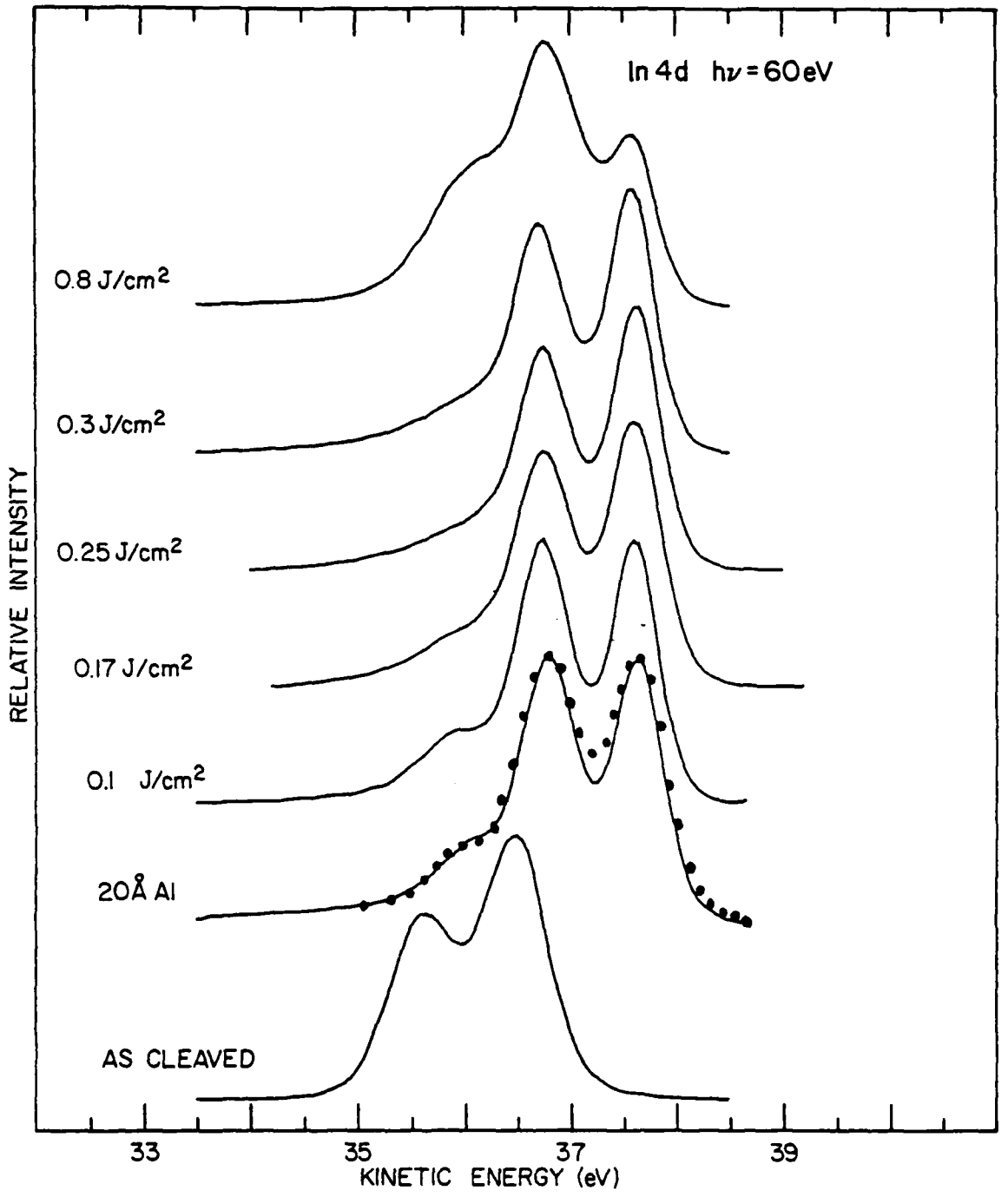
In 4d hν = 60eV
0.8 J/cm²
0.3 J/cm²
0.25 J/cm²
0.17 J/cm²
0.1 J/cm²
20Å Al
AS CLEAVED
RELATIVE INTENSITY
33
35
37
39
KINETIC ENERGY (eV)

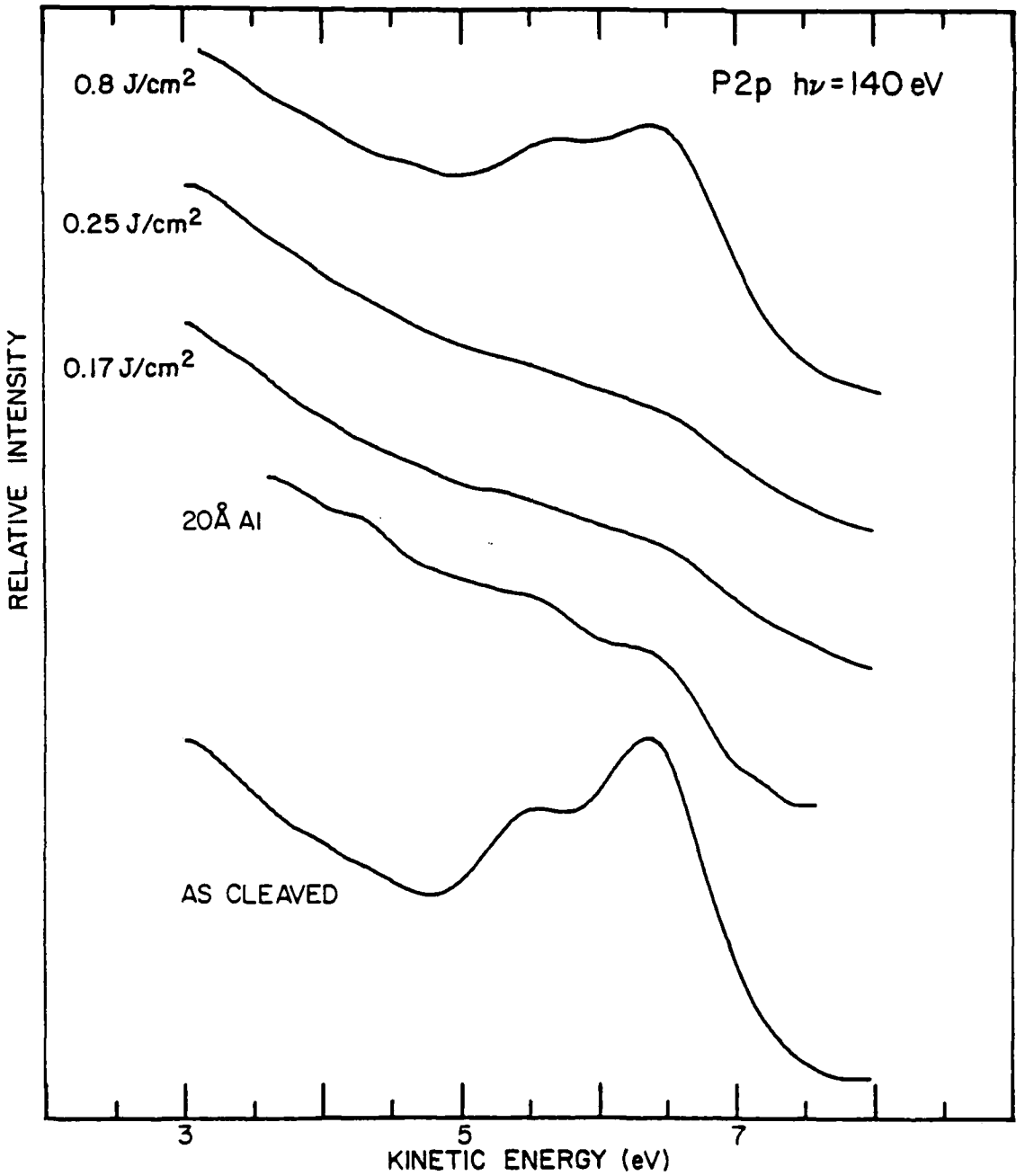
0.8 J/cm2
P2p hν = 140 eV
0.25 J/cm2
0.17 J/cm2
20Å Al
AS CLEAVED
RELATIVE INTENSITY
3
5
7
KINETIC ENERGY (eV)

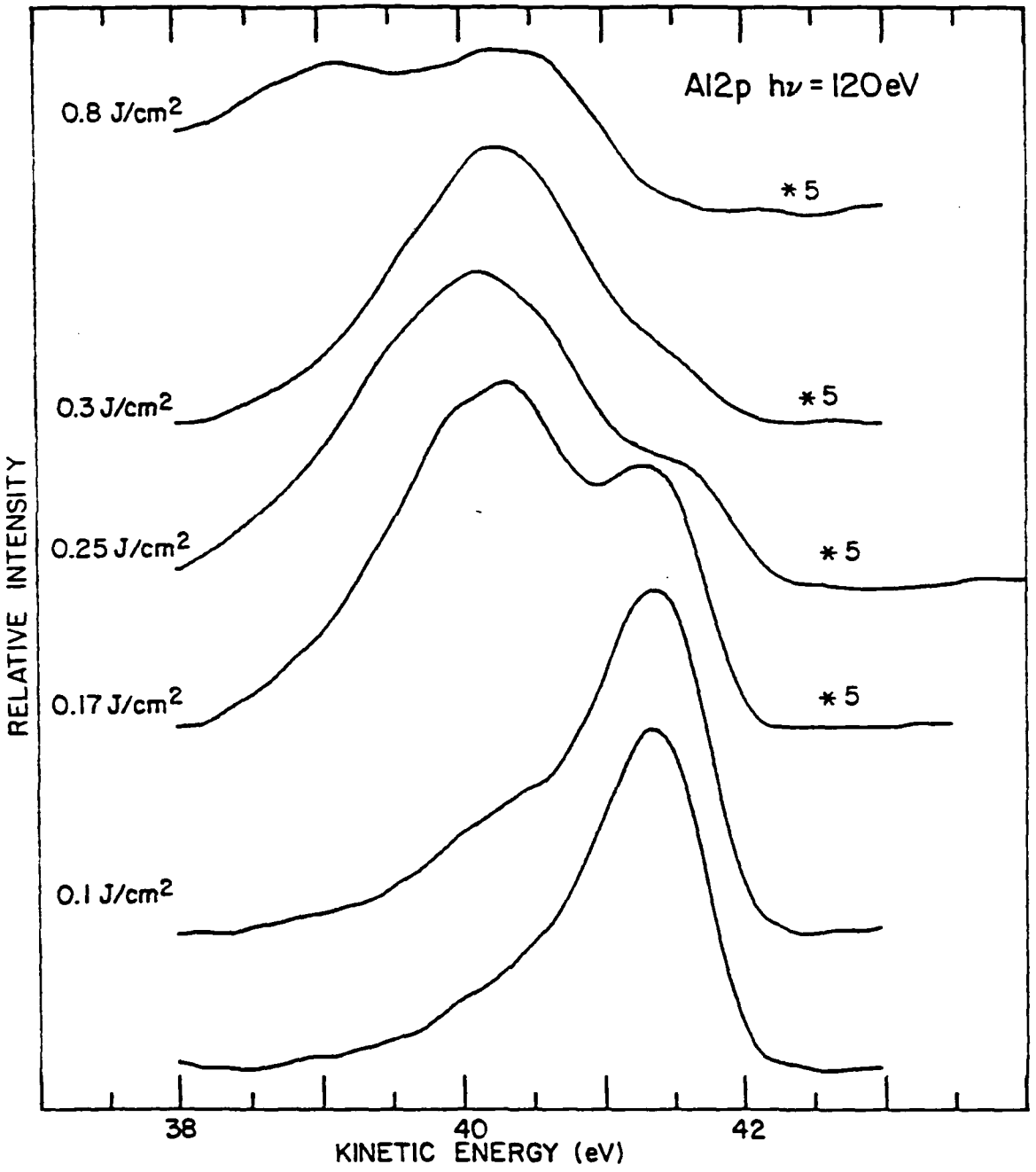
Al2p hν = 120eV
0.8 J/cm2
*5
0.3 J/cm2
*5
0.25 J/cm2
*5
0.17 J/cm2
*5
0.1 J/cm2
RELATIVE INTENSITY
38
40
42
KINETIC ENERGY (eV)

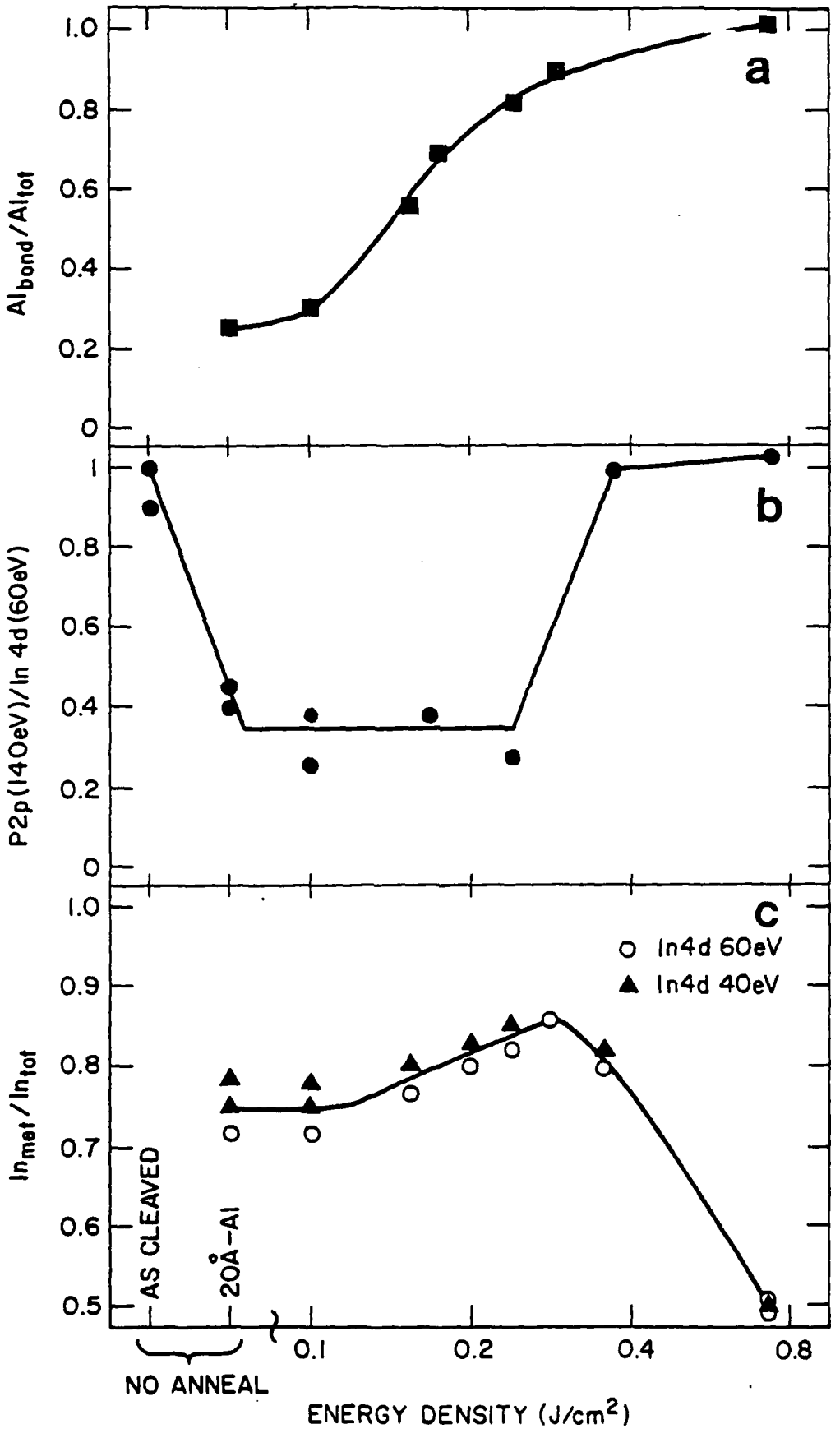
a
b
c
Al_{bond}/Al_{tot}
P2p(140eV)/In 4d(60eV)
In_{met}/In_{tot}
In4d 60eV
In4d 40eV
AS CLEAVED
20Å-Al
NO ANNEAL
ENERGY DENSITY (J/cm²)
1.0
0.8
0.6
0.4
0.2
0
0.9
0.7
0.5
0.1
0.2
0.4
0.8

LASER INDUCED CHEMICAL REACTIONS AT THE AL III-V SEMICONDUCTOR INTERFACE

H. W. Richter* and L. J. Brillson

Xerox · Webster Research Center, Webster, New York 14580

We have used pulsed laser annealing to produce highly localized chemical reactions at the interface between Al and various III-V semiconductors. We employed soft X-ray spectroscopy, Auger-electron spectroscopy and sputter depth profiling to characterize the interfacial chemical composition. From the variation of reaction threshold with the semiconductor substrate, we find that melting of both a thin layer of III-V compound and the metal overlayer initiates the chemical reaction.

Chemical reactions and diffusion at the metal-semiconductor interface have been studied quite extensively using surface science techniques /1-3/. Although such phenomena are usually localized within tens of Å at room temperature the resultant changes in chemical structure can strongly affect the macroscopic electronic properties of the metal-semiconductor contact. Interface reactions are strongly enhanced at elevated temperature, but they are generally accompanied by extensive interdiffusion. Laser annealing has not been used in many studies to modify the properties of Si/4/ and III-V semiconductors, in the latter case mostly to anneal ion implantation damage in GaAs. Relatively little work has been performed to induce metal-compound-semiconductors reactions via laser-annealing. Notably, Gold et al. /6/ and Barnes et al. /7/ have promoted the formation of ohmic contacts in the Au-Ge-GaAs systems. Kirkpatrick /8/ has suggested pulsed electron beam annealing of deposited Al on GaAs as a means of $Ga_{1-x}Al_xAs$ formation. Since laser annealing can be performed within very short times (<10ns) and depths (<100nm), such processing offers the potential of promoting strong localized chemical reaction without extensive interdiffusion.

In this study, we have combined pulsed ultraviolet laser annealing (5ns pulses from a 308 nm XeCl laser) to promote a chemical reaction near the Al-III-V semiconductor interface with surface sensitive techniques such as soft X-ray photoemission (SXPS) and Auger electron spectroscopy (AES) to monitor changes in atomic composition and bonding. All experiments were performed on (110) surfaces cleaved in ultrahigh vacuum (UHV) (pressure < 10^{-10} torr) from 5x5x15mm bars of GaP (doping level unknown) GaAs ($n = 0.47 \cdot 10^{18}$Te), GaSb ($p = 1.3 \cdot 10^{17}$Zn), InP ($p = 4.3 \cdot 10^{15}$Zn), InAs (nominally undoped) and InSb ($n = 0.9 \cdot 10^{18}$). Al overlayers ranging from 20 to 100 Å thickness were evaporated from a heated tungsten filament. The laser annealing was performed in the same UHV-chamber. Using a oval 0.6x0.3mm (1/e intensity) spot size, up to twenty single shot anneals could be performed on visually smooth surface areas of one cleave. AES-data were recorded from the center of the annealed spots with a fine focus (3μm) electron gun aligned by using the electron beam-induced image displayed by a TV-monitor. Auger-sputter depth-profile were taken for Al on InP. In this case, the entire 5x5mm surface was annealed by using repetitive pulses while scanning the laser beam over the surface.

The effect of the laser anneal on the Al-overlayer and near surface region of the semiconductor was characterized in two ways: 1) near surface atomic composition and 2) chemical state of the Al-atoms. Figure 1 shows atomic composition for a 50Å Al overlayer on two of the semiconductors investigated, GaAs and InSb, as a function of annealing energy density. The atomic composition was deduced from the intensitites of the strongest Auger peaks and calibration factors given in /9/. Prior to the laser annealing (i.e., zero energy density) we find in general a larger signal from the substrate than would be expected from the attenuation by a 50Å-Al overlayer. This behavior may be due to a non-continuous Al-overlayer as well as the interaction between the Al-overlayer and the semiconductor - especially the diffusion of the cation to the surface /10/. Annealing at low energy densities we find very little or no variation in the atomic composition until, within a relatively narrow energy range, the Al concentration decreases significantly. At high enough energy density the atomic concentration is again constant over a rather wide energy range. We define a reaction threshold by the midpoint between initial Al concentration and the high energy density plateau, thus making it independent of the intensity calibration. This threshold is characteristic for each material, ranging from 0.09 J/cm^2 for InSb to 0.19 J/cm^2 for GaP.

The sharp change in atomic composition is paralleled by a change in the chemical bonding of the Al-atoms. Well below the annealing theshold, the Al LVV transition is found at 68 eV, above the threshold at 64 eV. This indicates a change from metallic to covalent bonding as reported earlier using SXPS /10/. On the other hand, the position of the P-LVV transition is not affected, indicating little or no change in the chemical environment of the P-atoms.

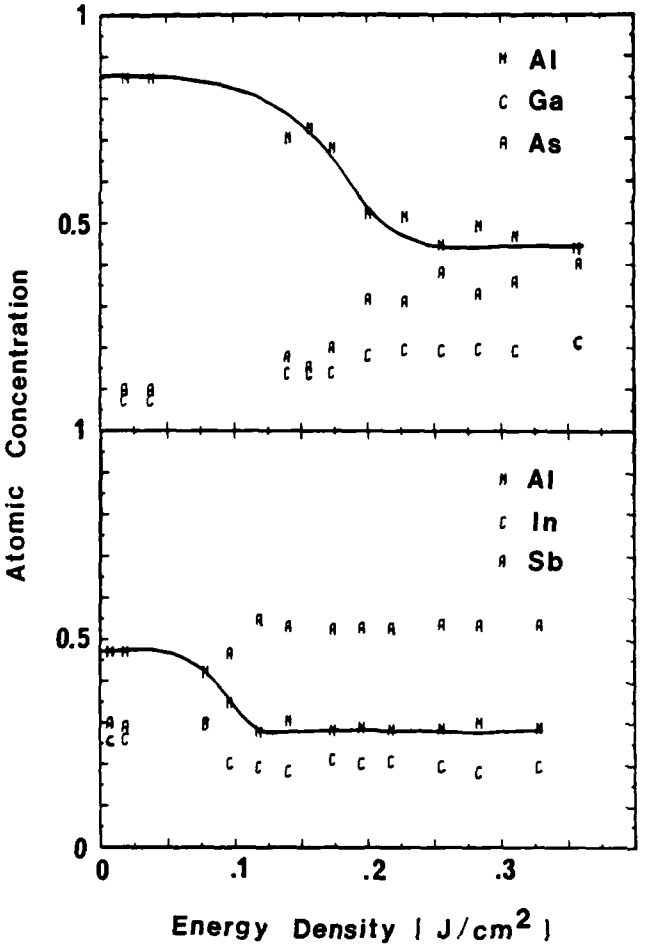

Fig. 1 Atomic Concentration of 50A Al on GaAs (top) and InSb (bottom) as a function of annealing energy density.

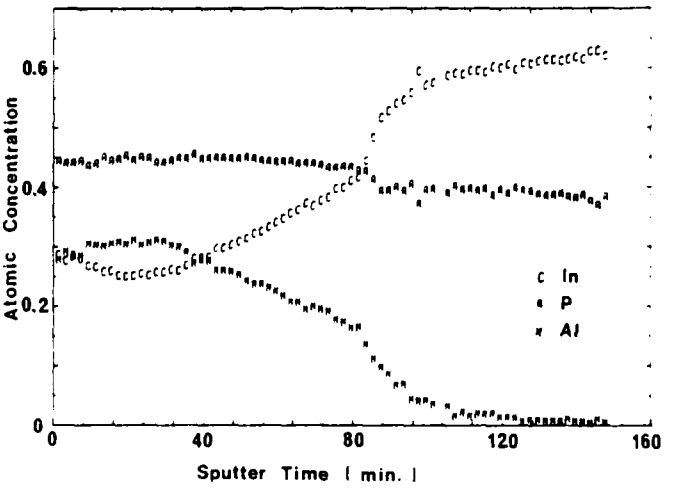

Fig. 2 Sputter depth profile of 50A-Al on InP annealed at an energy density of 0.14 J/cm^2 per pulse. The excess In above 120 min is due to preferential sputtering of P /11/. From the integration of the Al signal, we deduce a sputter rate of 2.25Å/min.

In order to demonstrate the localized nature of the chemical reaction, we show in Figure 2 a sputter-depth profile of a 50A-Al overlayer on InP annealed with a energy density of 0.14 J/cm^2. We observe a slight In segregation at the surface, a region of constant composition (8-32 min sputter-time), a very gradual decrease in the Al concentration (40 to 80 min sputter-time) and a rather sharp defined drop of the Al-concentration above 80 min. This sharp drop is even more remarkable, since in this experiment multiple shots were applied and every spot on the surface was annealed on average by 5 pulses. At low Al concentrations an exact measurement becomes difficult due to a weak structure in the In-spectrum in the same energy range. Above 100 min sputtered time, the Al concentration can only be considered as an upper limit. At this point, the spectra became almost indistinguishable from those taken from pure, sputtered InP surfaces. Therefore, we conclude that even after multiple pulses, the reaction and diffusion of the Al overlayer is well defined with a steep edge and localized to a depth of about 200Å.

In order to understand the systematics in the annealing behavior among the III-V semiconductors, we compared their optical and thermal properties (/12/). At 308mm (4eV) the reflectivity of all material are in the range from 42 to 56%, the absorption coefficient $8 \cdot 10^5$ to $12 \cdot 10^5 cm^{-1}$, a variation too small to explain the observed behavior even reduced by the common Al-overlayer. Likewise, we found no correlation between the reaction ΔH_R threshold and the heat of reaction released by the chemical reaction. While ΔH_R has proven effective in characterizing reactions at the metal-semiconductor interface /1,13/, it appears to be inappropriate in the case studied here. For example, GaP and GaAs show a similar threshold of 0.19 and 0.17 J/cm^2 but substantially different heats of reaction, e.g., 18.8 and 10.8 kcal/mol respectively. Thus, while the reactions are thermodynamically favorable, their rates are not determined by the difference in free energy. On the other hand, Figure 3 shows an excellent linear correlation between the reaction threshold and the heat of fusion H_{fus} /14/ for all materials. This fact suggests the following explanation of the metal-

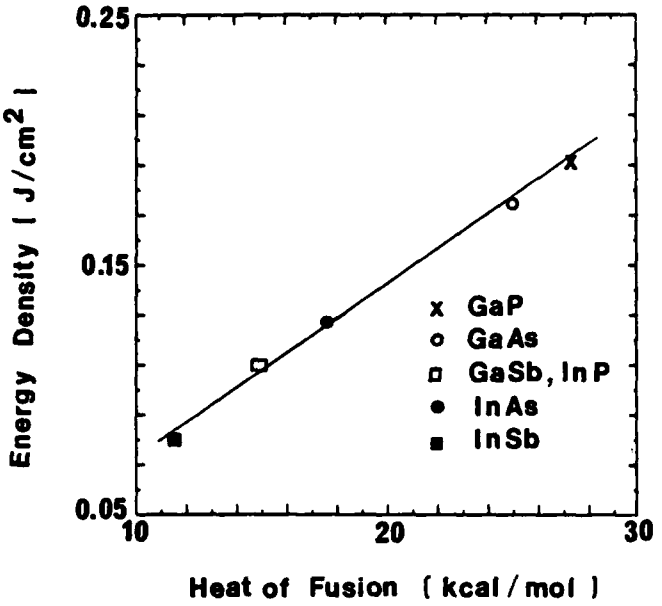

Fig. 3 Relationship between energy density of reaction threshold as defined in text and heat of fusion as compiled in /12/.

semiconductor reaction analogous to annealing of ion-implantion damages /5/. The laser pulse quickly heats the Al-layer and near surface region of the semiconductor. If enough energy is supplied, the Al overlayer and a thin layer of the substrate will melt. During the melt time (10-100ns) a fast interdiffusion of all atoms occurs and new bonds are formed. The assumption that the intermixing and reaction occurs almost exclusively in a thin molten layer can also account for the sharp interface after multiple pulse annealing: since the melt depth is constant from pulse to pulse, once the Al-overlayer is fully reacted, no significant increase in interdiffusion will occur.

Temperature profile calculations based on Baeri's and Compisano's heat flow model /15/ show that other thermal properties such as thermal conductivity, heat capacity and melting point influence the melting threshold of the semiconductor substrate. For the III-V compounds however, these properties in general follow the trend given by the heat of fusion. Our preliminary calculation show that the energy needed to melt the Al-overlayer and a 250A layer of the underlying semiconductor is, given the experimental error, in agreement with the observed threshold for the reaction. These calculations will be continued and refined and details will be published later.

In conclusion, we explain our observation on the laser induced Al-III-V compound reaction by a simultaneous melting of the metal and semiconductor substrate. The threshold in the Al-III-V semiconductor case is mainly controlled by thermal properties such as heat of fusion, melting temperature, thermal conductivity of the semiconductor substrate. This model explains not only experimental observations such as a sharp onset of the reaction and a sharp interface between a metal-rich layer and the underlying semiconductor substrate even after multiple pulses, but it can also be used to predict reaction thresholds for other systems on the basis of their thermal properties.

Partial support by the Office of Naval Research (ONR N00014-80-C0778) is gratefully acknowledged. We thank G. Margaritondo for valuable discussions and for supplying the GaP and InSb crystals.

*Present address: Max-Planck-Institute for Solid State Research, Stuttgart, West Germany.

References

1. L. J. Brillson, Surf. Sci. Repts. 2, 123 (1982); Int. J. Phys. Chem. Solids 44, 703 (1983).

2. G. Margaritondo, Solid State Electron. 26, 499 (1983).

3. R. H. Williams, Contemp. Phys. 23, 329 (1982).

4. G. Foti, E. Rimini, in "Laser-Annealing of Semiconductors", ed. J. M. Poate and J. W. Mayer (Academic Press, New York, 1982) p.203.

5. J. S. Williams, in "Laser Annealing of Semiconductors", ed. J. M. Poate and J. W. Mayer (Academic Press, New York, 1982) p. 383.

6. Gold, R. B. Powell, R. A., and Gibbons, J. F. in "Laser-Solid Interactions and Laser Processing", ed. S. D. Ferris, H. J. Leamy, and J. M. Poate (Am. Inst. Phys.. New York, 1979) p. 635.

7. Barnes, P. A., Leamy, H. J., Ferris, S. D., Williams, J. S., and Celler, G. K., in "Laser-Solid Interactions and Laser Processing", ed. S. D. Ferris, H. J. Leamy, and J. M. Poate (Am. Inst. Phys., New York, 1979) p. 647.

8. Kirkpatrick, A. R., In "Laser and Electron Beam Processing of Electronic Materials", ed. C. L. Anderson, G. K. Celler, and G. A. Rozgonyi (Electrochem. Soc., Pennington, New Jersey, 1980) p. 108.

9. L. E. Davis, N. C. MacDonald, P. W. Palmberg, G. E. Riach. and R. E. Weber, "Handbook of Auger Electron Spectroscopy", Physical Electronics Industries, Minnesota, 1976.

10. H. W. Richter, L. J. Brillson, M. K. Kelly, R. R. Daniels, and G. Margaritondo, J. Vac. Sci. Technol. B., in press.

11. Y. Shapira, and L. J. Brillson, J. Vac. Sci. Technol. B1, 618 (1983).

12. Landolt-Bornstein, "Numerical Data and Functional Relationships in Science and Technology", Group III, Vol. 17a, Berlin, 1982.

13. L. J. Brillson, Phys. Rev. Lett., 40, 260 (1978).

14. American Insitute of Physics Handbook, ed. D. E. Gray(New York, 1972).

15. P. Baeri, and S. U. Campisano, in "Laser Annealing of Semiconductors", ed. J. M. Poate and J. W. Mayer (Academic Press, New York, 1982) p. 75.

Laser Induced Chemical Reactions at the Al/III-V Compound Semiconductor Interface

H.W. Richter* and L.J. Brillson
Xerox Webster Research Center
Webster, NY 14580

We have used pulsed laser-annealing to promote and characterize highly localized chemical reactions at Al interfaces with III-V compound semiconductor. At successive stages of these laser-induced reactions, we have monitored atomic movement and chemical structure on a microscopic scale using soft x-ray photoemission spectroscopy (SXPS) and Auger electron spectroscopy (AES). For Al on each of the six III-V compound semiconductors investigated, we have found a finite range of energy density above a characteristic threshold energy density such that a chemical reaction is produced without disrupting the surface morphology. The systematic change of threshold with different semiconductors indicates a thermally activated reaction occurring in the molten phase of the Al-overlayer and a thin substrate layer. Heat-flow calculations which model the temperature profiles during and after the laser pulse confirm this model and also account for the highly abrupt interface between the reacted ternary overlayer and the binary substrate. The excellent agreement between experiment and theory demonstrates that thermal properties of the semiconductor have a dominant influence on the interfacial temperature profile and threshold energy density for reaction.

*Present address: Max-Planck Institute for Solid State Research, 7000 Stuttgart 80, W. Germany

Introduction

Chemical reactions and diffusion at metal-semiconductor interfaces are quite common phenomena, even if all interface fabrication steps are carried out at or near room temperature.[1-3] Research involving surface science techniques reveals that these effects are usually localized within a few tens of Å near the interface. Nevertheless, the resulting changes in chemical structure can strongly affect the macroscopic electronic properties of the metal-semiconductor contact. Thus, it is of interest to study how these chemical processes evolve for higher temperatures at which interface reactions and interdiffusion are strongly enhanced.[4] Such studies can provide new information on mechanisms of Schottky barrier formation, such as formation of interfacial dielectric layers, alloy layers, or defects within the semiconductor. They can also reveal modes of interface degradation for semiconductor interfaces at lower temperatures over relatively long times.

Laser annealing has been used in many studies to modify the properties of Si such as recrystallizing damage after ion implantation,[5] changing as-implanted doping profiles,[6] amorphizing crystalline silicon,[7] changing surface reconstruction,[8] and forming silicides from the elemental layers.[9] Comparatively little work has been done with III-V semiconductors, and most of that has been concerned with annealing ion implantation damage in GaAs.[10] Relatively few studies have been performed to induce metal-compound-semiconductors reactions via laser-annealing and these have focused primarily on the formation of Ohmic contacts.[11] Notably, Gold et al.[12] and Barnes et al.[13] have promoted the formation of ohmic contacts in the Au-Ge-GaAs systems. Kirkpatrick[14] has suggested pulsed electron beam annealing of deposited Al on GaAs as a means of $Ga_{1-x}Al_xAs$ formation. L.D. Laude[15] has used CW- and pulsed-laser annealing to form compound semiconductors such as CdTe and CdSe from the elements. A major problem with most of the annealing work in compound semiconductors seems to be a significant

loss of the more volatile component near the surface, leaving a non-stochiometric layer with rather unpredictable properties.[16-19]

Short UV-laser pulses provide a source of energy for semiconductor interfaces which is highly localized both spatially and temporally. Pulsed UV-laser annealing can promote processes far from thermal equilibrium, as is best illustrated by the amorphization of Si[7] by picosecond laser-pulses. In our study, we have used a pulsed ultra-violet (UV) laser (5 ns pulses from a 308 nm XeCl excimer laser) to anneal metal-semiconductor interfaces and promote highly localized chemical reactions. These interfaces were annealed in ultrahigh vacuum (UHV) and characterized by surface-sensitive techniques in order to monitor the chemical processes on a scale of monolayers. Because of the extremely short laser pulse (5 ns) and resultant heating (~ 100 ns), interdiffusion of the metal and semiconductor atoms could be limited to tens of Å. Longer heat treatments, even at lower temperatures, would produce extended diffusion, and a "washing out" of the interfacial structure, below the level of detectability of our spectroscopic techniques. In addition, the time structure of the laser pulses permits us to monitor the laser-induced process in discrete steps, using successive pulses. The UHV environment excludes ambient contamination which could interfere with or otherwise mask the metal-semiconductor interaction. Surface science techniques such as soft x-ray photoelectron spectroscopy (SXPS) and Auger electron spectroscopy (AES) combined with sputter-depth-profiling allow us to follow atomic movements on a monolayer scale and to determine the chemical state of these atoms.

We have systematically investigated laser-induced reactions at interfaces formed by depositing Al overlayers on ultrahigh vacuum (UHV) cleaved (110) surfaces of GaP, GaAs, GaSb, InP, InAs, and InSb. Considerable spectroscopic evidence[11] suggests that strong Al-anion bonding takes place at this interface, even with the semiconductor substrate held at room temperature. With the laser-induced

annealing technique, we have discovered that it is possible to induce strong chemical reactions at the Al/III-V compound semiconductor interface which are limited to depths on the order of a hundred Å and which involve all Al-Al bonds being replaced by Al-anion bonds. This can be achieved without severely disrupting the surface morphology - i.e., roughness as measured by optical microscopy and electron beam induced imaging with 3 μm resolution.

The materials investigated exhibit a wide range of energy density thresholds for laser-induced reactions. For example, the Al-GaP and GaAs system react only at highest energy densities of .19 and .17 J/cm^2 whereas InSb begins to react at energy densities as low as .08 J/cm^2, we explain these differences using a purely thermal model, in which the energy is absorbed near the metal-semiconductor interface much faster than the semiconductor substrate can reach thermal equilibrium. If enough energy is supplied, the Al-overlayer and near surface (tens of nm or less) regions of the substrate will melt and a fast intermixing and rearrangement of bonds takes place. From numerical heat flow calculations, we can explain the differences in threshold between the systems as the manifestation of different thermal and, to a much lesser extent, optical properties of the semiconductor materials. Taking into account variations in heat capacity, thermal conductivity, and reflectivity, we find that differences in semiconductor heat of fusion scale extremely well with the observed thresholds. In this time and temperature regime, differences associated with bulk melting appear to be dominant, whereas heats of of reaction released due to rearrangements of bonds do not seem to play an important role.

II. Experimental

All experiments were performed on visually smooth (110) surfaces cleaved in ultrahigh-vacuum ($p \leq 10^{-10}$ torr) from bars (5x5x15 mm) of the semiconducting material, thereby ensuring an atomically clean, reproducible starting point for the annealing and the surface characterization. Both SXPS and AES were applied to

GaAs (n type, 4.7×10^{17} cm^{-3} Te) and InP (p-type, 4.3×10^{15} cm^{-3} Zn), whereas GaP (doping unknown), GaSb (p-type, 1.3×10^{17} cm^{-3} Zn), InAs (nominally undoped) and InSb (n-type, 9×10^{17} cm^{-3}) was investigated by AES only. Al-overlayers ranging from 20 - 100 Å thickness (monitored with a quartz-crystal oscillator) were evaporated from heated tungsten filaments at rates of approximately 0.5 Å/s in the same UHV-chamber. The laser annealing was also performed in the same UHV-chamber immediately after the deposition of the Al-overlayer with an Excilite model XL-401 XeCl-laser operating at 308 nm with pulses of up to 5 mJ energy. The light was focused through a sapphire-window onto the specimen with a 350 mm quartz lens. Light reflected from the sample surface was directed out of the UHV-system through the entrance window in order to prevent laser light from impinging on the vacuum chamber walls, since the resultant desorption of ambient species could possibly contaminate the specimen surface under investigation.

Two different modes of annealing were used. Single shot anneals produced ~ .3 x .6 mm spots sufficiently large to perform AES with a fine focus (3 μm) electron gun and a PHI model 15-110A single pass cylindrical mirror electron energy analyzer (CMA). In this mode, anneals with up to 20 different pulse energies could be performed and analyzed on a single cleaved surface. For the AES-sputter profiles and the SXPS measurements at the Tantalus electron storage ring, large homogeneously annealed areas were required. We used repetitive pulses while scanning the laser beam to anneal the 5x5 mm^2 cleaved surface completely. Scan speed and pulse rate were chosen such that the individual laser spots overlapped with each surface point receiving 4 pulses. In both modes, special care was taken to align all specimens into exactly the same position relative to the focusing lens in order to assure good reproducibility of energy density from anneal to anneal. This was actually verified by repeating the same annealing steps on several specimen surfaces and comparing the associated spectroscopic features.

In the case of the single shot experiments, the annealed areas could be inspected with an optical microscope after removal from the system. From the dimension of the annealed area as a function of the pulse energy, the 1/e - values (assuming Gaussian profiles in both directions) of the oval spot could be determined accurately to be 0.3 and 0.6 mm for the short and long axes respectively. When the laser was scanned to cover the whole surface, this method could not be applied. In this case, we estimated the spot-size from the imaging properties of the optical system. Therefore the relative accuracy and reproducibility between different anneals in the same mode is estimated to be better than 10% (including shot-to-shot variations in the laser output), but the absolute value of the energy density, especially of the SXPS measurements, is only accurate to about 25%.

Up to the highest applied energy density, none of the materials exhibited any visual damage. The single shot experiments showed both in optical and electron beam-induced images a homogeneously annealed inner portion of each anneal, while the edges showed a number of concentric ring structures due to the decrease in energy density.

III. Results

The effect of the laser anneal on the Al overlayer and near surface region of the semiconductor was characterized in two ways: 1) near surface atomic composition and 2) chemical state of the Al-atoms. The most obvious changes due to the laser annealing appear in the Al 2p-SXPS spectra, as shown in Fig. 1 for the case of a 20 Å Al film on InP. In the Al 2p spectrum of the 20 Å overlayer before laser annealing in Fig. 1 (lowest curve), we observe a wing of significant intensity at lower kinetic (high binding) energy beside the major contribution from the metallic Al. This spectrum agrees with earlier observations[20-23] which indicate that Al reacts with the InP substrate and Al-P bonds are formed at the Al-InP interface.

Annealing the Al-overlayer with increasing densities, we observe the following: between 0.1 J/cm^2, the major intensity contribution in the photoelectron spectrum is shifted from 41.3 eV kinetic energy to 40.3 eV kinetic energy, indicating that more and more Al atoms change their chemical bonding from being bonded in a metal to a stronger covalent bond. This trend continues with higher annealing energy density until 0.3 J/cm^2, for which only a very small contribution from the 41.3 eV "metallic" peak is left. The two components can be separated quantitatively by fitting a model spectrum consisting of the Lorentzian doublet of metallic Al broadened by a Gaussian function (representing the experimental resolution) to the high energy side of the measured spectrum of the unannealed sample. For all spectra shown here, the model spectrum fits the metallic component very well, indicating that this peak does not broaden but that the intensity is transfered into the peak at higher binding energy. The intensity contribution from the "covalent" peak is plotted in Fig. 2a, illustrating a sharp onset of the reaction between 0.1 and 0.17 J/cm^2.

Up to 0.3 J/cm^2, the total Al-intensity drops by only 40% compared to the initial 20 Å-Al, indicating that the reaction is limited to a small volume near the surface. The details of the corresponding In 4d and P 2p spectra are discussed in Ref. 27 in detail and summarized in Figs. 2b and c. The Al overlayer strongly attenuates the P 2p intensity of the cleaved surface but as far as we can tell from the rather weak signal, there is no change in either peak position or peak shape. This indicates that the strength of chemical bonding between P atoms and its neighbors is affected very little by the Al overlayer, as expected because of the small difference between Al-P and In-P binding energies. During the anneal, both the intensity ratio P 2p/In 4d and the P 2p peak position change very little, again indicating that the chemical surroundings of the P-atoms are relatively unaltered. In contrast, the In 4d line changes drastically. After the evaporation of the Al we find two major peaks separated by 0.8 eV of approximately equal intensity and a rather small shoulder at higher binding energy. It has been shown earlier[20-27] that this In 4d is due to a

combination of two components representing two different chemical states of the In atoms: a) In in a covalent bonded, semiconductor-like environment and b) In in a metallic bonded state.

By deconvoluting these two In components, we can follow their intensity during the laser annealing, as shown in Fig. 2c. We find a gradual increase in the metallic component which parallels the increase of the covalently bonded Al (Fig. 2a), and which can be attributed to an exchange of the metal atoms. Only at the highest annealing energy does this trend reverse, along with a recovery of the P 2p intensity. We attribute this behavior to a partial evaporation of both In and P atoms from the surface, leaving an almost "as cleaved" surface.

The results for Al on GaAs from SXPS can be summarized as follows: the unannealed Al-overlayer shows a weaker interaction with the GaAs substrate: less Ga goes into the metallic phase (45% compared to 75% for In with the InP) and less Al-anion bonds are formed, as indicated by a less pronounced shoulder in the Al2p spectra. The reaction does not start until over 0.3 J/cm^2, but at 0.4 J/cm^2 almost all of the original Al 2p peak has shifted by 1 eV to higher binding energy, leaving few traces of the metallic component.

AES reveals information which is complementary to that of SXPS. Peak-to-peak height analyses allow us to determine the atomic composition of near surface layers. Also the significantly large chemical shift of 4 eV between the Al LVV Auger line of metallic and covalently bonded Al[28] permits us to determine easily the chemical state of the Al-layers at different stages of the anneal. Unfortunately a similar chemical shift cannot be observed for the In MNN and the Ga LMM lines, partially due to the intrinsic width and partially due to the reduced resolution of the CMA at higher kinetic energies. Significant chemical shifts in the PLVV Auger lines are in principle observable, but as in the case of SXPS we did not in fact observe any chemical shifts from the initial cleaved position. Figure 3 shows as an example the

AES spectra in the range 40 to 140 eV, displaying the Al LVV and P LVV transitions of 50 Å of Al on GaP after annealing at the indicated energies. Between 0.1 and 0.2 J/cm^2 the major part of the Al LVV shifts from 67 eV to 64 eV. At 0.2 J/cm^2 there is an indication of more than one component and at 0.3 J/cm^2 the transition is complete. Even though the total linewidth of the P LVV is comparable to that of Al and shifts on the order of 0.3 eV are observable, no shift could be detected here. The change in chemical state is paralleled by a drop in the intensity of the Al LVV line relative to the P LVV and, not shown here, the Ga LMM lines.

We have recorded Auger spectra at energy densities ranging from no anneal to 0.4 J/cm^2 for all six III-V compounds investigated here. Figure 4 shows the atomic composition for a 50 Å Al overlayer on two of the semiconductors investigated, GaAs and InSb, as a function of annealing energy density. The atomic composition was deduced from the intensities of the strongest Auger peaks and calibration factors given in Ref. 29. Prior to the laser annealing (i.e., zero energy density) we find in general a larger signal from the substrate than would be expected from the attenuation by a 50 Å-Al overlayer. This behavior may be due to a non-continuous Al-overlayer as well as to the interaction between the Al-overlayer and the semiconductor - especially the diffusion of the cation to the surface.[27] Annealing at low energy densities we find very little or no variation in the atomic composition until, within a relatively narrow energy range, the Al concentration decreases significantly. At high enough energy density the atomic concentration is again constant over a rather wide energy range. We define a reaction threshold by the midpoint between initial Al concentration and the high energy density plateau, thus making it independent of the intensity calibration. This threshold is characteristic for each material, ranging from 0.08 J/cm^2 for InSb to 0.19 J/cm^2 for GaP. (See also Table I).

In order to demonstrate the localized nature of the chemical reaction, we show in Fig. 5 a sputter-depth profile obtained with AES of a 50 Å-Al overlayer on InP annealed with energy density of 0.14 J/cm^2, i.e., just above the threshold. We observe a slight In segregation at the surface, a region of constant composition (8-32 min sputter-time), a very gradual decrease in the Al concentration (40 to 80 min sputter-time) and a rather sharp defined drop of the Al-concentration above 80 min. This sharp drop is even more remarkable in this experiment since multiple shots were applied and every spot on the surface was annealed on average by 5 pulses. At low Al concentrations, an exact measurement becomes difficult due to a weak structure in the In-spectrum in the same energy range. Above 100 min sputtered time, the Al concentration can only be considered as an upper limit. At this point, the spectra became almost indistinguishable from those taken from pure, sputtered InP surfaces. Therefore, we conclude that even after multiple pulses, the reaction and diffusion of the Al overlayer is well defined with a steep edge and localized to a depth of about 200 Å.

IV. Discussion

The AES and SXPS data can be summarized as follows: The laser annealing promotes a strong reaction of the Al-layer with the semiconducting substrates. Al-Al bonds are broken and Al-anion bonds are formed. At high enough energy we find a complete reaction of the metallic Al. While no anion loss near the surface is observed, cations segregrate near the surface and form metallic clusters. Even after multiple-shot annealing, the reaction is highly localized on a scale of 100 Å. For each material, we find a characteristic threshold for the onset of the reaction.

The long on-going controversy concerning the mechanisms of energy deposition during pulsed laser annealing experiments in silicon, has been resolved recently.[30] It is generally believed that, on a nanosecond (ns) timescale, essentially all of the deposited energy is converted into lattice vibrations or macroscopically to an increase

in temperature. All the observations involving diffusion of dopants, recrystallization etc. can be understood by thermally driven processes. For the balance of our discussion we will therefore assume that, on the ns-timescale of our experiments, the deposited energy is converted to thermal energy somewhere in the system. In order to understand especially the different thresholds for the different materials, we will discuss these topics: a) optical properties, b) interface heat of reaction between Al and III-V semiconductors, c) bulk thermal properties, and d) the resultant heat flow calculation.

a) Optical Properties

Aspnes and Studna[31] give a comprehensive overview on the optical properties of semiconductors at room temperature. According to their earlier data, the absorption coefficient for the materials investigated in our study range from $7 \cdot 10^5$ cm^{-1} for InP to $1.5 \cdot 10^6$ cm^{-1} for InSb and the reflectivity from 38% (InP) to 61% (InSb) at 4 eV. As reported for Si[32] at elevated temperature and photon energies above the direct bandgap, the optical properties of InSb change little up to temperatures close to melting[33] at 4 eV. Preliminary measurements[34] on GaAs up to 800K indicate the same behavior. Therefore, for further discussion, we will assume that the data in Ref. 31 are a reasonable approximation for the whole temperature of the individual material.

The influence of the absorption coefficient on to the temperature profile during and after the exciting laser pulse is discussed in Ref. 35. Under certain conditions the heat flow equation can be solved analytically. In this approximation, the temperature profile becomes independent of α if the light absorption length α^{-1} is small compared to the thermal diffusion length $\sqrt{Dt} = \sqrt{\kappa t/\rho C_p}$, where κ is the thermal conductivity, C_p the heat capacity, ρ the density of the material, and t the laser pulse duration. In simple terms this means that thermal diffusion during the pulse has already smeared out all temperature gradients near the surface which

would be expected due to the gradient in deposited energy. For the materials discussed here, $\sqrt{Dt}$ at all temperatures is larger than $2 \cdot 10^{-5}$ cm, which is an order of magnitude larger than the largest optical absorption length of $1.4 \cdot 10^{6}$ cm^{-1} (InP). Therefore, the temperature profile becomes independent of α and of changes in α due to temperature changes.

The energy deposited E_{dep} in the sample is directly related to the reflectivity R of the material via the formula $E_{dep} = E_{laser}(1 - R)$, where E_{laser} is the pulse energy. The differences in reflectivity (see Table I) cannot account for different annealing behavior - we find an anticorrelation between threshold and reflectivity. GaP, with the highest threshold, shows a relatively low reflectivity. Conversely InSb, with the highest reflectivity, shows the lowest threshold energy. The reflectivity of the Al-overlayer III-V semiconductor system can be calculated from the optical constants of both material using the formulas given in Ref. 36. Using n = 0.25 and k = 3.33 for Al,[36] these values are given in Table I for a 50 Å Al overlayer on the III-V compounds: in general, the surface reflectivity increases and differences between the substrates decrease. These are the values we have used for our heat flow calculations.

b) Interface heat of reaction

At room temperature, the reaction between monolayers of metal on various semiconductors, III-V's as well as others, can be explained by assuming that the driving force for this reaction is provided by the heat of reaction ΔH_R.[1,37] Systems react strongly if ΔH_R is large. Examples include Ti, Ni, and Al on InP.[20] If ΔH_R is small, the metal-semiconductor system behaves qualitatively different. For the systems investigated in this study, ΔH_R calculated from the difference in heats of formation given in Ref. 38 are listed in Table I. There is no obvious correlation between the observed threshold for the reaction and the change of enthalpy due to the reaction. Especially noteworthy is the comparison between Al-GaP and Al-

GaAs. While these two systems show rather similar thresholds of .19 J/cm^2 and 0.17 J/cm^2, their respective ΔH_R of 18.8 and 10.8 kcal/mol are substantially different. Thus, while the reactions are thermodynamically favorable, their rates and thresholds do not seem to be determined by the energy released from the metal-semiconductor reaction.

c) Bulk thermal properties

In contrast to the interface heat of reaction, the bulk heat of fusion provides a striking, linear correlation with E_{thres}. Figure 6 shows the reaction threshold E_{thres} for the six materials plotted versus the heat of fusion[42] H_{fus}. These results suggest that melting of the substrate is the important step in the reaction scheme that determines the reaction between the metal-overlayer and the substrate. The extremely good correlation shown in Fig. 6, is particularly significant, given that the heat of fusion is only one of several material parameters which determine the melting threshold for our interface laser annealing experiments. To verify that substrate melting is the basis for our observations given the particular thermal properties of these III-V compounds, we have performed extensive calculations to model the thermal behavior of the materials during and after the laser pulse. Since the thermal properties of heat conductivity κ and heat capacity C_p are strongly temperature-dependent (see Table II), the basic heat-flow equation[39]

$$\frac{\partial T}{\partial t} = \frac{\alpha}{\rho C_p} I(Z,t) + \frac{1}{\rho C_p} \frac{\partial}{\partial Z} \left(\kappa \frac{\partial T}{\partial z} \right) \qquad (1)$$

cannot be solved analytically. The numerical model used to solve the problem follows the lines given in Refs. 35 and 40. We section the interface and subsurface material into slabs, making use of the equations for the one-dimensional case given in Ref. 39. The Al overlayer is treated as a separate slab with κ = 2.37 W/cm K, C_p = 2.85 J/cm^3 K, and H_{fus} = 1.07 J/cm^3 treated as constants, since these parameters

are only slightly temperature-dependent.[41] For better accuracy near the surface, we use slabs of 50 Å or less near the surface, geometrically increasing in thickness with depth into the substrates. To facilitate the calculations, we assume that $C_p = C_{po} + \lambda T$, $T < T_{max}$, $C_p = \text{const}$, $T > T_{max}$, and $\kappa = \kappa_o T^{-x}$, where C_{po}, λ, κ_o, κ are fitted to the experimental data (see Table II). In the course of collecting the thermal properties, we discovered that for most of the materials only fairly old data are available,[42] and some cases taken only on polycrystalline materials.[43] Even for the commonly studied material GaAs, there are wide discrepancies between different sources.[35,43] Based on a survey of the literature, it is our judgment that the data collected in Table II are the most accurate values. For our specific calculations, the exact temperature dependence of C_p and κ is not important, but the overall functional behavior of these parameters can influence the results strongly. We have calculated the temperature profiles for all materials for a wide range of incident energies. In all cases, the actual energy absorbed was determined by the reflectivity for the system given in Table I. The profiles were calculated up to a depth of 10,000 Å, where with further increase no changes near the surface occurred. The elapsed time between iterations had to be chosen according to the stability condition given in Ref. 39 and was typically $2 \cdot 10^{-11}$ s. The melt duration near the threshold is typically 10-20 ns and the melt depth rises approximately linearly with energy density.

In order to compare the calculations with the experimental reaction threshold, we plot in Fig. 7 the reaction threshold as defined earlier over the calculated energy necessary to melt the Al overlayer and 250 Å of the substrate. For GaAs, two calculated values are given: 1) for thermal data from Ref. 35 and 2) from Ref. 43, indicating the uncertainties in the calculations arising from variations in the thermal properties from the literature. For InAs, the thermal conductivity varies by a factor of two with doping[43], and there are significant differences between nominally undoped samples. Since the thermal conductivity was measured on polycrystalline material only up to 800°K, there is some uncertainty in the accuracy of the thermal

properties used in our calculations. Also indicated in Fig. 7 is the estimated absolute error of the reaction threshold ($\approx$ 25%) for the highest energy. The relative error between the different materials is less than 10%. Except the InAs point, all points fall within the relative error of the measured threshold onto a best fit straight line, passing through the origin of the coordinate system with a slope of 1.02. This excellent correlation between calculated melt energies and measured threshold energies strongly supports the proposed model. The slope of nearly one also indicates that the experimental energy calibration is fairly accurate and free of systematic errors. Even though the thermal data on the III-V compounds are fairly old and sometimes taken on inferior material, they seem to describe the correct trend and also allow quantitative calculations. We have applied this model to estimate the reaction threshold for the Cu-CdS system in advance, and even with just approximate values for the thermal properties, the expected threshold was met quite accurately.[46]

V. Conclusions

In summary, we have used SXPS and AES measurements of chemical shifts and atomic spectral intensities at laser-annealed metal-III-V compound semiconductor interfaces to identify the probable mechanism which determines the threshold for metal-semiconductor reaction. Such reactions can be localized to depths of only tens of nanometers using pulsed excimer lasers and they exhibit a finite "window" of deposited energy density in which reaction can occur without disruption of the film-substrate surface morphology. An excellent correlation between the observed threshold in energy density and the semiconductor heat of fusion for six III-V compound semiconductors demonstrates that melting of the substrate within the laser pulse duration governs the metal-semiconductor interaction at elevated temperatures. Model calculations of laser-deposited heat transfer and temperature profile based on observed threshold energy densities and reacted interface depths

reveal very good agreement between observed and calculated thresholds based on available thermal data. In the case of GaAs, this systematic agreement permits us to discriminate between divergent reports of thermal data. Analogous laser-threshold studies are planned for metals with other classes of semiconductors, providing a basis for predicting and controlling the features of metastable metal-semiconductor interface layers.

Acknowledgements

Partial support by the Office of Naval Research (ONR N00014-80-C-0778) is gratefully acknowledged. We thank J. Iseler (Lincoln Labs) for supply of our InP crystals, Jim Zesch (Xerox Palo Alto Research Center) for cutting and orienting them. Our special thanks go to G. Margaritondo for supplying us with GaP and InSb crystals, for the opportunity to use his group's equipment at the Stoughton Synchrotron Radiation Center as well as for inspiring discussions. The Synchrotron Radiation Center is supported by the National Science Foundation and the assistance of its staff is gratefully acknowledged. We also thank M.K. Kelly and R.R. Daniels for their help with the SXPS measurements, Tom Orlowski (Xerox Webster Research Center) as well as Dave Zehner (Oak Ridge National Laboratory) for valuable discussions.

References

1. L.J. Brillson, Surf. Sci. Reports 2, 123 (1982); Int. J. Phys. Chem. Solids 44, 703 (1983).

2. G. Margaritondo, Solid State Electron. 26, 499 (1983).

3. R.H. Williams, Contemp. Phys. 23, 329 (1982).

4. A.K. Sinha and J.M. Poate, in "Thin Films - Interdiffusion and Reactions", ed. J.M. Poate, K.N. Tu and J.W. Mayer, (Wiley-Interscience, New York, 1978) p. 407 and references therein.

5. G. Foti and E. Rimini, in "Laser-Annealing of Semiconductors", ed. J.M. Poate and J.W. Mayer (Academic Press, New York, 1982) p. 203 and references therein.

6. S.U. Campisano, Appl. Phys. A30, 195 (1983).

7. P.L. Liu, R. Yen, N. Bloembergen, and R.T. Hodgson, Appl. Phys. Lett. 34, 864 (1979); R. Tsu, R.T. Hodgston, T.Y. Tan, and J.E. Baglin, Phys. Rev. Lett. 42, 1356 (1979); A.G. Cullis, H.C. Webber, N.G. Chew, J.M. Poate, and P. Baeri, Phys. Rev. Lett. 49, 219 (1982).

8. D.M. Zehner and C.W. White, in "Laser Annealing of Semiconductors", ed. J.M. Poate and J.W. Mayer (Academic Press, New York, 1982) p. 281.

9. M.F. v. Allmen and S.S. Lau, in "Laser-Annealing of Semiconductors", ed. J.M. Poate and J.W. Mayer (Academic Press, New York, 1982) p. 439.

10. J.S. Williams, Mat. Res. Soc. Symp. Proc. 13, 621 (1983).

11. J.S. Williams, in "Laser Annealing of Semiconductors", ed. J.M. Poate and J.W. Mayer (Academic, New York, 1982), Chap. 11, pp. 383-438.

12. R.B. Gold, R.A. Powell and J.F. Gibbons, in "Laser-Solid Interactions and Laser Processing", ed. S. D. Ferris, H.J. Leamy, and J.M. Poate (Am. Inst. Phys., New York, 1979) p. 635.

13. P.A. Barnes, H.J. Leamy, S.D. Ferris, J.S. Williams and G.K. Celler, in "Laser-Solid Interactions and Laser Processing", ed. S.D. Ferris, H.J. Leamy, and J.M. Poate (Am. Inst. Phys., New York, 1979) p. 647.

14. A.R. Kirkpatrick, in "Laser and Electron Beam Processing of Electronic Materials", ed. C.L. Anderson, G.K. Celler, and G.A. Rozgonji (Electrochem. Soc., Pennington, New Jersey, 1980) p. 108.

15. L.B. Laude, Mat. Res. Soc. Symp. Proc. 23, 611 (1984).

16. V. Gamo, Y. Yuba, A.H. Oraby, K. Murakami, S. Namba and Y. Kawasahi, in "Laser and Electron Beam Processing of Materials", ed. by C.W. White and P.S. Peercy, (Academic Press, New York, 1980) p. 322; H.B. Harrison and J.S. Williams, ibid., p. 481.

17. D. Eirug Davies, J.K. Kennedy and E.F. Kennedy, in "Gallium Arsenide and Related Compounds", ed. H.W. Thimm, Inst. of Phys., (Conf. Series 56, London, 1980) p. 229.

18. M. Okigawa, T. Nakayama, K. Morita and N. Hoh, Appl. Phys. Lett. 43, 1054 (1983).

19. A.G. Cullis, H.C. Webber and D.S. Robertson, in "Laser-Solid Interactions and Laser Processing 1978", ed. S.D. Ferris, H.J. Leamy and J.M. Poate (Am. Inst. Phys., New York, 1979) p. 653.

20. L.J. Brillson, C.F. Brucker, A.D. Katnani, N.G. Stoffel and G. Margaritondo, Phys. Rev. Lett. 46, 838 (1981); Appl. Phys. Lett. 38, 784 (1981); J. Vac. Sci. Technol. 19, 661 (1981).

21. L.J. Brillson, C.F. Brucker, A.D. Katnani, N.G. Stoffel, R. Daniels and G. Margaritondo, J. Vac. Sci. Technol. 21, 564 (1982).

22. T. Kendelewicz, W.G. Petro, I.A. Babalola, J.A. Silberman, I. Lindau and W.E. Spicer, J. Vac. Sci. Technol. B1, 623 (1983); T. Kendelewicz, W.G. Petro, I. Lindau, W.E. Spicer, Phys. Rev. B30, 5800 (1984).

23. A. Kahn, C.R. Bonapace, C.B. Duke and A. Paton, J. Vac. Sci. Technol. B1, 613 (1983).

24. T.-X. Zhao, R.R. Daniels, A.D. Katnani, G. Margaritondo and A. Zunger, J. Vac. Sci. Technol. B1, 610 (1983).

25. A. McKinley, G.J. Hughes and R.H. Williams, J. Phys. C15, 7049 (1982).

26. R.H. Williams, R.R. Varma and A. McKinley, J. Phys. C10, 4545 (1977); R.H. Williams, A. McKinley, V. Montgomery, and I.T. McGovern, J. Vac. Sci. Technol. 21, 594 (1982).

27. H.W. Richter, L.J. Brillson, J. Vac. Sci. Technol. B2, 591 (1984).

28. L.J. Brillson, Phys. Rev. Lett. 37, 245 (1977).

29. L.E. Davis, N.C. MacDonald, P.W. Palmberg, G.E. Riach, and R.E. Weber, "Handbook on Auger Electron Spectroscopy", Physical Electronics Industries, Minnesota, 1976.

30. D. VanderLinde, B. Wastman, M. Kemmler, and Z.H. Zu, Mat. Res. Soc. Symp. Proc. 23, 123 (1984); D.H. Lowndes, H.C. Webber and N.G. Chew, Mat. Res. Soc. Symp. Proc. 23, 105 (1984); G.J. Galvin, J.W. Mayer and P.S. Percey, Mat. Res. Soc. Symp. Proc. 23, 111 (1984).

31. D.E. Aspnes and A.A. Studna, Phys. Rev. B27, 985 (1983).

32. G.E. Jellison Jr. and F.A. Modine, Appl. Phys. Lett. 41, 180 (1982).

33. S. Logothetides, L. Vina and M. Cardona, unpublished.

34. P. Lautenschlager and L. Vina, private communcation.

35. P. Baeri and S.U. Campisano, in "Laser Annealing of Semiconductors", ed. J.M. Poate and J.W. Mayer (Academic Press, New York, 1982) p. 75.

36. American Institute of Physics Handbook, ed. D.E. Gray (McGraw-Hill, New York, 1972).

37. L.J. Brillson, Phys. Rev. Lett. 40, 260 (1978).

38. D.D. Wagman, W.H. Evans, V.B. Barker, I. Halow, S.M. Bailey and R.H. Schumm, Natl. Bur. Std. Technical Notes 270-3-270-7 (US Govt. Printing Office, Washington DC, 1968-1971.

39. F. Keith, Principles of Heat Transfer (Intext Educational Publishers, New York, 1973).

40. P. Baeri, S.U. Campisano, G. Foti and E. Rimini, J. Appl. Phys. 50, 788 (1980).

41. Y.S. Touloukian, R.W. Powell, C. Ho and P.G. Klemens, Thermodynamic Properties of Matter (Plenum, New York, 1970).

42. Landolt-Bornstein, "Numerical Data and Functional Relationships in Science and Technology", Group III, 17a (Springer-Verlag, Berlin, 1982).

43. E.F. Stegmeier and I. Kudman, Phys. Rev. 141, 767 (1966), E.F. Stegmeier and I. Kudman, Phys. Rev. 132, 508 (1963).

44. I. Kudman and E.F. Stegmeier, Phys. Rev. 133, A1665 (1964).

45. I. Barin, O. Knache and O. Kubaschewski, Thermodynamic Properties of Inorganic Solids" (Springer-Verlag, Berlin, 1977).

46. L.J. Brillson and H.W. Richter, to be published.

47. Y. Shapira and L.J. Brillson, JVST B1, 618 (1983).

TABLE I

Material	Reaction Threshold [J/cm^2]	Reflectivity at 4 eV [%]	Reflectivity with 50A-Al at 4 eV [%]	ΔH_R [kcal/mol]
GaP	0.19	45	57	18.8
GaAs	0.17	42	54	10.8
GaSb	0.11	58	68	13.0
InP	0.11	38	52	18.6
InAs	0.125	39	53	13.6
InSb	0.08	61	71	15.7

TABLE II

Thermal Properties of III-V Semiconductors

	T_{melt}[42] [K]	H_{fus}[42] [kcal/mol]	C_p[45] [cal/mol K]	κ [W/cm K]	Ref for κ
GaP	1740	27.7	$10+1.6\cdot10^{-3}T$	$1458\cdot T^{-1.33}$	43a
GaAs	1513	25.2	$10.8+1.45\cdot10^{-3}T$	$208\cdot T^{-1.09}$ $35.5\cdot T^{-.66}$	43 35
GaSb	985	14.8	$10.9+3\cdot10^{-3}T$	$633\cdot T^{-1.33}$	43a
InP	1335	14.8	$9.8+3.5\cdot10^{-3}T$	$200\cdot T^{-1.0}$	44
InAs	1215	17.6	$10.9+1.8$	$197\cdot T^{-1.16}$	43b
InSb	800	11.5	$10.6+3.6$	$20.61\cdot T^{-.847}$	41

Figure Captions

Fig. 1. Al 2p SXPS core level spectra taken at 120 eV photon energy: 20 Å Al on InP (110) surface as evaporated and after laser annealing with increasing energy density.

Fig. 2. Change in surface composition of 20 Å-Al overlayer on UHV-cleaved InP (110) surface as a function of annealing energy density.

a) covalently bonded Al versus total Al: conversion of metallic Al into covalent bonded Al.

b) P 2p versus In 4d: attenuation of P 2p level at surface due to Al overlayer and recovery after high energy density anneal.

c) metallic In 4d versus total In 4d: metallic segregation due to Al overlayer increases with energy density up to 0.3 J/cm^2 and then drops at higher energy densities.

Fig. 3. Chemical reaction in the Al-GaP system identified by AES: with increasing energy density, the Al LVV transition shifts from 67 eV ("metallic") to 64 eV ("covalent"), while decreasing in intensity. The P LVV feature unchanged in energy.

Fig. 4. Atomic concentration of 50 Å Al on GaAs (top) and InSb (bottom) as a function of annealing energy density.

Fig. 5. Sputter depth profile of 50 Å-Al on InP annealed at an energy density of 0.14 J/cm^2 per pulse. The excess In above 120 min is due to preferential sputtering of P.[47] From the integration of the Al signal, we deduce a sputter rate of 2.25Å/min.

Fig. 6. Relationship between energy density of reaction threshold as defined in text and heat of fusion as compiled in Ref. 42.

Fig. 7. Experimentally determined reaction threshold E_{mea} versus calculated melting threshold E_{cal} for 50 Å Al and a 250 Å semiconductor layer: X GaP, O GaAs, □ GaSb, △ InP, o InAs, □ InSb. For GaAs, two sets of thermal properties were used for the calculations: 1) from 35 and 2) from 43.

Table Captions

1. Reaction thresholds, reflectivities with and without 50 Å Al overlayers, and heats of reaction[37] ΔH_R for each of the six compound semiconductors.

2. Thermal properties for each of the six III-V compound semiconductors studied.

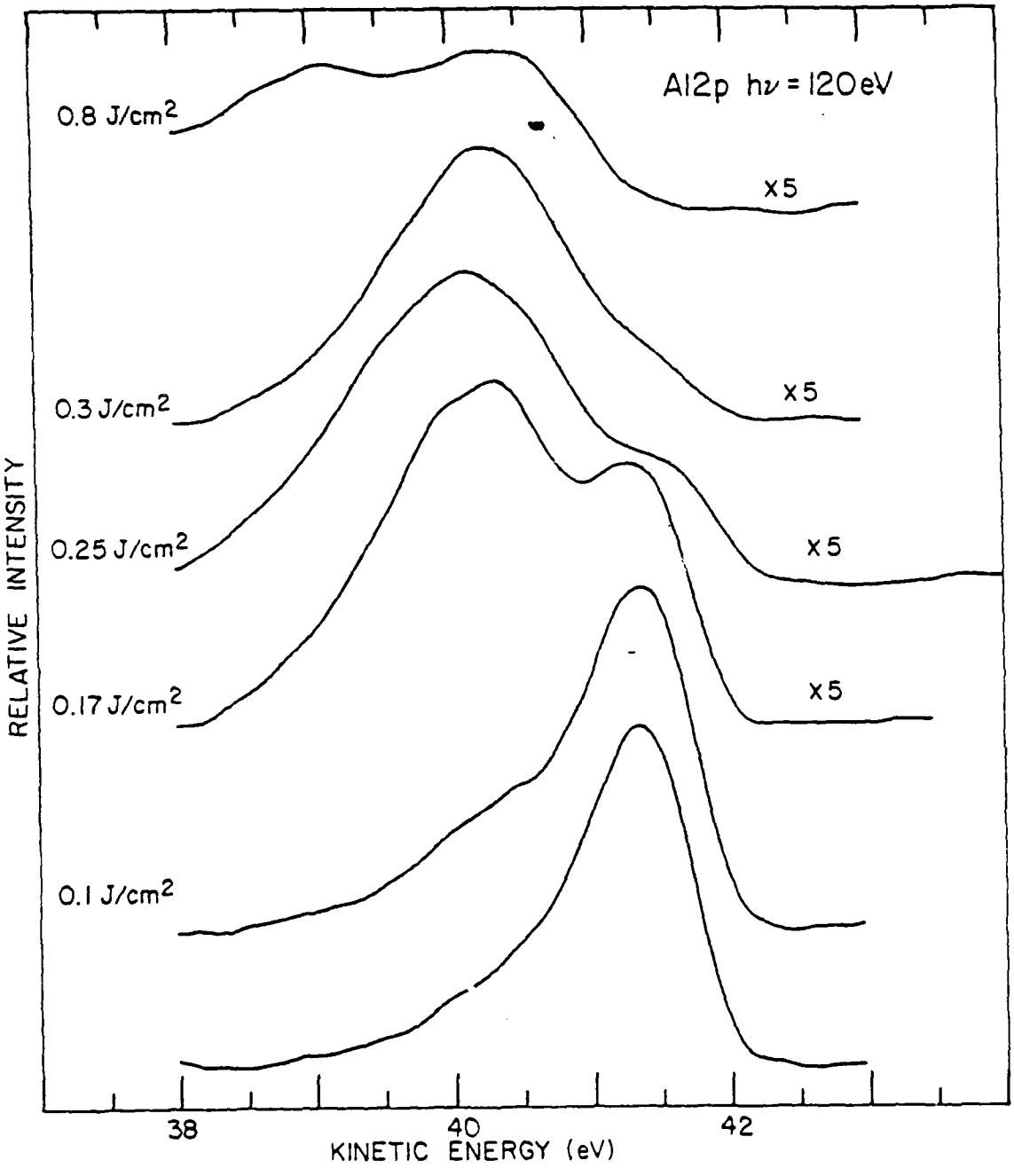
Al2p hν = 120eV
0.8 J/cm2
x5
0.3 J/cm2
x5
0.25 J/cm2
x5
0.17 J/cm2
x5
0.1 J/cm2
RELATIVE INTENSITY
38
40
42
KINETIC ENERGY (eV)

Figure 1

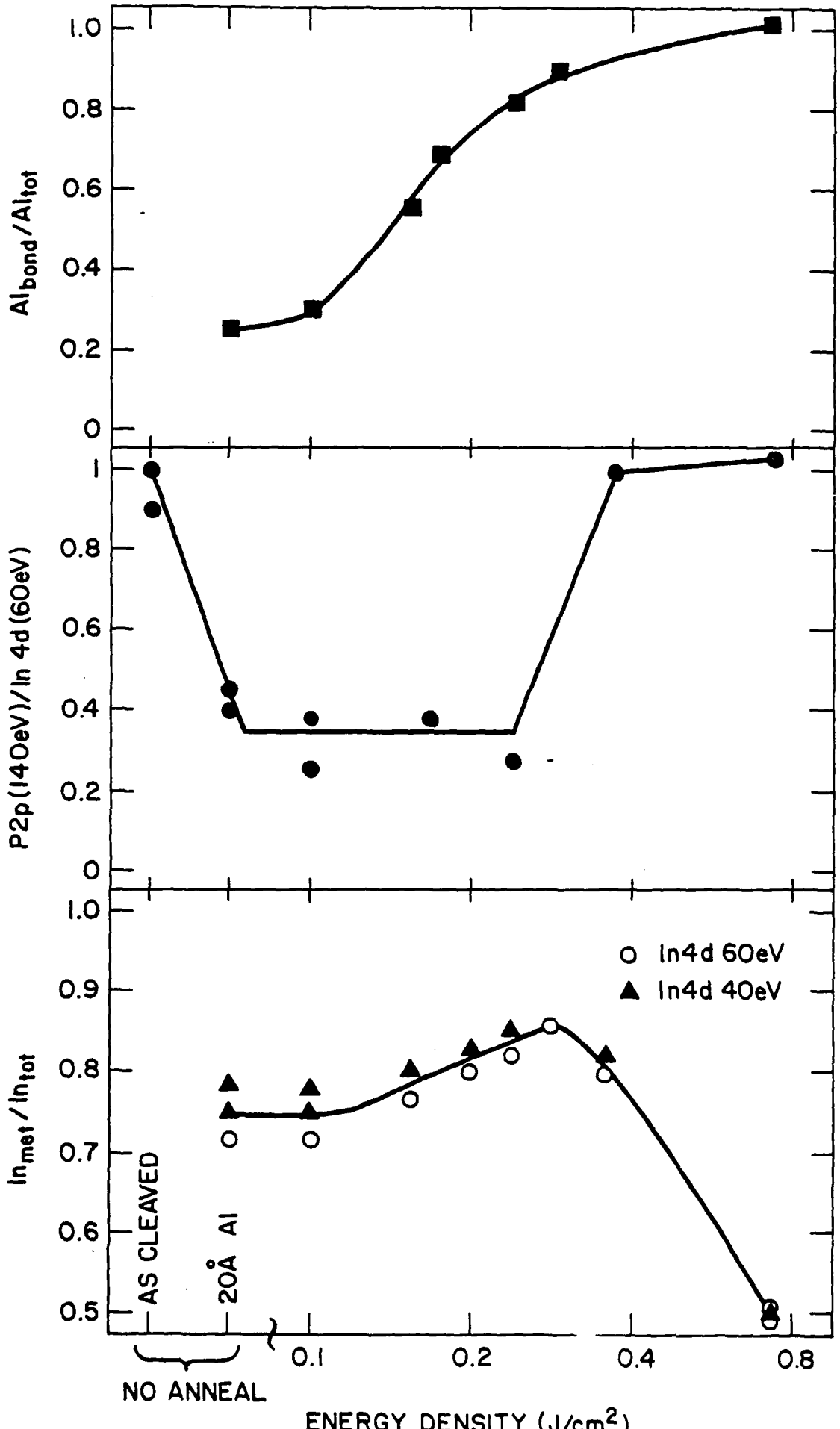
Al_{bond}/Al_{tot}
1.0
0.8
0.6
0.4
0.2
0
P2p(140eV)/In 4d(60eV)
1
0.8
0.6
0.4
0.2
0
In_{met}/In_{tot}
1.0
0.9
0.8
0.7
0.6
0.5
In4d 60eV
In4d 40eV
AS CLEAVED
20Å Al
NO ANNEAL
0.1
0.2
0.4
0.8
ENERGY DENSITY (J/cm²)

Figure 2

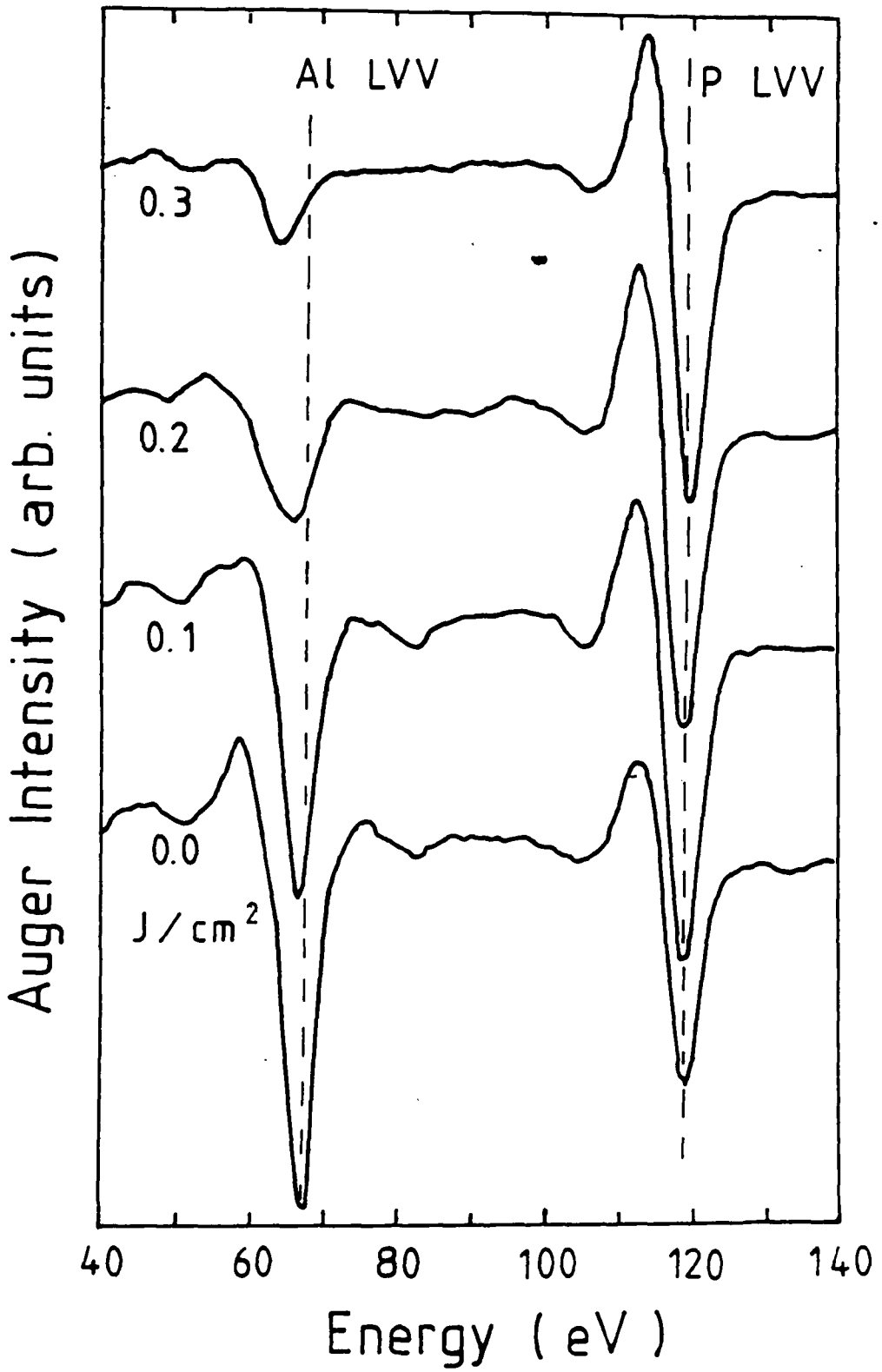
Al LVV
P LVV
0.3
0.2
0.1
0.0
J / cm²
Auger Intensity (arb. units)
40
60
80
100
120
140
Energy (eV)

Figure 3

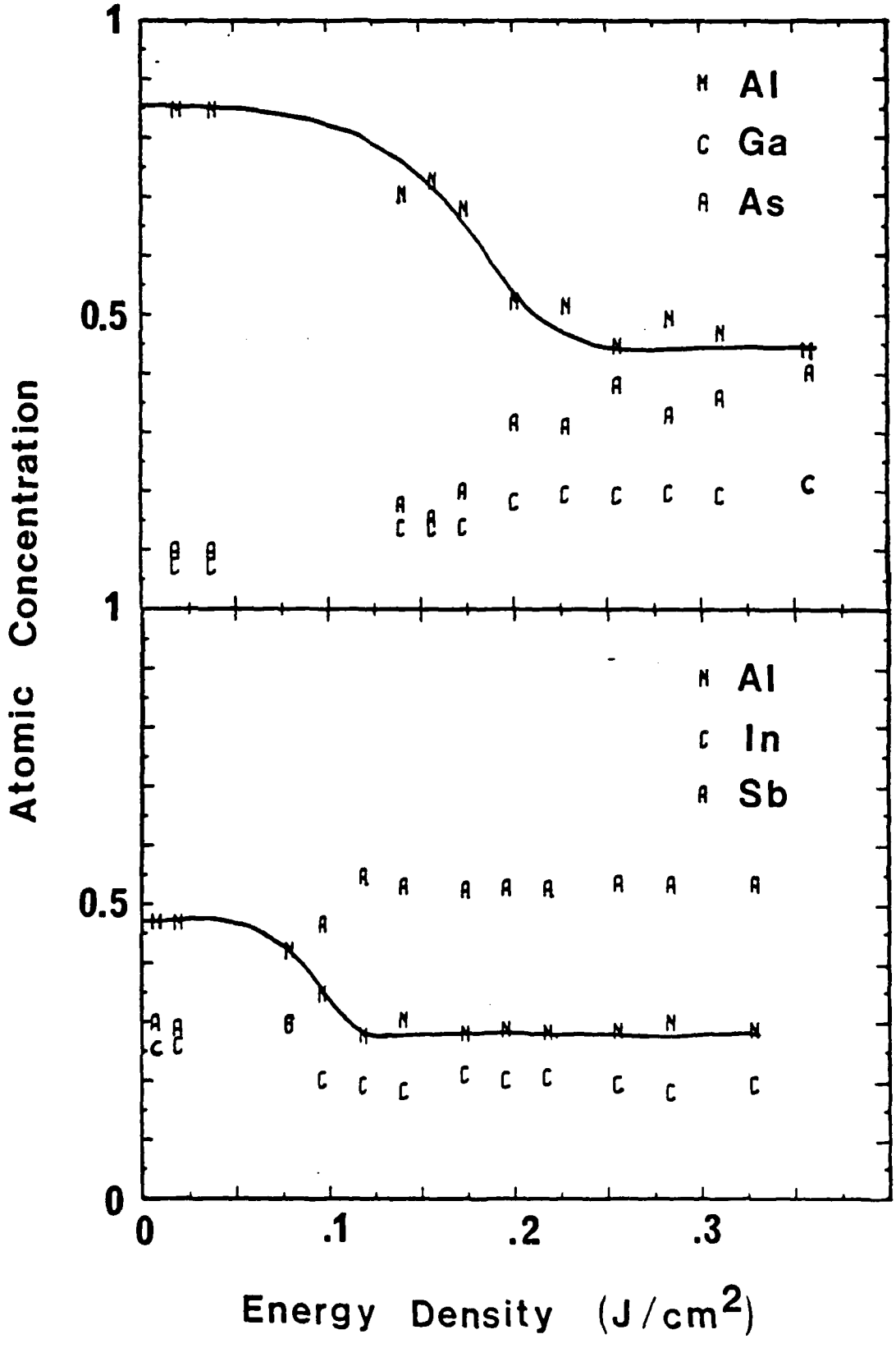
Atomic Concentration
1
0.5
1
0.5
0
0
.1
.2
.3
Al
Ga
As
Al
In
Sb
Energy Density (J/cm2)

Figure 4

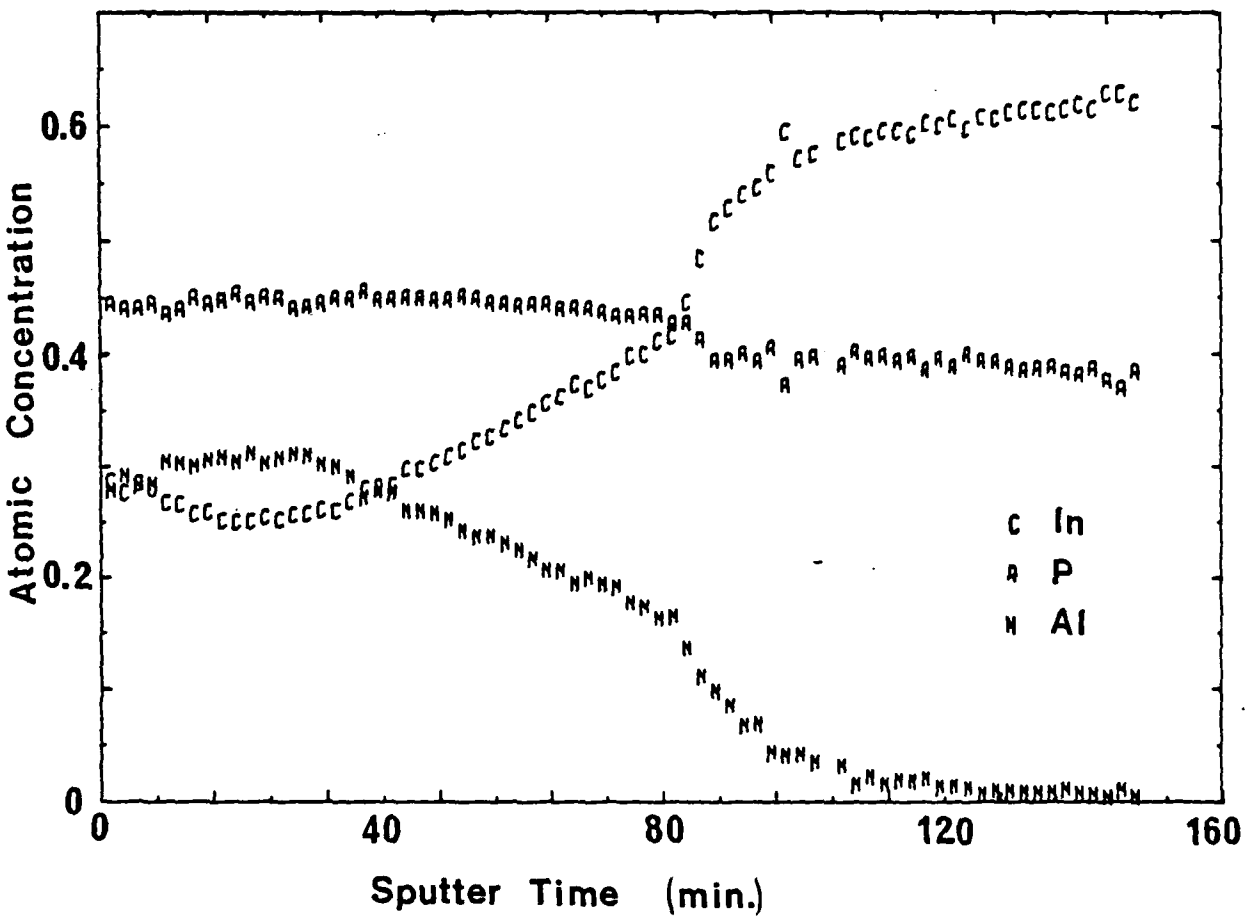
Atomic Concentration
0.6
0.4
0.2
0
0
40
80
120
160
Sputter Time (min.)
C In
A P
N Al

Fig. 5

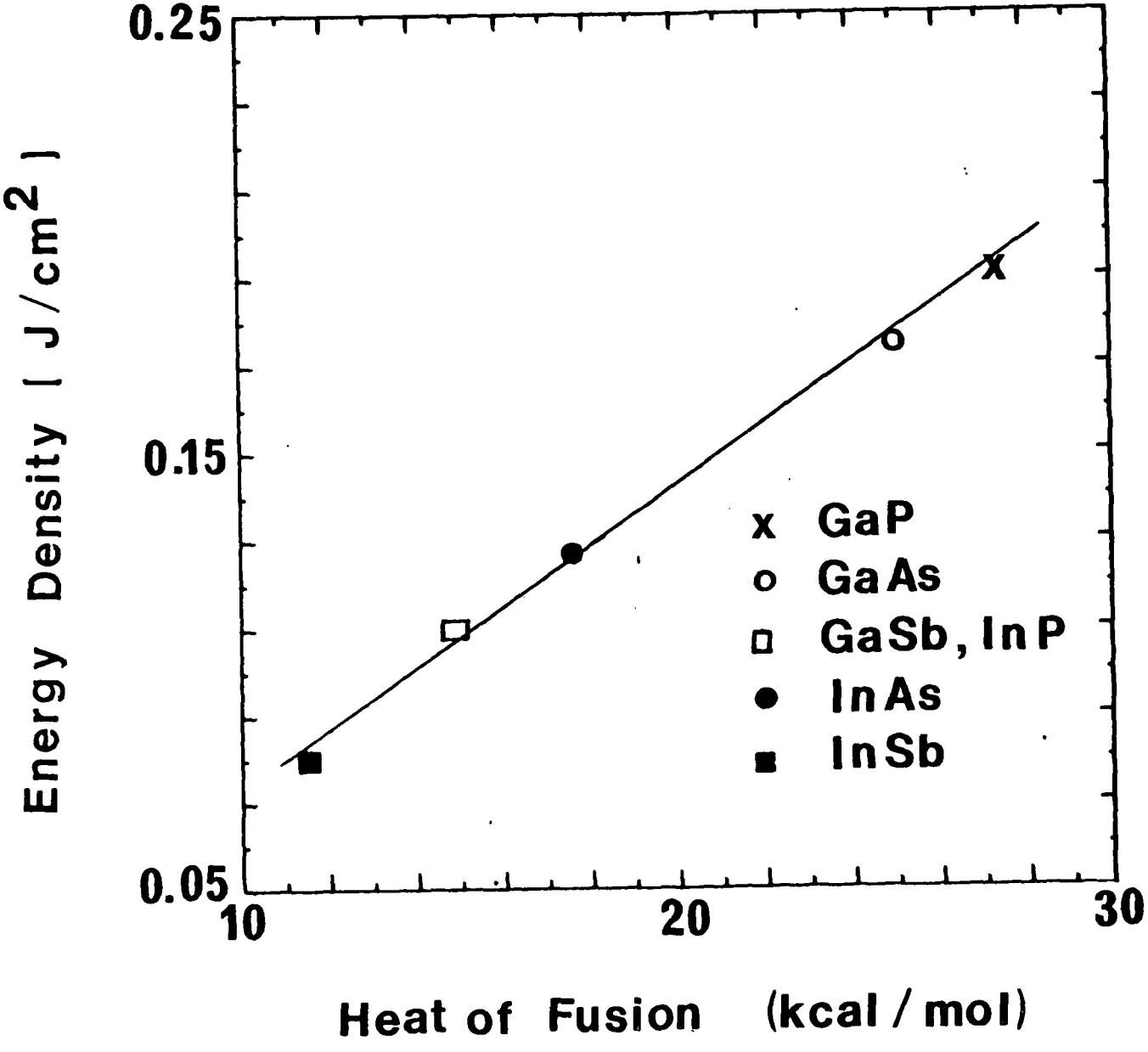
0.25
0.15
0.05
10
20
30
Energy Density [J/cm2]
Heat of Fusion (kcal / mol)
x GaP
o GaAs
□ GaSb, InP
● InAs
■ InSb

Figure 6

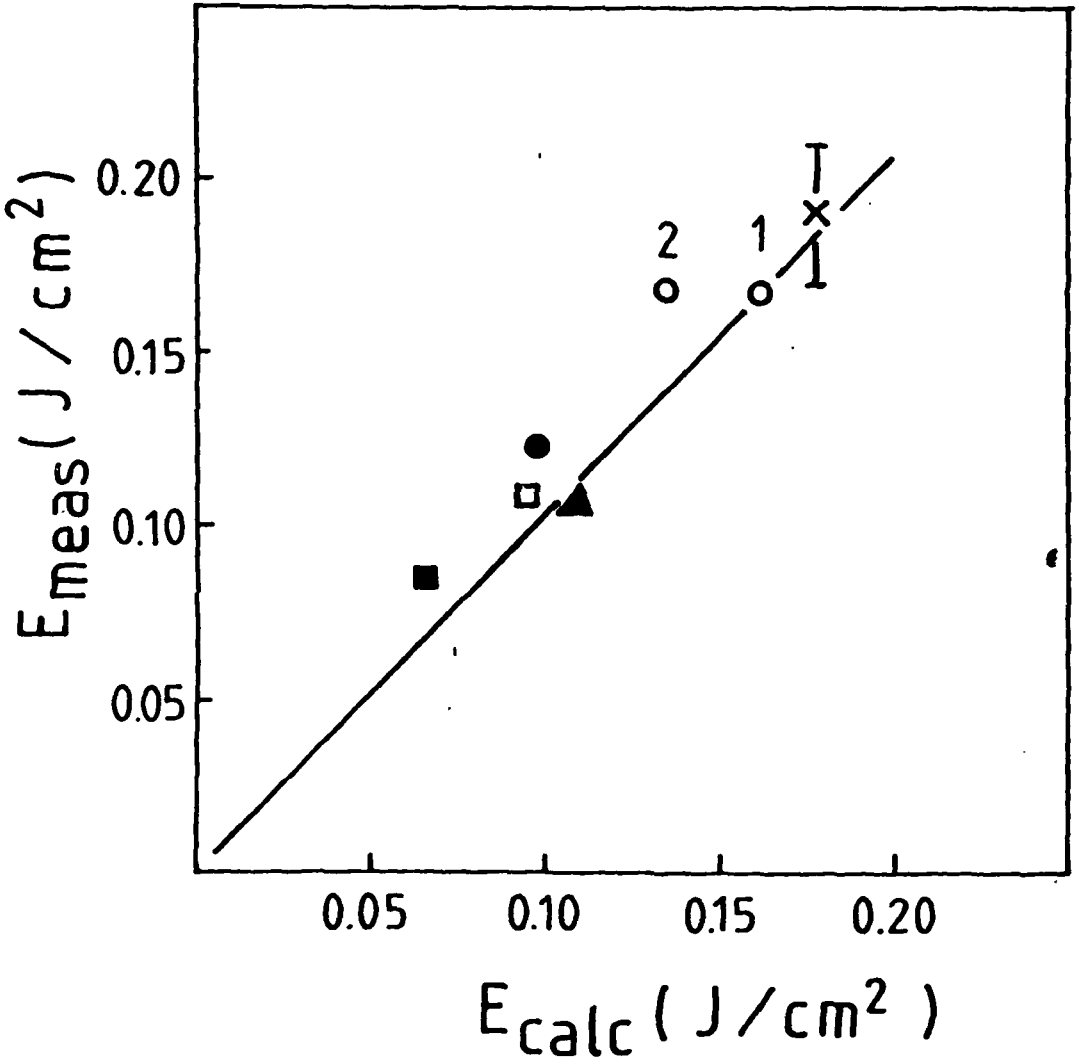

Figure 7

Ultrafast Laser-Induced Oxidation of Silicon: A New Approach Towards High Quality, Low Temperature, Patterned SiO_2 Formation

T.E. ORLOWSKI and H. RICHTER
Xerox Webster Research Center, Rochester, NY 14644

A new low temperature method of rapidly forming (>100Å/sec) high quality patterned silicon dioxide (SiO_2) layers on silicon substrates is presented. Ultraviolet pulsed laser excitation in an oxygen environment is utilized. Infrared absorption measurements indicate that the laser grown oxide is stoichiometric but with a higher degree of disorder than thermally grown oxide. From capacitance-voltage measurements we deduce a fixed oxide charge near the Si-SiO_2 interface of $6 \times 10^{10}/cm^2$ for oxides that have been thermally annealed following the laser induced growth making this material a candidate for applications in semiconductor devices.

There has been considerable activity in the search for efficient low temperature techniques for depositing thin dielectric films in semiconductor device fabrication processes. Low temperature techniques can reduce or eliminate problems such as substrate warpage, dopant redistribution and defect generation and propagation[1] associated with conventional high temperature processing steps. Much progress has been made in rapid low temperature deposition of Si_3N_4 and SiO_2 utilizing laser-initiated chemical vapor deposition (CVD) techniques[2,3]. Other studies have shown that oxygen trapped in amorphous silicon layers during pulsed laser annealing of silicon wafers rapidly forms SiO_2[4]. Although considerable work has been done using continuous-wave(CW) lasers[5,6] to grow thin SiO_2 layers on Si, growth rates reported for these measurements are comparable or only slightly larger than the rate for conventional thermal oxidation processes. The work reported here is concerned with a new low temperature method of rapidly forming high quality patterned silicon dioxide layers on silicon substrates utilizing pulsed ultraviolet (UV) laser excitation. We examine the growth kinetics and stoichiometry of the laser grown SiO_2 (L-SiO_2) and characterize the electrical properties of metal-oxide-silicon (MOS) devices made using L-SiO_2.

The technique involves optical excitation and subsequent rapid heating of a silicon substrate (p-type, 10-20 Ωcm, (100) surface) to near or above its melting point in an oxygen environment (1 atm.) using a XeCl excimer laser which provides 5 nsec pulses with up to 5mJ energy at 308 nm. Focusing the beam to a 1.0 x 0.5 mm spot on the sample results in energy densities of up to 0.9 J/cm^2. A laser pulse repetition rate of 100 Hz. is used which produces no residual substrate heating and even the surface of the sample cools within 1 μsec of excitation. In order to reduce the strain in the substrate during the rapid heating and cooling, the substrate was resistively heated to 400°C. Repetitive pulses combined with scanning the focused laser beam over the sample surface produced patterned oxide layers large enough to perform infrared (IR) and electrical measurements.

Figure 1 shows the thickness of L-SiO_2 as a function of laser exposure time. For thicknesses between 300 and 1800 Å the oxide growth rate is linear (~ 100 A/sec) and comparable to that found for deposition of SiO_2 by laser assisted CVD techniques[2,3]. For thicker oxides the growth kinetics appear to follow a quadratic behavior (i.e., X_{SiO_2} (Å) $\propto$ (Bt)½ where B is a time-averaged parabolic rate constant) indicating that the diffusion of oxygen across the SiO_2 layer toward the Si-SiO_2 interface is influencing the overall oxide formation rate. From the fit in Figure 1 (dotted line) we obtain a value of B ~ 8.5 μm^2/hr which is ~ 30X larger than that found for the thermal oxidation process at 1000°C and 1 atm. O_2 pressure[7]. These considerations do not take into account that the SiO_2 and the surface of the Si wafer stay at elevated temperatures for less than 1 μsec after each laser pulse. Taking this time as an upper limit, and with a laser repetition rate of 100 Hz, the effective parabolic rate constant would be 8.5 x 10^4 μm^2/hr or 3x10^5 times larger than in conventional thermal oxidation processes!

Several points can be made concerning these results. The onset of parabolic behavior of the growth kinetics for L-SiO_2 occurs at thicknesses a factor of two greater than for typical thermally grown oxides. This could happen if the diffusion of oxygen through the L-SiO_2 is faster or if the concentration of dissolved oxygen is larger than in thermally grown oxides. In order to understand the dramatic increase in the overall oxidation rate however, much more information is needed concerning the effect of Si electronic excitation upon the formation of Si-O bonds. Other investigators have reported enhanced oxidation of silicon using CW lasers[5,8] and in one case[5] dramatic differences in enhancement were found between visible and UV excitation. It was proposed[5] that electrons excited from the conduction band of Si into the conduction band of SiO_2 (barrier height 3.2 eV) by UV photons could combine with dissolved O_2 in the SiO_2 layer to form O_2^-. Many researchers have suggested[9,10] that a negatively charged species of oxygen plays a key role in the oxidation process. We observe a rather sharp onset to rapid oxide formation at incident pulse energy densities near 0.3 J/cm^2 which we attribute to the onset of melting of the Si surface. Other experiments using visible[11] and UV[12] laser pulse energy densities

exceeding the silicon melting threshold have been reported however only thin oxides (<500 A) were formed and no discussion of the electrical quality of the Si-SiO_2 interface was included. It is clear that more detailed experimental effort is needed to explain the entire catalytic effect of the laser upon the growth process. In any event, very thick oxides can be grown rapidly using this new method. With longer exposure times and tighter laser focusing oxide layers up to a thickness of 1μm have been made. Considerable effort has been expended to characterize the quality of the oxide formed by this laser induced process as discussed below.

Silicon dioxide shows three prominent IR absorption bands: 1070 cm^{-1} (Si-O stretching), 850 cm^{-1} (O-Si-O bending) and 450 cm^{-1} (Si-O-Si rocking). These bands obey a Lambert-Bouguer law and can therefore be used to determine the thickness of SiO_2 films on an IR transparent substrate.[13] The frequency, width and relative intensities also reveal information about stoichiometry and structure of SiO_2 films. The IR-spectra were recorded on a double beam Perkin-Elmer 283 IR-spectrometer with a bare silicon substrate (covered with native oxide $\approx$ 20-30 A on both sides) in the reference beam. Besides the above mentioned SiO_2-bands, no other absorption bands (e.g. hydroxyl-groups, etc.) were detected in the range from 4000 cm^{-1} to 200 cm^{-1}. Figure 2 shows a typical Si-O stretching band of a 2830 A-thick L-SiO_2 film in comparison with a 2800 A thermal oxide layer, grown at 1000°C in dry O_2. The peak position of the absorption band in both spectra is the same (1070 cm^{-1}), but the L-SiO_2 band is broader (133 cm^{-1}) than the thermal oxide (90 cm^{-1}). A similar but larger broadening is found in CVD-deposited SiO_2-films[14]. Recent work[6] reporting oxide films prepared using CW CO_2 lasers show the opposite effect (i.e., a slight narrowing of the Si-O stretching band compared to the thermal oxide). It has been shown earlier[15] that the Si-O stretching frequency in SiO_x is linearly related to the oxygen concentration x, whereas the band width is mainly determined by the O-Si-O bond angle variation. We therefore interpret our IR-data in the following way: The bulk of the L-SiO_2 is stoichiometric within the accuracy of the measurement and shows no oxygen deficiency. *The broadening of the bands on the other hand shows an additional degree of structural*

disorder like large variations in bond angle. Similar results are obtained from soft x-ray photoemission(SXPS) data: the bulk of the L-SiO_2 shows no sign of SiO_x suboxides while at the interface, a layer of SiO_x is found of comparable thickness as in thermally grown SiO_2.[16]

The strength of the 1070 cm^{-1} absorption band was used as the standard way of determining the thickness of the L-SiO_2 films (Figure 1) using the absorption coefficient of 3.4 x 10^4 cm^{-1} given in Ref. 17. The thicknesses determined in this way are in good agreement with standard color charts and the oxide thickness determined from capacitance measurements of MOS-capacitors using the standard SiO_2 dielectric constant ϵ_i = 3.5 x 10^{-13} F/cm.

Two critical parameters for the application of an insulating layer in metal-insulator-semiconductor devices are the fixed oxide charge density, D_f, and the interface state density, D_{it}. We have studied both parameters in the L-SiO_2 films using the combined high- and low-frequency capacitance, voltage (CV-) technique reviewed in Ref. 18. Al-contacts of .0033 cm^2 area were evaporated onto the L-SiO_2 layers with no post metallization annealling. For these capacitors, the CV-plots reveal fixed oxide charge densities in the range of $3x10^{11}$ - $8x10^{11}$ cm^{-2} and surface state densities of the same magnitude. The capacitors also show leakage currents of typically 10^{-6} A at $3x10^5$ V/cm. This electrical quality can be improved significantly with a short (20 min.) anneal at 900°C in 1 atm. O_2 prior to metallization. From the CV-plots shown in Fig. 3 one obtains characteristic values of $6x10^{10}$ cm^{-2} fixed charge and $2x10^{11}$ cm^{-2} eV^{-1} surface states near midgap following this treatment. Leakage is also reduced dramatically. Up to a field of $5x10^5$ V/cm (our experimental limit), leakage currents are less than our detection limit of 10^{-10} A. These values are in the same range as the values for plasma oxides[19] or CVD-oxides[20] following longer annealling treatments at higher temperatures. Further studies on the annealing behavior in a variety of ambients (H_2, N_2) and temperatures as well as measurements of pinhole density and breakdown voltage are in progress in order to determine the mimimum

requirements for achieving "good" oxide electrical properties. At the present time we know that the breakdown voltage of all capacitors made with L-SiO_2 is >5 x 10^5 V/cm. It should be noted that all results reported here were obtained without preoxidation cleaning of the silicon substrate, an elaborate multistep procedure found necessary for achieving good electrical properties in thermally-grown oxides[18].

We have presented a new, fast, essentially low temperature technique for growing high quality SiO_2 suitable for application in certain thin film devices. An important advantage of this technique is the use of a focussed laser beam which makes it possible to grow a patterned oxide thus eliminating two steps in the fabrication of integrated circuits (masking and subsequent etching to remove insulation layer for contacts). Since the oxidation process is very strongly temperature dependent, the oxide profile is usually much steeper than the laser beam profile. By varying the energy density it is also possible to modulate the oxide thickness in a controlled manner during the growth process as we have shown.

ACKNOWLEDGEMENTS

The encouragement and assistance of L.J. Brillson and technical advice of W.G. Hawkins is gratefully acknowledged. Partial support of this research was provided by the Office of Naval Research under Contract N0014-80-C-0778(G.B. Wright). We thank H. Vander Plas (Xerox Palo Alto Research Center) for supplying us with the silicon substrates.

REFERENCES

1. S. Su, Solid State Technol. 24, 72 (1981).
2. T.F. Deutsch, D.J. Silversmith and R.W. Mountain, Mat. Res. Soc. Symp. Proc. 17, 129 (1983).
3. P.K. Boyer, G.A. Rocke, W.H. Ritchie and G.J. Collins, Appl. Phys. Lett. 40, 716 (1982).
4. Y.S. Liu, S.W. Chiang and F. Bacon, Appl. Phys. Lett. 38, 1005 (1981).
5. S.A. Schafer and S.A. Lyon, J. Vac. Sci. Technol. 21, 422 (1982).
6. I.W. Boyd and J.I.B. Wilson, Appl. Phys. Lett. 41, 162 (1982).
7. B.E. Deal and A.S. Grove, J. Appl. Phys. 36, 3770 (1965).
8. E. M. Young and W. A. Tiller, Appl. Phys. Lett. 42, 63 (1983).
9. W.A. Tiller, J. Electrochem. Soc. 127, 619 (1980).
10. A. Redondo, W.A. Goddard III, C.A. Swarts and T.C. McGill, Jr., J. Vac. Sci. Technol. 19, 498 (1981).
11. A. Cros, F. Salvan and J. Derrien, Appl.Phys. A28, 241(1982).
12. Y.S. Liu, S.W. Chiang and W. Katz, Laser and Electron-Beam Interactions with Solids (Elsevier Science Publishing Co. Inc., 1982), p.249.
13. J.E. Dial, R.E. Gong and J.N. Fordemwalt, J. of Electrochem. Soc. 115, 326 (1968).
14. W.A. Pliskin and H.S. Lehman, J. of Electrochem. Soc. 112, 1013 (1965).
15. L. Schumann, A. Lehmann, H. Sobotta, V. Riede, U. Teschner and K. Hübner, Phys. Stat. Sol. B110, K69 (1982).
16. H.Richter, T.E. Orlowski, M. Kelly and G. Margaritondo (unpublished).
17. J. Wong, J. Appl. Phys. 44, 5629(1973).
18. E.H. Nicollian and J.R. Brews, MOS (Metal Oxide Semiconductor) Physics and Technology (Wiley, NY. 1982).
19. J.R. Ligenza and M. Kuhn, Solid State Technol. 13, 33 (1970).
20. G. Pananakakis, G. Kamarinos, M. El-Sayed and V. LeGoascoy, Solid State Electron. 26, 415 (1983).

FIGURE CAPTIONS

Fig. 1 Plot of SiO_2 thickness (from IR absorption data) as a function of laser exposure time. The observed growth rate is linear from 300 - 1800 Å SiO_2 thickness becoming quadratic at greater SiO_2 thicknesses.

Fig. 2 IR absorption spectra: Laser-grown SiO_2 (solid line) and thermally-grown (1000°C) SiO_2 (dotted line). From the SiO_2 absorption coefficient at 1070 cm^{-1} we obtain an oxide thickness of ~2800 Å.

Fig. 3 Typical high-frequency (HF) and low-frequency (LF) CV-plot of an Al-L-SiO_2-Si MOS capacitor. The HF-curve was taken at 1 MHz, the LF-curve at 1 kHz (no changes were observed at lower frequencies). From the HF data one obtains a fixed oxide charge density, D_f, of $6x10^{10}$ cm^{-2} and from the LF data, an interface state density, D_{it}, of $2x10^{11}$ $cm^{-2}eV^{-1}$.

AD-A160 403 CHEMICAL BONDING INTERDIFFUSION AND ELECTRONIC STRUCTURE AT INP GAAS ANN SI--ETAL INTERFACES(U) XEROX WEBSTER RESEARCH CENTER NY L J BRILLSON 01 OCT 85 3/3

UNCLASSIFIED N00014-80-C-0778 F/G 20/12 NL

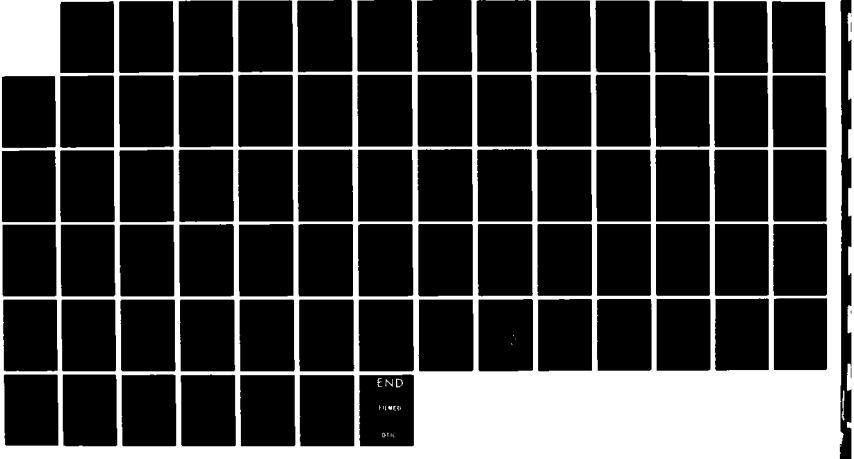

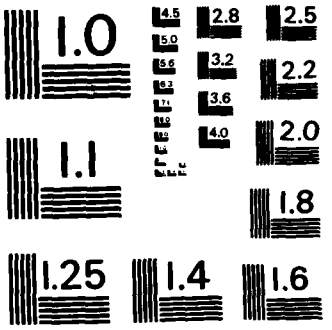

MICROCOPY RESOLUTION TEST CHART
NATIONAL BUREAU OF STANDARDS-1963-A

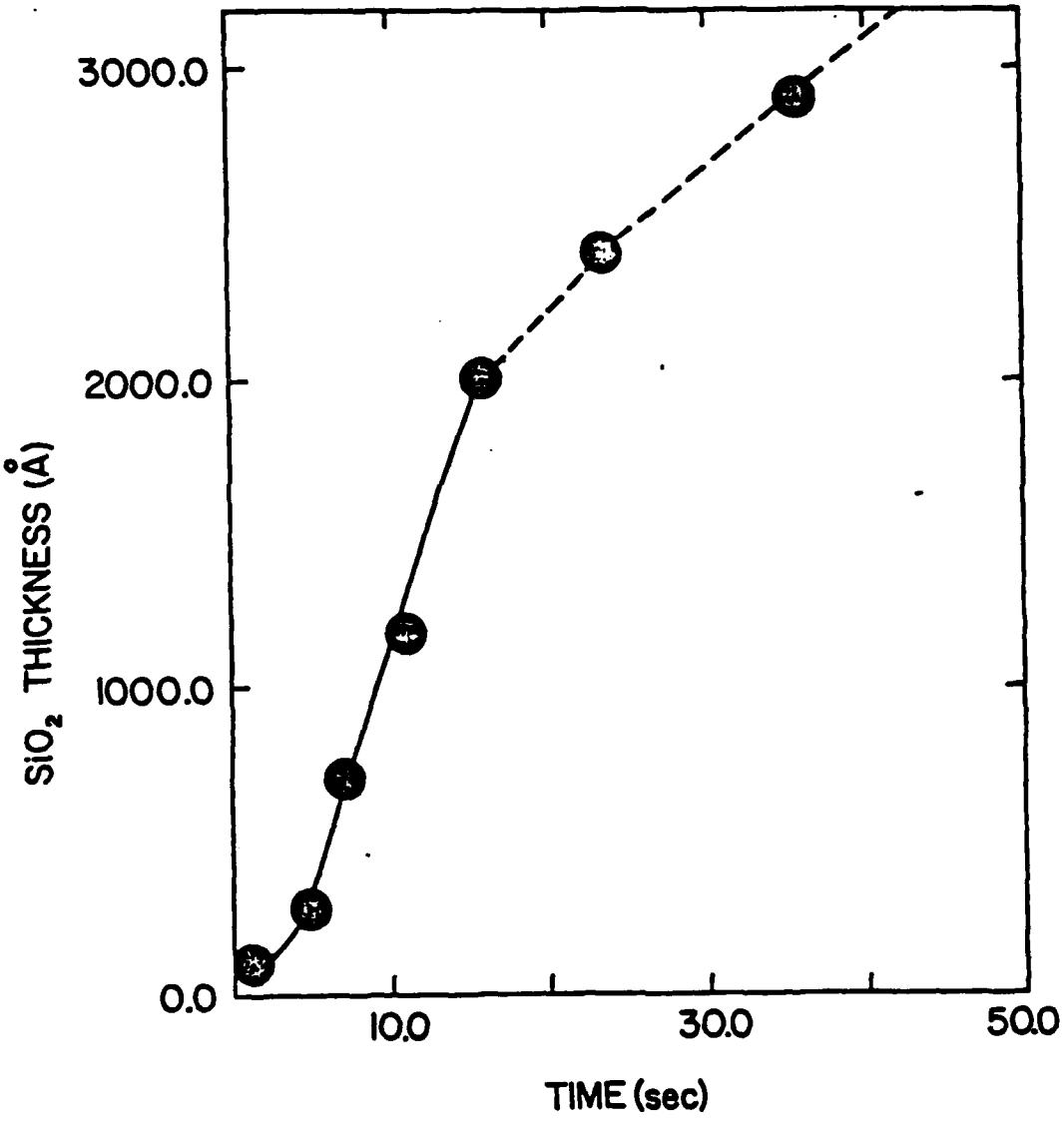
3000.0
2000.0
1000.0
0.0
SiO2 THICKNESS (Å)
10.0
30.0
50.0
TIME (sec)

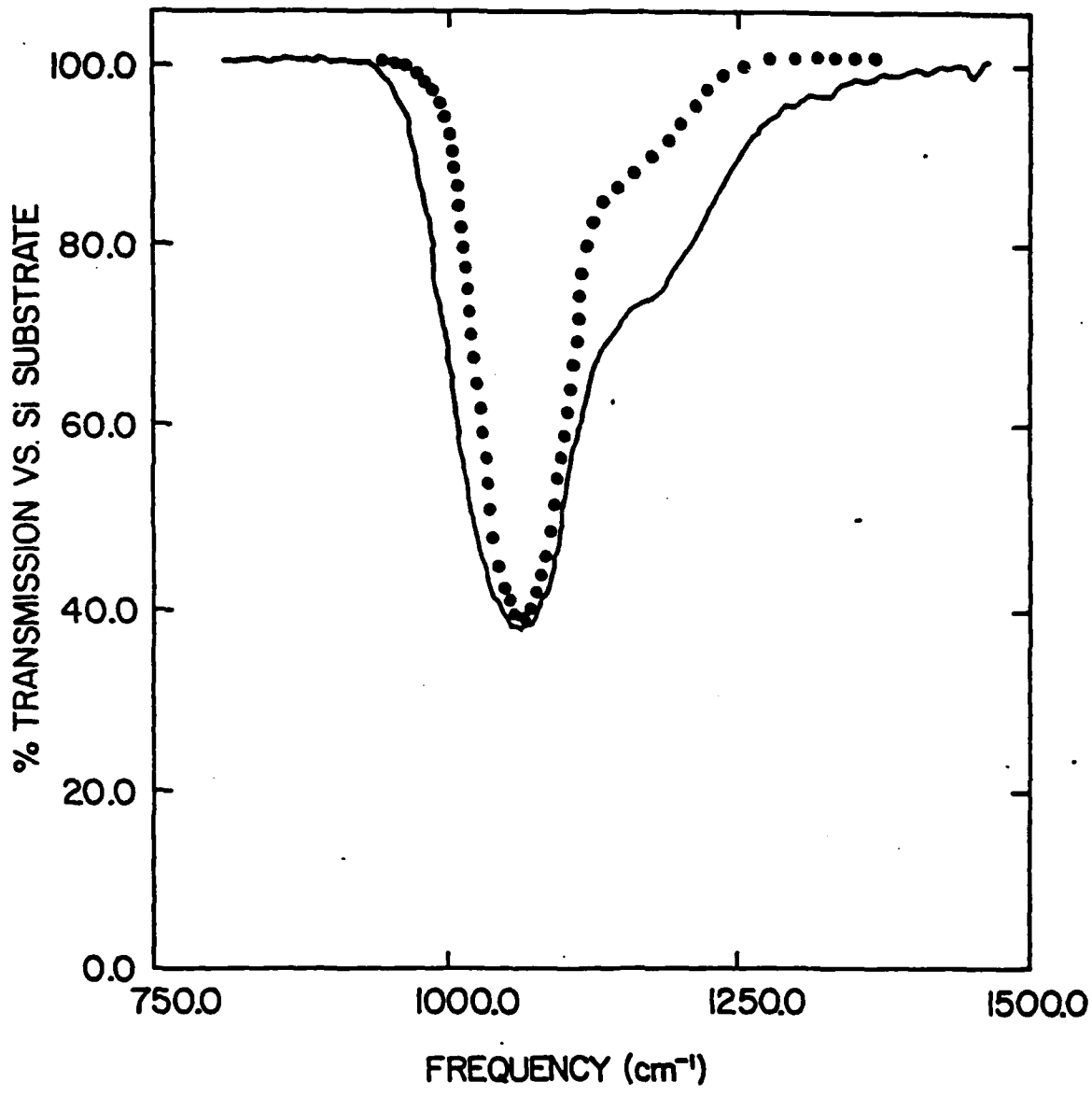
100.0
80.0
60.0
40.0
20.0
0.0
% TRANSMISSION VS. Si SUBSTRATE
750.0
1000.0
1250.0
1500.0
FREQUENCY (cm⁻¹)

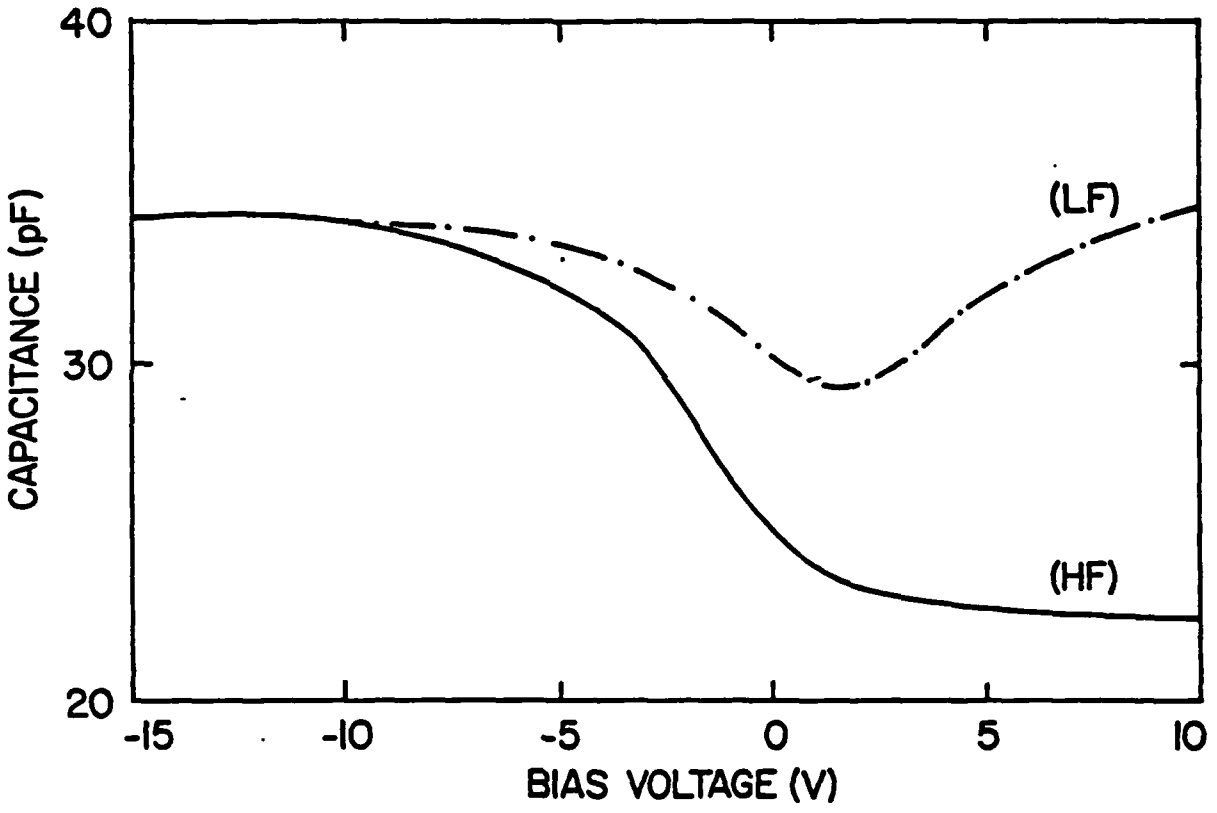
40
30
20
CAPACITANCE (pF)
(LF)
(HF)
-15
-10
-5
0
5
10
BIAS VOLTAGE (V)

Ultrafast UV-Laser Induced Oxidation of Silicon: Control and Characterization of the Si-SiO_2 Interface

H. RICHTER and T.E. ORLOWSKI
Xerox Webster Research Center, Rochester, NY 14644

M. KELLY and G. MARGARITONDO
Dept. of Physics, University of Wisconsin, Madison, WI 53706

A new low temperature method of rapidly forming (>100Å/sec) high quality patterned silicon dioxide (SiO_2) layers up to a thickness of 1 μm on silicon substrates is presented. Ultraviolet pulsed laser excitation in an oxygen environment is utilized. Infrared absorption spectroscopy, capacitance-voltage measurements, and soft x-ray photoemission are employed to characterize the oxide films and the Si-SiO_2 interface. No shift but a significant broadening of the Si-O stretching mode compared with thermally grown oxides is found indicating that the laser grown oxide is stoichiometric but with a higher degree of disorder. Similar results are obtained from soft x-ray photoemission data: the bulk of the laser grown SiO_2 shows no sign of SiO_x-suboxides while at the interface, a layer of SiO_x is found of comparable thickness as in thermally grown SiO_2. From capacitance-voltage measurements we deduce a fixed oxide charge near the Si-SiO_2 interface of $6 \times 10^{10}/cm^2$ for oxides that have been thermally annealed following the laser induced growth making this material a candidate for applications in semiconductor devices.

There has been considerable activity in the search for efficient low temperature techniques for depositing thin dielectric films in semiconductor device fabrication processes to eliminate problems such as substrate warpage, dopant redistribution and defect generation and propagation[1] associated with conventional high temperature processing steps. Much progress has been made in rapid low temperature deposition of Si_3N_4 and SiO_2 utilizing laser-initiated chemical vapor deposition (CVD) techniques[2,3]. Other studies have shown that oxygen trapped in amorphous silicon layers during pulsed laser annealing of silicon wafers rapidly forms SiO_2[4]. Although considerable work has been done using continuous-wave (CW) lasers[5,6] to grow thin SiO_2 layers on Si, growth rates reported for these measurements are comparable or only slightly larger than the rate for conventional thermal oxidation processes. The work reported here is concerned with a new low temperature method of rapidly forming high quality patterned silicon dioxide layers on silicon substrates utilizing pulsed ultraviolet (UV) laser excitation. We examine the growth kinetics, electronic structure, and stoichiometry of the laser grown SiO_2 (L-SiO_2) and characterize the electrical properties of metal-oxide-silicon (MOS) devices made using L-SiO_2.

Shown in Figure 1 is the apparatus developed for laser induced oxidation of silicon. The technique involves optical excitation and subsequent rapid heating of a silicon substrate (p-type, 10-20 Ωcm, (100) surface) to near or above its melting point in an oxygen environment (1 atm.) using a XeCl excimer laser which provides 5 nsec pulses with up to 5mJ energy at 308 nm. Focusing the beam to a 1.0 x 0.5 mm spot results in energy densities at the sample of up to 0.85 J/cm^2. Excitation at 308 nm in silicon (absorption coefficient = 1.2 x 10^6 cm^{-1})[7] provides over ninety percent absorption of the laser pulse within 200A of the sample surface. With a laser pulse duration of 5 nsec and a pulse repetition rate of 100 Hz., there is no residual substrate heating and even the surface of the sample cools within 1 μsec of excitation. In order to reduce the strain in the substrate during the rapid heating and cooling, the substrate was resistively heated to 400°C. Substrate temperature was measured using an infrared pyrometer operating at 5μm.

Repetitive pulses combined with scanning the focused laser beam over the sample surface produced patterned oxide layers large enough to perform infrared (IR) absorption and electrical measurements.

Figure 2 shows the thickness of L-SiO_2 as a function of laser exposure time. For oxides between 300 and 1800 A thick the growth rate is linear (~ 100 A/sec) and comparable to that found for deposition of SiO_2 by laser assisted CVD techniques[2,3]. For thicker oxides the growth kinetics appear to follow a quadratic behavior (i.e., X_{SiO_2} (A) $\propto$ (Bt)½ where B is a time-averaged parabolic rate constant) indicating that the diffusion of oxygen across the SiO_2 layer toward the Si-SiO_2 interface is influencing the overall oxide formation rate. From the fit in Figure 2 (dotted line) we obtain a value of B ~ 8.5 μm^2/hr which is ~ 30X larger than that found for the thermal oxidation process at 1000°C and 1 atm. O_2 pressure[8]. These considerations do not take into account that the SiO_2 and the surface of the Si wafer stay at elevated temperatures for less than 1 μsec after each laser pulse. Taking this time as an upper limit, and with a laser repetition rate of 100 Hz, the effective parabolic rate constant would be 8.5 x 10^4 μm^2/hr or 3x10^5 times larger than in conventional thermal oxidation processes.

Several points can be made concerning the dramatic increase in the overall oxidation rate. The diffusion of oxygen through the SiO_2 layer toward the Si-SiO_2 interface may be promoted by the UV photodissociation (multiphoton) of O_2 into oxygen atoms. In addition, the effect of Si electronic excitation upon the formation of Si-O bonds is not clearly understood. Other investigators have reported enhanced oxidation of silicon using CW lasers[5] and dramatic differences in enhancement were found between visible and UV excitation. It has been proposed[5] that electrons excited from the conduction band of Si into the conduction band of SiO_2 (barrier height 3.2 eV) by UV photons could combine with dissolved O_2 in the SiO_2 layer to form O_2^-. Many researchers have suggested[9,10] that a negatively charged species of oxygen plays a key role in the oxidation process. We observe a rather sharp onset to rapid oxide formation at incident pulse energy densities

near 0.35 J/cm^2 which we attribute to the onset of melting of the Si surface.[11] Other experiments using visible[12] and UV[13] laser pulse energy densities exceeding the silicon melting threshold have been reported however only thin oxides (<500Å) were studied and no discussion of the electrical quality of the Si-SiO_2 interface was included. It is clear that more detailed experimental effort is needed to explain the entire catalytic effect of the laser upon the growth process. In any event, very thick oxides can be grown rapidly using this new method. With longer exposure times and tighter laser focusing oxide layers up to a thickness of 1μm have been made. Considerable effort has been expended to characterize the quality of the oxide formed by this laser induced process as discussed below.

Silicon dioxide shows three prominent IR absorption bands: 1070 cm^{-1} (Si-O stretching), 850 cm^{-1} (O-Si-O bending) and 450 cm^{-1} (Si-O-Si rocking). It has been shown[14] that these bands obey a Lambert-Bouguer law and can therefore be used to determine the thickness of SiO_2 films on an IR transparent substrate. The frequency, width and relative intensities also reveal information about stoichiometry and structure of SiO_2 films.

The IR-spectra were recorded on a double beam Perkin-Elmer 283 IR-spectrometer with a bare silicon substrate (covered with native oxide $\approx$ 20-30 A on both sides) in the reference beam. The measurements scanned the frequency range from 4000 cm^{-1} to 200 cm^{-1}. Besides the above mentioned SiO_2-bands, no other absorption bands (e.g. hydroxyl-groups, etc.) were detected. Figure 3 shows a typical Si-O stretching band of a 2830 A-thick L-SiO_2 film in comparison with 2800 A of thermal oxide, grown on both sides of a Si wafer (<100> surface) at 1000°C in dry O_2. This figure shows that the peak position of the absorption band in both spectra is the same (1070 cm^{-1}), but the L-SiO_2 band is broader (133 cm^{-1}) than the thermal oxide (90 cm^{-1}). A similar but larger broadening is found in CVD-deposited SiO_2 films[15]. Recent work[6] reporting oxide films prepared using CW CO_2 lasers show the opposite effect (i.e., a slight narrowing of the Si-O stretching band compared to the thermal oxide).

It has been shown earlier[16] that the Si-O stretching frequency in SiO_x is linearly related to the oxygen concentration x, whereas the band width is mainly determined by the O-Si-O bond angle variation. We therefore interpret our IR-data in the following way: The bulk of the L-SiO_2 is stoichiometric within the accuracy of the measurement and shows no oxygen deficiency. The broadening of the bands on the other hand shows an additional degree of structural disorder like large variations in bond angle.

The strength of the 1070 cm^{-1} absorption band was used as the standard way of determining the thickness of the L-SiO_2 films (Figure 2) using the absorption coefficient of 3.4×10^4 cm^{-1} given in Ref. 17. The thicknesses determined in this way are in good agreement with standard color charts and the oxide thickness determined from capacitance measurements of MOS-capacitors using the standard SiO_2 dielectric constant $\epsilon_i = 3.5 \times 10^{-13}$ F/cm.

The electronic structure and the stoichiometry of L-SiO_2 was investigated by soft x-ray photoemission (SXPS) at the University of Wisconsin Storage Ring facility at the Stoughton Physical Science Laboratory. All data discussed here were taken on in-situ prepared L-SiO_2 samples transferred from a high pressure reaction chamber into the SXPS-spectrometer. The valence band density of states (DOS) as revealed by photoelectron spectra taken at 40 eV photon energy, and the conduction band DOS, as revealed by secondary electron yield measurements, (a measurement yielding information comparable to soft x-ray absorption data) are identical with corresponding data reported in the literature.[18,19] A combination of the two measurements was applied to determine the bandgap of L-SiO_2. In agreement with data on thermally grown SiO_2, a gap of 9.1 eV is found, while a double peak structure 1.8 eV below the conduction band edge in the secondary yield spectrum is interpreted as a core hole exciton, also found in earlier x-ray absorption measurements[20] (details will be published later).

Figure 4 shows the Si 2p photoelectron spectra of (a) thermally cleaved Si surface, (b)

7.5 Å L-SiO_2, (c) 15 Å L-SiO_2 and (d) $\approx$ 500 Å L-SiO_2 taken at 145 eV photon energy (resulting in maximum surface sensitivity). The Si 2p spectra of the 500 Å L-SiO_2 layer shows the characteristic chemical shift of 4.5 eV relative to the clean Si 2p spectra.[21] While the clean Si-surface as well as the 500 Å L-SiO_2 surface exhibit one distinct peak, the spectra of the thin SiO_2 layers (b,c) stretch out over the whole energy range between the "clean" Si 2p peak and the oxide SiO_2-peak. Spectra (b) and (c) can be deconvoluted into contributions from the underlying Si-substrate (no chemical shift), a stoichiometric SiO_2 layer (~4.5 eV shift), and a peak (dashed lines in Fig. 4b and 4c) that has been interpreted[21] as originating from a non-stoichiometric SiO_x interlayer at the Si-surface. From the relative intensities of the three components and the electron-mean free path (5 Å), the thickness of the SiO_2 layer and the SiO_x interlayer have been calculated. For a thickness of the L-SiO_2 layer ranging from 5 to 15 Å, the interlayer has a constant thickness of 2-3 Å, as also found in the case of thermally grown SiO_2-layers.[21] On the other hand, this component is completely absent in thicker L-SiO_2 where the film thickness is much larger than the electron escape depth, showing that the bulk of the L-SiO_2 is stoichiometric, with a suboxide layer of comparable dimension as in thermal SiO_2 localized at the Si-SiO_2 interface.

Two critical parameters for the application of an insulating layer in metal-insulator-semiconductor devices are the fixed oxide charge density, D_f, and the interface state density, D_{it}. We have studied both parameters in thick L-SiO_2 films (~3000Å). First, Al-contacts (.0033 cm^2 area) were evaporated onto the L-SiO_2 layers with no post metallization annealing. Then we used the combined high-frequency (HF) and low-frequency (LF) capacitance, voltage (CV-) technique first described by Castagne and Vapaille[22] and reviewed in Ref. 23 to obtain D_f and D_{it}. This CV technique relies on the measurement of capacitance by currents from an AC gate voltage applied to the MOS capacitor. At low frequencies ($\leq$1 kHz) interface trap response to the AC gate voltage is immediate whereas at high frequencies (~1 MHz) interface traps do not follow the AC gate voltage. One extracts the interface trap density from the difference in response at low and

high frequencies to the applied AC gate voltage and the fixed charge from the shift in flatband voltage[23]. Both HF and LF CV curves were taken with a Hewlett-Packard Model 4192A impedance analyzer. All HF CV measurements were performed at 1 MHz while LF measurements were taken in the range 200-1000 Hz. Further reduction in frequency did not alter the CV curve thus insuring that the measured response represents the LF case. Using LF AC measurements instead of a linear voltage ramp significantly reduces problems interpreting CV curves from leaky insulators. For these as prepared Al-L-SiO_2-Si capacitors, the CV-plots reveal fixed oxide charge densities in the range of $3x10^{11}$ - $8x10^{11}$ cm^{-2} and surface state densities of the same magnitude. The capacitors also show leakage currents of typically 10^{-6} A at $3x10^5$ V/cm.

The electrical quality of the as grown oxides can be improved significantly with a short (20 min.) anneal at 900°C in 1 atm. 0_2 prior to metallization. Under these conditions ~17A of "thermal" oxide will grow at the Si-L-SiO_2 interface. Although annealing of thermally grown oxides in O_2 (at temperatures lower than the growth temperature) typically causes an increase in D_f and D_{it},[24] for L-SiO_2 the opposite occurs. From the CV-plots shown in Fig. 5 one obtains characteristic values of $6x10^{10}$ cm^{-2} fixed charge and $2x10^{11}$ cm^{-2} eV^{-1} surface states near midgap with a narrow distribution within the number of samples following this annealing treatment. Leakage current is also reduced dramatically. Up to a field of $5x10^5$ V/cm (our experimental limit), leakage currents are less than our detection limit of 10^{-11} A. The reason for the deviation between the LF and HF CV curves shown in Fig. 5 at negative biases has not been explored fully. However, using the expression given in Ref. 23,

$$D_{it} = \frac{\Delta C}{q}\left[1 - \frac{C_{HF} + \Delta C}{C_{ox}}\right]^{-1} \qquad \left[1 - \frac{C_{HF}}{C_{ox}}\right]^{-1}$$

where $\Delta C = C_{LF} - C_{HF}$, q is the elementary charge and C_{ox} is the oxide capacity, this difference between C_{LF} and C_{HF} results in an increased density of interface states. Therefore the value of $D_{it} = 2 \times 10^{11}$ $cm^{-1}eV^{-1}$ represents an upper limit. Values of D_f and

D_{it} that we have obtained for annealed Si-L-SiO_2 structures are in the same range as values for plasma oxides[25] or CVD-oxides[26] following longer annealing treatments at higher temperatures and are lower than reported values for thermal oxides grown at 900°C.[23] Further studies on the annealing behavior in a variety of ambients (H_2, N_2) and temperatures as well as measurements of pinhole densities and breakdown voltage are in progress in order to determine the mimimum requirements for achieving "good" oxide electrical properties. At the present time we know that the breakdown voltage for all capacitors made with L-SiO_2 is > 5 x 10^5 V/cm. It should be noted that all results reported here were obtained without preoxidation cleaning of the silicon substrate, an elaborate multistep procedure found necessary for achieving good electrical properties in thermally-grown oxides[23].

Recently, experiments on the effects of laser annealing silicon substrates capped with thermally grown SiO_2 layers have been reported.[27] Using ruby laser pulses (694 nm) silicon substrates (<100> surface) were annealed exciting through the SiO_2 layer (3000 A) at various excitation densities in the range 0.6-1.0J/cm^2. From CV measurements obtained on MOS structures made following this treatment values of D_f~3 x 10^{11} cm^{-2} and D_{it}~6 x 10^{11} $cm^{-2}eV^{-1}$ were found at an incident pulse energy density equal to that used in our experiment (~0.8J/cm^2). These values are remarkably close to values reported here for unannealed Si-L-SiO_2 structures which indicates that the interface damage introduced by laser annealing the silicon surface of a Si-SiO_2 structure is similar to the residual interface damage in the laser grown Si-L-SiO_2 structure. It was also found that at excitation densities exceeding 0.8 J/cm^2 physical damage consisting of surface wrinkles appeared in the SiO_2 layer.[27] We find no evidence for this in our work. One final remark concerning laser annealing is that it has been reported[27] that minority carrier lifetimes dramatically decrease following annealing of Si-SiO_2 structures. We did not verify this for our Si-L-SiO_2 structures and mention it here for consideration.

We have presented a new, fast, essentially low temperature technique for growing high quality SiO_2 suitable for application in certain thin film devices. An important advantage of this technique is the use of a focussed laser beam which makes it possible to grow a

patterned oxide without using a mask and thus eliminating two steps in the fabrication of integrated circuits (masking and subsequent etching to remove insulation layer for contacts). Since the oxidation process is very strongly temperature dependent, the oxide profile is usually much steeper than the laser beam profile. By varying the energy density it is also possible to modulate the oxide thickness in a controlled manner during the growth process as we have shown.

ACKNOWLEDGEMENTS

The encouragement and assistance of L.J. Brillson and technical advice of W.G.. Hawkins is gratefully acknowledged. Partial support of this research was provided by the Office of Naval Research under Contract N0014-80-C-0778(G.B. Wright). We thank H. Vander Plas (Xerox Palo Alto Research Center) for supplying us with the silicon substrates.

REFERENCES

1. S. Su, Solid State Technol. 24, 72 (1981).
2. T.F. Deutsch, D.J. Silversmith and R.W. Mountain, Mat. Res. Soc. Symp. Proc. 17, 129 (1983).
3. P.K. Boyer, G.A. Rocke, W.H. Ritchie and G.J. Collins, Appl. Phys. Lett. 40, 716 (1982).
4. Y.S. Liu, S.W. Chiang and F. Bacon, Appl. Phys. Lett. 38, 1005 (1981).
5. S.A. Schafer and S.A. Lyon, J. Vac. Sci. Technol. 21, 422 (1982).
6. I.W. Boyd and J.I.B. Wilson, Appl. Phys. Lett. 41, 162 (1982).
7. G.E. Jellison Jr. and F.A. Modine, J. Appl. Phys. 53, 3745 (1982).
8. B.E. Deal and A.S. Grove, J. Appl. Phys. 36, 3770 (1965).
9. W.A. Tiller, J. Electrochem. Soc. 127, 619 (1980).
10. A. Redondo, W.A. Goddard III, C.A. Swarts and T.C. McGill, Jr., J. Vac. Sci. Technol. 19, 498 (1981).
11. M.O. Thompson, J.W. Mayer, A.G. Cullis, H.C. Webber, N.G. Chew, J.M. Poate and D.C. Jacobson, Phys. Rev. Lett. 50, 896 (1983).
12. A. Cros, F. Salvan and J. Derrien, Appl. Phys A28, 241 (1982).
13. Y.S. Liu, S.W. Chiang and W. Katz, Laser and Electron-Beam Interactions with Solids (Elsevier Science Publishing Co. Inc.,1982), p.249.
14. J.E. Dial, R.E. Gong and J.N. Fordemwalt, J. of Electrochem. Soc. 115, 326 (1968).
15. W.A. Pliskin and H.S. Lehman, J. of Electrochem. Soc. 112, 1013 (1965).
16. L. Schumann, A. Lehmann, H. Sobotta, V. Riede, U. Teschner and K. Hübner, Phys. Stat. Sol. B110, K69 (1982).
17. J. Wong, J. Appl. Phys. 44, 5629 (1973).
18. T.H. DiStefano, D.E. Eastman, Phys. Rev. Lett. 27, 1560 (1971).
19. F.C. Brown, R.Z. Bachrach, M. Skibowski, Phys. Rev. B15, 4781 (1977).
20. D.L. Griscom, J. Non-Cryst. Sol. 24, 155 (1977) and references therein.
21. G. Hollinger, Appl. of Surf. Sci. 8, 318 (1981).

22. R. Castagne and A. Vapaille, Surface Sci. 28, 557 (1971).

23. E.H. Nicollian and J.R. Brews, MOS (Metal Oxide Semiconductor) Physics and Technology (Wiley, NY, 1982).

24. F. Montillo and P. Balk, J. Electrochem. Soc. 118, 1463 (1971).

25. J.R. Ligenza and M. Kuhn, Solid State Technol. 13, 33 (1970).

26. G. Pananakakis, G. Kamarinos, M. El-Sayed and V. LeGoascoy, Solid State Electron. 26, 415 (1983).

27. V.G.I. Deshmukh, H.C. Webber and D.V. McCaughan, Appl. Phys. Lett. 39, 251 (1981).

FIGURE CAPTIONS

Fig. 1 Schematic diagram of the apparatus: the XeCl excimer laser produces SiO_2 patterns on the Si substrate (<100> surface) by lens translation.

Fig. 2 Plot of SiO_2 thickness (from IR absorption data) as a function of laser exposure time. The observed growth rate is linear from 300 - 1800 A SiO_2 thickness becoming quadratic at greater SiO_2 thicknesses.

Fig. 3 IR absorption spectra: Laser-grown SiO_2 (solid line) and thermally-grown (1000°C) SiO_2 (dotted line). From the SiO_2 absorption coefficient at 1070 cm^{-1} we obtain an oxide thickness of ~2800 A.

Fig. 4 SXPS-spectra of Si-2p core level: (a) thermally cleaned Si-surface; (b) 7.5 A - L-SiO_2; (c) 15 A - L-SiO_2, and (d) ~ 500 A - L-SiO_2. The dashed curves show the contribution from a non-stoichiometric interface layer, after subtraction of bulk SiO_2 and substrate Si contributions.

Fig. 5 Typical high-frequency (HF) and low-frequency (LF) CV-plot of an Al-L-SiO_2-Si MOS capacitor. The HF-curve was taken at 1 MHz, the LF-curve at 500 Hz. From the data one obtains a fixed oxide charge density, D_f, of $6x10^{10}$ cm^{-2} and an interface state density, D_{it}, of $2x10^{11}$ $cm^{-2}eV^{-1}$.

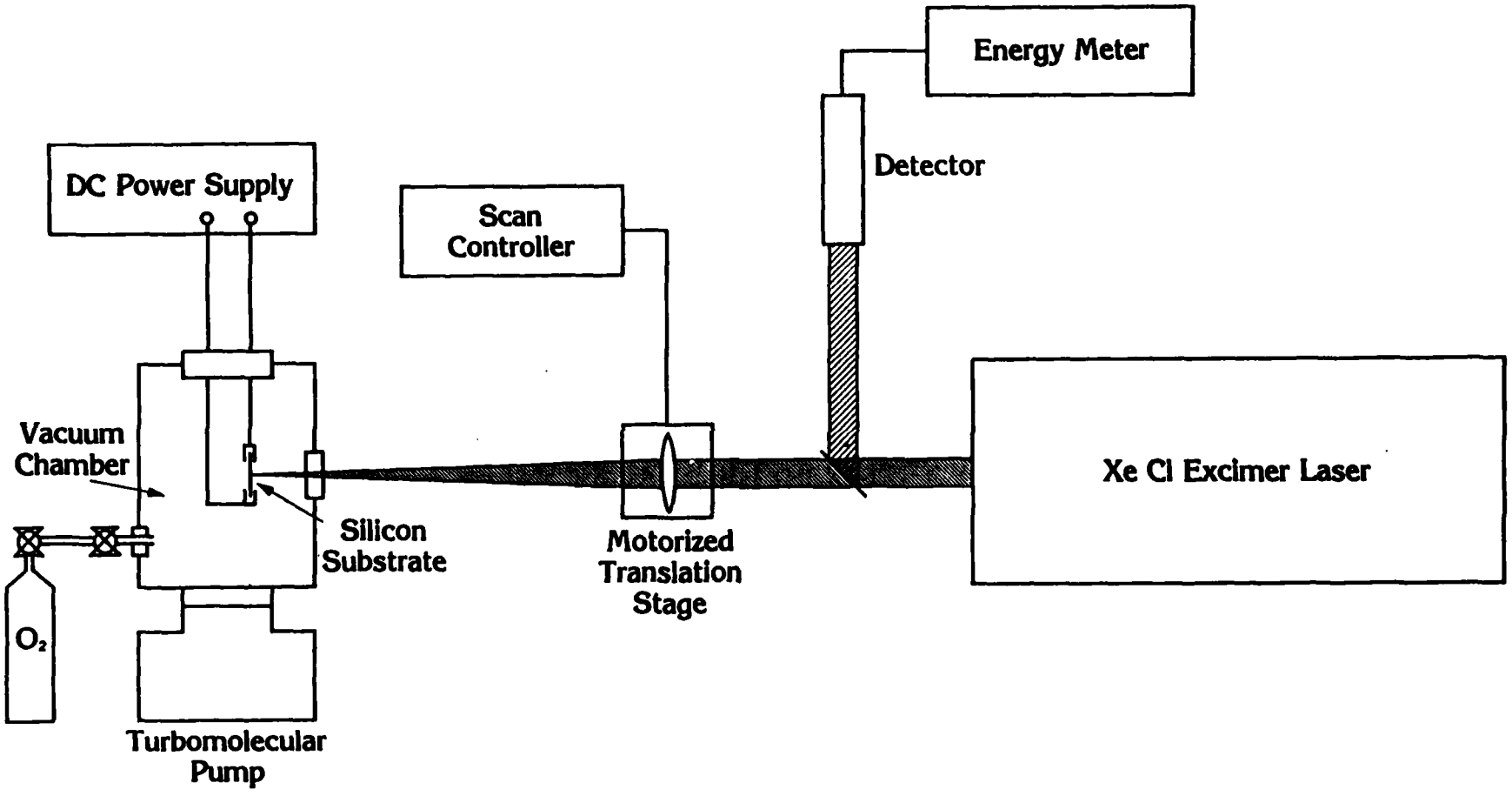
Energy Meter
Detector
DC Power Supply
Scan Controller
Vacuum Chamber
Silicon Substrate
Motorized Translation Stage
Xe Cl Excimer Laser
O_2
Turbomolecular Pump

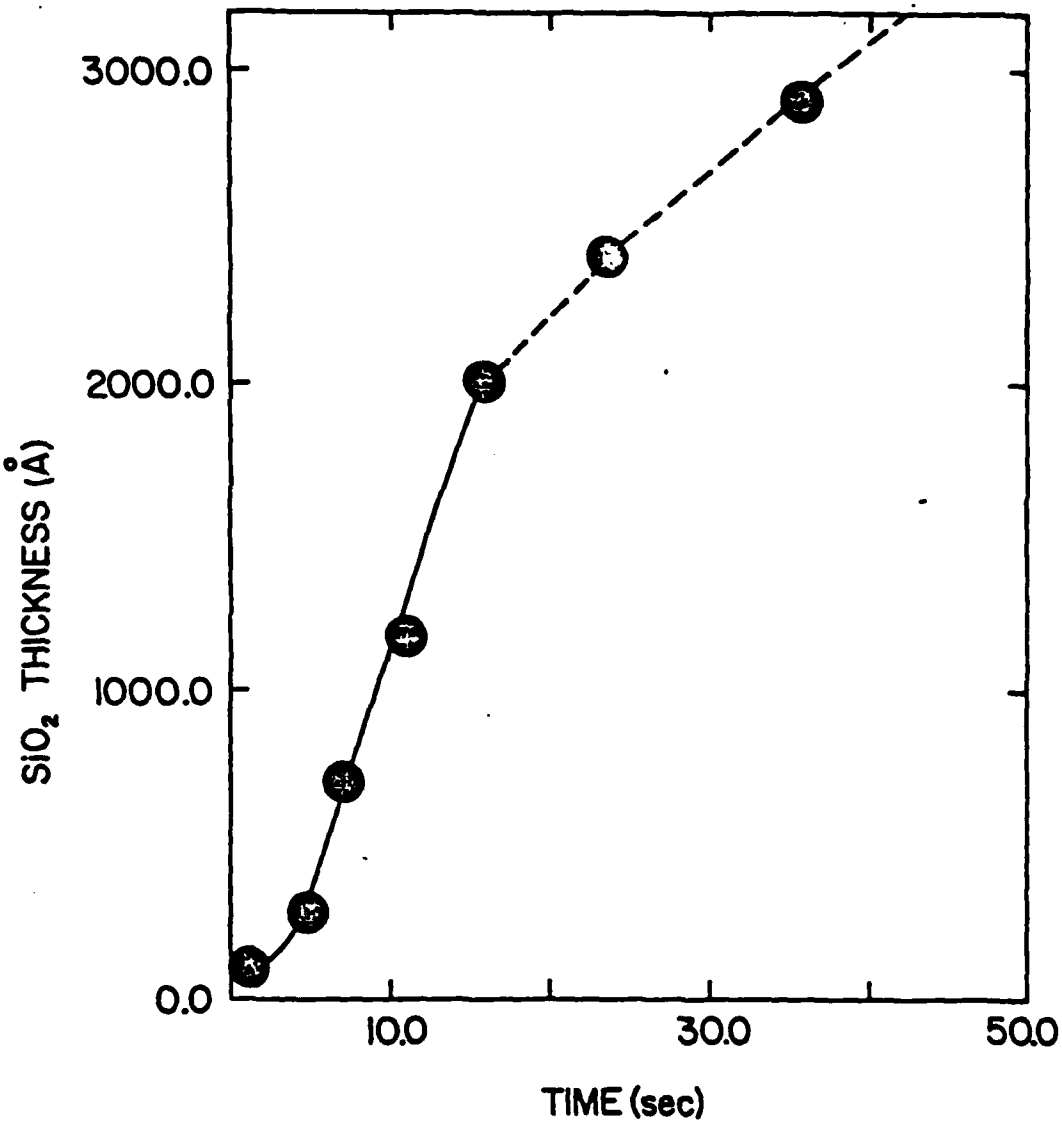
3000.0
2000.0
1000.0
0.0
SiO_2 THICKNESS (Å)
10.0
30.0
50.0
TIME (sec)

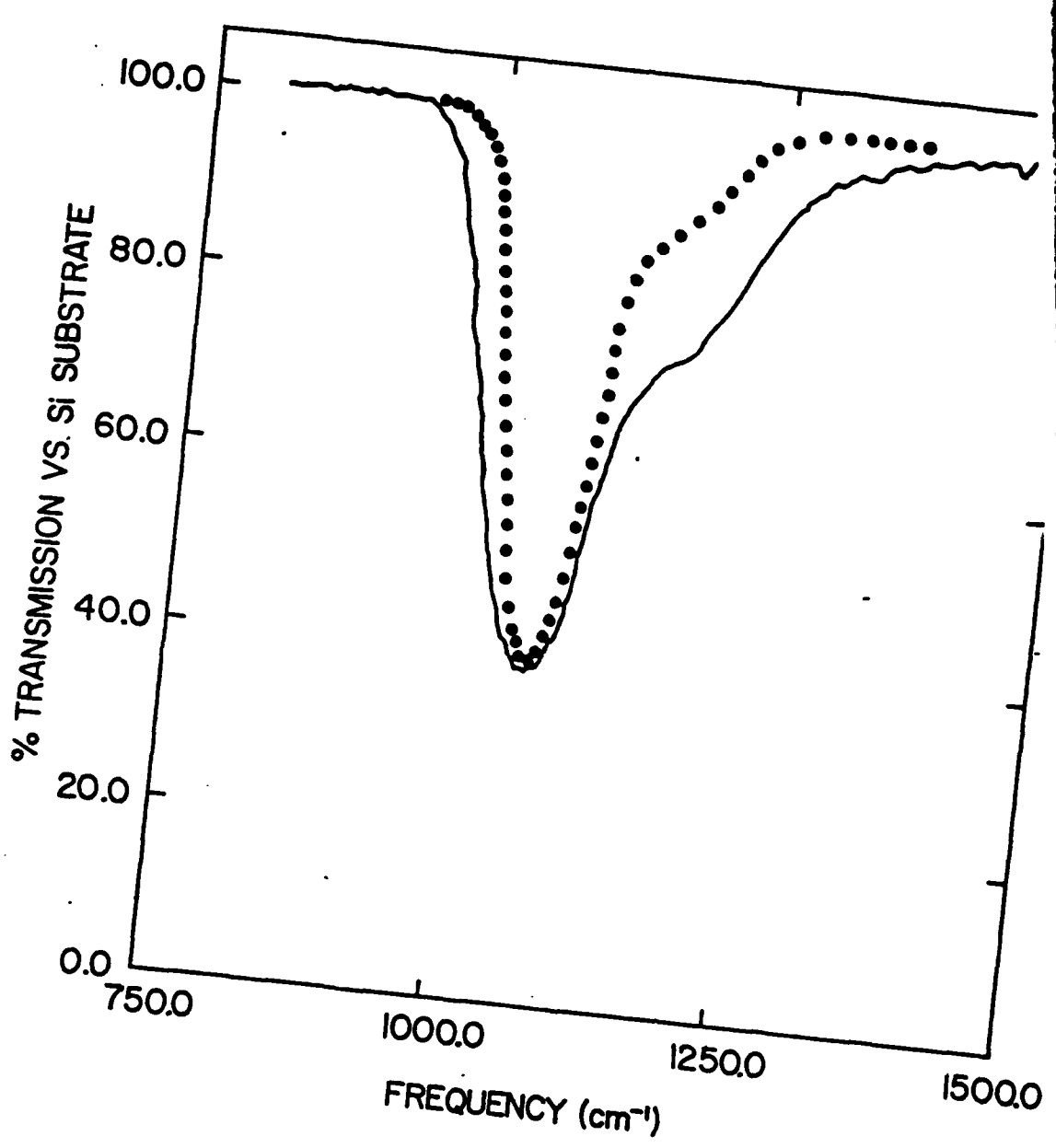
100.0
80.0
60.0
40.0
20.0
0.0
% TRANSMISSION VS. Si SUBSTRATE
750.0
1000.0
1250.0
1500.0
FREQUENCY (cm⁻¹)

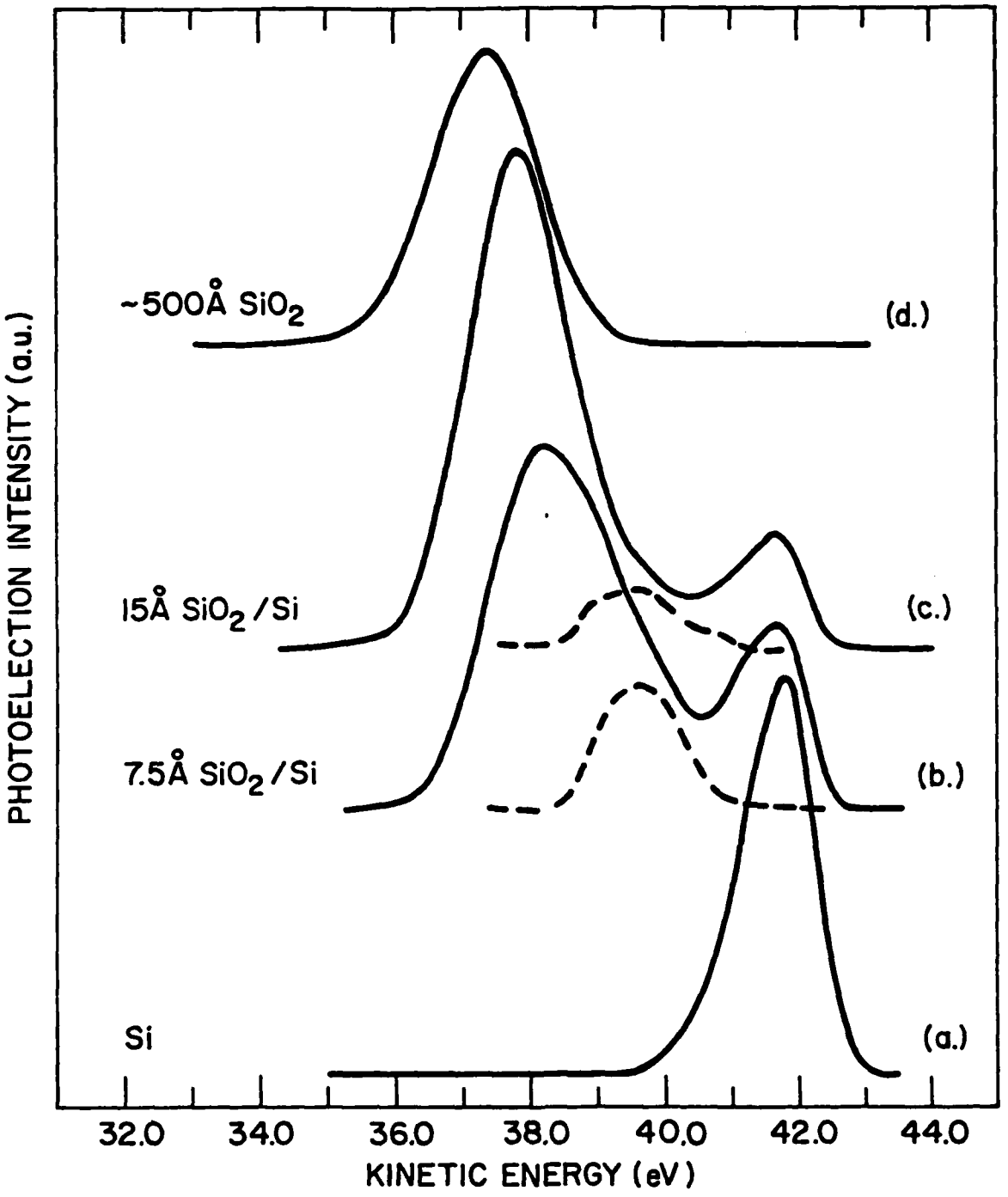
~500Å SiO2
(d.)
15Å SiO2 / Si
(c.)
7.5Å SiO2 / Si
(b.)
Si
(a.)
PHOTOELECTION INTENSITY (a.u.)
32.0
34.0
36.0
38.0
40.0
42.0
44.0
KINETIC ENERGY (eV)

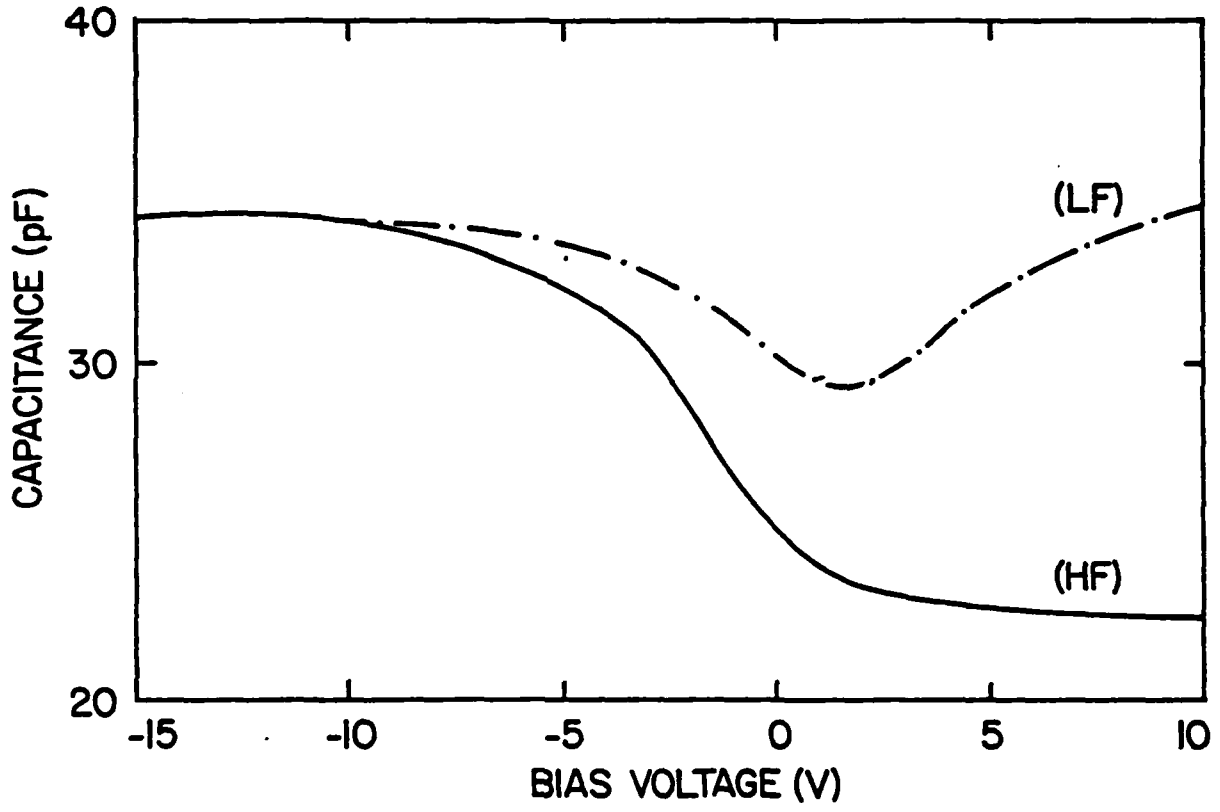
40
30
20
CAPACITANCE (pF)
(LF)
(HF)
-15
-10
-5
0
5
10
BIAS VOLTAGE (V)

UPS, XPS, and AES Studies of CaF_2-CdSe Interfaces

Yoram Shapira*
School of Engineering, Tel Aviv University
Ramat Aviv 69978, Israel

and

C.F. Brucker** and L.J. Brillson
Xerox Webster Research Center
Webster, NY 14580

Abstract

We have investigated overlayers of CaF_2 deposited in ultra high vacuum on CdSe surfaces using ultraviolet and x-ray photoemission spectroscopy and Auger electron spectroscopy. The interfaces exhibit very little reaction or interdiffusion and are remarkably abrupt. The results are compared with metal-CdSe interfaces and possible applications are discussed.

*Work done during sabbatical year at Xerox Research Center, Webster, NY, USA

**Permanent address: Eastman Kodak Co., Rochester, NY, 14650, USA

Acceptor-Like Electron Traps and Thermally-Reversible Barrier Heights for Al on UHV-Cleaved (110) InP

John H. Slowik, H.W. Richter[a] and L.J. Brillson
Xerox Webster Research Center, Webster, NY 14580

Temperature-dependent current-voltage (I-V) and capacitance-voltage (C-V) measurements reveal that a low but non-zero barrier is present at the interface of Al deposited on ultrahigh-vacuum-cleaved n-InP (110), and that the true barrier height lies between 0.21 - 0.26 eV. An analysis which allows for the presence of of trapped charge near the interface provides the most accurate and consistent determination of the effective barrier. The effective barrier is strongly and reversibly temperature-dependent, corresponding to movement of the Fermi level with temperature. The trapped interfacial charge resides in acceptor-like electron traps 0.10 eV below the conduction band edge. The traps are distributed 100-200 A into the space charge region. These results are discussed in terms of models of defect electrical activity at metal-semiconductor interfaces, and are related to results of annealing studies.

PACS numbers: 73.40.Ns, 71.55.Ht, 73.30.+y, 73.40.Gk

I. INTRODUCTION

The Al contact to InP is of high importance for both scientific and technological reasons. It forms microscopically abrupt junctions with semiconductors including InP, and the Al/InP contact is particularly stable under heating.[1,2] Al also shields the interface on some semiconductors from ambient contamination.[3] Contact stability is particularly desirable for high power InP devices like microwave oscillators and injection lasers.

Reproducible Al Schottky barriers on pure (shallow donor doping density, $N_D = 5 \times 10^{15}$ cm^{-3}) InP have been reported with ideality factor $n \approx 1$ only if the InP surface is first treated.[4,5] Such processing alters the surface or interface state density, presumably by adding states, since the barrier increases[4] from a low value before treatment to a highly reproducible 0.5 eV. On unprocessed vacuum-cleaved InP, relatively unreactive metals[6] (Au, Ag, Cu) form barriers with the same energy,[7] suggesting that both cases involve defects with the same energy level.[8]

The clean unprocessed interface between InP and a reactive metal[6] such as Al is less well understood. The free surface lacks detectable surface states,[2,7,9] and Al deposition results in a low barrier. It has been suggested that metal-induced defect states could control this barrier formation,[10-14] though few electrical measurements have been published.[4,5,7,15] This may be due to the fact that the standard analysis of the I-V characteristic[16] leads to a large ideality factor, and a lack of reproducibility has been reported.[4] Thus a better understanding of this interface is desirable for both theoretical and technological reasons. Theoretical studies of InP processing are usually designed as perturbations on the simple unprocessed interface, since the multitude of states likely to be introduced by processing are mathematically

intractable. The unprocessed interface is also important as a point of departure for understanding the empirical results of processing technology.

The work reported here is based on thermal measurements of the I-V and C-V characteristics of Al deposited in situ on vacuum-cleaved InP. It is found that the non-ideal I-V characteristics result from metal-induced defect states, as suggested by Williams,[10,13] which form acceptor-like electron traps. These states are distributed into the semiconductor about 100-200 Å, and are 0.10 eV below the conduction band. Because of their influence on the C-V and I-V characteristics, physically meaningful barrier parameters can be extracted only by an analysis which takes account of their presence. The effective barrier is non-zero at all temperatures, though reduced by tunneling effects, and shows a strong, reversible temperature dependence related to the thermal motion of the Fermi level. The sample-to-sample fluctuation in the barrier is attributed to small changes in interfacial state density, and may account for the reported lack of reproducibility. The true barrier height at the metallurgical junction is between 0.21-0.26 eV.

Experimental details are presented in Sec. II. The reverse-biased capacitance characteristics and the forward-biased current characteristics are presented in Sec. III, and analyzed in Secs. IV and V, respectively. The consistency between these two and also with the forward-biased capacitance is discussed in Sec. VI. Section VI also points out the similarity of the proposed electronic structure of the interface to that of an MIS device, and relates the present results to annealing studies. The results are summarized in Sec. VII.

II. EXPERIMENTAL

Samples were formed on three crystals of n-InP, $N_D = 1$ to 5×10^{15} cm^{-3}, obtained from MCP Ltd. (Cambridge, England) and Lincoln Laboratories. A large area

("ohmic") back contact was formed by heating a 5000 Å Sn layer at 350°C for 15 minutes in forming gas of 10-20% H_2 in N_2. The crystals were then cleaved in ultrahigh vacuum. An array of 5 to 8 Al electrodes were deposited with 200 Å thickness and 500 μm diameter. Surface current effects were eliminated using a guard ring structure in the manner of Padovani.[17] An additional large-area electrode was applied for determining spreading resistance and the residual resistance associated with the ohmic Sn contact and the external circuit.[16]

Since the barriers are low and the interfaces are abrupt, the method of establishing electrical contact with the 200 Å Al electrodes is important. The continuity must endure thermal cycling, yet contact must be gentle enough to avoid piercing the barrier. A mechanical pressure contact made by a spring-loaded In pin yielded good results.

Current and capacitance were measured with a Keithley 616 electrometer and a Boonton 72B capacitance meter operating at 1 MHz. Measurements were made between 80K and 360K. Forward currents were kept sufficiently low so that spreading and residual resistances could be neglected. Usually the applied potential was kept above 3 kT/q, although some very low bias measurements were also made. In such cases special care was taken to interpret the current response by correctly handling[18] the exponential terms containing kT. For the magnitude of $d(C^{-2})/dV$ presented here, the influence of series resistance[19] was negligible. At each temperature both capacitance and current were studied following a variety of bias conditions, to gauge the effect of trapped charge.

III. CAPACITANCE AND CURRENT RESULTS

Capacitance was determined as a function of temperature and applied potential.

V. After subtracting stray capacitance, $(A/C)^2$ was plotted versus V, where A is the electrode area. One representative set of data is shown in Fig. 1, where $V<0$ indicates the reverse-biased condition. These plots have a distinctive two-regime structure. Between zero and –60 meV, the curves are linear with V-axis intercepts at tenths of volts, from which the barrier height may be calculated, as discussed later. At higher reverse bias, the curves asymptotically approach a different linear behavior having a smaller slope and intercepts between 1 and 3.5 V. This smaller slope is related to bulk carrier density, though somewhat modified by the presence of deep bulk traps. At the highest temperature, reverse currents saturate the amplifier,[20] introducing an artifical nonlinearity. Data distorted by this effect are deleted from the figure.

Current characteristics were obtained under forward bias at a variety of temperatures between 84K and 360K. A set of such data is shown in Fig. 2 which was taken at the same time as the capacitance data in Fig. 1. These characteristics are highly non-ideal. Interpretation according to thermionic emission theory is not valid since it leads to large field-dependent values of the ideality factor. A correct analysis, leading to a physically meaningful picture of the barrier region, is deferred until Sec. V.

IV. ANALYSIS OF REVERSE-BIASED CAPACITANCE CHARACTERISTICS

The nonlinear capacitance characteristics result from acceptor-like electron traps 0.10 eV below the conduction band edge, rather than from an interfacial layer or doping variation. Variation in the density of shallow donors can be eliminated since the interfaces were prepared on uniformly doped, cleaved single crystals. A bias-dependent surface state charge does not lead to non-linear behavior, though the presence of an interfacial layer can account for large offsets of the voltage intercept,

such as are observed at high reverse bias.[21] The characteristic in the presence of such a layer has a slope equal to $2/q\epsilon_s n_0$ when the surface state charge is coupled to the metal, but much larger when decoupled by a thick intervening layer.[21] The free carrier density is n_0 and the semiconductor dielectric constant is ϵ_s. Slopes at low bias in Fig. 1 significantly exceed $2/q\epsilon_s n_0$ if n_0 is taken to be equal to the doping density of shallow donors. However, there is no intervening oxide to provide decoupling. AlP probably forms at the interface,[22,23] but in a layer too thin for effective decoupling. Decoupling requires that the states which form during Al metallization extend from the metallurgical junction to some depth within the semiconductor. An effective decoupling would then result from trapped charge in these states being isolated from the metal. Hereafter, such states are referred to as interfacial states with the understanding that their distribution penetrates into the semiconductor.

The existence of such states is also suggested by considering the usual analysis[18] in which the nonlinearity of the capacitance characteristic is used to determine a nonuniform doping distribution. In that analysis the slope at V is given by $\partial(C^{-2})/\partial(-V) = 2/q\epsilon_s n_0(w)$, where $n_0(w)$ is the free carrier density at the edge of the depletion width, w, and w increases with reverse bias. Applying this to the data in Fig. 1, the higher slope between zero and –60 meV would indicate a thin interfacial region in which there is significant compensation due to acceptors or acceptor-like traps (neutral when empty). A related effect was reported for ideal Au contacts on etched epitaxial (110)n-InP of low doping, and attributed to incomplete depletion.[24] In the case of incomplete depletion, the effect is more pronounced at higher temperatures due to diffusion of mobile carriers. In the present case the slope is constant for fields between zero and -60 meV, independent of temperature, as would be expected if the slope change were related to the penetration depth of the states into the body of the semiconductor.

The zero-bias capacitance, C_0, increases with temperature, as listed in Table I.[25] This suggests the level becomes more negatively charged at low temperature. Thus the state is an acceptor-like trap rather than a shallow acceptor. Further confirmation of the presence of these traps is presented in the Discussion section.

The linear capacitance characteristic indicates that the occupancy of the traps is not altered at low bias. When traps are present within the top layers of the semiconductor, the zero-bias barrier, φ_{co}, determined from the capacitance characteristic,

$$(A/C)^2 = 2(\varphi_{co} - qV - \zeta - kT)/q^2\epsilon_s n_{oo}, \quad (1)$$

can differ significantly from the true zero-bias barrier at the metallurgical junction, φ_o. This is because φ_{co} is determined by extrapolating a parabolic potential back to the semiconductor surface,[26] whereas trapped charge may make the depletion-region potential non-parabolic. Here n_{oo} represents a modified carrier density which is less than the density of shallow donors due to trapping by the acceptor-like states,[18,27] and

$$\zeta = E_c - E_F = kT \ln(U_c/n_o), \quad (2)$$

where E_c is the conduction band edge, E_F the Fermi level, and U_c the effective density of states in the conduction band. Values of φ_{co} and n_{oo} obtained by applying Eq. (1) to the data in Fig. 1 are listed in Table I, and plotted in Fig. 3 as a function of inverse temperature.

Although data could not be obtained above room temperature,[20] both Table I

and Fig. 3 show a clear increase in n_{oo} above 170 K. If the rise is assumed to proceed linearly to n_o at high temperature, as the dashed line in Fig. 3, an activation energy can be determined according to

$$n_{oo}(T) = n_o \exp(-E_a/kT) \tag{3}$$

where E_a represents the depth of the trap below E_c. The resulting value of E_a is 101±4 meV. At room temperature, emission from such a level, populated by tunneling from the metal, would account for the strong current under reverse bias. At lower temperatures this emission would be much reduced, as is observed. Since the doping density is low, trapped electrons repel free carriers at the depletion edge, further increasing the φ_{co} value obtained at low temperature by extrapolating the bands to the surface. Thus φ_{co} would be larger than the true zero-bias barrier, φ_o, throughout the temperature range, with $\varphi_{co}=\varphi_o$ only when the traps are fully ionized.

V. ANALYSIS OF FORWARD-BIASED CURRENT CHARACTERISTICS

Analysis of the I-V characteristics according to a model which includes trapped charge near the interface results in physically meaningful barrier parameters. However, since such analysis is less well known, we consider first the application of familiar Schottky barrier transport mechanisms. Forward I-V characteristics are usually interpreted in terms of thermionic emission[18,28] (TE) over an ideal Schottky barrier:

$$J = A^*T^2 \exp(-\varphi_{BO}/kT) \exp(qV/nkT) \tag{4}$$

where φ_{BO} is the effective zero-bias barrier height, and the ideality factor, n, expresses the increase in barrier height under applied field. For TE in an ideal

Schottky barrier this increase is small, so that n exceeds unity by only a few percent. Large n values occur when a thin interfacial layer is present on high resistivity semiconductors.[29] Large n is found in the present data due to the traps near the surface. In either case the characteristic is said to be non-ideal, transport does not proceed by TE over an ideal barrier, and φ_{BO} cannot be accurately determined from Eq. (4).

There are four other transport mechanisms possible at an ideal Schottky barrier which do lead to $n \neq 1$. All can be formally described[16] by Eq. (4). The four are: thermionic-field emission (TFE), field emission (FE), recombination in the space charge region (RSC), and minority carrier injection from the back contact with recombination occurring in the bulk (RB). The n values derived from tangents to the curves in Fig. 2 are too high for TE or RSC. RB could not account for the magnitude of the observed current since the minority carrier injection ratio[30,31] is less than 3×10^{-3} for all of the fields and temperatures which were applied, even assuming a barrier height as large as the band gap. The remaining tunneling modes, TFE and FE, can be analyzed using Eq. (4) by setting[16]

$$n = (E_{oo}/kT) \coth (E_{oo}/kT) \tag{5}$$

where

$$E_{oo} = (qh/4\pi) (N_D/m^*\varepsilon)^{1/2}. \tag{6}$$

Here N_D is the density of the fully ionized donors, m^* the effective mass, and ε the dielectric constant. Modification of the prefactor is also necessary,[16] but is omitted here since it does not affect the discussion. The large n values derived from Fig. 2 imply, because of Eq. (5), that $E_{oo} >> kT$. This indicates FE rather than TFE. The slope of ln J is nearly temperature independent, further suggesting FE. However,

for FE the reverse-biased current should exceed[16] the forward current when n >2. This was not observed. Furthermore, values of N_D calculated from Eq. (6) exceed the bulk doping density by more than a factor of 10^5. Thus the data conform to none of the ideal Schottky barrier transport mechanisms. The conclusion is that the barrier is not ideal, but rather contains an interfacial layer, which was ruled out earlier, or interfacial states. A model which includes charge trapped in interfacial states is required to interpret correctly the I-V characteristics.

The case where charged states are present near the barrier has been analyzed by Levine.[32] This model is useful here, although it is not decisively physical,[33-35] because its generality encompasses a variety of situations where charge is present at, as well as near, the surface. It is equivalent[35] to the Bardeen interface if the states are at the surface and distributed over an energy greater than kT, and possibly equivalent[35] to a modified doping profile at the surface if less than kT. For the full analysis the reader is referred to the original work.[32] Use of the model to interpret data begins with[32]

$$1/T_0 = 2(\varphi_B - qV - \zeta - kT)/TE_0, \tag{7}$$

where T_0 is nearly independent of temperature at constant current. φ_B is the field-dependent barrier height. E_0 is a constant characterizing the energy distribution of the interface states. The procedure is to obtain T_0 empirically from

$$\partial(\ln J)/\partial V = q/k(T+T_0), \tag{8}$$

and use the derivative of Eq. (7) with respect to V to obtain $E_0 = -2q/(T+T_0)(\partial T_0^{-1}/\partial V)$. This requires using the field dependence[32] of φ_B, which is related to the magnitude of T_0:

$$\partial\varphi_B/\partial V = qT_o/(T+T_o). \quad (9)$$

In situations where surface states produce a modest deviation from ideal TE behavior, T_o is small.[36,37] In the present data $T_o >> T$ so that

$$\partial\varphi_B/\partial V \approx q. \quad (10)$$

In analyzing the present data it was established that both T_o and E_o depend only weakly upon temperature at constant current. With E_o and T_o determined, φ_B versus V can be plotted for various temperatures by using Eq. (7). The values of φ_B obtained in this way are shown in Fig. 4 for 101K and 223K.

The strong field dependence of φ_B shown in Fig. 4 is a direct consequence of Eq. (10). Because of the physical limitations of the model,[33-35] it is prudent to attribute little physical significance to this field dependence. However, the saturation current part of Eq. (4) contains only the zero-bias value φ_{BO}. Any refinement of the model that resulted in a different field dependence would not affect the intercept, φ_{BO}. For this reason, and because φ_B is empirically observed to extrapolate to a constant value of φ_{BO} independent of the bias magnitude, as in Fig. 4, the derived values of φ_{BO} should reflect accurately the effective zero-bias barrier for electrons emitted from the conduction band. Note that φ_{BO} may be significantly less that the true zero-bias barrier height because of tunneling through the tip of the barrier.

The value of φ_{BO} shifts monotonically higher as ambient temperature increases, as shown in Table I and Fig.3. This shift is reversible with temperature. It is much stronger than, and opposite in direction to that reported for Al deposited onto a polished and heated InP surface.[4]

At fixed temperature and bias, the values of T_0 fluctuated between samples by as much as a factor of two, even for diodes on the same cleavage face. Such behavior has been noted before.[17] Dopant fluctuations have been proposed as a cause of such variation for lightly doped semiconductors.[33,35] A variability in trap density at the interface might have a similarly strong effect here. The fluctuation in T_0 is a mathematical consequence of J variation according to Eq. (8). Less fluctuation was observed at reduced temperature. The influence of the fluctuation upon both φ_{BO} and $\partial\varphi_B/\partial V$ values was somewhat less than 10%.

The Richardson coefficient, A^*, as derived from the above analysis, centers around $4x10^{-3}$ A/cm^2 at room temperature. This is smaller than expected, but interfacial layers are known to reduce the current in a manner[18] equivalent to reducing A^*. For example, an SIS device having a thin ($\leq$ 20 Å) SnO_2 layer on n-Si and a barrier near 0.2 eV was reported[38] to show $A^* \sim 10^{-2}$ A/cm^2.

VI. DISCUSSION

Values determined for φ_{CO} and φ_{BO} agree with published descriptions, as shown in Table I. As indicated earlier, few electronic barrier determinations have been published, which is remarkable considering the high level of interest in the structure of this interface, and its relevance to the technology of practical processed Al/InP interfaces. It is likely that this situation reflects the difficulty of analyzing the C-V and I-V characteristics, rather than a lack of interest. There are no well-developed models for analyzing the I-V characteristic of a barrier which specifically include a penetrating population of traps localized near the interface. The correctness of the model of Levine for analyzing the forward I-V characteristics, is confirmed below by a) pointing out consistency between the barriers derived from the forward-biased C-V and I-V characteristics, and b) the demonstration that a similar φ_{BO} results from analyzing the I-V characteristic as if it were that of an MIS layer. Such results

cannot conclusively establish the applicability of Levine's analysis, but they do lead to a consistent picture of the interfacial electronic structure. In the final part of this Discussion, c) the results of studies of the annealing of processed interfaces are related to the proposed electronic structure.

Using a differential technique, dC/dV was measured as a function of forward bias. Maxima were observed at $V_M = 0.03$ eV (85K) and 0.18 eV (295K). If these maxima are due to the shallow donors at, for example, $E_D = 5$ meV so that the 1 MHz test frequency is low compared to their emission rate, then φ_{BO} can be determined from[39]

$$\varphi_{BO} = E_D + V_M. \tag{11}$$

The resulting values of φ_{BO} are in good agreement with the values shown in Fig. 3 as determined from Levine's analysis.

In Fig. 3, φ_{BO} rises faster when $\varphi_{BO} \gtrsim 0.1$ eV. This is not due to the Fermi level passing above the top of the trap distribution at $E_a = 0.10$ eV. Rather it is due to the temperature dependence of ζ, since over the entire temperature range φ_{BO} is closely approximated by

$$\varphi_{BO} \approx 38 \text{ meV} + \zeta + kT. \tag{12}$$

This suggests a model of the barrier as shown in Fig. 5. At high temperature, Fig. 5a, the traps in a thin interfacial layer are fully ionized. Since they are acceptor-like, they are neutral when empty and do not perturb the space charge. At low temperature, Fig. 5b, some of the traps may be filled and negatively charged, depending on the details of their distribution. In both cases, forward bias would

tend to populate the traps, with greater effect at low temperature due to the reduced emission rate. Since the trap density is locally greater than the doping density, as indicated by the behavior of n_{oo}, the band structure would be modified as if there were strong local compensation. In Fig. 5b, the effective barrier, φ_{BO}, is less than φ_o because carriers activated thermally to φ_{BO} with subsequent tunneling, constitute a larger emission current than carriers thermally activated over the full barrier height.

The shape of the conduction band in the presence of trapped charge is similar to that of an MIS structure,[28] and transport could be expected to behave similarly over small ranges of temperature and applied bias. To determine the nature of an MIS device with the same I-V characteristic as the Al/InP interface, the I-V data are shown as a Richardson plot in Fig. 6a. Two regimes are evident. The current at high temperature is more likely to be Schottky emission,[28] which for an MIS is

$$J = A^*T^2 \exp\{[q(qV/4\pi\epsilon_i d)^{1/2} - \varphi_{BO}]/kT\}. \quad (13)$$

The low temperature current is more likely to be tunneling,[28]

$$J \sim V^2 \exp\{-1.89\, m^{*1/2}\, \varphi_{BO}^{3/2} d/q\hbar V\}, \quad (14)$$

where ϵ_i is the insulator dielectric constant, taken here to be identical to that of InP. Physically the MIS thickness, d, would be associated with the penetration depth of the traps. Both φ_{BO} and d could also depend on the occupancy of the traps. Thus the values resulting from an MIS analysis would merely approximate the actual effective barrier and penetration depth.

According to Eq. (13), the slopes, s, at high temperature in Fig. 6a are given by

$$s = [q(qV/4\pi\epsilon_i d)^{1/2} - \varphi_{BO}]/k. \quad (15)$$

A plot of s versus $V^{1/2}$, as in Fig. 6b, then yields φ_{BO} from the intercept and d from the slope. The linearity of Fig. 6b suggests that the higher temperature transport mechanism is indeed Schottky emission. The resulting φ_{BO} is 0.05 eV, as compared to an average value over a comparable temperature range of about 0.13 eV from Fig. 3. The low estimate of φ_{BO} resulting from this MIS analog is probably due to the absence of a true insulator layer. No temperature variation of φ_{BO} is discernible because of scatter in the data. Eq. (15) yields d = 160 Å, a reasonable value which suggests moderate trap penetration. Williams[40] discusses the liklihood that electrically active states may be distributed several layers into the semiconductor, as found here, and he points out that this implies an energy distribution consistent with Levine's model. Finally, the value of A^* determined according to Eq. (13) is unphysically small, about 10^{-5} A/cm^2, due to the influence of trapped charge.

The low temperature characteristics can be analyzed according to Eq. (14), by plotting $\ln(J/V^2)$ versus V^{-1} as in Fig. 7. As the applied potential increases and the temperature drops, the data cluster toward nearly temperature-independent values, which indicates tunneling. The slope in this region yields $\varphi_{BO}^{3/2}$ d = 1.9 eV$^{3/2}$ Å. If we use d = 160 Å, as derived above, then φ_{BO} = 0.05 eV. This value is slightly below the 0.07 eV value from Fig. 3 at comparable temperature, again because of the absence of a true insulator layer.

Thus the results of the C-V analysis, and the I-V analysis according to Levine's technique, can be consistently understood by postulating acceptor-like traps at 0.1 eV below E_c. Since $\varphi_{co} \geq \varphi_o \geq \varphi_{BO}$, and since φ_{co} and φ_{BO} converge as the traps ionize at upper temperatures, the zero-bias barrier height at the metallurgical junction is 0.21 eV $\leq \varphi_o \leq$ 0.26 eV. Furthermore, the interpretation of the I-V characteristics according to MIS analogs yields values of φ_{BO} and trap penetration which are in reasonable agreement. The unusual, but fully reversible, temperature-

dependence of φ_{BO}, Eq. (12), can be understood as resulting from the thermal movement of E_F. The values in Fig. 3 and Table I, with φ_{BO} understood as an effective barrier lowered by tunneling, constitute the most complete picture to date of the barrier formed by Al on vacuum-cleaved (110) n-InP.

This picture suggests an interesting interpretation of annealing studies of Al on processed InP surfaces. In contrast to the low, non-ideal barrier on cleaved n-InP, stable higher barriers, ~0.5 eV, are formed if the n-InP is etched and heated before Al deposition.[1,2,4,7] Williams, et al.[2] studied the thermal stability of the Al interface on the processed (110) surface by measuring the barrier height as the sample was heated. As indicated by the last entry in Table I, they found that the initial 0.52 eV barrier at 100°C decreased toward 0.22 eV as the sample was heated to 400°C. The initial value is well understood as being the consequence of defect levels at the surface.[13] We speculate that annealing removes the original defect levels, creates more metal-induced states by further reacting the Al, or both. As a result the electronic structure becomes more like that of the UHV-cleaved interface. By the same token, the fact that the Al barrier on (100) epitaxial InP does not drop with annealing[1] could be due to a higher density of surface defects, rather than the different crystal orientation as has been suggested.[2]

VII. CONCLUSIONS

The principal results of this work are as follows:

(1) A low, but non-zero, barrier is present at all temperatures at the interface of Al deposited in situ on vacuum-cleaved (110) n-InP. The convergence at high temperature of the effective barrier under forward bias and the extrapolated barrier under reverse bias indicate that the true barrier height lies between 0.21-0.26 eV.

(2) The effective barrier governing the I-V characteristic is more accurately determined from an analysis which allows for the presence of a thin interfacial layer of trapped charge, than by analyses appropriate to an ideal Schottky barrier. A fully satisfactory model is lacking, but Levine's analysis yields a barrier in general agreement with MIS analogs, and close agreement with the forward-biased C-V analysis.

(3) The effective barrier is strongly and reversibly temperature-dependent. Between 80-360K, its value for semi-insulating n-InP is $\varphi_{BO} \approx 38\text{meV} + \zeta + kT$. This behavior is attributed to the thermal movement of the Fermi level.

(4) The trapped interfacial charge resides in acceptor-like electron traps separated by 0.10 eV from the conduction band edge.

(5) The traps are not restricted to the surface, but penetrate 100-200 Å into the depletion region.

(6) The traps proposed here are distinct from the donors invoked to explain certain InP barrier heights[7] according to the unified defect model.[41] Like the donors, they are at 0.10 eV below E_c and emit electrons into the conduction band. However these traps are negatively charged when filled, and thus are properly termed acceptor-like, whereas true donors would be neutral. Note, however, that the character of the unified defect model donors is uncertain. They could be acceptors instead,[42,43] and could then be identical to the traps described here. Calculations indicate that an amphoteric character is also possible.[44]

(7) The density and distribution of the Al-induced traps relative to that of process-induced defects may be the key to a deeper understanding of the annealing behavior of Al on InP.

VIII. ACKNOWLEDGEMENTS

We wish to thank Dr. C. B. Duke and Professors A. Kahn and M. Shaw for useful conversations. One of the authors (L.J.B.) acknowledges partial support by the Office of Naval Research, (Contract N00014-80-0778).

References

[a]Present address: Max-Planck Institut für Festkörperforschung, Stuttgart, W. Germany.

[1]H.B. Kim, A.F. Lovas, G.G. Sweeney, and T.M.S. Heng, in Proceedings of Sixth International Symposium on GaAs and Related Compounds, Inst. Phys. Conf. Ser. No. 33b, p.145, (1976).

[2]R.H. Williams, R.R. Varma, and A. McKinley, J. Phys. C 10, 4545 (1977).

[3]J.H. Slowik, L.J. Brillson, and C.F. Brucker, J. Appl. Phys. 53, 550 (1982).

[4]B. Tuck, G. Eftekhari, and D.M. deCogan, J. Phys. D 15, 457 (1982).

[5]Some samples recently produced by slow and interrupted deposition of Al onto InP in UHV exhibit a significant barrier and low n $\approx$ 1.05, see T. Kendelewicz, N. Newman, R.S. List, I. Lindau, and W.E. Spicer, Bull. Am. Phys. Soc. 30, 591 (1985). It is presently unclear why such a low n resulted. However, under slow and interrupted deposition in UHV, the first few layers of Al on CdS getter sufficient foreign atoms to affect the diode electrical behavior, see reference 3. Al could behave similarly when deposited onto InP, with foreign atoms modifying barrier characteristics.

[6]L.J. Brillson, Phys. Rev. Lett. 40, 260 (1978).

[7]R.H. Williams, R.R. Varma, and V. Montgomery, J. Vac. Sci. Technol. 16, 1418 (1979).

[8]W.E. Spicer, I. Lindau, P. Skeath, and C.Y. Su, J. Vac. Sci. Technol. 17, 1019 (1980).

[9]Y. Shapira and L.J. Brillson, Phys. Rev. B29, 6824 (1984).

[10]R.H. Williams, J. Vac. Sci. Technol. 18, 929 (1981).

[11]L.J. Brillson, C.F. Brucker, A.D. Katnani, N.G. Stoffel, and G. Margaritondo, Appl. Phys. Lett. 38, 784 (1981).

[12]L.J. Brillson, C.F. Brucker, A.D. Katnani, N.G. Stoffel, R. Daniels, and G. Margaritondo, J. Vac. Sci. Technol. 21, 564 (1982).

[13]R.H. Williams, J. Vac. Sci. Technol. 21, 594 (1982).

[14]Y. Shapira and L.J. Brillson, J. Vac. Sci. Technol. B1, 618 (1983).

[15]R.H. Williams, V. Montgomery, and R.R. Varma, J. Phys. C 11, L735 (1978).

[16]M. Shaw, in Handbook on Semiconductors, edited by T.S. Moss and C. Hilsum, (North-Holland, New York, 1981), Vol. 4, p. 1.

[17]F.A. Padovani, in Semiconductors and Semimetals, edited by R.K. Willardson and A.C. Beer, (Academic, New York, 1971), Vol. 7A, p.75.

[18]E.H. Rhoderick, Metal-Semiconductor Contacts (Clarendon, Oxford, 1980).

[19]A.M. Goodman, J. Appl. Phys. 34, 329 (1963).

[20]Figures in refs. 7 and 15 show a zero barrier at room temperature for Al on vacuum-cleaved (110) n-InP of low doping, as determined from C-V characteristics. However, a zero barrier implies an infinite capacitance, which is not measurable. The zero value merely represents a "low barrier" as stated in the text of these articles. A low barrier may be inferred from the fact that large reverse-bias currents interfere with capacitance measurements at room temperature.

[21]A.M. Cowley, J. Appl. Phys. 37, 3024 (1966).

[22]L.J. Brillson, Phys. Rev. Lett. 38, 245 (1977).

[23]L.J. Brillson, C.F. Brucker, A.D. Katnani, N.G. Stoffel, and G. Margaritondo, Phys. Rev. Lett. 46, 838 (1981).

[24]B.L. Smith, J. Phys.D 6, 1358 (1973).

[25]Depletion widths are not derived from C_0 since the presence of a nonuniform space-charge barrier on lightly doped material reduces the capacitance below the value corresponding to the actual barrier width, see ref. 17.

[26]C.R.Crowell and G.I. Roberts, J. Appl. Phys. 40, 3726 (1969).

[27]The relaxation frequency of the level is less than the measurement frequency if the level is deep, see ref. 17.

[28]S.M. Sze, Physics of Semiconductor Devices, (Wiley, New York, 1969).

[29]C.R. Crowell and S.M. Sze, Sol. St. Electron. 9, 1035 (1966).

[30]D.L. Scharfetter, Sol. St. Electron. 8, 299 (1965).

[31]M.A. Green and J. Shewchun, Sol. St. Electron. 16, 1141 (1973).

[32]J. Levine, J. Appl. Phys. 42, 3991 (1971).

[33]C.R. Crowell, J. Vac. Sci. Technol. 11, 951 (1974).

[34]E.H. Rhoderick, J. Appl. Phys. 46, 2809 (1975).

[35]C.R. Crowell, Sol. St. Electron. 20, 171 (1977).

[36]F.A. Padovani and G.G. Sumner, J. Appl. Phys. 36, 3744 (1965).

[37]A.N. Saxena, Surf. Sci. 13, 151 (1969).

[38]A.K. Ghosh, T. Feng, J.I. Haberman, and H.P. Maruska, J. Appl. Phys. 55, 2990 (1984).

[39]G.I. Roberts and C.R. Crowell, Sol. St. Electron. 16, 29 (1973).

[40]R.H. Williams, Surf. Sci. 132, 122 (1983).

[41]W.E. Spicer, I. Lindau, P. Skeath, C.Y. Su, and P. Chye, Phys. Rev. Lett. 44, 420 (1980).

[42]A. Nedoluha, J. Vac. Sci. Technol. 21, 429 (1982).

[43]W.E. Spicer and S.J. Eglash, in VLSI Electronics: Microstructure Science, edited by N.G. Einspruch and R.S. Bauer (Academic, New York, 1984).

[44]M.S. Daw and D.L. Smith, Phys. Rev. B20, 5150 (1979).

TABLE I. Temperature dependence of zero-bias capacitance, carrier density and barrier height as determined from Eq. (1), and barrier height determined from I-V characteristics. Entries without a reference are from the present work, for a single sample with $n_0 = 3.2 \times 10^{15}$ cm^{-3} bulk carrier density. Excess significant figures are retained to show systematic variation in φ_{BO}. Data for further samples appear in Fig. 3. NI = cited as being measurable but non-ideal with no numerical value given. NM = not measurable; see comment about room temperature φ_{CO} measurements, reference 20. Last line refers to a much different sample, processed by etching before Al deposition, and annealed after deposition at 400°C.

$10^3/T$(K)	C_o(pF)	$n_{oo} \times 10^{-12}$ (cm^{-3})	φ_{CO}(eV)	φ_{BO}(eV)
A. UHV-cleaved				
13			.46[a]	NI[a]
9.91	1.96	4.7	.44	.070
9.04	1.96	3.8	.37	.080
8.17	2.42	4.4	.29	.095
6.01	3.05	6.2	.29	.107
5.28	3.85	7.6	.25	.121
4.47	6.85	24.	.27	.141
3.40	NM	NM	NM,low[a,b]	.180
B. Etched and annealed				
1.5				.22[c]

[a]Ref. 7.

[b]Ref. 15.

[c]Ref. 2.

Figure Captions

1. Capacitance characteristics of one sample at (top to bottom) 110, 101, 123, 166, 189 and 225 K. Negative values of applied potential correspond to reverse bias. Data in lower left-hand corner, distorted by amplifier saturation, are deleted.

2. Forward I-V characteristic of same sample as in Fig. 1, at (top to bottom) 293, 223, 190, 167, 122, 111 and 101 K. If the ideality factor at 101 K were unity, slope would be as indicated by dashed line.

3. Temperature-dependence of effective barrier height, φ_{BO}, determined from forward I-V, and φ_{co} and n_{oo} from reverse C-V according to Eq. (1). As traps ionize with rising temperature, n_{oo} rises to the bulk free carrier density, n_o. Approximating the rise of n_{oo} by the dashed line yields 0.10 eV activation energy.

4. φ_B versus forward-bias resulting from analysis of I-V characteristics according to Levine's model. Intercepts equal zero-bias effective barrier, φ_{BO}. Upper data at 223 K, lower at 101 K. Shift of φ_{BO} with ambient temperature is reversible.

5. Schematic electronic structure of Al/n-InP interface assuming constant φ_o. Dashed part of conduction band indicates tunneling region. a) At high temperatures the effective barrier, φ_{BO}, increases with ζ. Barrier from reverse C-V, φ_{co}, equals true barrier, φ_o, at junction (neglecting image charge) when traps at $E_c - E_a$ are empty and neutral. b) At low temperatures φ_{BO} and ζ are small. Trapped majority carriers distort rigid band structure so that φ_{co} determined by parabolic extrapolation (dotted line) overestimates φ_o.

6. Forward I-V data analyzed as Schottky emission at MIS layer, Eq. (13). a) Richardson plot at (top to bottom) 0.9, 0.8, 0.7, . . . , 0.1 V (solid points), and 0.15 and 0.05 V (open points). High temperature slopes, s, are given by Eq. (15). b) Linearity of s versus $V^{1/2}$ is consistent with Schottky emission.

7. Forward I-V data analyzed as field emission through MIS layer, Eq. (14). Data are for (top to bottom) $10^3/T$ = 3.4, 4.5, 6.0, 8.2, 9.0 and 9.9 K^{-1}. Convergence at low temperatures indicates tunneling regime with $\varphi_{BO}^{3/2}\, d \approx 1.9\ eV^{3/2}$ A.

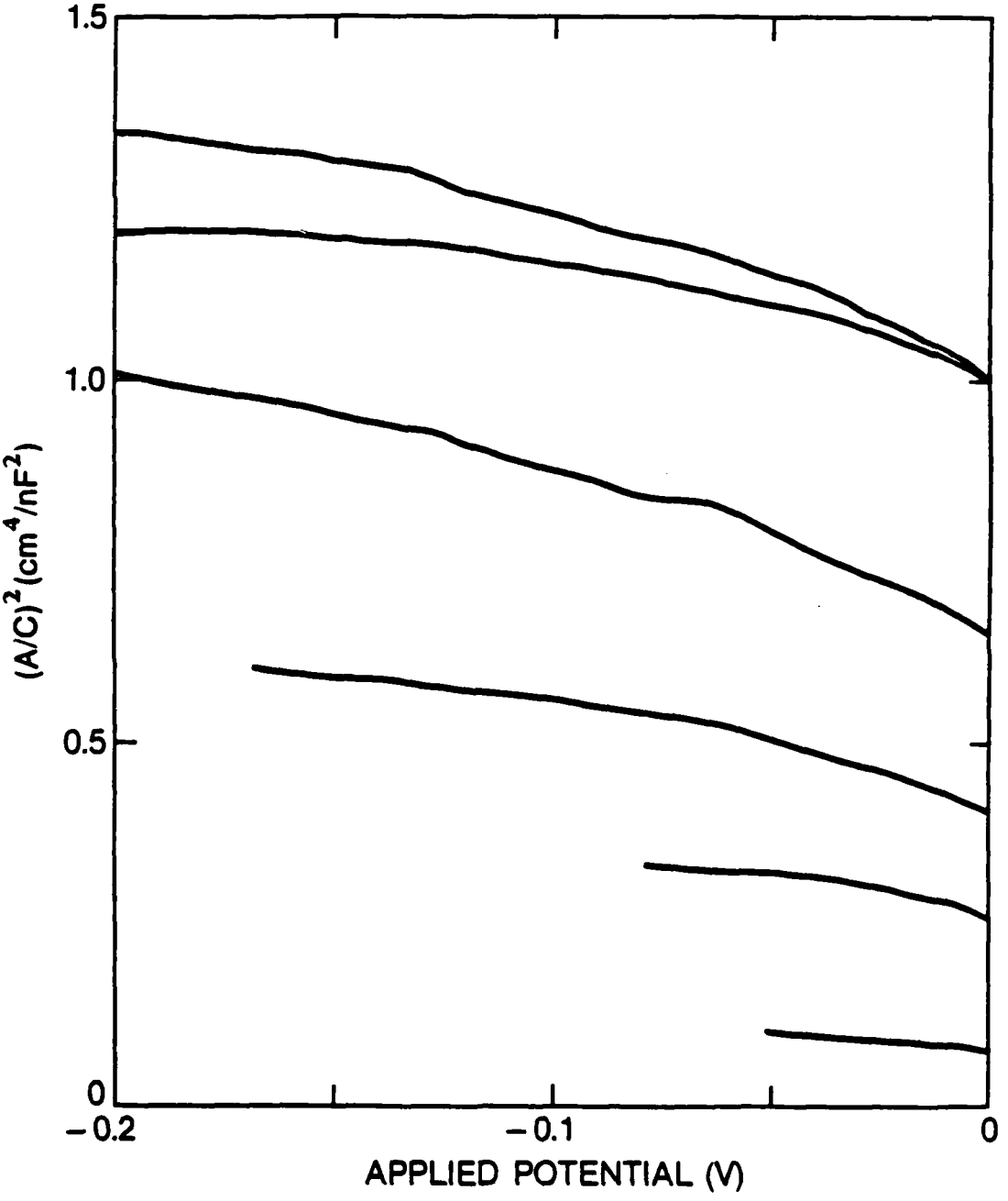

Fig. 1

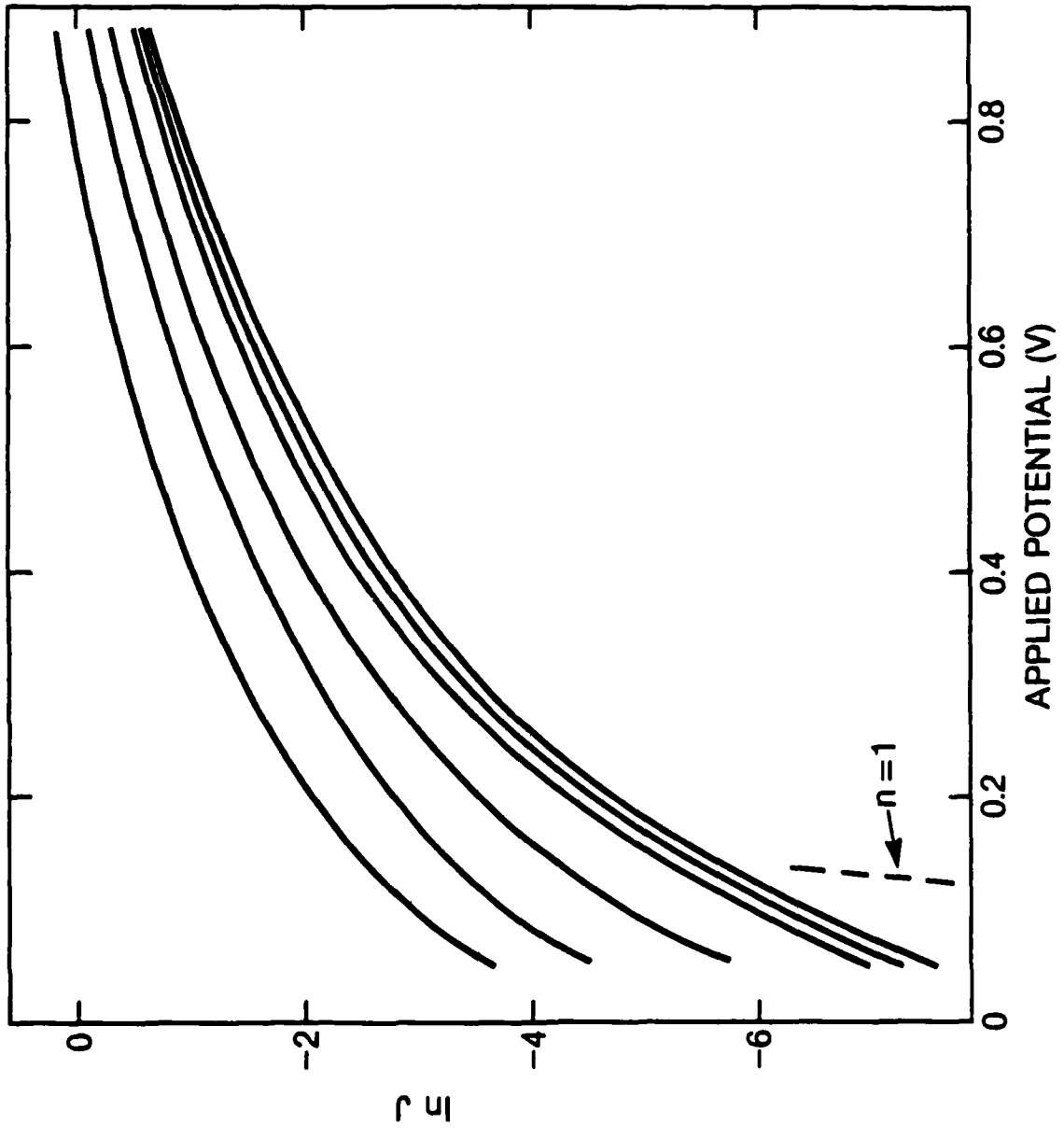

Fig. 2

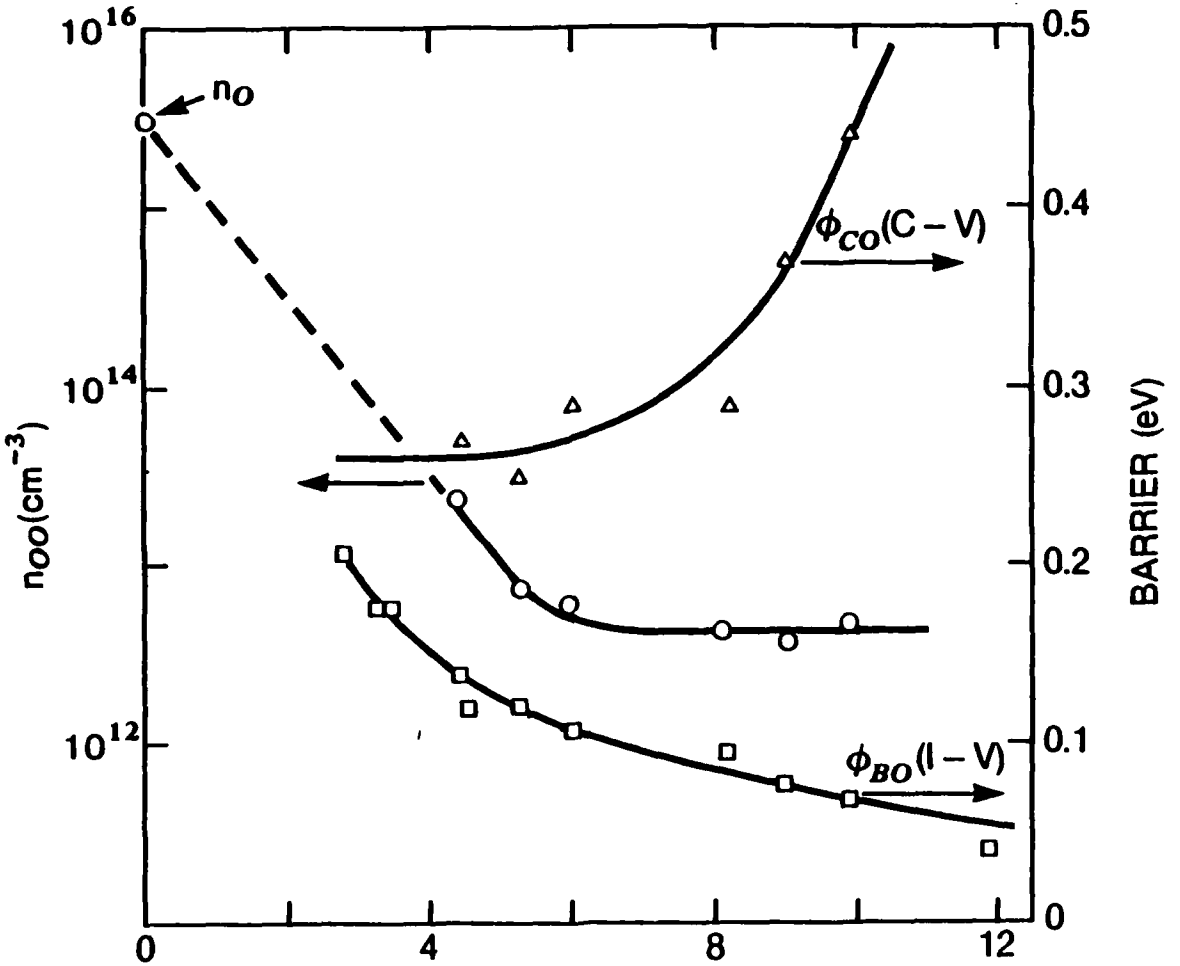
10^{16}
10^{14}
10^{12}
n_O
$n_{OO}(cm^{-3})$
$\phi_{CO}(C-V)$
$\phi_{BO}(I-V)$
0.5
0.4
0.3
0.2
0.1
0
BARRIER (eV)
0
4
8
12
$10^3T^{-1}(K^{-1})$

Fig. 3

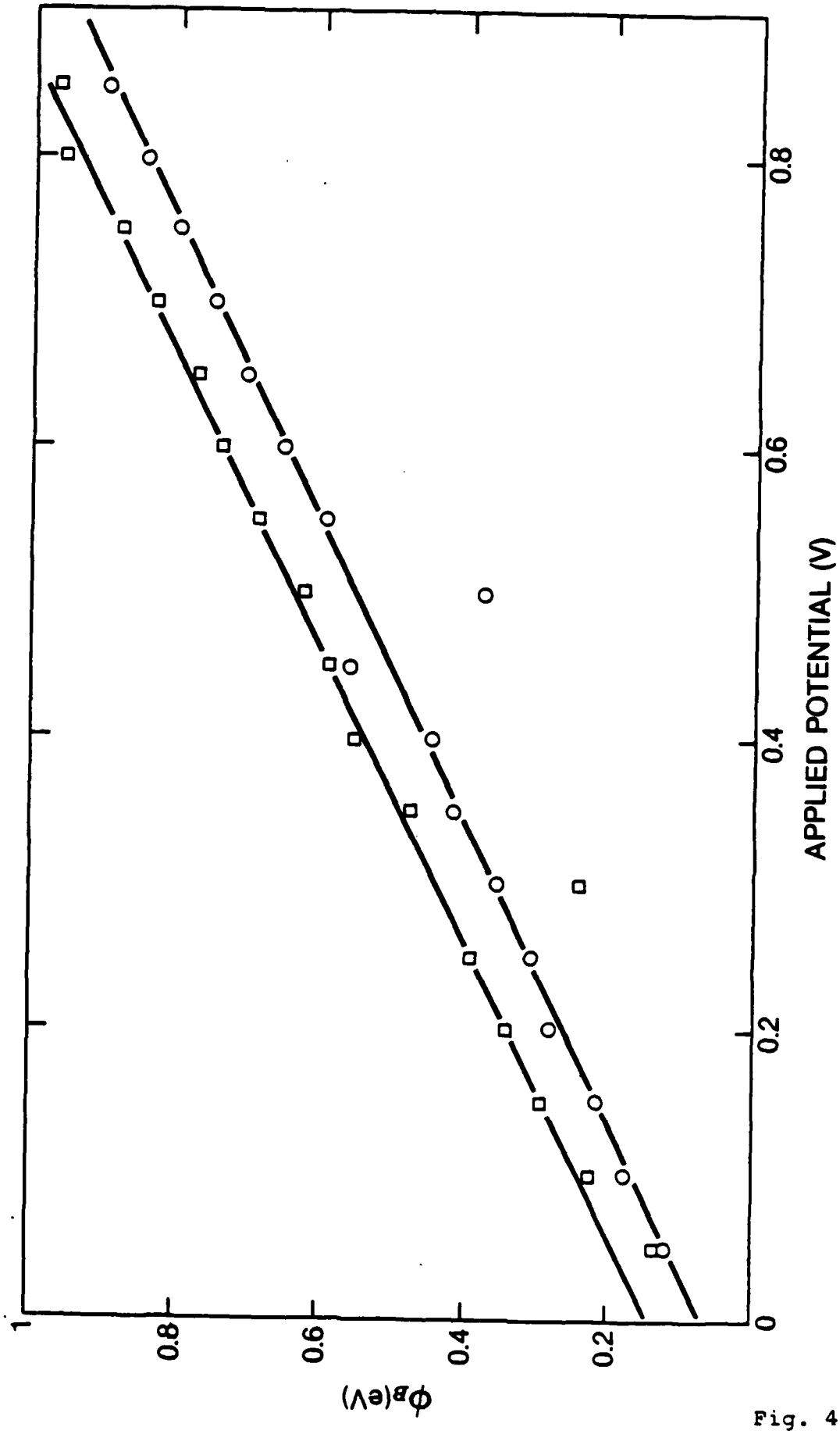

Fig. 4

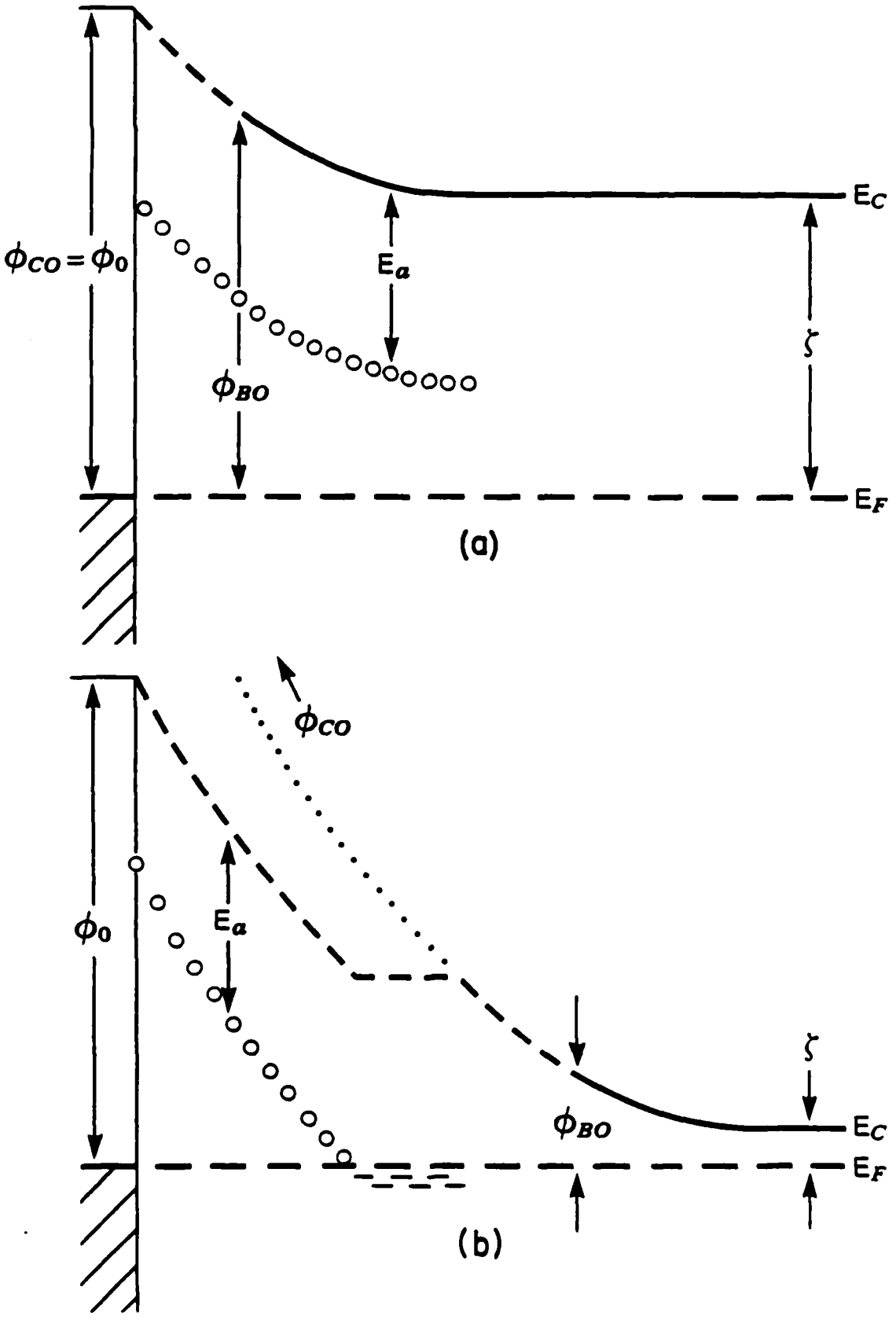
$\phi_{CO} = \phi_0$
E_a
ϕ_{BO}
ζ
E_C
E_F
(a)
ϕ_{CO}
ϕ_0
E_a
ζ
ϕ_{BO}
E_C
E_F
(b)

Fig. 5

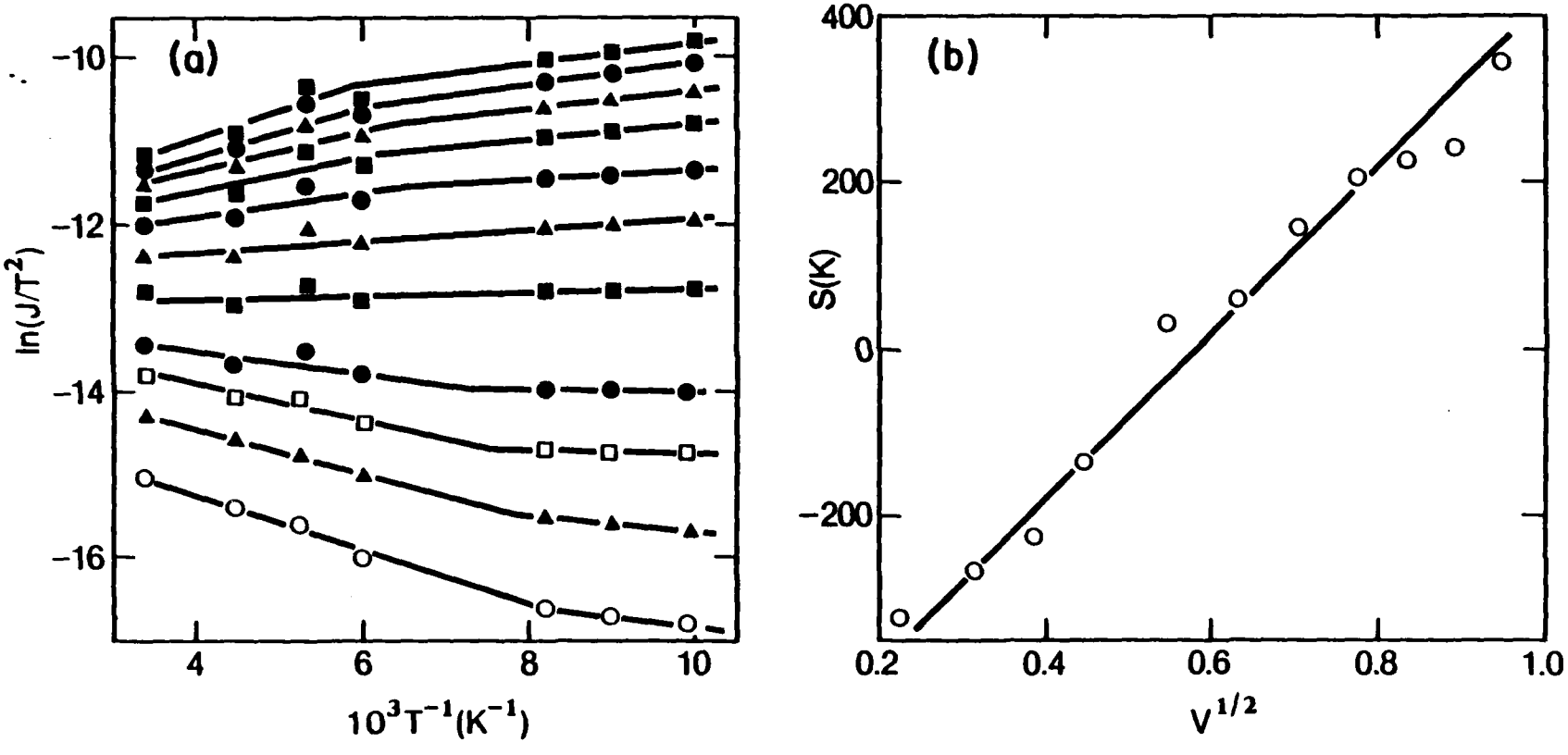
(a)
-10
-12
-14
-16
ln(J/T²)
4
6
8
10
10³T⁻¹(K⁻¹)
(b)
400
200
0
-200
S(K)
0.2
0.4
0.6
0.8
1.0
V^1/2

Fig. 6

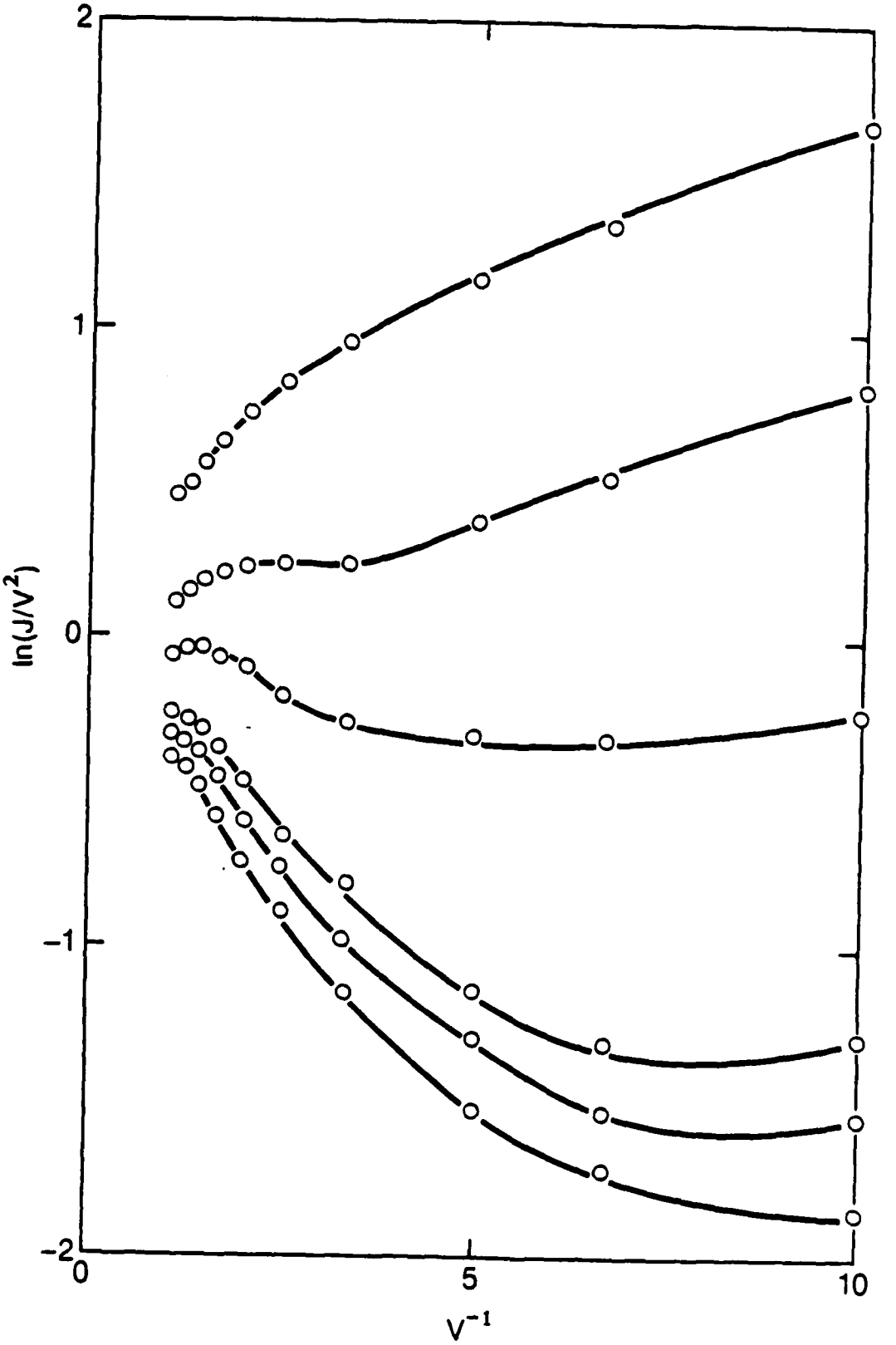

Fig. 7

Control of Titanium-Silicon and Silicon Dioxide Reactions by Low Temperature Rapid Thermal Annealing

L.J. Brillson, M.L. Slade and H.W. Richter
Xerox Webster Research Center, 800 Phillips Road, Webster, NY 14580

and

H. Van der Plas and R.T. Fulks
Xerox Palo Alto Research Center, 3333 Coyote Hill Road, Palo Alto, CA 94304

ABSTRACT

Auger electron spectroscopy/depth profiling measurements demonstrate that titanium silicide forms between titanium and silicon dioxide at conventional annealing temperatures. Low temperature rapid thermal annealing provides a process window in time and temperature to suppress this parasitic reaction relative to silicide formation at titanium-silicon interfaces within the same thin film structure.

PACS Numbers: 66.30.Ny, 68.40.+e, 73.40.-C, 73.40.Qr

INTRODUCTION

The formation of titanium silicide is of considerable interest for microelectronic applications because of its resistivity, the lowest of all refractory metal silicides,[1] and its compatibility with standard metal-oxide-semiconductor (MOS) processing.[2-7] In particular, titanium silicide finds application as low-resistivity interconnects for very-large-scale-integrated (VLSI) circuits and as gate electrodes for MOS devices. One application involves the simultaneous reaction of elemental Ti with polycrystalline Si (polysilicon) gates and with crystalline Si in the source and drain of a MOS transistor. Shorting between the source/drain and the gate is prevented by an SiO_2 spacer on the sidewall of the polysilicon line. High temperature (900-1000°C) annealing promotes silicide formation wherever the Ti is in contact with exposed Si. The resultant silicide pattern forms a self-aligned gate and source/drain for MOS transistors.

An undesirable byproduct of annealing such a Ti-Si-SiO_2 structure is the formation of titanium silicide on the SiO_2 sidewall, which can open a conducting pathway across the gate insulator. Initially, this unwanted reaction product was attributed to Si diffusion from the substrate through the conformal Ti overlayer. In this paper, we identify a second effect which may also be responsible for this parasitic silicide – namely, the reaction between Ti and SiO_2. In addition, we demonstrate how the silicide reaction at the Ti-Si interface can be enhanced over that at the Ti-SiO_2 interface by rapid thermal annealing[8] at low temperatures. Specifically we find that 1) reactions and diffusion occur at Ti-Si and Ti-SiO_2 interfaces on short time scale (seconds) at conventional processing temperatures (e.g., 400-1000°C) and not over the course of tens of minutes or hours,[9] 2) these chemical

interactions evolve for thin films (e.g., <100 nm) in a manner similar to multi-micron thicknesses, 3) Ti silicide forms at the Ti-SiO_2 interface due to the dissociation of SiO_2, 4) at a temperature of 475°C or less, a process window in time exists such that Ti silicide can form at source, gate, and drain before SiO_2 can dissociate and form a silicide at the insulator, 5) reactions at the Ti-Si interface are very sensitive to interface contamination, which can form a strong barrier to Si diffusion into Ti, and 6) ion sputter-cleaning of Si and SiO_2 before Ti deposition accelerates dissociation of SiO_2 and outdiffusion of Si into Ti..

We used Auger electron spectroscopy (AES) with 3 keV Ar^+ sputter profiling to characterize the Ti-Si and Ti-SiO_2 interfaces under ultrahigh vacuum (UHV) conditions. Base pressure of our stainless steel UHV chamber was $p = 1x10^{-10}$ torr with the pressure rising during Ti deposition to the mid-10^{-9} torr range. AES displayed no evidence (< 1%) of 0 incorporation within the Ti film. Our specimens consisted of 6x12 mm sections of Si (100) wafer (intrinsic, p-type), patterned with thermally-grown 140 nm SiO_2 areas across the surface. These surfaces were heat-cleaned prior to Ti deposition by passing current through the wafer section via Ta support clips. After a 1050°C anneal for 2 minutes, AES analysis revealed no detectable C or O surface contamination. We used a similar geometry for rapid thermal annealing of the Ti-covered surfaces. An Optitherm radiometer (Barnes Engineering) focused on the heated surface through a sapphire window provided a measure of surface temperature. Ti deposition was intentionally over only part of the surface so that the exposed Si provided reliable emissivity values, as measured previously.[10] AES analysis was confined to Ti-Si and Ti-SiO_2 interfaces located within a few tens of microns laterally of the exposed Si surface to minimize any possible discrepancy between the probe area and the bare surface. Because of the

low thermal mass of the Si wafer section and Ta heater clips, the specimen temperature could be ramped up to temperatures of 300-1000°C in a matter of only a few seconds. Radiant cooling limits the rate of temperature decrease such that 15-30 sec. are required to reach temperatures below 200°C.

AES analysis of Ti-Si interfaces - both patterned and uniform, large areas - reveal that silicides of various stoichiometry form at temperatures of 500-1000°C. The surface stoichiometry of these silicides increases with increasing anneal temperature, consistent with the proportions of TiSi and TiS_2 formed,[9] as well as with the reported Si surface segregation.[11,12] However, the AES results show that such silicides form at the same temperatures in much shorter times than are conventionally employed - less than two minutes vs. 30-60 minutes by furnace anneal. Furthermore, these reactions evolve even for relatively thin Ti overlayers (e.g. 40 nm) vs. the multimicron thicknesses typically studied. Butz et al.[13] obtained similar results, albeit with even thinner films for longer times at 500°C. Hence, our Ti-Si AES studies complement earlier thick film, rapid thermal annealing work[2,4] as well as thin film, extended annealing studies[11,13] of Ti-Si interfaces. Exposition of this Ti-Si work will appear elsewhere.[14]

Here we focus primarily on the reaction products at the Ti-SiO_2 interface - both patterned and uniform, large areas - and the temperature dependence of such reactions over periods of minutes or less with respect to the temperature dependence of Ti-Si reactions over similar time periods. Ti reactions with SiO_2 *slowly* begin at temperatures below 500°C and eventually result in the formation of a Ti silicide and an overlayer of Ti oxide. Figure 1 shows an Auger depth profile of 40 nm Ti on 140 nm SiO_2 on a Si substrate, annealed at 700°C for 2 minutes. The sputter profile

reveals at least three discrete regions above the Si substrate: a layer of Ti oxide at the outer (free) surface, a layer of Ti silicide, and the SiO_2 film on the Si substrate. The abrupt changes in Si concentration at the Ti-Si and SiO_2 interface may signal the presence of an additional phase or mixture of phases, but with a thickness of only a few monolayers or less. Overall, Fig. 1 reveals that all of the deposited Ti has been consumed by Si and O in only two minutes, that an oxide forms at the free surface which is not due to contamination above or within the Ti film, and that a silicide forms above the SiO_2 film. Clearly the presence of a Ti silicide across the SiO_2 gate oxide could lead to a low resistance path between gate and source/drain of a self-aligned, Ti-SiO_2 gate structure.

The stoichiometry of the Ti oxide and silicide in Fig. 1 can be extracted by consideration of the ternary phase diagram for Ti-SiO_2 recently presented by Beyers.[15] Assuming that the constituents have reached thermodynamic equilibrium (which is likely since diffusion into discrete phases has occurred throughout the Ti film), the phase diagram indicates that several Ti silicides are stable next to SiO_2 but that only Ti_5Si_3 is stable in contact with both SiO_2 and a Ti oxide. Thus, the Ti:Si ratio is established for the intermediate layer in Fig. 1. Since the Si:O ratio in the SiO_2 layer is determined as well, we can derive the stoichiometry of the outer oxide layer which is that of TiO. This oxide layer evolves from the decomposition of SiO_2 and not from any ambient contamination above or within the initial Ti film.

Figure 1 illustrates that the appearance of TiO on SiO_2 is an indication of SiO_2 dissociation and subsurface silicide formation. Likewise, the appearance of Si at the free surface of Ti on clean Si provides an indicator of Ti silicide formation.[11-14] We have used these signs to uncover a process window in time during which Ti silicide

can form on Si before dissociation of SiO_2 on the same Si substrate begins. Figure 2 illustrates the evolution of Auger intensities on the deposited Ti surface as a function of anneal time for a representative temperature of 425°C. The differences in surface chemical composition between Ti on Si in Fig. 2(a) and Ti on SiO_2 in Fig. 2(b) derive from interface areas spaced less than 20 microns apart laterally on the same Si substrate. From Fig. 2a, the Si Auger signal appears almost immediately at the free Ti-on-Si surface, whereas the appearance of O on Ti/SiO_2 in Fig. 2b requires between 8 and 12 minutes. After this time interval, almost the entire Ti film on Si has reacted to form Ti silicide(s), whereas dissociation of the SiO_2 interface has only begun. Furthermore, at these relatively low temperatures, Si diffusion from the substrate will be limited to lengths of tens of nm vertically – enough to form silicide at a gate, source and drain, but not enough for significant lateral diffusion through the conformal Ti film across the gate insulator. These results suggest that rapid thermal annealing at low temperatures can be used to limit such unfavorable reactions while promoting silicide formation where desired.

The Ti silicide(s) formed in Fig. 2a after 10 min. are not yet completely $TiSi_2$. As a result, a piranha etch ($5H_2SO_4 + 2H_2O_2$) used to remove residual Ti from above the SiO_2 may remove some Ti from the $TiSi_x$ ($X \leq 2$) as well, leading to increased silicide resistivity. This may be remedied by repeating the low temperature metallization and annealing process.

Interfaces free of contamination[10] are required to achieve the results presented in Fig. 2. Our studies show that air-exposed wafers require higher temperatures, typically 700°C or more, to initiate these reactions because of a thin contamination layer (primary O and C) which must be dissociated first. At such temperatures, dissociation of the SiO_2 could not be controlled.

An alternative to heating the Si substrate to high temperature for obtaining a clean surface is sputter-etching the surface prior to metal deposition. AES analysis of surface composition vs. time shows that a process window in time exists for Ti on sputter-cleaned surfaces as well. However, this time interval is considerably shorter than that for heat-cleaned Si. At 475°C, O appears on Ti/SiO_2 after only 120 seconds.

We are currently investigating the competition between the Ti silicide formation and Ti/SiO_2 dissociation processes at even lower temperatures in order to determine if the process window can be expanded further in time. Critical to the success of such a low temperature, rapid thermal anneal are 1) the absence of any oxide on the Si prior to Ti deposition, which will inhibit the silicide formation and 2) the absence of any temperature spikes during the anneal procedure, which if even for a few seconds or less above 500°C can accelerate Ti/SiO_2 dissociation.

In conclusion, we find that Ti silicide forms at the Ti/SiO_2 interface due to the dissociation of SiO_2, and that at a temperature of 475°C or less, a process window in time exists such that Ti silicide can form at Ti-Si interfaces before SiO_2 can dissociate at the $Ti-SiO_2$ interface. These reactions are very sensitive to interface contamination and ion sputter damage.

ACKNOWLEDGMENTS

The authors wish to thank C.B. Duke, J. Knights and J. Mort for their encouragement and support.

REFERENCES

1. S.P. Murarka, Silicides for VLSI Applications (Academic, New York, 1983).

2. R.A. Powell, R. Chow, C. Thridandam, R.T. Fulks, J.A. Blech and J-D. T. Pan, IEEE Electron Device Letters, EDL-4, 380 (1983).

3. M. Tanielian, S. Blackstone, and R. Lajos, Appl. Phys. Lett. 45, 444 (1984).

4. C.S. Wei, J. Van der Spiegel, J.J. Santiago, and L.E. Seiberling, Appl. Phys. Lett. 45, 527 (1984).

5. M. Tanielian and S. Blackstone, Appl. Phys. Lett. 45, 673 (1984).

6. T.P. Chow, W. Katz and G. Smith, Appl. Phys. Lett. 46, 41 (1985).

7. G.G. Bertini, R. Nipoti, A. Armigliato, M. Berti, A.V. Drigo and C. Cohen, J. Appl. Phys. 57, 270 (1985).

8. R.T. Fulks, C.J. Russo, P.R. Hanley and T.I. Kamins, Appl. Phys. Lett. 39, 604 (1981).

9. S.P. Murarka and D.B. Fraser, J. Appl. Phys. 51, 342 (1980).

10. L.J. Brillson, M.L. Slade, A.D. Katnani, M. Kelly and G. Margaritondo, Appl. Phys. Lett. 44, 110 (1984).

11. M.A. Taubenblatt and C.R. Helms, J. Appl. Phys. 53, 6308 (1982).

12. A.E.T. Kuiper, G.C.J. Van der Ligt, W.M. Van de Wijgert, M.F.C. Williemson and F.H.P.M. Habraken, J. Vac. Sci. Technol. B3, 830 (1985).

13. R. Butz, G.W. Rubloff, T.Y. Tan, and P.S. Ho, Phys. Rev. B30, 5421 (1984).

14. L.J. Brillson, M.L. Slade, H.W. Richter, H. Van der Plas, and R.T. Fulks, unpublished.

15. R. Beyers, J. Appl. Phys. 56, 147 (1984).

FIGURE CAPTIONS

Figure 1. Auger depth profile of 40 nm Ti over SiO_2 on Si, annealed at 700°C for two minutes.

Figure 2. Evolution of Auger intensities as a function of 425°C anneal time for 40 nm Ti on heat-cleaned Si (a) and SiO_2 (b).

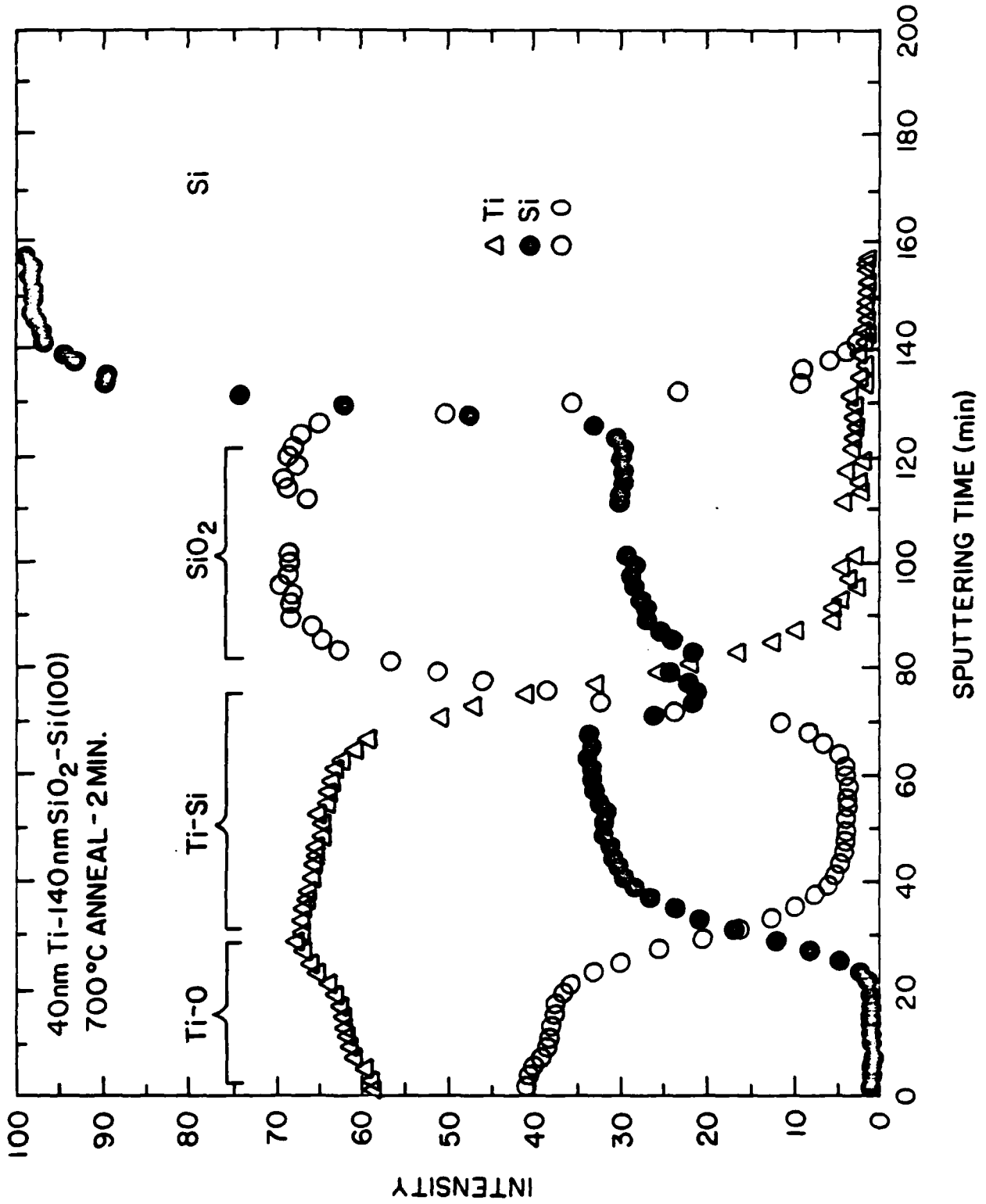
40nm Ti-140nmSiO2-Si(100)
700°C ANNEAL - 2MIN.
Ti-O
Ti-Si
SiO2
Si
Ti
Si
INTENSITY
SPUTTERING TIME (min)
0
10
20
30
40
50
60
70
80
90
100
0
20
40
60
80
100
120
140
160
180
200

Fig. 1

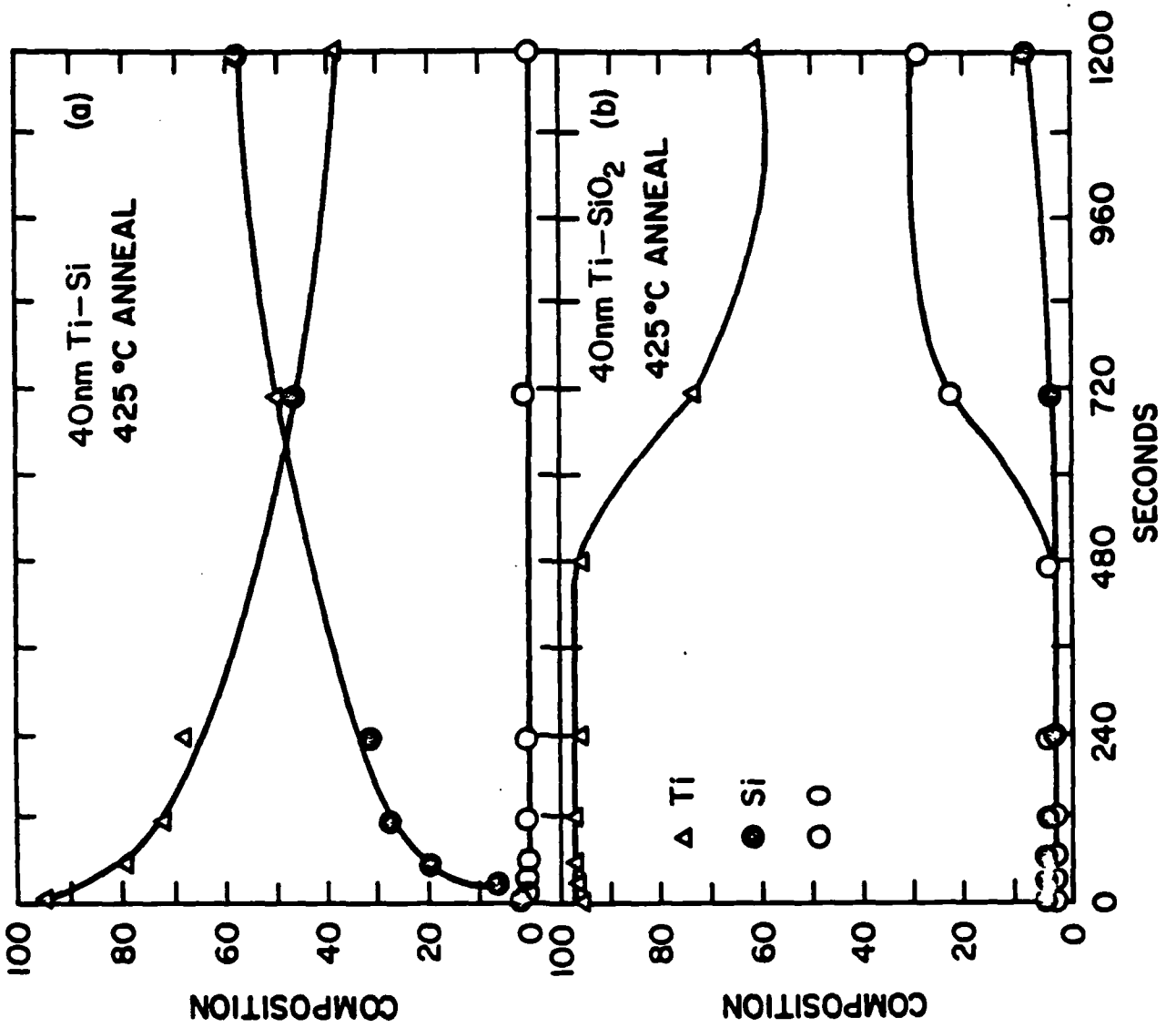
(a)
40nm Ti–Si
425 °C ANNEAL
(b)
40nm Ti–SiO2
425 °C ANNEAL
Ti
Si
O
COMPOSITION
SECONDS
0
240
480
720
960
1200
100
80
60
40
20
0

Fig. 2

V. Cumulative List of Publications Under Navy Contract N00014-80-C-0778

80-C-0778 - 1. Atomic and Electrical Structure of InP-Metal Interfaces: A Prototypical III-V Compound Semiconductor, L.J. Brillson, C.F. Brucker, A.D. Katnani, N.G. Stoffel, and G. Margaritondo, Journal of Vacuum Science and Technology 19, 661 (1981).

80-C-0778 - 2. Chemical Basis for InP-Metal Schottky Barrier Formation, L.J. Brillson, C.F. Brucker, A.D. Katnani, N.G. Stoffel, and G. Margaritondo, Applied Physics Letters 38, 784 (1981).

80-C-0778 - 3. Fermi Level Pinning and Chemical Structure of InP-Metal Interfaces, L.J. Brillson, C.F. Brucker, A.D. Katnani, N.G. Stoffel, R. Daniels and G. Margaritondo, Journal of Vacuum Science and Technology 21, 564 (1982).

80-C-0778 - 4. Leading Semiconductor Research in China, Scientific Bulletin, Dept. Navy, Office of Naval Research Tokyo 6, 48 (1981).

80-C-0778 - 5. Abruptness of Semiconductor-Metal Interfaces, L.J. Brillson, C.F. Brucker, A.D. Katnani, N.G. Stoffel, and G. Margaritondo, Physical Review Letters 46, 838 (1981).

80-C-0778 - 6. Interface Chemical Reaction and Interdiffusion of Thin Metal Films on Semiconductors, L.J. Brillson, Thin Solid Films 89, 461 (1982).

80-C-0778 - 7. Interaction of Metals with Semiconductor Surfaces, L. J. Brillson, Applications of Surface Science; 11/12, 249 (1982).

80-C-0778 - 8. Chemical and Electronic Structure of Compound Semiconductor-Metal Interfaces, L.J. Brillson, Journal of Vacuum Science and Technology 20, 652 (1982).

80-C-0778 - 9. Systematics of Chemical Structure and Schottky Barriers at Compound Semiconductor-Metal Interfaces" L.J. Brillson, C.F. Brucker, N.G. Stoffel, A.D. Katnani, R. Daniels, and G. Margaritondo, Proceedings of the Second IUPAP Semiconductor Symposium on Surfaces and Interfaces, Surface Science 132, 212 (1983).

80-C-0778 - 10. Photoemission Studies of Reactive Diffusion and Localized Doping at II-VI Compound Semiconductor Interfaces, L.J. Brillson, C.F. Brucker, N.G. Stoffel, A.D. Katnani, R. Daniels, and G. Margaritondo, Proceedings of the 16th International Conference on the Physics of Semiconductor, Physica 117B&C, 848 (1983).

80-C-0778 - 11. Contact Technology in 3-5 Device Analysis and Modification of Metal-Semiconductor Contact Interface in 3-5 Devices, L.J. Brillson, IEEE Technical Digest of the International Electron Devices Meeting, p. 111.

80-C-0778 - 12. Soft X-Ray Photoemission Techniques for Characterizing Metal-Semiconductor Interfaces, L.J. Brillson, Proceedings of the Brookhaven Conference on Advances in Soft X-Ray Science and Technology, Eds. F.J. Himpsel and R.W. Klaffky (SPIE, Bellingham, WA, 1984) p. 89.

80-C-0778 - 13. InP Surface States and Reduced Surface Recombination Velocity, L. J. Brillson, Y. Shapira, and A. Heller, Applied Physics Letters, 43, 174 (1983).

80-C-0778 - 14. Investigation of InP Surface and Metal Interfaces by Surface Photovoltage and Auger Electron Spectroscopies, Y. Shapira, L.J. Brillson and A. Heller, *Journal of Vacuum Science and Technology* A1, 766 (1983).

80-C-0778 - 15. Studies of Surface Recombination Velocity Reduction of InP Photoelectrochemial Solar Cells, Y. Shapira, L.J. Brillson, and A. Heller, Proceedings of the Fifth EC Photovoltaic Solar Energy Conference, Athens, Greece (1983).

80-C-0778 - 16. Origin of Surface and Metal-Induced Interface States on InP, Y. Shapira, L.J. Brillson, and A. Heller, Physical Review B29, 6824 (1984).

80-C-0778 - 17. Auger Depth Profiling Studies of Interdiffusion and Chemical Trapping at Metal-InP Interfaces, Y. Shapira and L. J. Brillson, Journal of Vacuum Science and Technology B1, 618 (1983).

80-C-0778 - 18. Reduction of Silicon-Aluminum Interdiffusion by Improved Semiconductor Ordering, L.J. Brillson, M. Slade, A. Katnani, M. Kelly, and G. Margaritondo, Applied Physics Letters 44, 110 (1984).

80-C-0778 - 19. Photoemission Studies of Atomic Redistribution at Gold-Silicon and Aluminum-Silicon Interfaces, L.J. Brillson, A.D. Katnani, M. Kelly, and G. Margaritondo, Journal of Vacuum Science and Technology, A2, 551 (1984).

80-C-0778 - 20. Ultrafast UV-Laser Induced Oxidation of Silicon, T.E. Orlowski and H. Richter, Materials Research Society Symposium Proceedings 23, 327 (1984).

80-C-0778 - 21. Ultrafast Laser-Induced Oxidation of Silicon: A New Approach Towards High Quality, Low Temperature, Patterned SiO_2 Formation, T.E. Orlowski and H. Richter, Applied Physics Letters 45, 241 (1984).

80-C-0778 - 22. Ultrafast UV-Laser-Induced Oxidation of Silicon: Control and Characterization of the Si-SiO_2 Interface, H. Richter, T.E. Orlowski, M. Kelly, and G. Margaritondo, Journal of Applied Physics 56, 2351 (1984).

80-C-0778 - 23. Interdiffusion and Chemical Trapping at InP (110) Interfaces with Au, Al, Ni, Cu and Ti, Y. Shapira, L.J. Brillson, A.D. Katnani and G. Margaritondo, Physical Review B30, 4586 (1984).

80-C-0778 - 24. Control and Characterization of Metal-InP and GaAs Interfaces Formed by Laser-Enhanced Reactions, H. Richter, L.J. Brillson, R. Daniels, M. Kelly, and G. Margaritondo, Journal of Vacuum Science and Technology B2, 591 (1984).

80-C-0778 - 25. Laser-Induced Chemical Reactions at the Al/III-V Semiconductor Interface, H. Richter and L.J. Brillson, Proceedings of the 17th International Conference on the Physics of Semiconductors (Springer-Verlag, New York, 1985), p. 137.

80-C-0778 - 26. Advances in Characterizing and Controlling Metal-Semiconductor Interfaces, Applications of Surface Science 22/23, 948 (1985).

80-C-0778 - 27. Cathodoluminescence Spectroscopy Studies of Laser-Annealed Metal-Semiconductor Interfaces, Journal of Vacuum Science and Technology A3, 1011 (1985).

80-C-0778 - 28. Laser-Induced Chemical Reaction at the Al/III-V Compound Semiconductor Interface, H.W. Richter and L.J. Brillson, submitted to Physical Review B.

80-C-0778 - 29. UPS, XPS and AES Studies of CaF_2-CdSe, C.F. Brucker, Y. Shapira and L.J. Brillson, submitted to Thin Solid Films.

80-C-0778 - 30. Acceptor-Like Electron Traps and Thermally-Reversible Barrier Heights for Al on UHV-Cleaved (110) InP, John H. Slowik, H.W. Richter, and L.J. Brillson, *Journal of Applied Physics*, in press.

80-C-0778 - 31. Promoting and Characterizing New Chemical Structure at Metal-Semiconductor Interfaces, L.J. Brillson, Surface Science, in press.

80-C-0778 - 32. Control of Titanium-Silicon and Silicon Dioxide Reactions by Low Temperature Rapid Thermal Annealing, L.J. Brillson, M.L. Slade, H.W. Richter, H. Vander Plas, and R.T. Fulks, Applied Physics Letters, in press.

VI. Postdoctoral Fellows Involved in Navy Contract N00014-80-C-0778 Research for the Period October 1, 1984, through September 30, 1985

1. Prof. Yoram Shapira, School of Engineering, Tel Aviv University, Tel Aviv, Israel.

2. Dr. Harald Richter, Max Planck Institut für Festkörperforschung, Stuttgart, West Germany.

3. Dr. Enrique Viturro, Solid State Institute, The Technion, Israel Institute of Technology, Haifa, Israel.

VII. Publications/Patents/Presentations/Honors for the Period October 1, 1984, to September 30, 1985

a) *Papers Submitted to Refereed Journals (and not yet published)*

1. Laser-Induced Chemical Reaction at the Al/III-V Compound Semiconductor Interface, H.W. Richter and L.J. Brillson, submitted to Physical Review B.

2. UPS, XPS and AES Studies of CaF_2-CdSe, C.F. Brucker, Y. Shapira and L.J. Brillson, submitted to Thin Solid Films.

3. Acceptor-Like Electron Traps and Thermally-Reversible Barrier Heights for Al on UHV-Cleaved (110) InP, John H. Slowik, H.W. Richter, and L.J. Brillson, Journal of Applied Physics, in press.

4. Control of Titanium-Silicon and Silicon Dioxide Reactions by Low Temperature Rapid Thermal Annealing, L.J. Brillson, M.L. Slade, H.W. Richter, H. VanderPlas, and R.T. Fulks, Applied Physics Letters, in press.

b) *Papers Published In Refereed Journals*

1. Ultrafast UV-Laser Induced Oxidation of Silicon, T.E. Orlowski and H. Richter, Materials Research Society Symposium Proceedings 23, 327 (1984).

2. Ultrafast Laser-Induced Oxidation of Silicon: A New Approach Towards High Quality, Low Temperature, Patterned SiO_2 Formation, T.E. Orlowski and H. Richter, Applied Physics Letters 45, 241 (1984).

3. Ultrafast UV-Laser-Induced Oxidation of Silicon: Control and Characterization of the Si-SiO_2 Interface, H. Richter, T.E. Orlowski, M. Kelly, and G. Margaritondo, Journal of Applied Physics 56, 2351 (1984).

4. Interdiffusion and Chemical Trapping at InP (110) Interfaces with Au, Al, Ni, Cu and Ti, Y. Shapira, L.J. Brillson, A.D. Katnani and G. Margaritondo, Physical Review B30, 4586 (1984).

5. Control and Characterization of Metal-InP and GaAs Interfaces Formed by Laser-Enhanced Reactions, H. Richter, L.J. Brillson, R. Daniels, M. Kelly, and G. Margaritondo, Journal of Vacuum Science and Technology B2, 591 (1984).

6. Laser-Induced Chemical Reactions at the Al/III-V Semiconductor Interface, H. Richter and L.J. Brillson, Proceedings of the 17th International Conference on the Physics of Semiconductors (Springer-Verlag, New York, 1985), p. 137.

7. Characterization and Control of Metal-Semiconductor Interfaces, Applications of Surface Science 22/23, 948 (1985).

8. Cathodoluminescence Spectroscopy Studies of Laser-Annealed Metal-Semiconductor Interfaces, Journal of Vacuum Science and Technology A3, 1011 (1985).

9. Metal-Semiconductor Interface Studies by Synchrotron Radiation Techniques, in Handbook of Synchrotron Radiation, L.J. Brillson, Volume II, Ed. G.V. Marr (North-Holland, Amsterdam, 1985), in press.

c) *Books (and Sections Thereof) Submitted for Publication*

NONE

d) *Books (and Sections Thereof) Published*

NONE

e) *Patents Filed*

NONE

f) *Patents Granted*

NONE

g) *Invited Presentations at Topical or Scientific/Technical Society Conferences*

1. Surface Science Analysis of Metal-Semiconductor Interfaces, L.J. Brillson, University of Florida, Gainesville, FL, November 12, 1984. Supported by Xerox Corporation.

2. Chemical and Electronic Structure at Metal-Semiconductor Interfaces, L.J. Brillson, RCA David Sarnoff Research Center, Princeton, NJ, November 15, 1984. Supported by Xerox Corporation.

3. Progress in Understanding Metal-Semiconductor Interfaces by Surface Science Techniques, L.J. Brillson, The 1984 International Chemical Congress of Pacific Basin Societies, Honolulu, Hawaii, Dec. 19, 1984. Supported by the American Chemical Society.

4. Characterization and Control of Metal-Semiconductor Interfaces, L.J. Brillson, Electronics Department, General Motors Research Laboratories, Warren, MI, January 22, 1985. Supported by General Motors.

5. Understanding Semiconductor Surfaces and Interfaces Using Surface Science Techniques, L.J. Brillson, Special Lecture Series on Electronic Materials, University of Pennsylvania, Philadelphia, PA, February 20, 1985. Supported by the University of Pennsylvania.

6. Modelling and Modifying the Formation of Schottky Barriers, L.J. Brillson, Special Lecture Series on Electronic Materials, University of Pennsylvania, Philadelphia, PA , February 21, 1985. Supported by the University of Pennsylvania.

7. Metal-Semiconductor Interface Characterization and Control, L.J. Brillson, Arizona Chapter, American Vacuum Society, Phoenix, AZ, February 26, 1985. Supported by the American Vacuum Society.

8. The Physics and Chemistry of Metal-Semiconductor Interfaces, L.J. Brillson, Department of Physics, Brooklyn College, New York, NY, March 20, 1985 Supported by Brooklyn College.

9. Advanced Techniques for Characterizing Metal-Semiconductor Interfaces. L.J. Brillson, Special Lecture Series on Electronic Materials, University of Pennsylvania, Philadelphia, PA, April 3, 1985. Supported by the University of Pennsylvania.

10. Processing and Control of Electronic Materials, L.J. Brillson, Special Lecture Series on Electronic Materials, University of Pennsylvania, Philadelphia, PA, April 4, 1985. Supported by the University of Pennsylvania.

11. Chemical and Electronic Properties of Metal-Semiconductor Interfaces, L.J. Brillson, Department of Physics, Pennsylvania State University, State College, PA, May 15, 1985. Supported by Pennsylvania State University.

12. Promoting and Characterizing New Chemical and Electronic Structure at Metal-Semiconductor Interfaces, L.J. Brillson, International Conference on the Formation of Semiconductor Interfaces, Marseilles, France, June 11, 1985. Supported by ICSFS.

13. Understanding Chemical Interactions at Metal-Semiconductor Interfaces for Improved Adhesion, L.J. Brillson, Department of Energy Panel on Bonding and Adhesion, Aspen, CO, August 14, 1985. Supported by the Department of Energy.

14. Chemical Bonding and Diffusion at Metal-Semiconductor Interfaces, L.J. Brillson, Department of Physics, Ohio State University, Columbus, OH, August 30, 1985. Supported by Xerox Corporation.

15. Characterization and Control of III-V Compound Semiconductor/Metal Interfaces, L.J. Brillson, Advanced Technology Department, Bell Northern Research Laboratories, Ottawa, Canada, September 13, 1985. Supported by Xerox Corporation.

16. Characterization and Control of Metal-Semiconductor Interfaces, L.J. Brillson, Department of Physics, University of Maryland, College Park, MD, September 19, 1985. Supported by the University of Maryland.

h) *Honors/Awards/Prizes*

1. Fellow, American Physical Society

VIII. Money Spent of Equipment

NONE

IX. Transitions of Research to Industry

The low temperature thermal annealing technique (80-C-0778-32) is being picked up by the Integrated Circuits Laboratory of Xerox's Palo Alto Research Laboratory as a possible means to avoid shorting across gate dielectrics in self-aligned transistor gate structures. Such prototype VLSI structures will ultimately go into custom chips manufactured in Xerox's El Segundo plant.

X. Collaborations With Workers From Academic Institutions

Professor Giorgio Margaritondo, Department of Physics, University of Wisconsin, Madison, WI - Soft X-ray Photoemission Spectroscopy of Metal-Semiconductor Interfaces.

END

FILMED

12-85

DTIC